Rheological, Thermal and Isostatic Constraints on Continental Lithosphere Extension and Compression.

Stuart S. Egan

Thesis Submitted for the Degree of Doctor of Philosophy

Department of Geology

University of Keele

December 1988

ABSTRACT

Deep seismic reflection data has shown the importance of low angle faults and detachments in continental extensional tectonics. A quantitative model of continental lithosphere extension is presented, incorporating geometric, thermal and isostatic components. The upper lithosphere extends by simple shear associated with low angle faults, while the lower lithosphere deforms by pure shear.

The resulting sedimentary basin geometry and crustal structure are dependent upon the amount of lithosphere extension, the distribution of the pure shear, the depth of the horizontal detachment, the geometry of the low angle fault and the isostatic response of the lithosphere during rifting and thermal subsidence.

The Jeanne d'Arc basin, Newfoundland is most closely represented by models incorporating the flexural isostatic response of the lithosphere to applied loading. Stratigraphic data shows that the basin was generated by several pulses of extension and rifting was followed by erosion. Modelling techniques are used to assess the implications of these phenomena.

A two dimensional study of the rheological strength of the lithosphere shows it to be determined by the interaction between the pre-rift thermal state of the lithosphere, the position of simple shear deformation with respect to that of pure shear, time since rifting and the rate of extension.

Model predictions of lithosphere shortening on low angle thrusts have been combined with the extensional modelling technique to explore the process of basin inversion. Model predictions are compared with observations from the North Celtic Sea Basin.

Extension on planar faults is modelled by considering the footwall and hanging wall as two interacting cantilevers, which flex in response to the isostatic forces created during extension. The construction has been applied to extension on a sequence of planar faults and predicts the familiar "domino-style" block rotation.

Acknowledgements

I would like to thank my supervisor, Nick Kusznir, for his constant interest and involvement in this research project. I would also like to thank Paul Collis and Gerry Pratt of the Computer Centre for their assistance with programming problems, members of the Department of Geology for helping to provide a friendly environment in which to work and last, but not least, Antonia Tomoszek for proof reading this thesis and offering constant encouragement.

Most of all I would like to thank my parents, Iris and Peter, for their support throughout my academic career.

I was supported during this study by a research studentship awarded by the University of Keele.

Contents

CHAPTER 1

Introduction

The theory of plate tectonics states that the outer rigid shell of the earth, the lithosphere, is broken into a number of plates (eg. Wilson 1966, Dewey and Bird 1970, Wilson et al. 1972, Dewey 1982) and convection currents in the sub lithosphere mantle cause these plates to be in relative motion to one another (McKenzie 1969). The elastic strength of the lithosphere allows the stresses produced by the interactions that take place at plate boundaries to be transmitted to relatively weak regions where they cause deformation. These deformational effects and their relationship to the plate tectonic process are described by the Wilson Cycle (Wilson 1966 and 1972) such that under tension the lithosphere is extended along normal faults and a rift valley is produced. If the horizontal stresses are prolonged or of a particularly high magnitude further extension of the rift valley leads to the formation of a sea floor spreading centre. As the cycle continues, sea floor at the oceanic margin grows older, becoming thicker and more dense until eventually it sinks and subduction begins. In some cases the rate of subduction exceeds the rate of sea floor spreading, which causes the size of the ocean to gradually decrease until continental collision occurs - the resulting compressional stresses initiate mountain building.

Research for this thesis has concentrated on quantifying certain aspects of the Wilson Cycle and, in particular, the deformational effects caused by continental lithosphere extension, with emphasis placed upon the basin and

stratigraphic geometries generated by the rifting. Mathematical modelling techniques have been used combining elementary physical principles, as applied to lithospheric behaviour, under extension, with observations from geological and geophysical data. Later sections show the results of a thermo-rheological investigation of extended lithosphere, an adaptation of the extensional modelling technique to lithosphere shortening and, finally, how both extensional and compressional processes have been combined to explore sedimentary basin inversion. The models have been tested against geological and geophysical data from examples including the Jeanne d'Arc basin, the North Celtic Sea basin and the Viking Graben.

1.1 Pure Shear Lithosphere Extension Models.

Extension of the continental lithosphere causes a thinning of the crust, which produces subsidence. The lithosphere-asthenosphere boundary is also brought nearer to the surface, causing an overall heating of the lithosphere, which generates a surface uplift (McKenzie 1978). The extension therefore generates two opposing phenomena; crustal thinning and thermal expansion (figure 1.1). Perturbations caused to the geotherm are temporary and after rifting cooling and contraction occurs as the isotherms within the lithosphere return back to their original state. This thermal contraction, in the absence of crustal thinning, returns any uplifted surface back to sea level or to some position below sea level if the crust has been attenuated. Both the thinning of the crust and the heating associated with rifting perturb the force balance of the

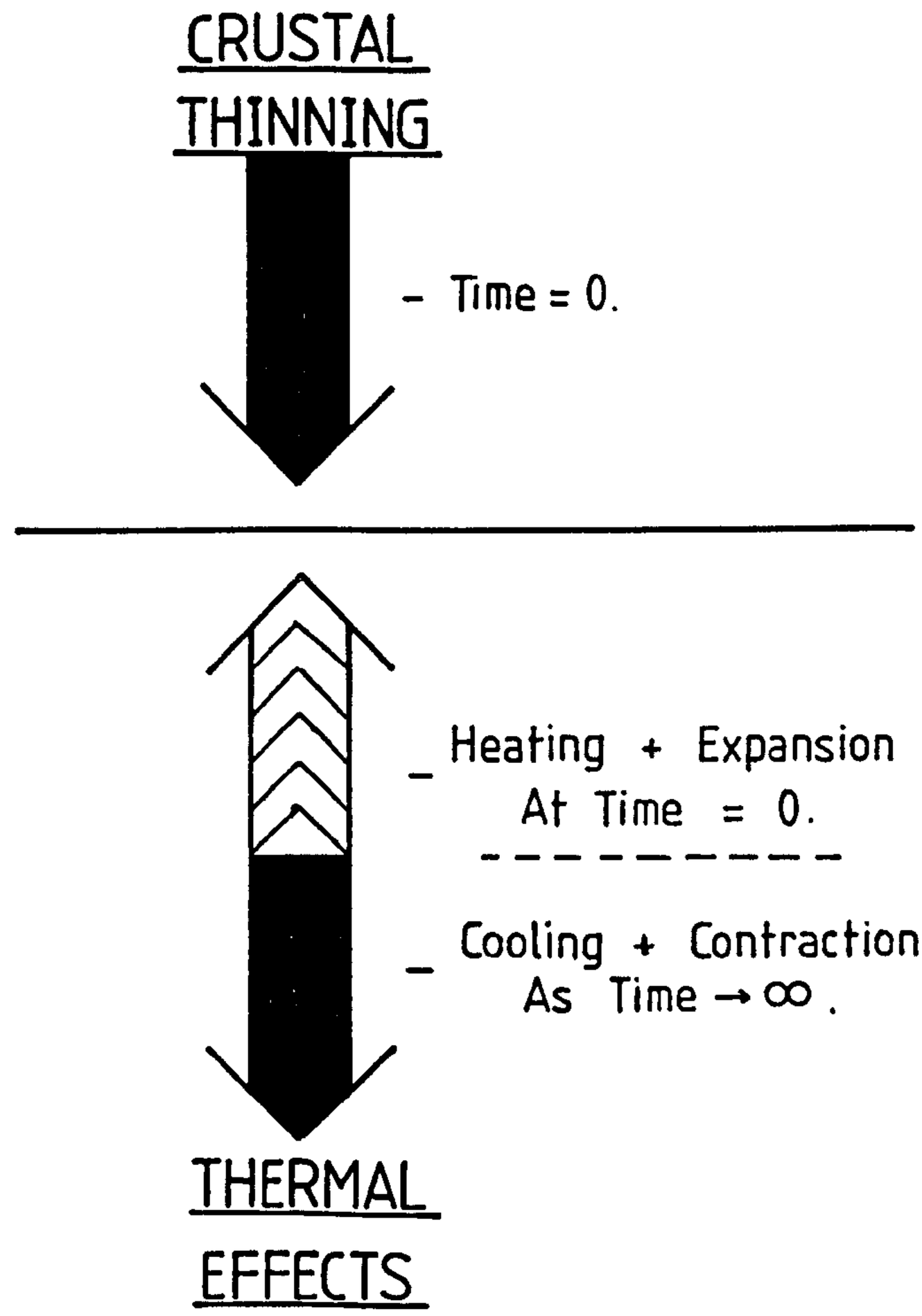

Figure 1.1 - Diagrammatic representation of lithosphere extension. At rifting the crust is thinned, which produces a surficial hole. At the same time the lithosphere is heated, producing a component of uplift. After rifting the lithosphere temperature field cools back to its original state, which is reflected by a gradual surface subsidence. Density contrasts arising from the deformation are isostatically compensated

lithosphere. The final form of the basin, stratigraphic geometries and Moho topography are controlled by the isostatic response of the lithosphere as a force balance is again achieved through subsidence and/or uplift.

The McKenzie model (1978) was the first quantitative model to successfully link continental lithosphere extension to extensional sedimentary basin formation and evolution. The model (figure 1.2) calculates the effect of instantaneously rifting a section of lithosphere uniformly from top to bottom. In response to this the crust is thinned and the lithosphere is heated due to the raising of hotter material nearer to the surface. The Airy isostatic effects arising from these two phenomena, as well as the infilling of any subsided area with water, are also included in the model. Crustal thinning, thermal expansion and isostatic compensation are combined in the following equation to give the vertical position, S_1, of the lithosphere surface following rifting:

$$S_1 = \{a.[(p_m-p_c).(c_o/a).(1-((\alpha.T_o.c_o)/(2.a))) - (\alpha.T_o.p_m/2)] . (1-1/\beta)\} / (p_m.(1-\alpha.T_o) - p_w) \quad \text{-----1.1}$$

where a is the thickness of the lithosphere, c_o is the original thickness of the crust, α is the thermal expansion coefficient, T_o is the temperature at the base of the lithosphere (equal to 1333°C), β is the stretching factor and p_m, p_c and p_w are the densities of mantle, crust and water respectively. A definition of each of the symbols is repeated in Table 1.

TABLE 1

List of Symbols

a	Lithosphere thickness.	125km
α	Thermal expension coefficient.	$3.28 \times 10^{-5} °C^{-1}$
β	Extension factor.	-----
β'	Lower lithosphere stretching factor.	-----
c_o	Original crustal thickness.	35km
k	Thermal diffusivity.	$7.99 \times 10^{-7} m^2.s^{-1}$
p_c	Density of crustal material.	$2800 kg.m^{-3}$
p_m	Density of mantle material.	$3300 kg.m^{-3}$
p_w	Density of water.	$1000 kg.m^{-3}$
S_i	Depth to basement after rifting.	-----
δ	Upper lithosphere stretching factor	-----
S_t	Thermal subsidence.	-----
t	Time	-----
T_o	Temperature at the base of the lithosphere.	1333°C
Γ	Dyke intrusion.	-----
y	Lithosphere decoupling depth.	-----

THE McKENZIE MODEL

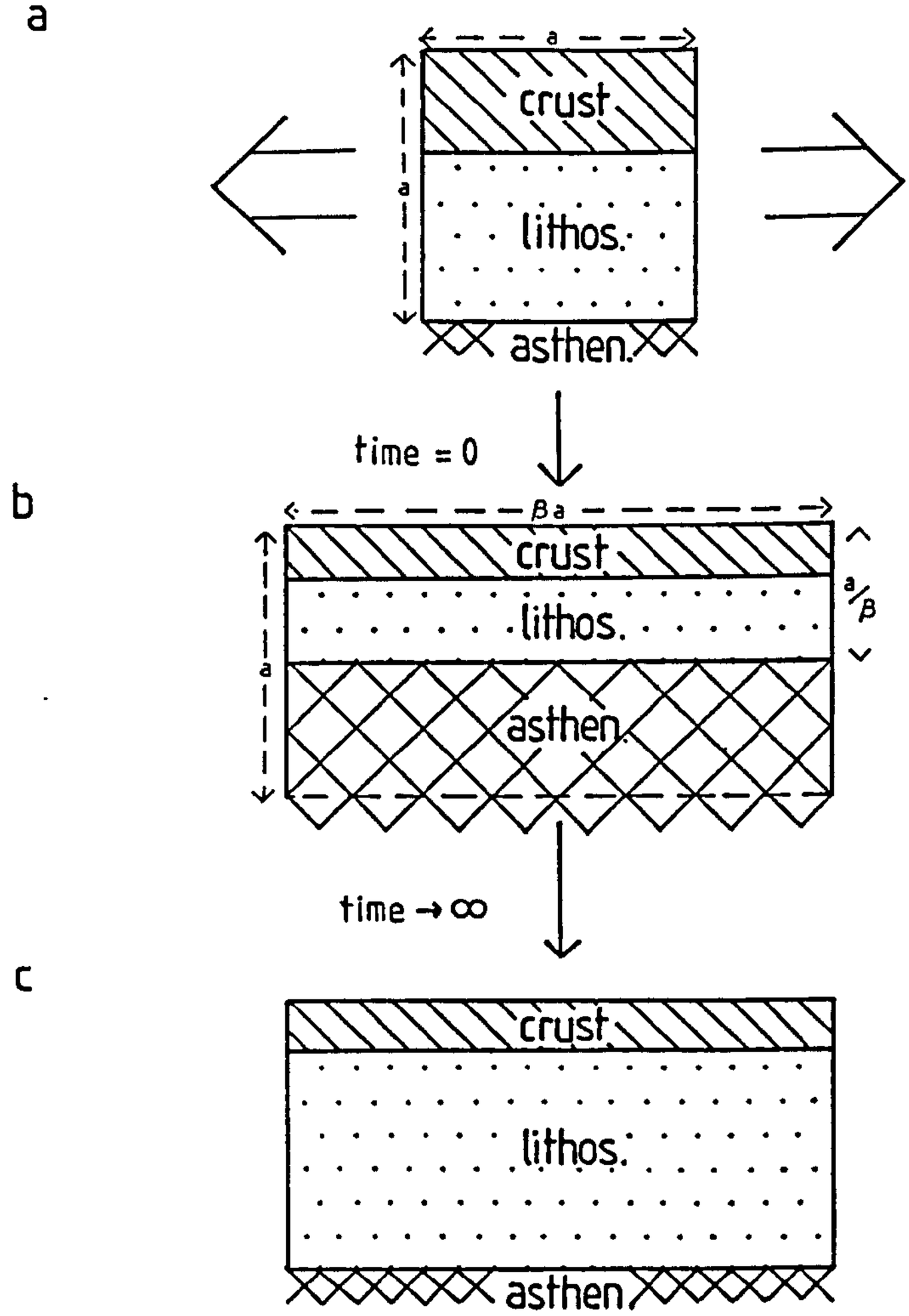

(adapted from McKenzie, 1978)

Figure 1.2 - The McKenzie model assumes that a section of lithosphere with width and depth, a, is extended uniformly with depth by an amount, Beta (a). This causes a thinning of the crust and a raising of the lithosphere/asthenosphere boundary (b), which is defined by the 1333°C isotherm. The section of lithosphere now has a new length of a.Beta and a thickness reduced to a/Beta. After the instantaneous rift phase the geotherm reequilibrates and a thinned crust remains (c). The elevation of the surface is determined by the Airy isostatic response of the lithosphere to the thinned crust and density reductions caused by heating.

After rifting the model predicts the thermal subsidence arising from the re-equilibration of the lithosphere temperature field. This thermal subsidence, S_t, exponentially decays over times of the order of 100 to 300 Ma and is defined by:

$$St = e_{(t=o)} - e_{(t)} \quad \text{----- 1.2}$$

where t is time and $e_{(t)}$ defines the elevation, at a particular time after rifting, above the final depth to which the surface of the lithosphere thermally subsides and is given by:

$$e_{(t)} = (a.p_m.\alpha.To)/(p_m-p_w) \; . \; \{(4/\pi^2) \; . \sum_{m=o}^{\infty} 1/(2.m+1)^2 \; . \; [\beta/((2.m+1).\pi) \; . \; \sin(((2.m+1).\pi)/\beta)] \; \exp(-(2.m+1)^2 \; . \; t/\tau)\} \text{ --- 1.3}$$

and:

$$\tau = a^2 /\pi^2.k \quad \text{---- 1.4}$$

where k is thermal diffusivity.

Total subsidence, S, is given by:

$$S = S_i - S_t \quad \text{----- 1.5}$$

The capabilities of the McKenzie model in terms of the basin geometries that it can generate are relatively limited - figure 1.3 shows basin geometries predicted by the model at rifting (dotted ornament) and at several times throughout the post-rift thermal subsidence phase (shaded ornament). In this particular example lithosphere extension reaches a maximum of 100 percent (Beta = 2) in the central region of

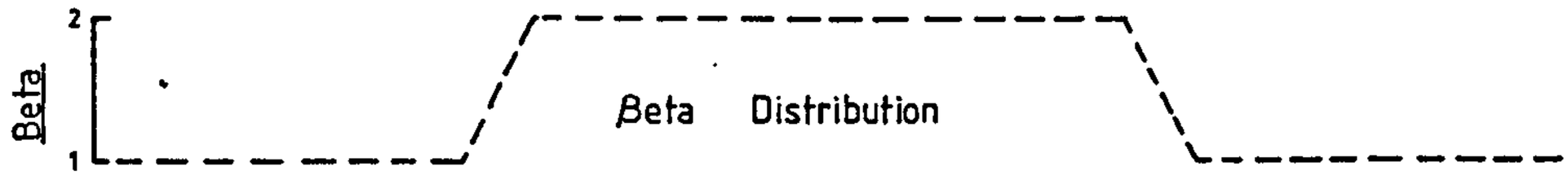

a) Water infill.

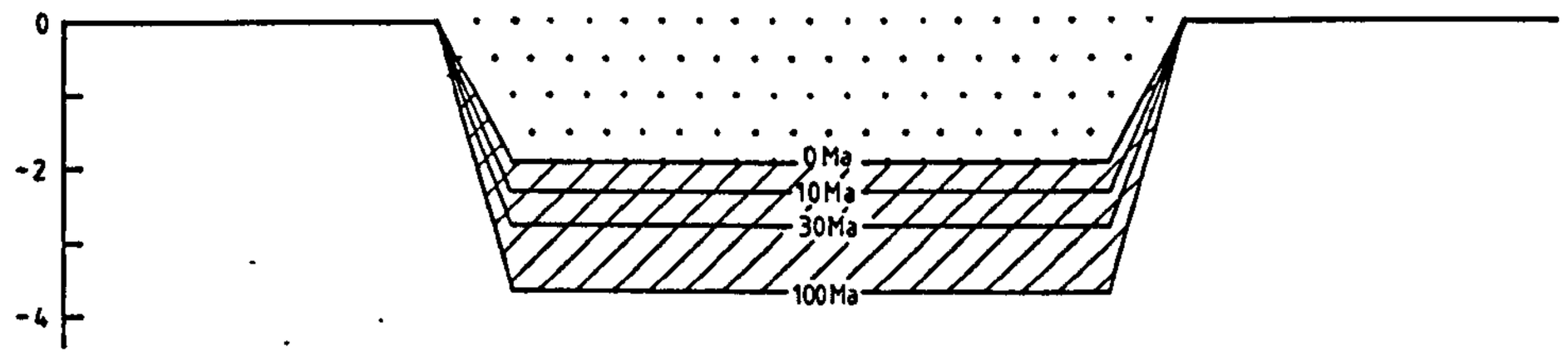

b) Sediment infill.

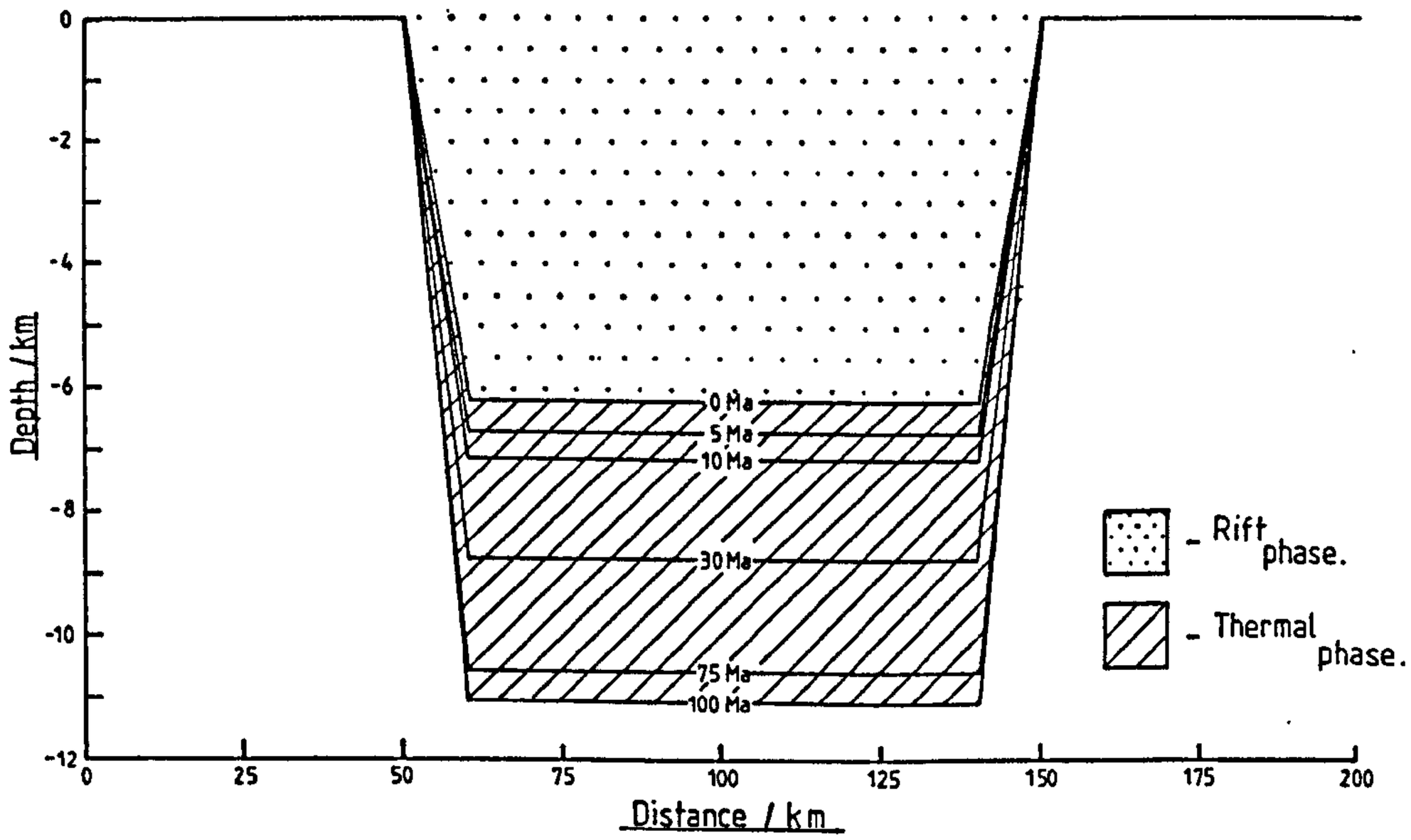

Figure 1.3 - Basins generated by using the mathematics of the McKenzie model. The lithosphere has been extended according to the Beta profile, which shows extension factors up to a maximum of 2. Dotted ornament represents the basin following instantaneous rifting, whereas shaded ornament denotes thermal subsidence. Basement is shown at various times from rifting through to 100Ma. The effect of filling the basin with water (a) and sediment (b) are shown.

the basin. In figure 1.3a any subsided region of the basement is loaded by water to sea level, while the greater depths displayed by the basin in figure 1.3b are a direct consequence of its infilling by sediment, which has an average density some 2.5 times greater than water (cf. 2500 $kg.m^{-3}$ to 1000 $kg.m^{-3}$ respectively).

The McKenzie model assumes that the lithosphere extends uniformly with depth - it is a pure shear model. This predicts extensional basins with laterally coincident syn- and post-rift components. While some large regions of extension display this vertical stacking of rift and thermal subsidence depocentres (eg. the Jeanne d' Arc basin, Grand Banks), other basins, such as the Brazilian Tucano basin (Ussami et al. 1986), show an absence of post-rift thermally driven subsidence. A possible cause of this is a relatively low amount of subcrustal attenuation beneath the region of rifting, which implies that the formation of these basins by a depth independent process must be questioned.

The Nova Scotian and Labrador continental shelves experienced rifting during the Jurassic/Cretaceous, to be followed by a gradual thermally induced subsidence due to the cooling of the lithosphere. Royden and Keen (1980) show that the subsidence history of the Nova Scotian margin can be accurately predicted by the uniform extension model (McKenzie, 1978). However the Labrador shelf displays a subsidence pattern which suggests that the mantle lithosphere was extended more than the crust. Similarly, the Viking Graben in the northern North Sea shows a high ratio of thermal subsidence to syn-rift deposition (Badley et al.

1988). In contrast, Hellinger and Sclater (1983) have shown that the thinning of the crust in the central part of the Pattani Trough in the intracratonic Gulf of Thailand has to be approximately 20 percent greater than the attenuation of the subcrustal lithosphere in order to explain the high thickness of syn-rift sediment.

To allow for the inhomogeneous behaviour of the lithosphere with depth under extension, Royden and Keen (1980) and Sclater et al. (1980) expanded upon the McKenzie model (1978) such that the upper and lower lithosphere are decoupled at a depth, y. Extension takes place by a factor δ above the decoupling depth, whereas the lower lithosphere extends independently by a factor β'. This non-uniform extension model is illustrated diagrammatically in figure 1.4 where it is also contrasted against the uniform stretching model in which the whole lithosphere is extended by a factor β. Similar to the McKenzie model (1978), the position of the surface, following rifting, predicted by the non-uniform extension model depends upon the isostatic response of the lithosphere to both the thinned crust and the reduced density due to heating. The position of the surface following crustal thinning is given by:

$$S_o = -((p_m-p_o)/(p_m.(1-\alpha T_o))) \; . \; c_o \; . \; (1-(1/\delta)+(\Gamma/\delta)) \; .$$
$$(1-((T_o.\alpha.c_o)/(2.a))) \quad \text{---- 1.6}$$

for $y > c_o$.

and:

$$S_\sigma = (-(p_m-p_\sigma)/(p_m.(1-\alpha.T_o))) \; . \; [y.(1-(1/\delta)+(\Gamma/\delta)) \; .$$

$$(1-((\alpha.T_o.y)/(2.a))) + (c_o-y) \; . \; (1-(1/\beta)+(\Gamma/\beta)) \; .$$

$$(1-(((\alpha.T_o)/(2.a)).(y+c_o))] \text{ ---- } 1.7$$

for $y \leq c_o$.

where Γ defines the amount of dyke intrusion (see Table 1 for a list of the other symbols).

The uplift of the surface created by heat added to the lithosphere during rifting is given by:

$$S_t = (T_o.\alpha.a.H)/(2.(1-(\alpha.T_o))) \text{ ----- } 1.8$$

where H is the amount of heat added to the lithosphere such that:

$$H = [(1-(1/\beta)) + ((y^2/a^2)-((2.y)/a)) \; .$$

$$((1/\delta)-(1/\beta))] \; . \; (1-\Gamma) + \Gamma \text{ ---- } 1.9$$

Therefore, the elevation of the surface, S, after the effects of crustal thinning and lithosphere heating is given by:

$$S = S_\sigma + S_t \text{ ---- } 1.10$$

Following extension the lithosphere temperature field re-equilibrates from its disturbed state and the associated cooling causes subsidence which is defined such that the elevation of top basement above the final subsided position is given by:

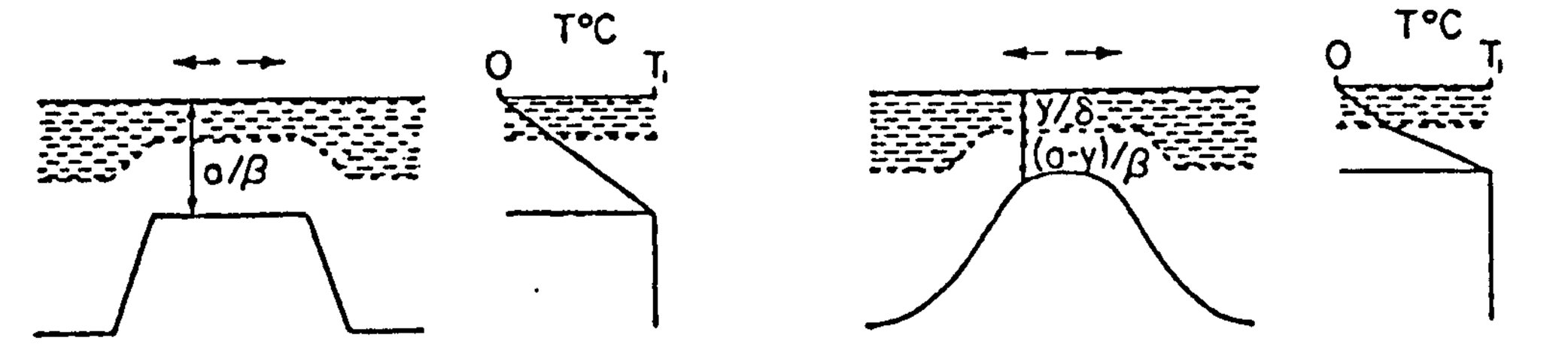

(after Royden and Keen, 1980)

Figure 1.4 - Diagram contrasting the uniform (a) and non-uniform (b) extension models. During uniform extension the entire lithosphere extends by β and is thinned by 1/β. However, during non-uniform extension the lithosphere is divided into two layers such that the upper layer (above y) is extended by δ, while the lower layer (below y) is extended by β - a non linear geotherm results.

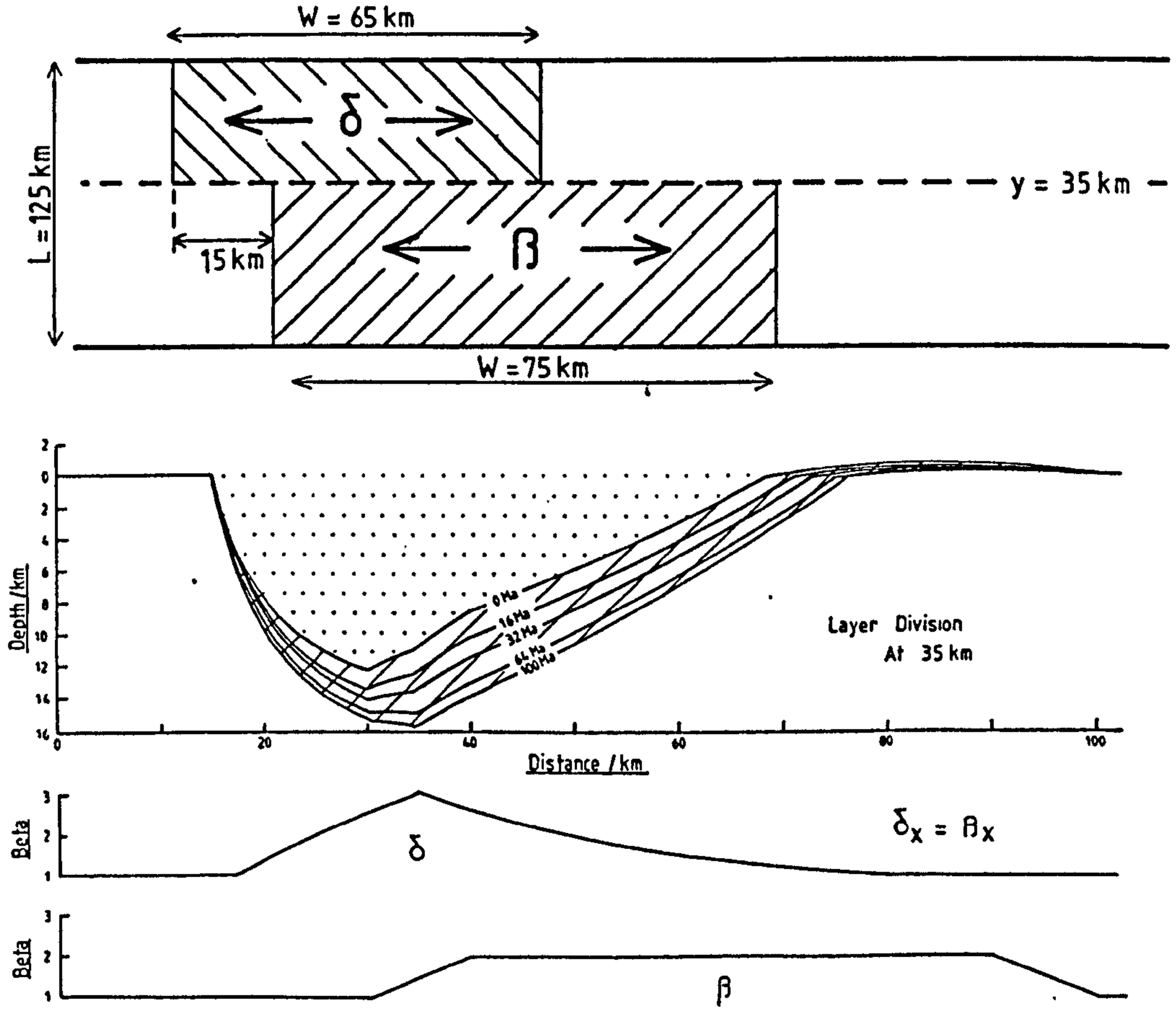

Figure 1.5 - Sedimentary basin generated using a non-uniform extension model. The lithosphere has been divided at the Moho such that the extension of the upper layer, δ, thins the crust only. The distribution of the upper layer extension has been arranged to simulate simple shear extension along a fault. Extension of the lower lithosphere, β, has been regionally distributed to represent deformation by plastic failure (Jackson and McKenzie 1983). The lateral offset of the lower lithosphere extension with respect to the deformation in the upper lithosphere has produced thermal uplift in the distal region of the basin at rifting - post-rift thermal subsidence reduces this uplift back to sea level.

$$e_{(t)} = (\alpha.a.T_o)/(1-\alpha.T_o) \; . \; (4/\pi^2) \; . \sum_{m=0}^{\infty} x_{(2.m+1)}/(2.m+1)^2 \; .$$

$$\exp[-(2.m+1)^2.\pi^2.k.t/a^2] \quad \text{--- 1.11}$$

where:

$$x_{(2.m+1)} = \Gamma + \{(1-\Gamma).[(\delta-\beta).\sin((2.m+1).\pi.H) +$$

$$\beta.\sin((2.m+1).\pi.G)] \; .$$

$$(-1)2.m+2/(2.m+1).\pi\} \quad \text{---- 1.12}$$

and:

$$H = 1 - y/(a.\delta) \quad \text{----- 1.13}$$

$$G = 1 - y/(a.\delta) - (1-(y/a))/\beta \quad \text{----} \quad 1.14$$

The amount of thermal subsidence, S_t, at a particular time, t, is given by:

$$S_t = e_{(t=o)} - e_{(t)} \quad \text{----} \quad 1.15$$

The non-uniform stretching model considers the upper and lower lithospheric layers as being separate in so far as one layer can be extended by a different amount and/or at a different lateral position with respect to the other. Uniform extension occurs when the two layers are extended by the same amount and in the same position. The two-layer stretching model allows a greater flexibility in terms of the basin geometries that can be generated as is shown in figure 1.5 - the lithosphere has been decoupled at the base of the crust. This means that the subcrustal deformation has not thinned the crust, but has perturbed the geotherm, which, in the absence of crustal thinning in the distal

region of the basin, has generated uplift.

The non-uniform extension model allows a redistribution of the thermal subsidence component, by dividing the lithosphere so that the lower lithosphere deformation, which mainly causes perturbations to the geotherm, can be offset with respect to the crustal thinning due to the upper lithosphere deformation. Leeder (1983) has acknowledged non-uniform extension as being a possible cause of uplifts around the periphery of the North Sea graben system during the Middle Jurassic. These marginal hinterlands were later eroded to form the major fluvial deltaic clastic wedges which now form the major hydrocarbon resevoirs.

1.2 The Role of Fault-Detachment Horizons in Continental Extensional Tectonics.

Deep seismic profiling of the continental lithosphere shows unequivocally that extensional basin evolution is controlled by major low angle faults. The British Institutions Reflection Profiling Syndicate (BIRPS) have provided an abundance of seismic reflection data across Upper Palaeozoic-Mesozoic basins on the North West European shelf (eg Hall et al., 1984, BIRPS and ECORS, 1986). The SWAT and MOIST seismic reflection sections, acquisitioned by BIRPS, are shown in figures 1.6a and 1.6b respectively. The SWAT survey shows major crustal reflectors across the North and South Celtic Sea basins (BIRPS and ECORS, 1986) , while the MOIST reflection line shows the Lewis basin in the West and the Orcadian basin in the East (Smythe et al, 1982, Brewer and Smythe, 1984, McGeary and Warner, 1985, Blundell et al.,

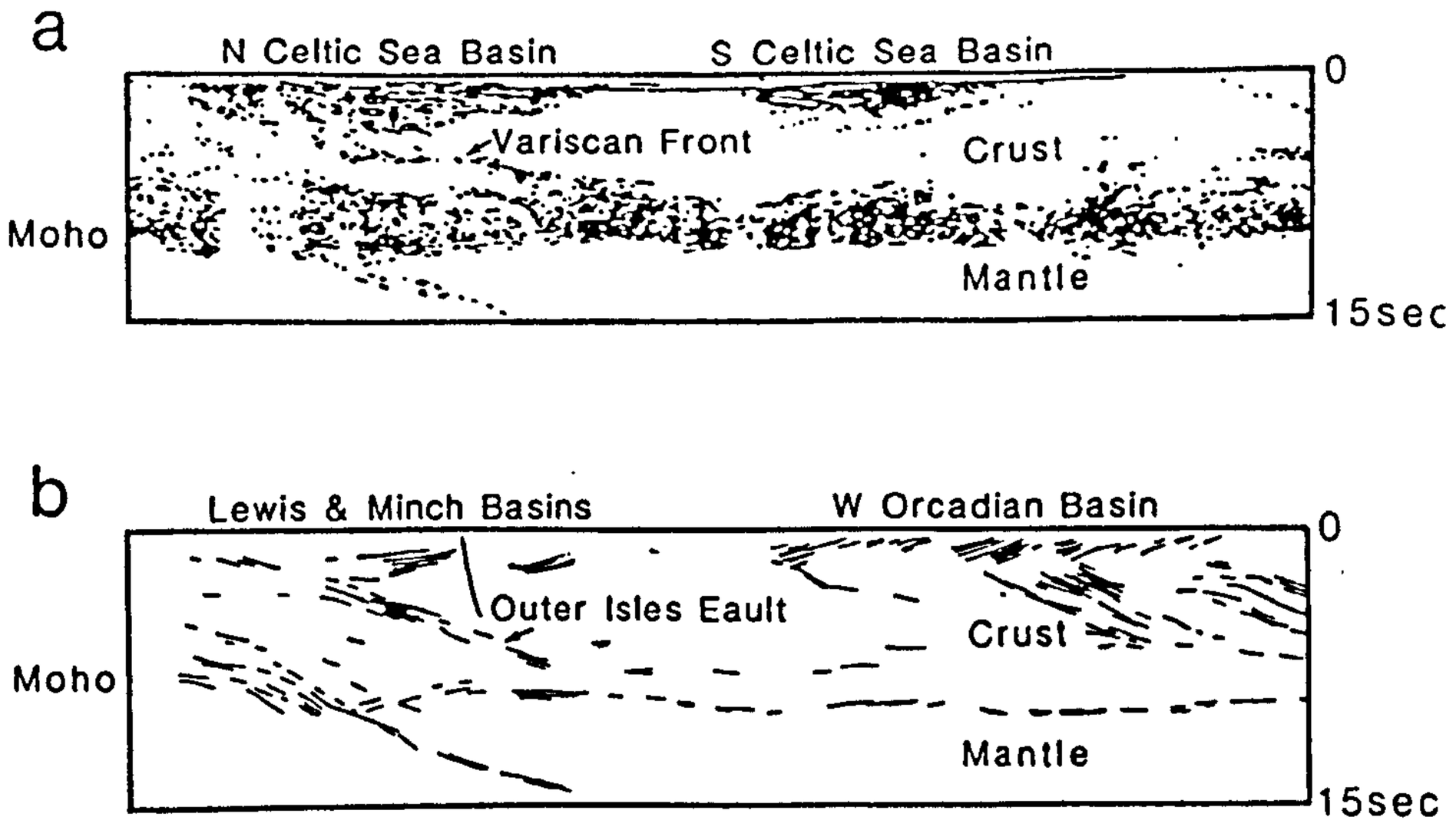

Figure 1.6 - Deep seismic reflection profiling showing the relationship between extensional basins and major low angle faults. The SWAT line (a) shows the North Celtic Sea basin which has formed by hanging wall collapse following extension along a major low angle fault. The MOIST reflection section (b) shows the Lewis basin in the west, which has formed in the hanging wall of the Outer Isles Fault. In the east of the section, the strongly apparent easterly dipping reflectors denote the faults which have controlled the formation of the Orcadian basin. The Jeanne d'Arc basin (c) also shows a strong relationship between sedimentary basin and major low angle fault, while the Viking Graben (d) has evolved by extension on several closely spaced low angle faults (Beach 1986).

1985). The North Celtic Sea basin evolved during the Mesozoic by hanging wall collapse following extension along the low angle fault forming the strong set of reflectors in the left of the section. Similarly, the Lewis basin, also of Mesozoic age, developed in the hanging wall of the Outer Isles fault. The East of the MOIST section shows a series of easterly dipping linear reflectors denoting major low angle faults which have controlled the extensional evolution of the Orcadian basin. Similarly, the Jeanne d' Arc basin (figure 1.6c) to the East of Newfoundland has formed in the hanging wall of the Murre fault (Keen et al., 1987), whereas the Viking Graben in the northern North Sea (figure 1.6d) shows several closely spaced major faults and their associated rift basins (Beach, 1986).

A consistent feature of these major low angle faults is that they are more or less planar down to at least mid crustal levels after which they flatten into horizontal detachments. Jackson and McKenzie (1983) analysed a number of active normal faults in Greece and Turkey using a variety of seismological techniques and found these faults to dip between 40° and 50° to a depth of about 10 km, after which they gradually flatten into the lower crust.

The concept of detachments in extension arose from work carried out in the Basin and Range province by Wernicke and Burchfiel (1982) and Wernicke (1985) as a means for the fault controlled extension in the upper lithosphere to be accommodated at greater depths (figure 1.7). Their work suggests that major basin bounding faults in the upper lithosphere continue as detachment structures down to the

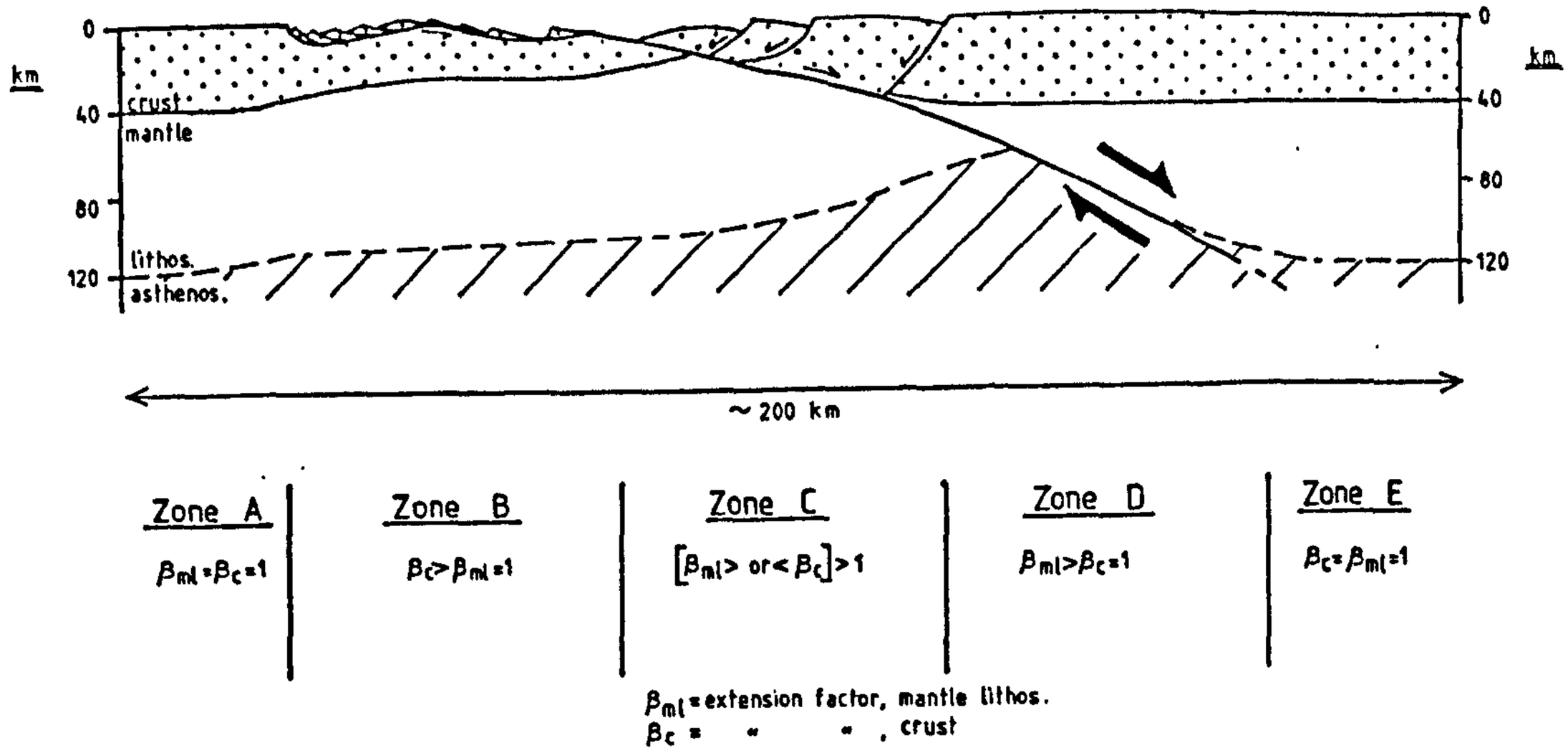

Figure 1.7 - Qualitative model for the extensional development of the Basin and Range province (Wernicke, 1985). The extension of the region has occurred along a single fault-detachment horizon, which shallowly dips down to the lithosphere-asthenosphere boundary. The simple shear deformation both thins the crust and brings hotter material nearer to the surface, producing thermal uplift in the distal region ("discrepant zone") of the basin.

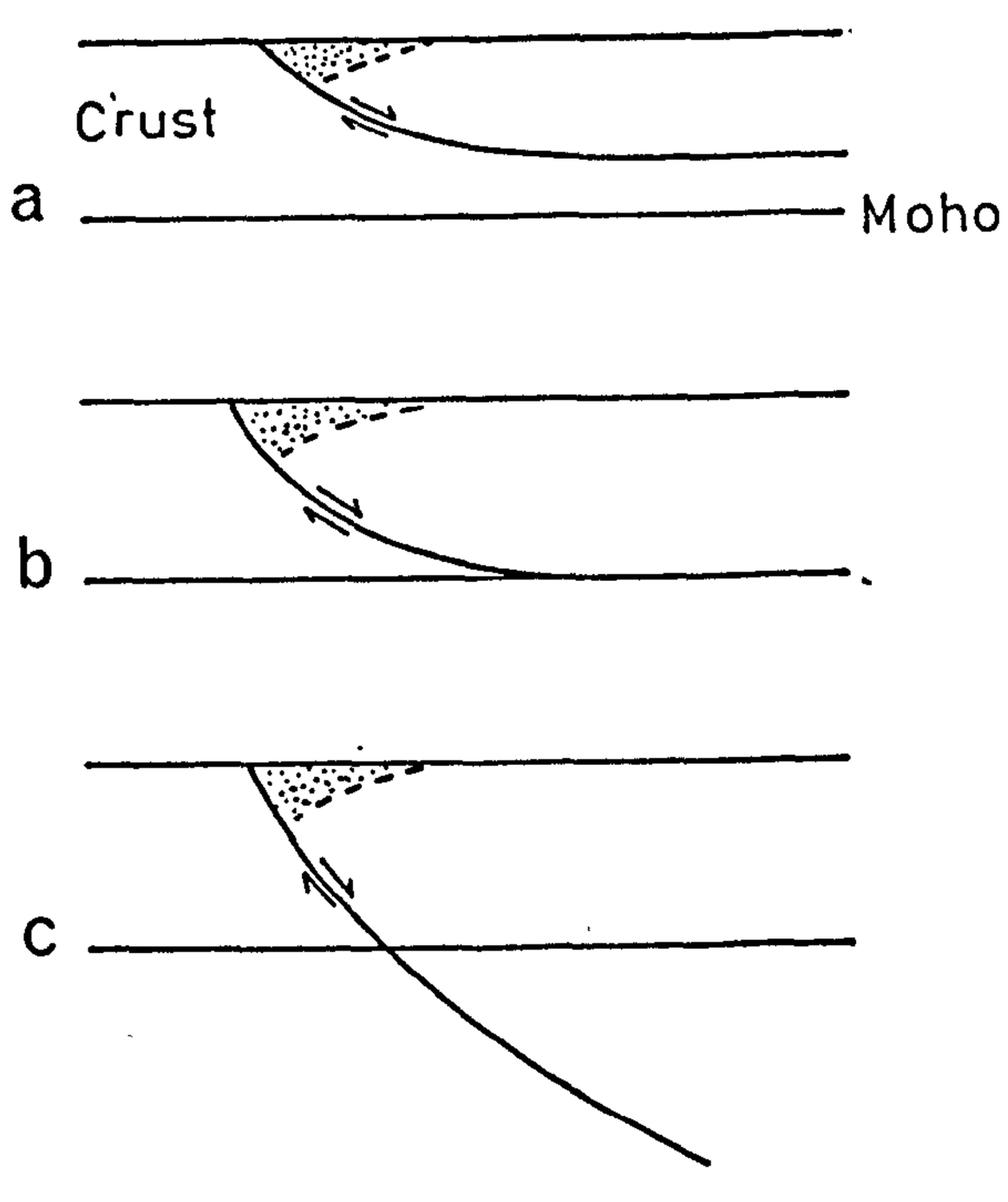

(after Kusznir, Karner and Egan,1987)

Figure 1.8 - Evidence suggests that low angle faults flatten into horizontal detachment horizons at three different levels: a) intracrustal, b) at the base of the crust and c) at the base of the lithosphere.

lithosphere-asthenosphere boundary, which allows a lateral separation of the rift depocentre from that of the region of thermally induced uplift and subsidence. Wernicke (1985) terms this thermally influenced region, caused by the thinning of the lower lithosphere, the "discrepant zone" (figure 1.7).

Geological and seismic data suggest three fault-detachment configurations (figure 1.8); a fault flattening into a detachment within the crust (eg. the Orcadian basin fault), a fault detaching at the Moho (eg. the Outer Isles fault) and a fault dipping from the surface down to the deep lithosphere (eg the Basin and Range province), although in no case yet has the seismic record revealed a fault continuing uninterrupted from the surface down to the lithosphere-asthenosphere boundary, as suggested by Wernicke's qualitative model for the Basin and Range (figure 1.7). Therefore the bearing of the Wernicke model upon reality in this respect, must be somewhat questionable.

What controls the depth at which faults flatten at intracrustal and basal crustal levels? Information from the MOIST reflection line is combined with that from the LISPB seismic refraction survey (figure 1.9). The seismic velocities from the LISPB refraction survey (Bamford, 1979) indicate an upper crustal composition of amphibolite facies rocks of Caledonian age and a middle crust composed of an intermediate granulite facies of Lewisian age, which overlies an mafic lower crust (Hall and Al-Haddad, 1976). Kusznir and Park (1987) constructed a thermo-rheological model based on the crust imaged by MOIST, as interpreted by

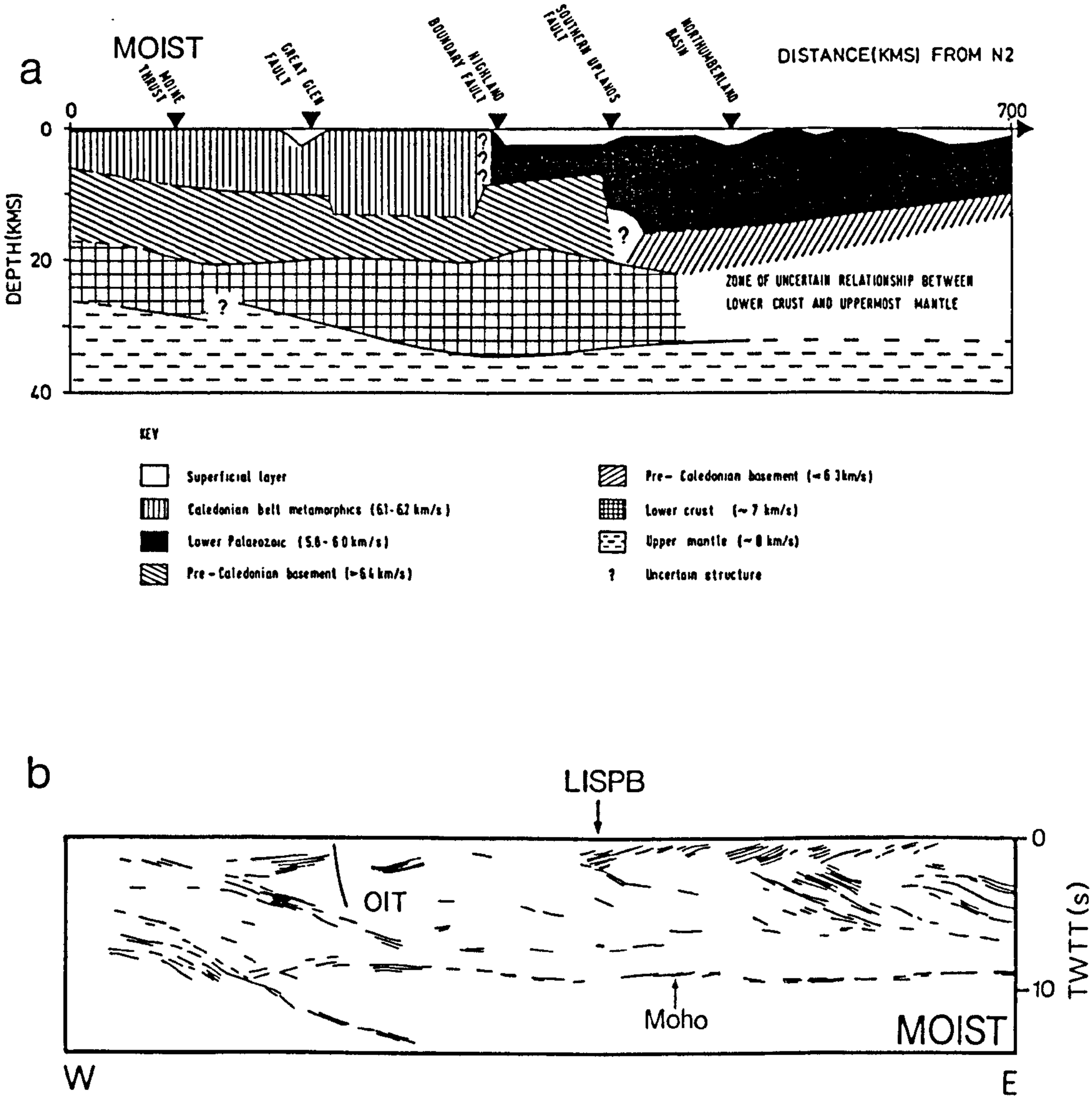

Figure 1.9 - Seismic velocities from the LISPB seismic refraction survey (a) indicate that the composition of the crust in the region imaged by the MOIST reflection line (b) is one of amphibolite facies for the upper crust, intermediate granulite facies for the middle crust and a granulite mafic lower crust.

Blundell (1985), and using the compositional layering indicated by LISPB. The model assumes the following rheologies; wet quartz for the upper crust, dry quartz for the middle crust, plagioclase for the lower crust and a mantle of olivine. They then calculate stress-depth distributions resulting from the application of a tensile force to the above compositions for different geothermal states of the lithosphere (figure 1.10a). Their models predict that extended lithosphere with surface heat flows of 60mW.m^{-2} to 70 mW.m^{-2} has low stress-low strength regions at mid-crustal levels (at approximately 22km), where the dry quartz upper crust gives away to the stronger plagioclase rheology of the lower crust, and at the Moho, caused by the rheological change from a plagioclase lower crust to a stronger olivine rheology in the mantle. It is suggested that these low stress-low strength regions facilitate the formation of the horizontal detachments into which the major low angle faults flatten. The faults that have controlled the extension of the Orcadian basin flatten into the low strength region in the mid crust, whereas the Outer Isles Fault, related to the Lewis basin, detaches in the weak region at the base of the crust (figure 1.10b).

The major faults that influenced the evolution of both the Lewis and Orcadian basins are inherited from the Caledonian orogeny when they assumed a major role in the thrust movements of that period. During the Mesozoic extensional reactivation of this inherited structural framework occurred leading to the basins in existence at the present. But why do these faults detach at different depths taking into account that they experienced a similar deformational

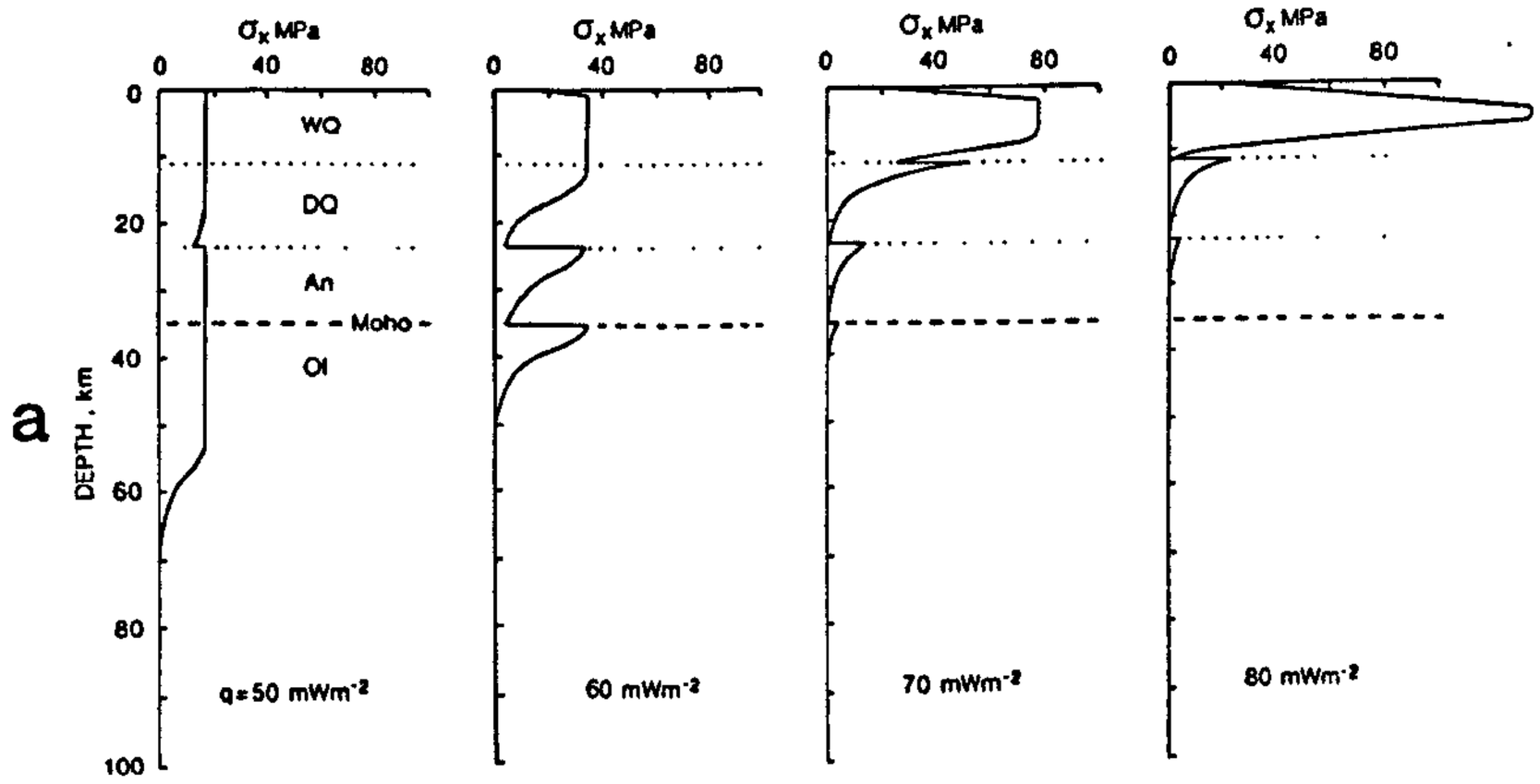

(after Kusznir and Park, 1987)

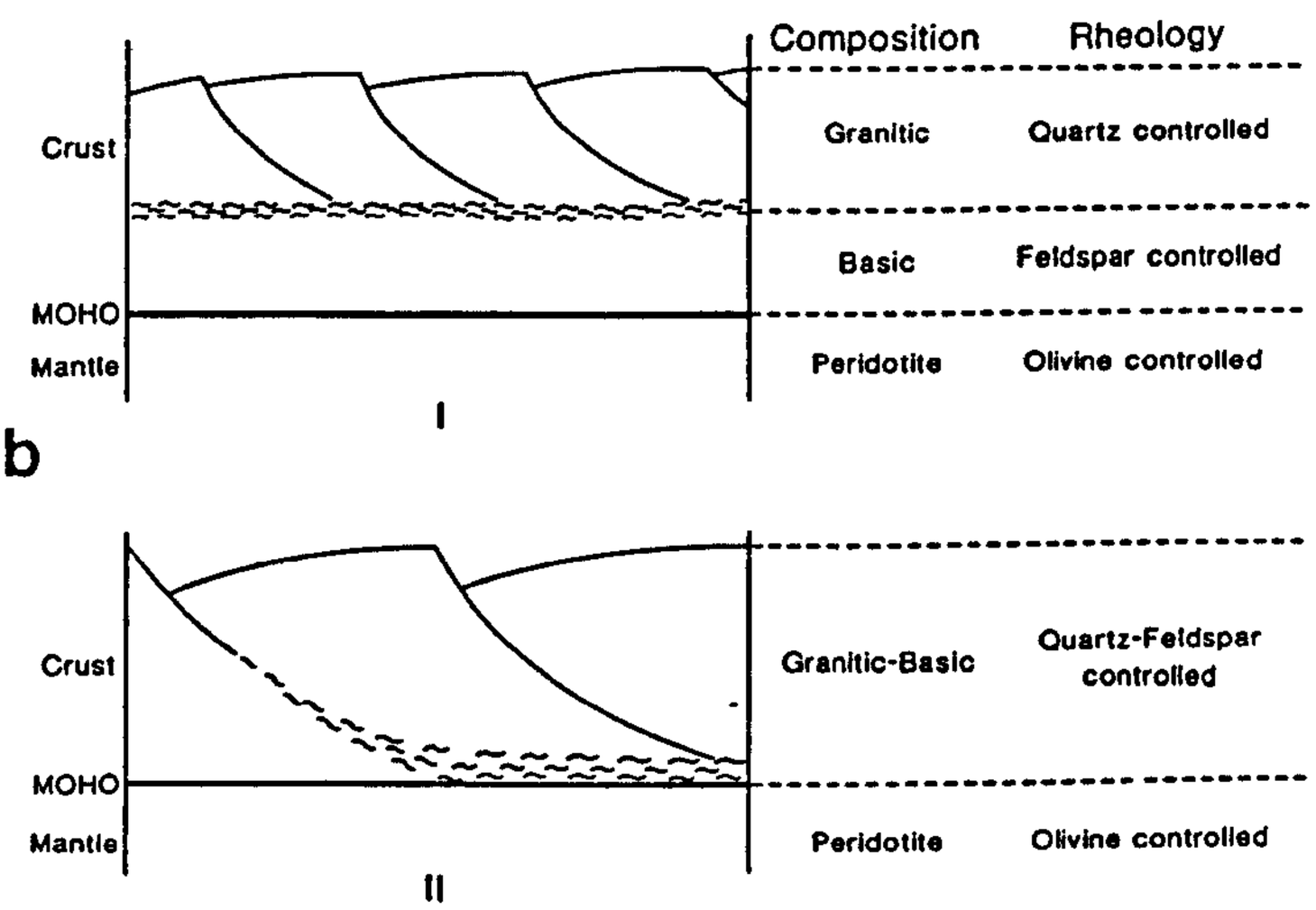

(after Kusznir et al., 1987)

Figure 1.10 - The thermo-rheological control on the development of detachment horizons. The production of low stress-low strength regions within the lithosphere is controlled by the rheological behaviour of its internal mineral assemblage. Intermediate to high heat flow enhances the development of low stress-low strength regions (a). It is suggested that these weak regions facilitate the flattening of the low angle faults which have controlled basin formation at shallow depths (b).

history? The deeper detachment shown by the Outer Isles fault in the western part of the MOIST section could have been caused by a cooler geothermal gradient, which generates a relatively deep brittle-ductile transition. This is supported by its location on the periphery of the Caledonian earth movements, where the exposed Lewisian craton suggests a cool crust depleted somewhat in upper crustal radioactive heat input.

1.3 Summary

This section has shown that while pure shear lithosphere extension might be adequate to use for the modelling of the low strength plastic region in the lower lithosphere, it is inadequate for predicting the effect of the upper lithosphere deformation where extension is accommodated by a fault controlled, simple shear process. The non-uniform extension model (Royden and Keen 1980) can be used to approximate the effect of lithosphere extension by simple shear (see figure 1.5, Karner 1984 and Coward 1986), however, to use a pure shear process to predict the simple shear extensional phase of basin evolution is an unrealistic assumption.

In the next chapter a numerical model is presented in which the extension of the upper brittle region of the lithosphere is modelled as a fault controlled or simple shear process, which is balanced by a similar amount of pure shear extension in the lower lithosphere. Upper and lower lithosphere deformational regimes are separated by a detachment horizon into which the major low angle faults

flatten.

CHAPTER 2

The Geometric, Thermal and Airy Isostatic Consequences of Simple Shear - Pure Shear Extension of the Continental Lithosphere.

2.1 Introduction

Deep seismic reflection profiling of the continental lithosphere has revealed the importance of major low angle faults (McGeary and Warner 1985, Matthews and Cheadle 1986, Matthews and Smith 1987) in continental extensional tectonics. These faults, on the application of a tensile force, are normally activated and rift basins form within their collapsed hanging walls (figure 1.6). In this chapter a mathematical model is presented (see also Kusznir et al 1987, Kusznir and Egan, in press) in which the upper, brittle region of the lithosphere is assumed to extend by simple shear along a low angle fault (figures 2.1a and 2.1b). This fault soles out with depth into a horizontal detachment horizon below which the lithosphere behaves plastically and deforms by pure shear (Jackson and McKenzie 1983). The model also calculates perturbations caused to the geotherm by the extension (figure 2.1c), including temperature gradients set up by the tectonic juxtaposition of cool hanging wall next to warmer footwall material, and heating from the raising of the lithosphere-asthenosphere boundary, causing an initial surface uplift. After rifting the isotherms return back to their original state and the surface subsides. The model predicts the familiar sedimentary basin configuration of rift basin overlain by a blanket of post rift thermal sag deposition. Any loading

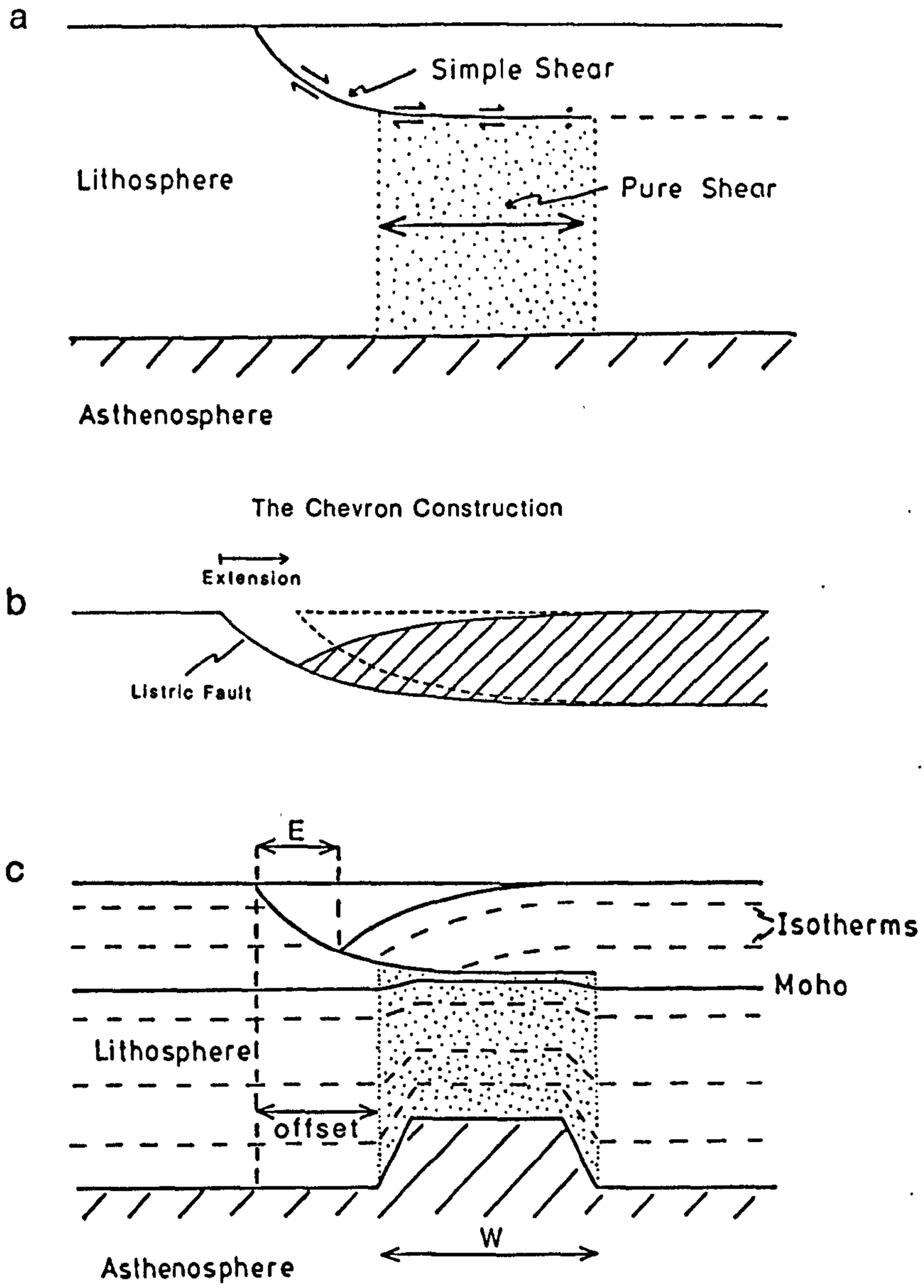

Figure 2.1 -

a. Upper lithosphere extension by simple shear along a low angle fault gives away with depth to pure shear beneath a horizontal detachment horizon. The detachment depth corresponds to the brittle-ductile transition.

b. Crustal thinning due to simple shear is calculated using the Chevron construction, whereby any unsupported section of the hanging wall, after extension, collapses directly downwards onto the footwall.

c. Lithosphere extension leads to crustal thinning by both simple and pure shear, depending on the detachment depth. The deformation also perturbs the lithosphere temperature field - the collapse of the hanging wall after simple shear extension causes a temperature discontinuity across the fault and pure shear raises the lithosphere-asthenosphere boundary, bringing hot material nearer to the surface, which causes a heating of the lithosphere.

forces imposed on the lithosphere from its extension are isostatically compensated.

2.2 Mathematical Model Formulation.

a) Geometric component

The upper lithosphere is extended by simple shear along a low angle fault. The geometry of this fault is defined such that exponential faults are given by:

$$D_{(x)} = 0 \qquad \text{for} \quad x \leq x_o$$

$$D_{(x)} = Z_a \,.\, (1 - \exp(-x'/Z_a)) \qquad \text{for } x > x_o \quad \text{----- 2.1}$$

where $D_{(x)}$ is the depth of the fault in the x-coordinate frame, Z_a is the depth of the detachment and x_o defines the horizontal position of the outcrop of the fault at the surface (all of the symbols are further defined in Table 2.1).

The fault geometry produced by equation 2.1 has a surface dip of 45°, which is similar to dip angles exhibited by presently active normal faults (Jackson and McKenzie 1983).

Planar faults are defined by the following set of equations:

$$D_{(x)} = 0 \qquad \text{for} \quad x \leq x_o$$

$$D_{(x)} = \tan\Theta.x \qquad \text{for} \quad x > x_o \quad \text{----} \quad 2.2$$

where Θ is the angle of dip of the fault.

The "Chevron construction" (Verall 1982, Gibbs 1983) has been used to predict the surficial subsidence arising from simple shear extension (figure 2.1b), whereby the hanging

Table 2.1

List of Symbols

a	Thickness of the lithosphere	125km
α	Coefficient of thermal expansion	$3.28 \times 10^{-5} {}^{o}C^{-1}$
β	Extension factor	-----
$B_{(x,t)}$	Basement depth	-----
C_o	Original crustal thickness	-----
$D_{(x)}$	Detachment depth	-----
E	Amount of horizontal extension	-----
g	Acceleration due to gravity	$9.81 m.s^{-2}$
h_m	Thickness of the mantle lithosphere	-----
k	Thermal conductivity	$2.5 W.m^{-1}.{}^{o}K^{-1}$
$L_{(x)}$	Laterally varying load distribution	-----
$M_{(x)}$	Moho depth	-----
p_{air}	Density of air	0.0
p_o	Surface density of crustal material	$2800 kg.m^{-3}$
p_i	Density of basin infill	-----
p_m	Surface density of mantle material	$3300 kg.m^{-3}$
$P_{(x)}$	Crustal thinning by pure shear	-----
$S_{(x)}$	Crustal thinning by simple shear	-----
σ	Specific heat capacity	$1 kJ.kg^{-1}.{}^{o}K^{-1}$
t	Time	-----
T_o	Temperature at the base of the lithosphere	$1333 {}^{o}C$
$T_{(z)}$	Temperature with respect to depth in ^{o}C	-----
x	Lateral/horizontal coordinate frame	-----
W	Width of pure shear	-----
w(x)	Isostatic response	-----
Z_d	Depth of detachment	-----

wall is laterally displaced by the amount of extension. The resulting unsupported section of the hanging wall then collapses directly downwards onto the footwall and generates a roll-over structure. The amount of crustal thinning, $S_{(x)}$, arising from the simple shear deformation is given by:

$$S_{(x)} = D_{(x)} - D_{(x-E)} \quad \text{----- 2.3}$$

where E is the amount of horizontal extension.

Below the detachment horizon into which the fault flattens, the lithosphere is extended by pure shear, which is defined by a series of extension factors, $\beta_{(x)}$ (McKenzie, 1978), such that for small strains:

$$\beta = 1+\epsilon \quad \text{----- 2.4}$$

where ϵ defines the change in length of a section of lithosphere parallel to the direction of stretching. Therefore, a β value of 1 denotes no extension, 2 implies 100 percent extension, 3 denotes 200 percent extension, etc.

If the detachment is within the crust then lower crustal thinning, $P_{(x)}$, occurs due to pure shear deformation:

$$P_{(x)} = (C_o - Z_a) \cdot (1 - 1/\beta_{(x)}) \quad \text{----- 2.5}$$

where C_o is the original thickness of the crust.

The Beta factors defining the pure shear deformation have been given a sinusoidal distribution within limits that can be set at any lateral position. The Beta distribution can be defined by:

$$\beta_{(x)} = (1+D_o) \cdot \sin(\pi.x/W) \quad \text{----- 2.6}$$

where $1+D_o$ is the maximum Beta value at the peak of the

sinusoidal distribution and W is the width over which the pure shear has been distributed.

In order to avoid mass balance problems, extension due to simple shear in the upper lithosphere, E, must be balanced by the extension in the lower lithosphere caused by pure shear. Therefore:

$$E = \int_{o}^{w'} (\beta_{(x)} - 1)\, dx = \int_{o}^{w'} D_o \,.\, \sin(\pi.x/W)\, dx \quad \text{----- 2.7}$$

where W' is the pre-extension width of the pure shear region.

As W' = W - E then,

$$D_o = (\pi/2).(E/(W-E)) \quad \text{----- 2.8}$$

This equation is valid provided that E is much smaller than W.

b) Thermal component

The lithosphere temperature field in its undisturbed state is assumed to have a constant geothermal gradient such that,

$$T_{(z)} = (T_o/a) \,.\, z \quad \text{----- 2.9}$$

where $T_{(z)}$ is the temperature in °C, z is the depth beneath top basement, T_o is the temperature at the base of the lithosphere and a is the thickness of the lithosphere.

During rifting both simple and pure shear perturb the temperature field (figure 2.1c). Simple shear extension, occurring above the detachment, tectonically juxtaposes cool

hanging wall next to warmer material in the footwall, thus generating a temperature discontinuity across the fault. The tectonic denudation of the hanging wall exposes warm footwall material at the surface and causes a shallow depth perturbation to the geotherm. The temperatures in the footwall can be defined such that:

$$T = T_{(z+s)} \quad \text{----- 2.10}$$

While the temperatures in the hanging wall are defined such that:

$$T = T_{(z)} \quad \text{---- 2.11}$$

where z defines the depth beneath top basement.

Below the horizontal detachment pure shear thins the lower lithosphere and as a result hot asthenospheric material is brought to shallower depths, causing a relatively deep perturbation to the geotherm. The temperatures beneath the horizontal detachment are defined such that:

$$T = T_{(z')} \quad \text{----- 2.12}$$

where $z' = z_a + [(z+S-z_a).\beta_{(x)}]$.

The lithosphere temperature field is represented as a rectangular grid and each intersection or node in the grid is assigned a temperature, defined according to equation 2.9. If a node is within the region of extension then its temperature will be modified according to the amount of simple shear-pure shear deformation it has experienced (equations 2.10, 2.11 and 2.12).

After rifting the temperature field gradually returns back

to its original state over times of the order of 100Ma to 300Ma. The equation for time dependent heat conduction is used to calculate the re-equilibration of the lithosphere temperature field with time. A two-dimensional consideration of this equation is used such that:

$$p.\sigma.dT/dt = k.(d^2T/dx^2 + d^2T/dy^2) \quad \text{-----} \quad 2.13$$

where p is density, σ is specific heat capacity, t is time, k is thermal conductivity and y denotes the depth co-ordinate frame.

The finite difference method has been used to solve equation 2.13, and is described in section 2.3.

c) Airy isostatic component.

Extension by a simple shear-pure shear process subjects the lithosphere to a suite of loads which vary both in magnitude and time. These loads are as follows:

i) $L_m(x)$, the buoyancy load arising from the surficial hole created by simple shear crustal thinning (equation 2.3).

ii) $L_p(x)$, the load function arising from pure shear crustal thinning (equation 2.5) and occurs only when the detachment is within the crust.

iii) $L_{th}(x,t)$ arises from the heating of the lithosphere during rifting (equations 2.10, 2.11 and 2.12). This load varies with both horizontal distance and time.

iv) $L_i(x,t)$, the loading resulting from the infill of

subsided basement with water and/or sediment. This is also time dependent due to additional subsidence created by post-rift re-equilibration of the geotherm.

The total amount of loading, L(x,t), experienced by a vertical section of lithosphere is therefore a function of both its horizontal position and time and is given by,

$$L(x,t) = L_m(x) + L_p(x) + L_{th}(x) + L_i(x,t) \quad \text{---- 2.14}$$

The superposition of these loads is to change the vertical force balance of the lithosphere, which, in turn, responds by isostatic adjustment. The initial models generated in this chapter assume that the isostatic compensation of the loads is achieved using Airy isostatic theory (Airy 1855). It is fundamental to Airy isostasy that the low density continental crust, which has a mean density of 2800 kg.m^{-3}, "floats" on mantle rocks with a higher mean density of 3300 kg.m^{-3}. The continental crust is buoyed up by a force equal to the weight of mantle rocks it displaces. The application of a load to the lithosphere causes a positive or negative displacement of mantle material, depending on the nature of the load, while an opposing force, known as the isostatic restoring force, restores the deflected lithosphere to its original configuration.

i) Airy isostatic response to simple shear crustal thinning.

The simple shear thinning of the crust, $S_{(x)}$, imposes a negative load upon the lithosphere due to the fact that the removed crustal rocks have been replaced by air of zero density (figure 2.2a). The load function due to simple shear

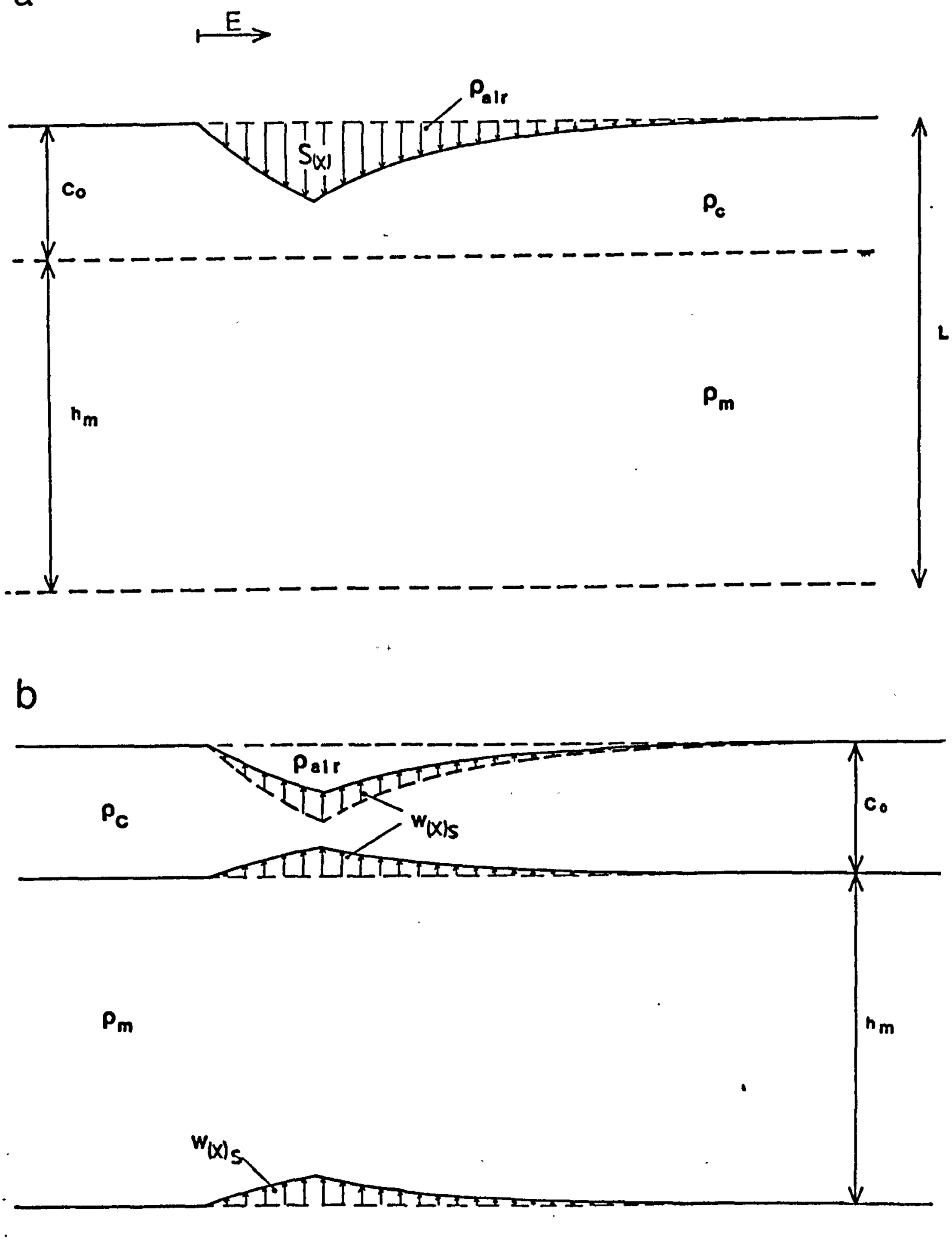

Figure 2.2 - Simple shear crustal thinning, S_x, creates a surficial hole and upsets the isostatic balance of the lithosphere (a). Isostatic equilibrium is again achieved by the influx of mantle material into the base of the lithosphere (b).

crustal thinning is given by,

$$L_w(x) = S_{(x)} \cdot ((p_{air}-p_c).g) \quad \text{----- 2.15}$$

The isostatic balance of the lithosphere is maintained by the isostatic restoring force, which induces additional mantle material into the lower lithosphere to compensate for the crustal material removed (figure 2.2b). The uplift or isostatic rebound, $w_{(x)w}$, does not return the surface back to its original position as less volume of relatively high density mantle rocks are required to compensate for the low density crust removed.

It is convenient to formulate the effects of Airy isostasy by comparing a vertical section of undisturbed lithosphere in isostatic equilibrium with a section that has been deflected due the application of a load. The mass per unit area of an unloaded vertical section of lithosphere is given by:

$$(C_o.p_c.g) + (h_m.p_m.g) = U \quad \text{-----} \quad 2.16$$

where g is the acceleration due to gravity, h_m is the thickness of the mantle lithosphere and p_c and p_m are the densities of crustal and mantle rocks respectively.

The mass per unit area of a vertical section of lithosphere which has experienced simple shear crustal thinning (figure 2.2b) is given by:

$$((C_o-S_{(x)})).p_c.g) + ((h_m+w_w(x)).p_m.g) = D \quad \text{-----} \quad 2.17$$

where $w_w(x)$ is the buoyant deflection of the lithosphere. The effects of basin fill are ignored until section iv

below.

The principle of isostatic equilibrium states that all vertical lithosphere sections must exert the same pressure. Therefore:

$$U = D$$

Substituting for U and D gives:

$$(C_o.p_c.g) + (h_m.p_m.g) = ((C_o-S_{(x)}).p_c.g) + (h_m+w_s(x)).p_m.g) \quad \text{---- 2.18}$$

Simplifying and rearranging,

$$w_s(x) = S_{(x)} . (p_c/p_m) \quad \text{----- 2.19}$$

$W_s(x)$ denotes the rebound experienced after simple shear crustal thinning, and so the resultant basin geometry, $B_{(x,t)}$, is given by,

$$B_{(x,t)} = S_{(x)} - w_s(x) \quad \text{----- 2.20}$$

$$= S_{(x)} . (1-(p_c/p_m)) \quad \text{---- 2.21}$$

ii) Airy isostatic response to pure shear crustal thinning.

Pure shear thinning of the lower crust causes its replacement with higher density mantle material and subsidence results. Using a similar treatment to section i, equation 2.19 is modified to:

$$w_p(x) = P_{(x)} . ((p_m-p_c)/p_m) \quad \text{----- 2.22}$$

iii) Airy isostatic response to thermal loading

Similarly, the uplift resulting from the heating of the

lithosphere, $w_{th}(x,t)$, is given by,

$$w_{th}(x,t) = L_{th}(x,t)/(p_m.g) \quad \text{-----} \quad 2.23$$

The load imposed upon the lithosphere by the perturbation of the temperature field is calculated for each vertical section of the lithosphere. Sections unaffected by extensional deformation will have experienced zero temperature perturbation at rifting. Within the rifted region the temperature of each node will be modified according to equations 2.10, 2.11 and 2.12, depending on the amounts of simple and pure shear deformation experienced. The temperature perturbation is defined by the temperature difference, ΔT, between a perturbed node and an unperturbed node (given by equation 2.9) at a particular depth. The thermal load for any vertical section of lithosphere, $L_{th}(x,t)$, is therefore given by,

$$L_{th}(x,t) = \int_o^a \alpha.\Delta T.p.g \quad dz \quad \text{-----} \quad 2.24$$

where α is the coefficient of thermal expansion and p is defines either the density of crust or mantle material depending on the depth at which the perturbation is being considered.

iv) Airy isostatic response to basin infill.

The isostatic response of the lithosphere to loads imposed by extension modify the surficial hole created by the simple shear deformation. The basin geometry can be further modified by infill, i, which causes subsidence, $w_i(x,t)$ such that:

$$w_i(x,t) = B_{(x,t)} \cdot p_i/(p_m-p_i) \quad \text{-----} \quad 2.25$$

where:

$$B_{(x,t)} = S_{(x)} - w_m(x) + w_p(x) + w_{th}(x,t) \quad \text{-----} \quad 2.26$$

Substituting for $w_m(x)$, $w_p(x)$ and $w_{th}(x)$ in equation 2.26 gives:

$$B(x,t) = \{(S_{(x)}.g.(1-p_o)) + (P_{(x)}.g.(p_m-p_o)) + \left[\int_o^a \alpha.\Delta T.p.g \, dz \right]\} / (p_m.g) \quad \text{--} \quad 2.27$$

Surface density values of mantle and crustal material have been assumed for the above initial treatment of Airy isostasy. More realistically density decreases with an increase in temperature and therefore depth. For example, isostatic adjustment occurring in response to simple shear crustal thinning compensates for attenuated crust by the addition of mantle material to the lower lithosphere. The density of this compensating mass, p_m', is modified from the surface value of 3300kg.m^{-3} by the higher temperatures in the lower lithosphere such that:

$$p_m' = p_m.(1-\alpha.T_o) \quad \text{-----} \quad 2.28$$

where α is the thermal expansion coefficient and T_o is the temperature at the base of the lithosphere.

In order to take into account the decrease in density with depth, equation 2.27 can be modified such that:

$$B(x,t) = (S_{(x)}.g.(1-p_o)) + ((P_{(x)}.g.(p_m-p_o)) + \left[\int_o^n \alpha.\Delta T.p.g \; dz \right] / (p_m.(1-\alpha.T_o).g) \text{ --- } 2.29$$

Both original Moho topography, $M_{(x)}$, and the fault-detachment geometry, $D_{(x)}$, are also modified by the isostatic response of the lithosphere to loading. The depth to the Moho can be defined as:

$$M_{(x)} = C_o - S_{(x)} - P_{(x)} + B_{(x,t)} + w_i(x,t) \text{ ----- } 2.30$$

and the depth to the fault-detachment, $D'_{(x)}$, is:

$$D'_{(x)} = M_{(x)} - (C_o - D_{(x)} - P_{(x)}) \text{ ----- } 2.31$$

where $D_{(x)}$ is the depth profile of the original fault.

2.3 A Solution of the Heat Conduction Equation by the Finite Difference Method.

Finite difference is a numerical method for solving differential equations by replacing the equation under consideration by a difference series. This series approximates the precise mathematical solution to the equation being solved. An explicit formulation of the method is used here whereby the temperatures at each of the nodes are directly calculated at small successive increments of time. The differential equation to be solved here is the time dependent heat conduction equation:

$$p.\sigma.dT/dt = k \; . \; (d^2T/dx^2 + d^2T/dy^2) \text{ ---- } 2.32$$

Thus, by rearrangement:

$$(d^2T/dx^2 + d^2T/dy^2) = p.\sigma/k \; . \; dT/dt \text{ ---- } 2.33$$

where T is the temperature, t is time, k is thermal conductivity, p is the density of the medium and σ is the specific heat capacity.

If a denotes the separation between the temperature nodes and $T_{(x)}$ is the temperature of a particular node in the x-coordinate frame then by Taylor's theorem (figure 2.3a):

$$T_{(x+a)} = T_{(x)} + a.T'_{(x)} + 1/2.a^2.T''_{(x)} + 1/6.a^3.T'''_{(x)}... \quad \text{--- 2.34}$$

and

$$T_{(x-a)} = T_{(x)} - a.T'_{(x)} + 1/2.a^2.T''_{(x)} - 1/6.a^3.T'''_{(x)}... \quad \text{--- 2.35}$$

Adding equations 2.34 and 2.35 gives:

$$T_{(x+a)} + T_{(x-a)} = 2.T_{(x)} + a^2.T''_{(x)} + R \quad \text{----} \quad 2.36$$

where R combines the terms containing fourth and higher powers.

If R is assumed to be negligible, then equation 2.36 can be rearranged such that:

$$T''_{(x)} = (T_{(x+a)} + T_{(x-a)} - 2.T_{(x)})/a^2$$

$$= d^2T/dx^2 \quad \text{------ 2.37}$$

Similarly for the y-coordinate frame:

$$d^2T/dy^2 = (T_{(y+a)} + T_{(y-a)} - 2.T_{(x)}) / a^2 \quad \text{---- 2.38}$$

By combining equations 2.37 and 2.38, and using T_o to define

a

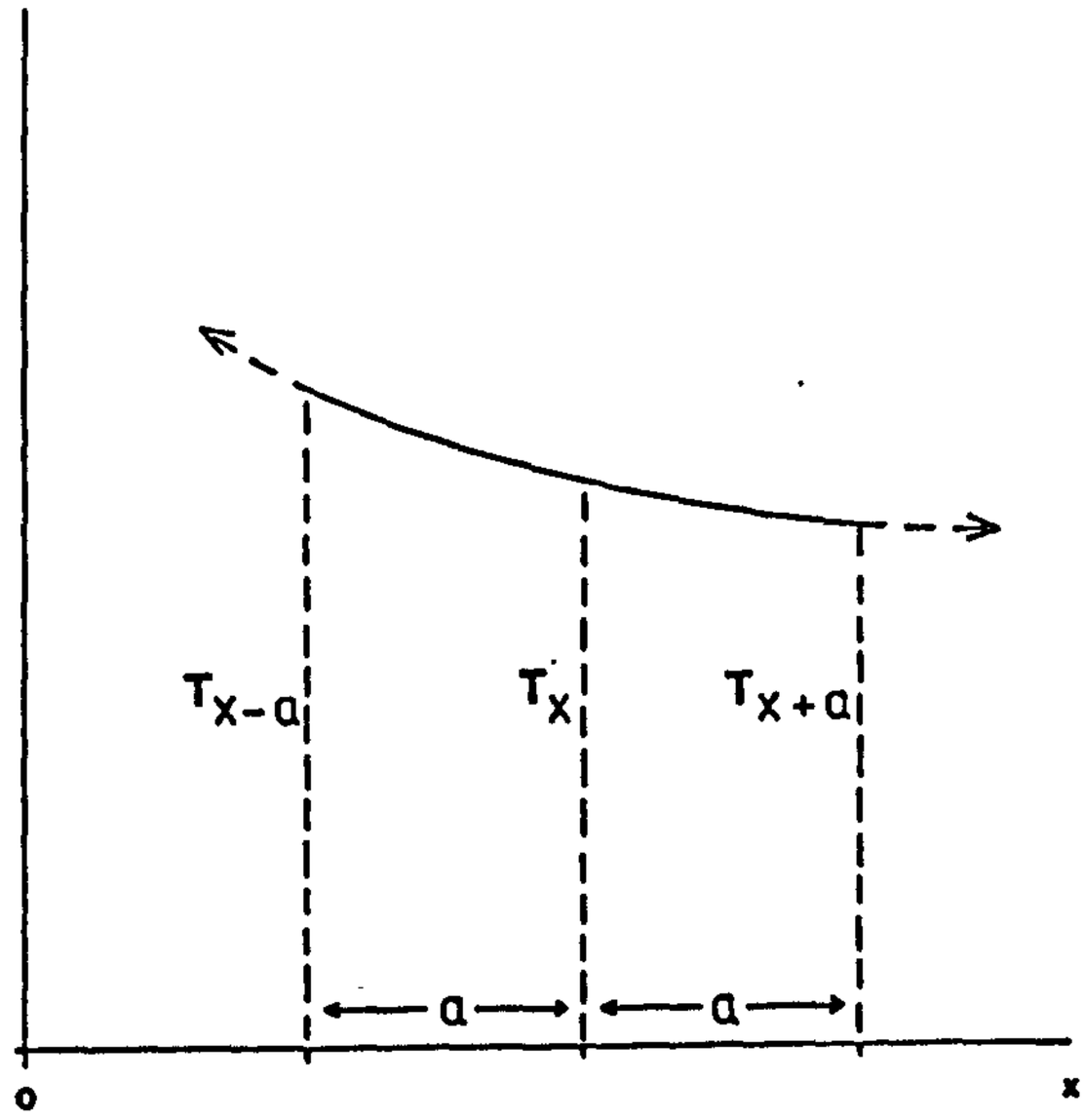

b

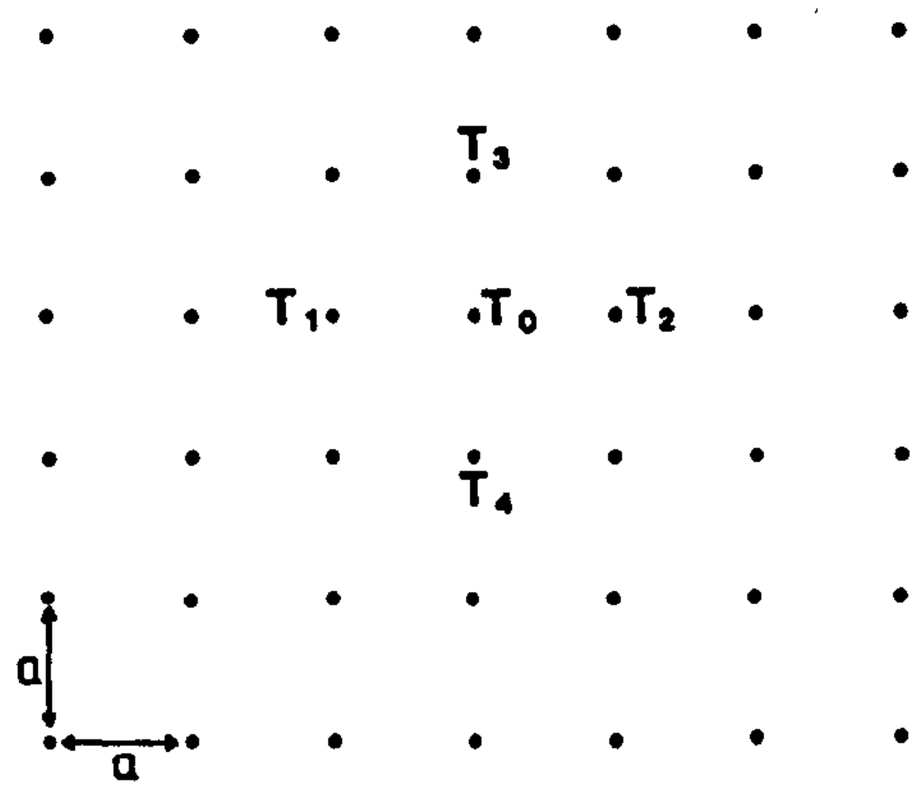

Figure 2.3 -

a. Taylor's theorem is utilised by the finite difference method to provide a solution for the heat flow equation at a particular time interval.

b. the two-dimensional temperature grid.

the temperature of a particular node in the two-dimensional grid (figure 2.3b),

$$d^2T/dx^2 + d^2T/dy^2 = ((T_1+T_2+T_3+T_4) - (4.T_o))/a^2 \text{ ----- } 2.39$$

Substituting into equation 2.33 gives,

$$(T_1+T_2+T_3+T_4 - 4.T_o)/a_2 = p.\sigma/k \; . \; dT/dt \text{ ---- } 2.40$$

If m and m+1 represent successive time intervals which are a small time increment, dt, apart then equation 2.40 becomes:

$$((T_{1(m)}+T_{2(m)}+T_{3(m)}+T_{4(m)})-(4.T_{o(m)})) \; / \; a^2$$

$$= (T_{o(m+1)}-To_{(m)})/dt \; . \; (p.\sigma/k) \text{ ---- } 2.41$$

Rearranging:

$$T_o(m+1) = (dt.k/p.\sigma.a^2) \; . \; ((T_{1(m)}+T_{2(m)}+T_{3(m)}+T_{4(m)}$$

$$-(4.T_{o(m)})) + T_{o(m)}$$

$$= r \; . \; (T_{1(m)}+T_{2(m)}+T_{3(m)}+T_{4(m)})$$

$$+ (1-4r) \; . \; T_{o(m)} \text{ ---- } 2.42$$

where $r = dt.k/p.\sigma.a^2$

Thus each nodal temperature, $T_{o(m+1)}$, within a vertical section of lithosphere is calculated from the corresponding temperature, $T_{o(m)}$, at the preceding time step.

To maintain the stability of the finite difference process the length of the time increment, dt, is critical. Instability arises due to the use of too great a time step relative to the grid size. Several texts are available which cover in detail the stability of this numerical process (eg.

Noble and Daniel 1980), however, there are two rules of thumb which guarantee stability:

a) the coefficient of $T_{o(m)}$ cannot be negative.

b) the sum of the coefficients of $T_{o(m)}$ must not exceed 1.

Applying the above criteria to equation 2.42 the following limiting conditions arise:

$$1 - 4r > 0$$

$$1 - 4r < 0$$

Therefore the maximum allowable time step, which maintains stability, is given by:

$$dt = (p.\sigma.a^2)/(k.4) \quad ---- \quad 2.43$$

A computer algorithm has been used to calculate the re-equilibration of the lithosphere temperature field after its perturbation by the extensional deformation. The algorithm is based on the following steps,

a) Input of temperature field including the perturbation caused by rifting.

b) The cooling, ΔT, of each temperature node is calculated using the finite difference method, for a small increment of time, dt, following rifting.

c) The modified temperature of each node is calculated such that:

$$T = T + \Delta T$$

d) Steps b and c are repeated for the next time interval, dt.

The finite difference method is constrained by boundary conditions which remain fixed throughout the incremental time steps. The boundary conditions were set such that the temperatures at the top and bottom (at 125km) of the lithosphere remain unmodified at 0°C and 1333°C respectively. The edge of the region is maintained at an equilibrated geotherm (equation 2.9) in order to provide a reference with which to compare the perturbations within the area of rifting.

2.4 Model Predictions for Continental Lithosphere Extension by a Coupled Simple Shear - Pure Shear Process.

The formulation described above for the geometric, thermal and isostatic aspects of continental lithosphere extension have been combined into a coupled simple shear-pure shear model which predicts basin geometry, timeline stratigraphy and crustal structure following extensional deformation (see also Kusznir et al, 1987, Kusznir and Egan, in press). In figure 2.4 a basin generated by the model is shown at 100Ma following 30km extension along a listric fault which soles out within the crust at a depth of 20km. Pure shear deformation, occurring below the detachment, balances the simple shear extension in the upper lithosphere and is distributed over a width of 100km, while it has a 30km distal offset with respect to the start of simple shear (the footwall cut-off). This offset causes a broadening of the basin into the distal region and allows a regional dispersal

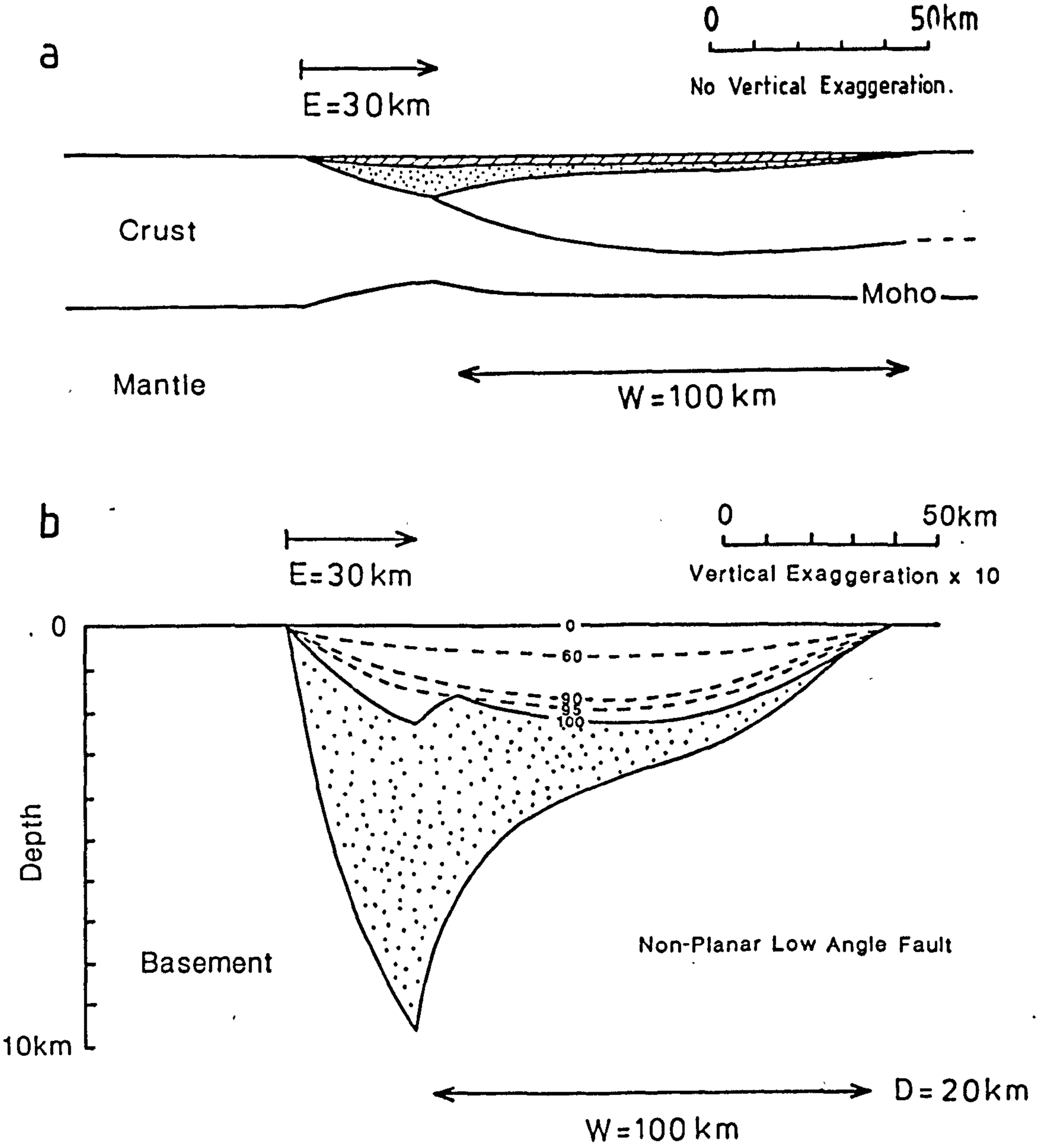

Figure 2.4 -

a) Model predictions showing basin geometry and crustal structure caused by coupled simple shear-pure shear lithosphere extension by 30km along a low angle listric fault, which gradually soles out into a detachment. Dotted ornament represents the syn-rift basin, while diagonal ornament denotes 100Ma of post-rift thermal subsidence. Airy isostasy and sediment loading to sea level are assumed throughout all phases of basin evolution. Pure shear extension in the lower lithosphere is offset 30km with respect to the start of simple shear and is distributed over a width of 100km.

b) Basin at 10x vertical exaggeration to show timeline stratigraphy at 100, 95, 90, 60 and 0Ma within the thermally induced deposition.

of the thermal subsidence.

The basin amplification shown in figure 2.4b illustrates stratigraphic timelines, which are caused by the post-rift re-equilibration of the lithosphere temperature field, at 100, 95, 90, 60 and 0Ma. Further consideration of the results predicted by the coupled simple shear-pure shear model will be made in chapter 3 where the response of the lithosphere to increasing the amount of fault controlled extension, varying the lateral position of the pure shear, deepening the detachment depth, etc. will be examined.

2.5 Summary

In this chapter the extension of the continental lithosphere has been assumed to be depth dependent such that the deformation of the upper brittle region of the lithosphere takes place by simple shear associated with low angle faults, whereas the lower plastic lithosphere extends by pure shear. The formulation of this simple shear-pure shear process has been divided into the following:

a) A geometric component arising from the thinning of the crust.

b) A thermal component caused by the perturbation of the lithosphere temperature field.

c) An Airy isostatic component, which compensates for surface and sub-surface loads arising from geometric and thermal effects.

A combination of the above components allows the prediction of sedimentary basin geometry, basin subsidence history and

stratigraphy, and crustal structure following lithosphere extension by a coupled simple shear-pure shear process.

CHAPTER 3

The Application of the Simple Shear - Pure Shear Model to Extensional Basin Formation on Low Angle Faults.

3.1 Introduction.

The mathematical formulation of the geometric, thermal and Airy isostatic components of simple shear-pure shear extension described in chapter 2 have been combined to calculate basin geometry and crustal structure. The models quantify the effect of varying the following parameters:

a) the amount of extension along the fault.

b) the lateral position of the pure shear deformation with respect to the simple shear extension.

c) the width over which the pure shear is distributed.

d) the detachment depth.

e) the fault-detachment shape.

In each case the models show syn-rift deposition (dotted ornament) generated by instantaneous extension, overlain by thermal subsidence to 100 Ma (shaded ornament). Sediment loading of any subsided region to sea level and Airy isostasy are assumed throughout all phases of basin evolution.

3.2 The Effect of Varying the Amount of Extension Along the Fault.

Model predictions are shown in figure 3.1 following extensions of 10km, 30km and 50km along a fault with

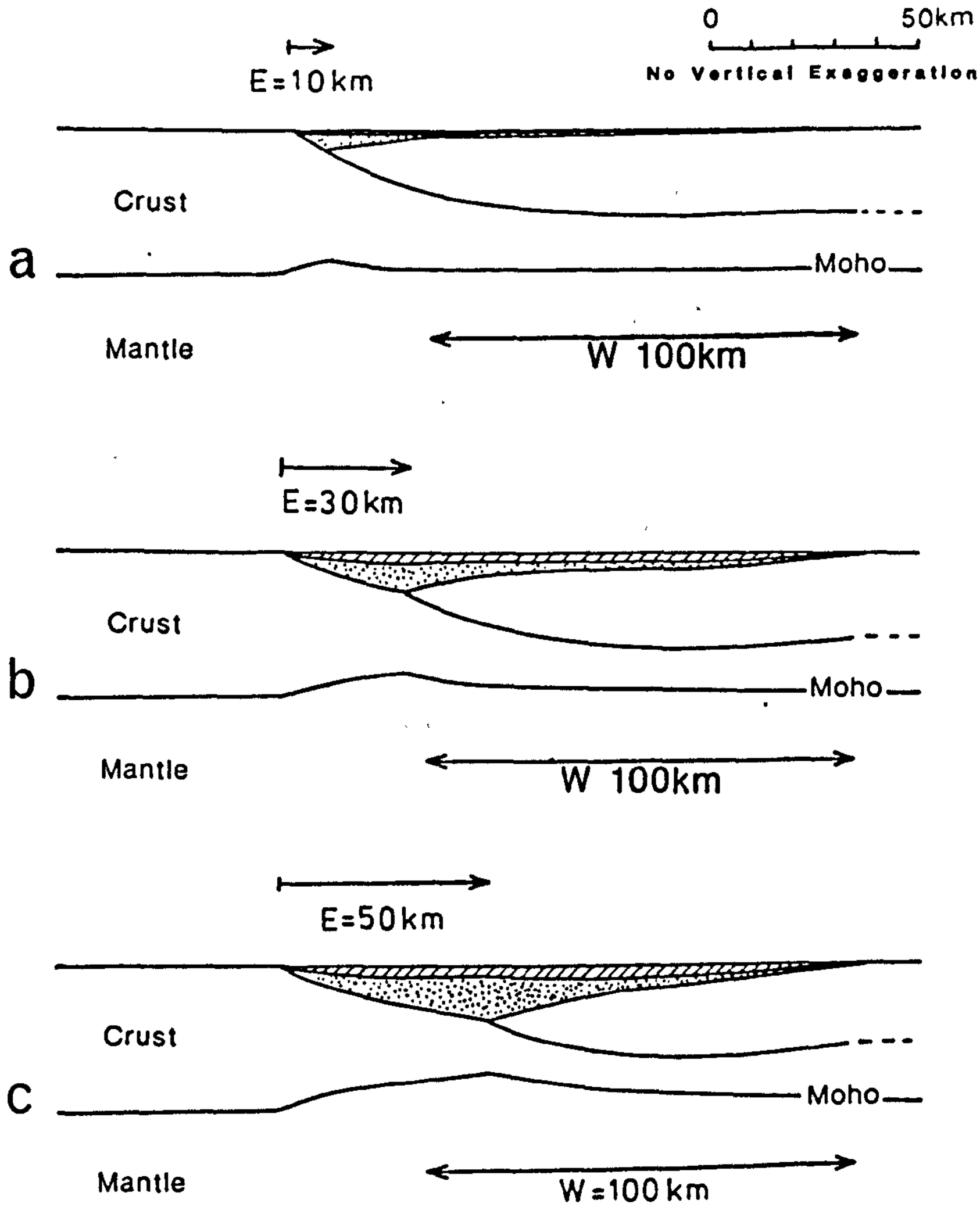

(after Kusznir et al., 1987)

Figure 3.1 - Model predictions for simple shear-pure shear extension of the continental lithosphere. Extensions of 10km (a), 30km (b) and 50km (c) are shown along an exponential fault which flattens into an intracrustal detachment at 20km. Below the detachment extension occurs by pure shear over a distance of 100km and begins 30km on the distal side of the simple shear. The geometrical configuration of both syn- (dotted ornament) and post-rift (shaded ornament) basin components, along with crustal structure, are shown at a time of 100Ma after instantaneous extension. Both sediment loading to sea level and Airy isostasy are assumed throughout all phases of basin evolution.

exponential geometry, which detaches within the crust at a depth of 20km. Pure shear deformation below the detachment has been distributed over 100km and laterally offset 30km to the distal side of the simple shear extension. The models show that the magnitude of the basin increases as the extension along the fault becomes greater. The maximum depth of the basin rises from 4km to 10km in response to an increase in extension from 10km to 30km. There is also a corresponding widening of the basin into the distal region. The increase in basin depth is less pronounced for an extension of 50km because the footwall, onto which the hanging wall collapses, is almost flat at this far distal position. Most sedimentary basins display extensions along a single fault in the range of 5 to 30km, therefore the 50km extension displayed in figure 3.1c is rather extreme. Most of the models presented in this thesis show extensions of 30km and while some basins exhibit this amount of extension (eg. the North Jeanne d'Arc basin), the main reason for using this figure was that it provided adequate visual resolution for comparing basin geometries.

3.3 The Effect of Varying the Lateral Position and Width of the Pure Shear.

In figure 3.2a to 3.2c the extension along the fault has been kept constant at 30km, while the lateral offset between the start of simple shear (the footwall cut-off) and pure shear has been increased. Offsets of 0, 30km and 60km are investigated in figures 3.2a, 3.2b, and 3.2c respectively. No offset between the simple and pure shear concentrates the extensional deformation into a relatively small region and a

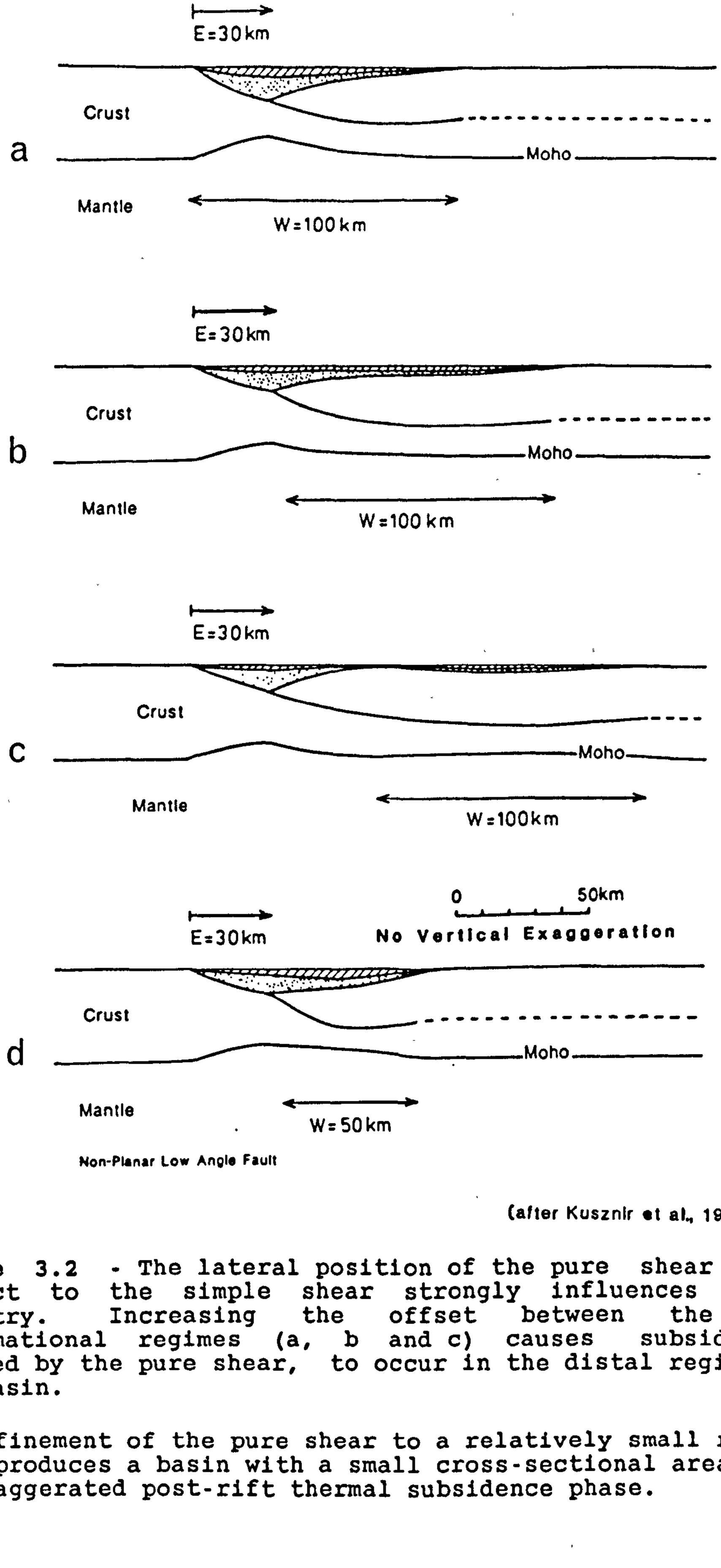

(after Kusznir et al., 1987)

Figure 3.2 - The lateral position of the pure shear with respect to the simple shear strongly influences basin geometry. Increasing the offset between the two deformational regimes (a, b and c) causes subsidence, induced by the pure shear, to occur in the distal region of the basin.

A confinement of the pure shear to a relatively small region (d) produces a basin with a small cross-sectional area and an exaggerated post-rift thermal subsidence phase.

narrow, deep basin is generated. Increasing the offset to 30km or 60km reduces the maximum basin depth by approximately 3km, while subsidence, induced by pure shear deformation, extends into the distal region, producing an almost separate sub-basin, which is composed almost entirely of thermal sag deposition.

Reducing the width of the pure shear concentrates its deformational effects into a relatively small region (figure 3.2d). As the pure shear produces dominantly thermal subsidence the resultant basin has an exaggerated thickness of thermal sag deposition, yet at the same time it has a narrow lateral extent.

In figure 3.3a and 3.3b model predictions are again shown for 30km and 60km offsets of the lower lithosphere pure shear deformation. The basins have been plotted at ten times vertical exaggeration and show timeline stratigraphy within the thermal subsidence component. Timelines have been calculated for 100, 95, 90, 60 and 0Ma and reflect the amount of thermal subsidence over these intervals. For example, the subsidence shown between 100 and 95Ma represents the amount of thermal subsidence occurring over the first 5Ma after rifting. The exponentially decaying nature of the thermal subsidence is clearly indicated by the fact that the thermal subsidence thickness produced during the first 10Ma after rifting is greater than that produced between 40 and 100Ma after initial extension.

The model showing 60km offset between the start of simple shear and pure shear (figure 3.3b) predicts two separate sub basins that are separated by a region of low subsidence.

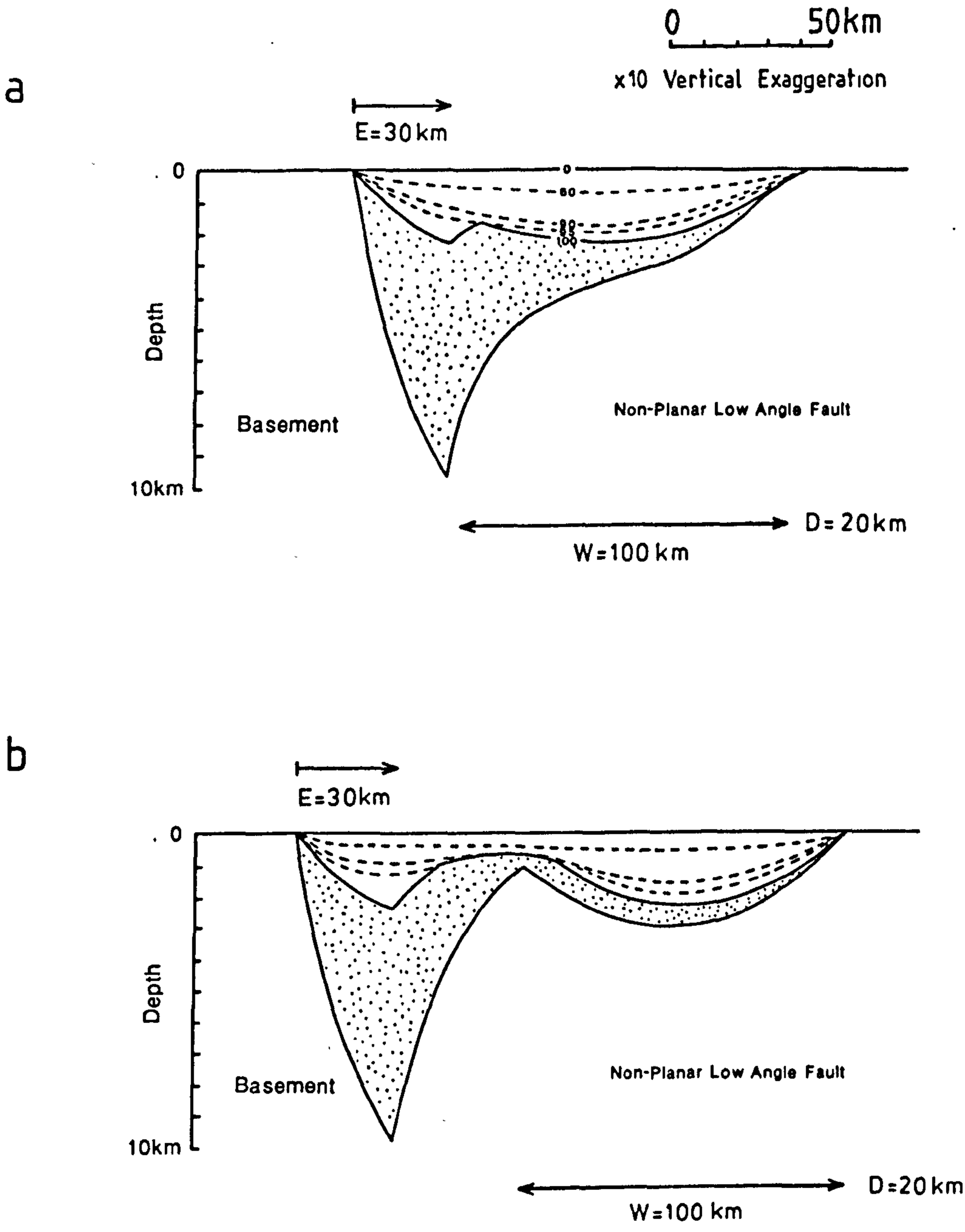

Figure 3.3 - Basin shown at 10x vertical exaggeration for 30km (a) and 60km (b) offset of the pure shear with respect to the start of simple shear. Subsidence history is shown by timelines at 100, 95, 90, 60 and 0Ma. At extreme offsets between the two deformational regimes (b) two distinct sub basins are generated, separated by a basement high.

This basement high reflects the region of separation between simple shear and pure shear. After 10Ma following rifting this basement high also experiences thermal subsidence due to lateral heat flow regionally perturbing the geotherm in the lower lithosphere.

3.4 The Effect of Varying Detachment Depth.

In chapter 1 three fault-detachment configurations have been described from evidence provided by geological and seismic data (figure 1.7). These are investigated in figures 3.4a, 3.4b and 3.4c with models showing a fault flattening into a detachment within the crust at 20km, at the Moho at 35km and at the lithosphere/asthenosphere boundary.

An intracrustal detachment (figure 3.4a) allows pure shear thinning of the lower crust. This creates additional syn-rift subsidence, which causes a widening of the basin into the distal region, especially when the pure shear is widely dispersed and/or offset relative to the simple shear. A detachment at the base of the crust (figure 3.4b) eliminates the pure shear deformation in the crust. In this case the pure shear is responsible for perturbing the geotherm only, thus causing uplift in the distal region of the basin at rifting. This is not seen in the model as thermal subsidence has brought the surface back to a position at or very near sea level - assuming no erosion occurs.

In figure 3.4c lithosphere extension by simple shear alone has been modelled along a fault dipping down to the deep lithosphere. The fact that the whole of the crust has been faulted produces a unique basin geometry and Moho

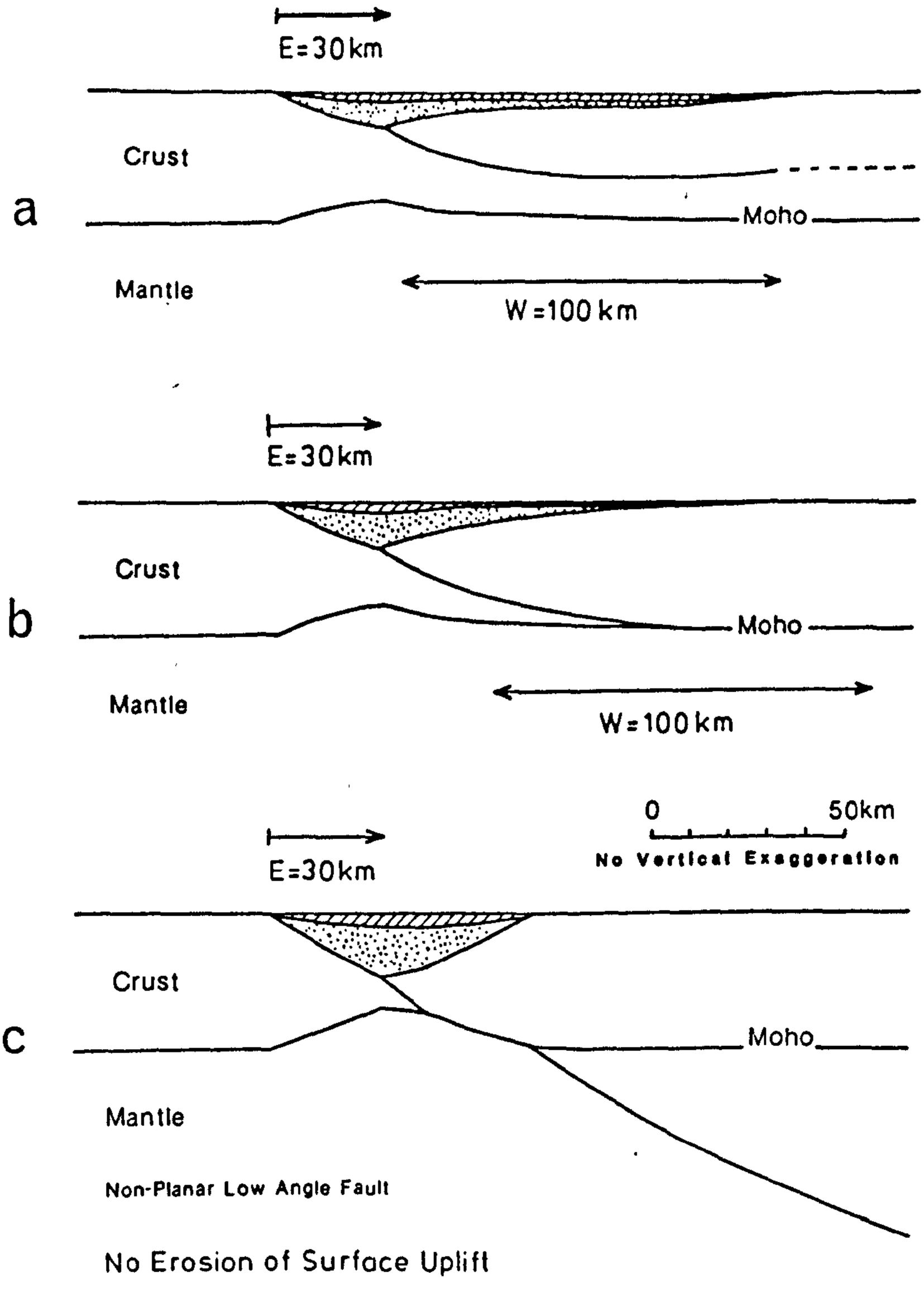

(after Kusznir et al., 1987)

Figure 3.4 -

a. An intracrustal detachment causes pure shear thinning of the lower crust, which produces subsidence in the distal parts of the basin.

b. Increasing the detachment depth to the base of the crust means that there is no pure shear thinning of the lower crust and as a result the width of syn- and post-rift basin components are reduced.

c. Extension along a fault detaching in the deep lithosphere causes a rifting of the whole of the crust - a unique basin geometry and crustal structure result.

Both models b and c predict syn-rift thermal uplift in the distal region of the basin.

topography. However, the existence of such continuous deeply detaching faults is not supported by deep seismic reflection data.

3.5 The Effect of Varying the Fault Geometry.

The model results so far have assumed an exponential fault geometry as defined in equation 2.1. In figure 3.5a the effect of extension along an initially planar fault with a dip of 30° is shown. The basin geometry generated, when compared to that produced by extension along a listric fault (figure 3.5b), is very symmetrical due to extension being taken up along a flat lying detachment - the implications of this are discussed in chapter 10.

3.6 The Application of the Coupled Simple Shear - Pure Model to Uniform Lithosphere Extension.

The mathematical formulation described in chapter 2 and applied in this chapter quantifies lithosphere response to extension by a simple shear-pure shear process. The formulation can also be used to investigate lithosphere extension and associated basin formation by an entirely simple shear mechanism, as shown in figure 3.4c, or alternatively by a wholly pure shear process.

Equation 2.29, which has been derived to give basin geometry, $B_{(x,t)}$, following the geometric, thermal and isostatic consequences of simple shear-pure shear lithosphere extension, can be simplified for pure shear deformation alone such that:

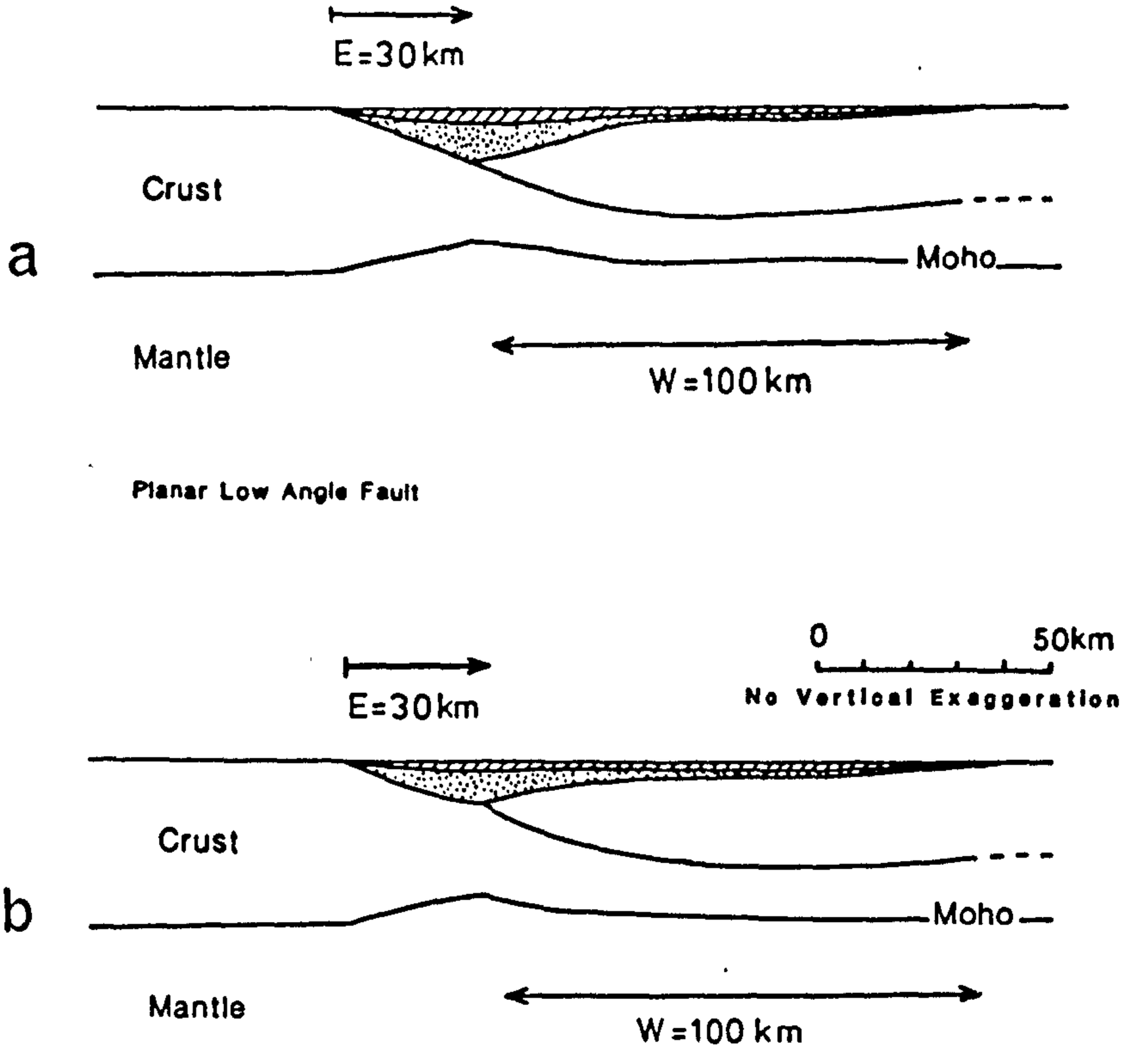

Figure 3.5 - Extension along a planar (a) and an exponential (b) fault are compared. The symmetrical, flat-bottomed basin produced by rifting along an originally planar fault is a result of much of the extension being accommodated along the horizontal detachment.

$$B_{(x,t)} = [(P_{(x)}.g.(p_m-p_c)) + L_{tn}(x,t)]$$

$$/ (p_m.(1-\alpha.T_o).g) \quad \text{---- 3.1}$$

where g is acceleration due to gravity (9.81 $m.s^{-2}$), p_m and p_c are the densities of mantle (3300$kg.m^{-3}$) and crust (2800$kg.m^{-3}$) respectively, a is the thickness of the lithosphere (125km), T_o is the temperature at the base of the lithosphere (1333°C), and $P_{(x)}$ is the amount of crustal thinning by pure shear defined such that:

$$P_{(x)} = C_o \,.\, (1-(1/\beta_{(x)}) \quad \text{----} \quad 3.2$$

where C_o is original crustal thickness (35km) and $\beta_{(x)}$ is the extension factor.

$L_{tn}(x,t)$ defines the load on the lithosphere created by the perturbation of the geotherm such that:

$$L_{tn}(x,t) = \int_o^a \alpha.p'.g.\Delta T \;\; dz \quad \text{-----} \quad 3.3$$

where α is the thermal expansion coefficient (3.28×10^{-5} $°C^{-1}$), ΔT defines the temperature difference at a particular depth z between perturbed lithosphere, where the temperature is given by $T_o.z.\beta/a$, and unperturbed lithosphere, where the temperature is given by $T_o.z/a$. p' is the density of crust or mantle depending on the depth at which the temperatures are being considered. Equation 3.3 can be written more precisely to reflect both the comparison between the temperatures of perturbed and unperturbed lithosphere and the change in density with depth such that:

$$L_{th}(x,t) = \int_{o}^{co} p_c.\alpha.g.T_o.z/a\ dz + \int_{co}^{a} p_m.\alpha.g.T_o.z/a\ dz$$

$$- \int_{o}^{co/\beta} p_c.\alpha.g.T_o.z.\beta/a\ dz - \int_{co/\beta}^{a/\beta} p_m.\alpha.g.T_o.z.\beta/a\ dz$$

$$- \int_{a/\beta}^{a-b} p_m.\alpha.g.T_o\ dz \quad \text{--- 3.4}$$

Figure 3.6a shows basement generated by using the above formulation after instantaneously extending the lithosphere by $\beta = 2$ for a width of 100km. The effects of sediment loading have also been included using equation 2.25. Basin geometry is shown at 0, 5, 10, 40 and 100Ma after rifting. The re-equilibration of the lithosphere temperature field following extension has been calculated using the finite difference method to solve the heat conduction equation as described in section 2.3. A two-dimensional solution of the equation has been used to take into account both the lateral and vertical flow of heat. It is the former phenomena which has caused relative deepening at the basin peripheries during thermal subsidence (heat is lost from the edges of the basin by lateral heat flow more readily than from the centre).

The formulation of lithosphere extension by pure shear as described above allows a direct comparison with the McKenzie model (McKenzie 1978, also see chapter 1). In figure 3.6b the solid line represents the subsidence history of lithosphere, to 100Ma, extended by a β of 2 as generated by equations 3.1 to 3.4, while the dotted line represents basement subsidence predicted by the McKenzie model (see equations 1.1 to 1.5), which has been modified to include

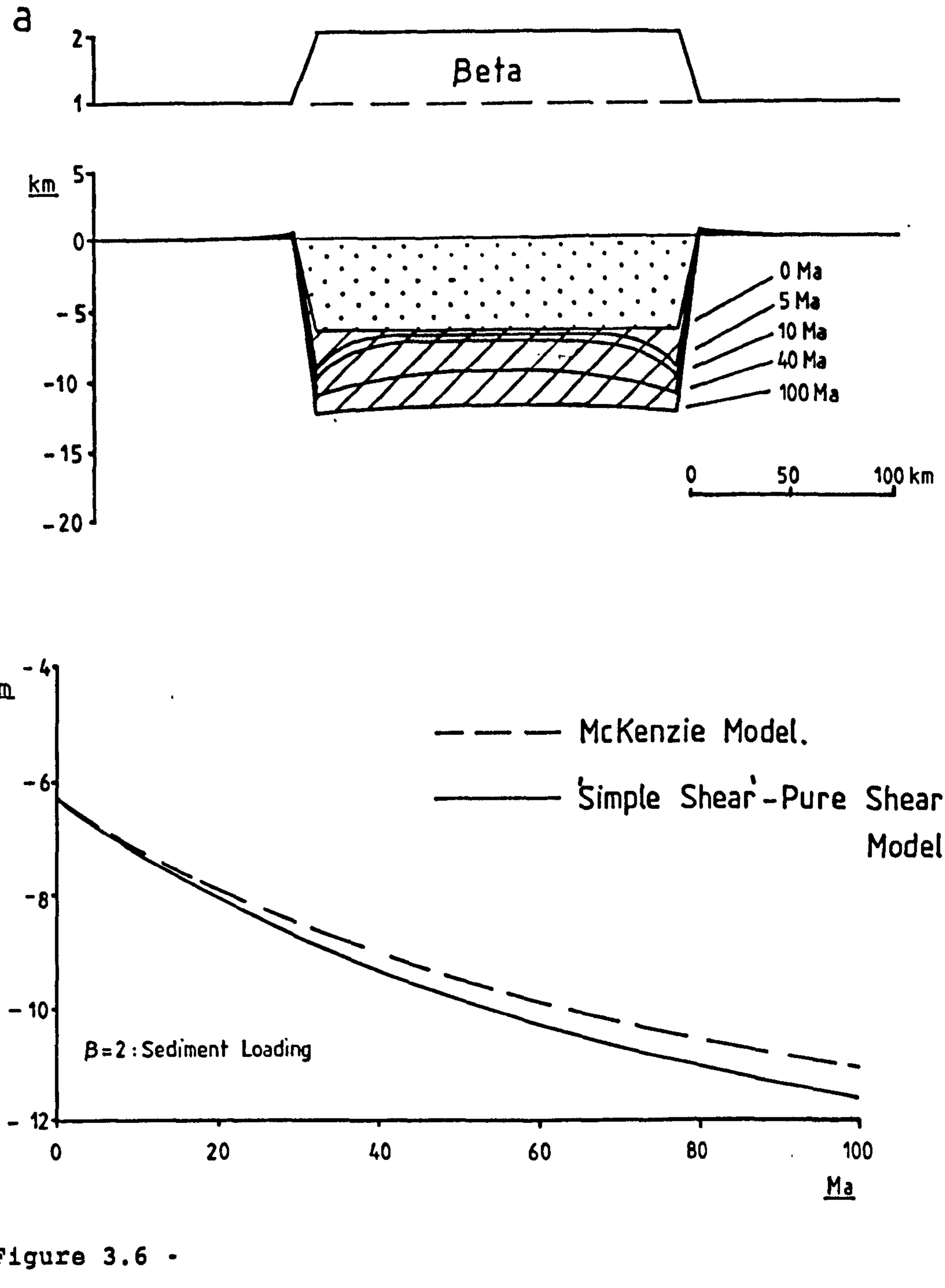

Figure 3.6 -

a) Basin predictions following an instantaneous pure shear stretching of the lithosphere by β = 2 over a width of 100km. Basement is shown immediately after rifting and during thermal subsidence to 100Ma. The loading effect of sediment fill to sea level has been included. The deepening seen after rifting at the basin peripheries is a result of lateral heat flow.

b) Subsidence history of lithosphere extended by a β = 2 as predicted by the McKenzie model (dotted line) and the simplified simple shear-pure shear model (solid line). Both formulations predict the same amount of basin subsidence directly after rifting, although the McKenzie model generates a lesser amount of thermal subsidence at 100Ma.

the effects of sediment loading. All parameters used in the two formulations have been made identical. Both models predict the same amount of subsidence immediately following rifting.

The two formulations do not agree, however, for the amount of thermal subsidence following rifting and the reason for this is partly due to the different mathematical methods used; McKenzie uses fourier analysis to solve the heat conduction equation and considers vertical heat flow only, whereas the method formulated above uses the finite difference method and considers both vertical and lateral heat flow. The McKenzie model also contains some inconsistency when calculating thermal loading. For any vertical section at time t the thermal load should include a density variation as described in equation 3.4, which for low β values and small basin depths can be approximated to:

$$L_{th}(x,t) = \int_{o}^{co} \alpha.\Delta T.p_{o}.g\ dz + \int_{co}^{a} \alpha.\Delta T.p_{m}.g\ dz \text{ ---- } 3.6$$

McKenzie assumes this density variation during initial rift induced subsidence, but allows density to be a depth independent value of p_m for the calculation of thermal loading during the post rift re-equilibration of the geotherm. As a consequence the McKenzie model under estimates the amount of thermal subsidence (see figure 3.6b). The mathematics of the McKenzie model, in fact, mean that it is not possible to incorporate a depth-dependent density in the calculation of thermal subsidence.

3.7 Summary.

A quantitative consideration of the geometric, thermal and isostatic consequences of continental lithosphere extension has been made in this chapter. These components have been combined into a coupled simple shear-pure shear model which predicts basement geometry, time line stratigraphy and Moho topography. The model has been used to show the effect of:

a) increasing the extension along the fault, which ultimately controls the size of the basin both vertically and laterally, such that large amounts of extension produce bigger basins.

b) varying the lateral position and width of the pure shear, which dictates the lateral coincidence between the simple shear and pure shear depocentres.

c) varying the detachment depth. This parameter controls the importance of crustal thinning by pure shear during extension, such that deeper detachment depths produce decreasing amounts of pure shear crustal thinning.

d) varying the shape of the fault. This parameter strongly determines the geometry of the basin produced following rifting.

Certain assumptions have been made in the generation of the above models, some of which are unrealistic. Later sections of this thesis largely concentrate on improvements made to the model, mostly using ideas gained from geological and geophysical data. For instance, one of the assumptions made

for this initial work was to assume that any loads imposed on the lithosphere were compensated by Airy isostasy. More realistically the lithosphere has a lateral strength and flexes in response to applied loads - it possesses a finite flexural rigidity (eg. Watts et al. 1982). The effect of flexural rigidity on basin geometry and crustal structure is considered in the next chapter.

CHAPTER 4

The Effect of Finite Flexural Rigidity During Extensional Basin Formation.

4.1 Introduction.

In Chapter 3 basin geometry and crustal structure have been generated assuming an Airy isostatic response to lithosphere loading caused by simple shear pure shear extension. Airy isostasy treats the lithosphere as if it is divided into an infinite number of independent vertical sections and that loading of a section produces uplift or subsidence of that section only. In reality the lithosphere is more analogous to an elastic plate, possessing a finite flexural rigidity, whereby loading causes either regional uplift or subsidence depending on the nature of the load (Walcott 1970, Sleep and Snell 1976, Beaumont 1978 and 1981, Beaumont et al 1982, Watts et al 1982).

4.2 The Flexural Isostatic Response of the Lithosphere to Load Forces Created During Rifting.

Extension disrupts the isostatic balance of the lithosphere - simple shear crustal thinning and heating at rifting constitute negative loads and produce uplift, whereas pure shear crustal thinning, basin fill and thermal re-equilibration after rifting generate downward flexing loads. The flexural isostatic deflection, w(x), caused by these loads can be determined by assuming that the lithosphere behaves as an elastic plate, which is in equilibrium under the action of all of the applied forces (Turcotte and Schubert 1982), such that:

$$(d^2/dx^2).(D.d^2w(x)/dx^2) = L(x) - (P.d^2x/dx^2) \quad \text{----} \quad 4.1$$

where L(x) is the applied load at a point and P is the horizontal force per unit length acting parallel to x and D is flexural rigidity given by the following equation:

$$D = (E.T_e^3) / (12.(1 - v^2)) \quad \text{-----} \quad 4.2$$

where E is Young's modulus and v is Poisson's ratio. Elastic thickness, T_e, is the main parameter controlling lithosphere flexural strength and is dependent on the composition and thermal structure of the lithosphere (Kusznir and Karner 1985). At high geothermal gradients the elastic layer is thin and as a consequence the flexural strength of the lithosphere is low. In fact if the thickness of the elastic layer is zero the lithosphere behaves as an Airy body. On the other hand, cool lithosphere has a relatively deep elastic-plastic transition and therefore a thick elastic layer, resulting in a high flexural strength.

When applied to the lithosphere equation 4.1 has to be modified to incorporate the isostatic restoring force to allow for the fact that loads are compensated by the negative or positive replacement of mantle rocks at the base of the lithosphere:

$$[(d^2/dx^2).(D.d^2w(x)/dx^2)] + [(p_m-p_i).g.w(x)] = L(x) \quad \text{----} \quad 4.3$$

where p_m and p_i are the densities of the mantle and infill loads respectively and L(x) defines the load on the lithosphere (P is assumed to be zero).

At zero flexural rigidity the isostatic restoring force is equivalent to the loading force itself, but for finite

flexural strengths some of the imposed load is supported by the rigidity of the lithosphere and the isostatic restoring force is reduced.

As described in chapter 2 simple shear extension along a fault thins the upper crust by an amount $S_{(x)}$, which is modified by an isostatically induced rebound, $w_m(x)$. Equation 4.3 can be modified to include this process such that:

$$[(d^2/dx^2).(D.d^2w_m(x)/dx^2)] + [(p_m-p_{air}).g.w_m(x)] = -(p_c.g.S_{(x)}) \quad \text{---- 4.4}$$

Similarly, thinning of the lower crust by pure shear, $P_{(x)}$, can be represented as:

$$[(d^2/dx^2).(D.d^2w_p(x)/dx^2)] + [(p_m-p_{air}).g.w_p(x)] = (p_m-p_c).g.P_{(x)} \quad \text{---- 4.5}$$

Thermal uplift at rifting can be expressed as:

$$[(d^2/dx^2).(D.d^2w_{th}(x,t=0)/dx^2)] + [(p_m-p_{air}).g.w_{th}(x,t=0)] = \int_0^a \alpha.\Delta T.p'.g \; dz \quad \text{---- 4.6}$$

where α is the coefficient of thermal expansion, ΔT is the temperature perturbation and p' is dependent upon the density at which the perturbation is being considered (all symbols are defined in table 4.1).

Equation 4.6 can also be used to predict the lithospheric response to post-rift re-equilibration of the geotherm as the only changing parameter is the magnitude of the

Table 4.1

List of Symbols

a	Thickness of lithosphere	125km
α	Thermal expansion coefficient	$3.28 \times 10^{-5} °C^{-1}$
$B_{(x,t)}$	Basin geometry	-----
D	Flexural rigidity	-----
$D_{(x)}$	Fault-detachment geometry	-----
E	Young's Modulus	$70 \times 10^{9} Pa$
f_N	Nyquist frequency	-----
g	Acceleration due to gravity	$9.81 m.s^{-2}$
λ	Wavelength of load	-----
$L_{(x)}$	Load function	-----
ρ_{air}	Density of air	0.0
ρ_c	Density of crust	$2800 kg.m^{-3}$
ρ_l	Density of load	-----
ρ_m	Density of mantle material	$3300 kg.m^{-3}$
$P_{(x)}$	Pure shear crustal thinning	-----
s	Width of load	-----
$S_{(x)}$	Simple shear crustal thinning	-----
t	Time	-----
ΔT	Temperature perturbation	-----
T_e	Elastic thickness	-----
v	Poisson's ratio	0.25
w(x)	Flexural uplift/subsidence	-----
x	Horizontal coordinate	-----

temperature perturbation, ΔT, which gradually decreases to zero.

The basin geometry, $B_{(x,t=0)}$, created during rifting is given by:

$$B_{(x,t=0)} = S_{(x)} + W_m(X) + W_p(X) + W_{th}(X,t=0) \quad \text{----} \quad 4.7$$

For a flexural rigidity of zero ($T_e=0$) equation 4.3 can be solved to predict the Airy isostatic response of the lithosphere to loading such that:

$$w(x) = L(x)/((p_m-p_1).g) \quad \text{----} \quad 4.8$$

For finite values of flexural rigidity the fourth order derivative in equation 4.3 must be solved. For simplicity a sinusoidally distributed load is considered initially such that:

$$L(x) = L_o \,.\, \sin(2.\pi.x/\lambda) \quad \text{----} \quad 4.9$$

where L_o defines the peak of the load and λ is its wavelength.

Equation 4.3 shows that the deflection of the lithosphere, w(x), is directly proportional to the applied load, which implies that if the load varies sinusoidally, so must the deflection it produces. Therefore:

$$w(x) = w_o \,.\, \sin(2.\pi.x/\lambda) \quad \text{----} \quad 4.10$$

where w_o is the maximum deflection of the lithosphere.

Substituting for $w_{(x)}$ into equation 4.3 gives:

$$[(D.(2.\pi/\lambda)^4).(w_o.\sin(2.\pi.x/\lambda))]$$

$$+ [(p_m-p_1).g.w_o.\sin(2.\pi.x/\lambda)] =$$

$$L_o.\sin(2.\pi.x/\lambda) \quad ---- \quad 4.11$$

simplifying:

$$(D.(2.\pi/\lambda)^4.w_o) + ((p_m-p_1).g.w_o) = L_o \quad ---- \quad 4.12$$

By rearrangememt the maximum deflection of the lithosphere is obtained:

$$w_o = L_o / [(D.(2.\pi/\lambda)^4)+((p_m-p_1).g)] \quad ---- \quad 4.13$$

More realistically lithospheric loads are not sinusoidally distributed, but are highly variable and a convenient means of representation is as a series of sine and cosine components which are combined in a Fourier series (eg Papoulis 1962) such that:

$$L(x) = (b_o/2) + \sum_{n=1}^{\infty} [A_n \,.\, \sin(2.\pi.n.x/s)] +$$

$$[B_n \,.\, \cos(2.\pi.n.x/s)] \quad ---- \quad 4.14$$

where b_o, A_n and B_n are the Fourier coefficients such that:

$$b_o = 1/s \,.\, \int_a^b L(x)\, dx \quad ---- \quad 4.15$$

$$A_n = 2/s \,.\, \int_a^b L(x) \,.\, \sin(2.\pi.n.x/s)\, dx \quad ---- \quad 4.16$$

$$B_n = 2/s \,.\, \int_a^b L(x) \,.\, \cos(2.\pi.n.x/s)\, dx \quad ---- \quad 4.17$$

where s is the width of the load, b-a. The wavelength of each sine and cosine component of the load is given by s/n.

It follows therefore that a large number of components are required in order to accurately represent a load function. If s is 100km then the wavelength of the first component (n=1) will be 100km and for the hundredth component the wavelength will be 1km. Furthermore, the number of sampling points across the width of the load also controls the fidelity with which the load function is represented. Constraint on the sampling interval is provided by the Nyquist frequency, f_N, which states that:

$$f_N = 0.5.\delta t \quad \text{----} \quad 4.18$$

where δt is the sampling interval.

It follows from equation 4.18 that there is no significant loss of information from the load being sampled so long as the sampling interval is at least twice as high as the highest frequency component in the sampled function. For the work carried out here a careful monitoring of the number of fourier components relative to the load sampling interval has been made in order to achieve maximum fidelity in the representation of the load and to optimise on the number of calculations.

By combining the equation 4.13 with the Fourier series the flexural response of the lithosphere to a varying load can be calculated such that

$$w(x) = (b_o'/2) + \sum_{n=1}^{\infty} [A_n' . \sin(2.\pi.n.x/s)] + [B_n' . \cos(2.\pi.n.x/s)] \quad \text{----} \quad 4.19$$

Similarly, the Fourier coefficients are now modified such that:

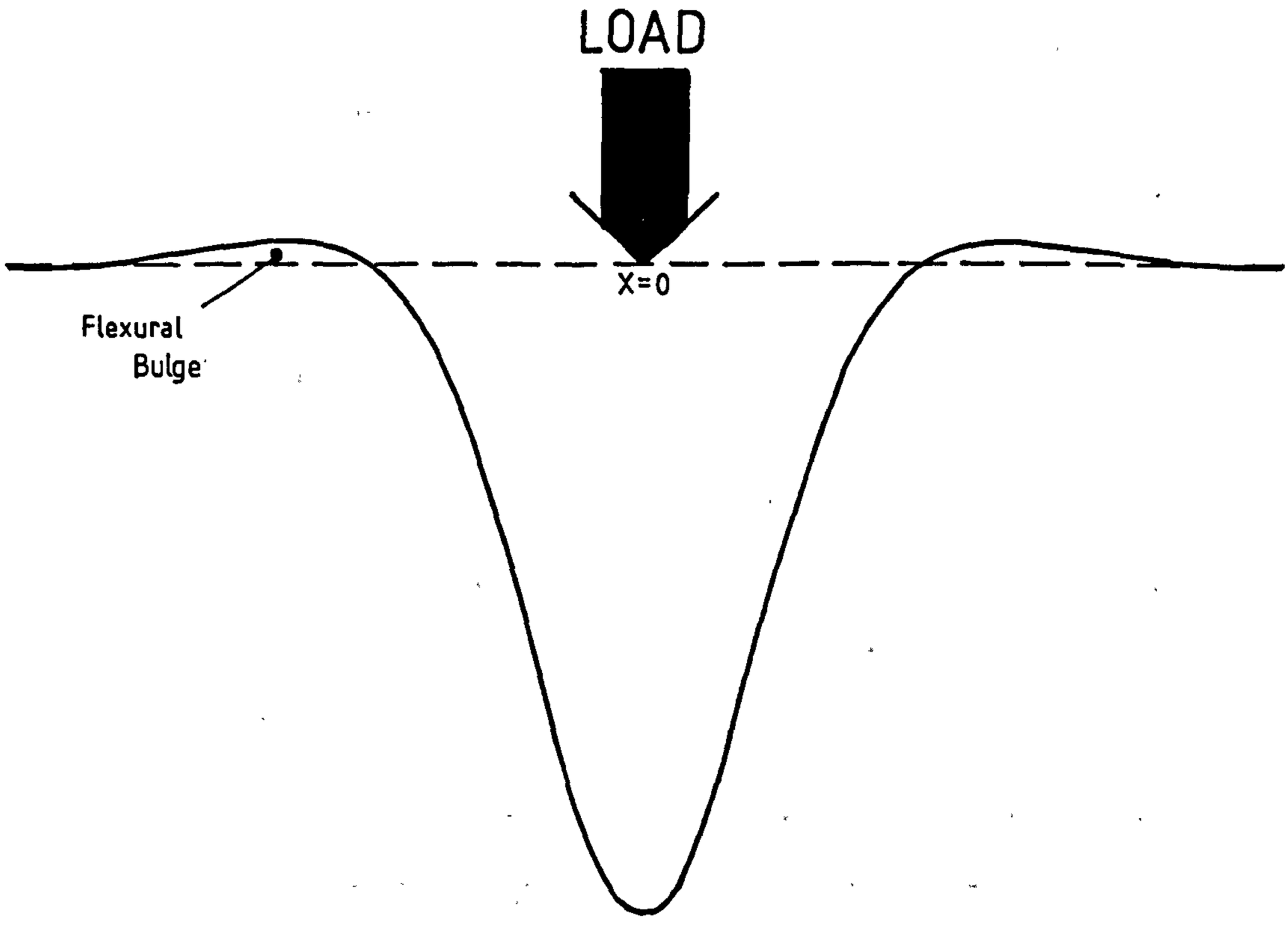

Figure 4.1 - Diagrammatic representation of the flexing of the lithosphere to a point load. Small amplitude flexures occur peripherally to the large subsidence caused directly by the load.

$$B_o' = 1/s \cdot \int_a^b L(x) / (p_m - p_1).g \; dx \quad \text{----- 4.20}$$

$$A_n' = 2/s \cdot \int_a^b [L(x) / ((D.(2.\pi.n.x/s)^4)+((p_m-p_1).g))] \cdot \sin(2.\pi.n.x/s)\, dx \quad \text{----- 4.21}$$

$$B_n' = 2/s \cdot \int_a^b [L(x) / ((D.(2.\pi.n.x/s)^4)+((p_m-p_1).g))] \cdot \cos(2.\pi.n.x/s)\, dx \quad \text{---- 4.22}$$

The end points a and b must be set so that they do not experience any flexural effects from loading. This means a and b must be defined so that there are a large number of zero-amplitude components are included either side of the load variation to take into account laterally distributed small amplitude flexural deflections occurring peripherally to the load itself (figure 4.1). The extent and magnitude of these deflections, which are only a fraction of the deflection of the lithosphere beneath the load, are dependent on the flexural rigidity of the lithosphere (see Turcotte and Schubert, 1982).

4.3 The Effect of Flexural Rigidity on the Rifting of Continental Lithosphere by a Simple Shear-Pure Shear Process.

A computer algorithm, incorporating the above theory, has been developed to calculate the flexural response of the lithosphere to load functions resulting from simple shear-pure shear extension. In figure 4.2 each rift induced load is considered and the associated flexural response profile is shown. Flexural rigidity is defined by a constant elastic

a) Simple Shear Crustal Thinning

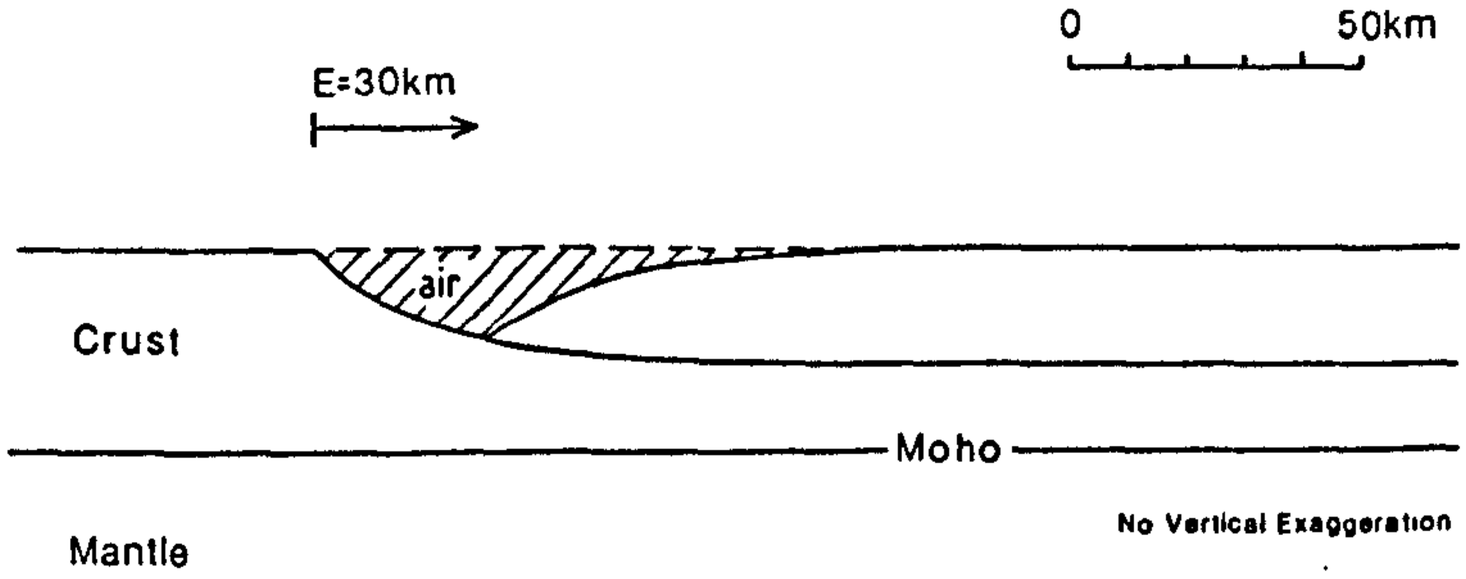

b) Flexural Rebound

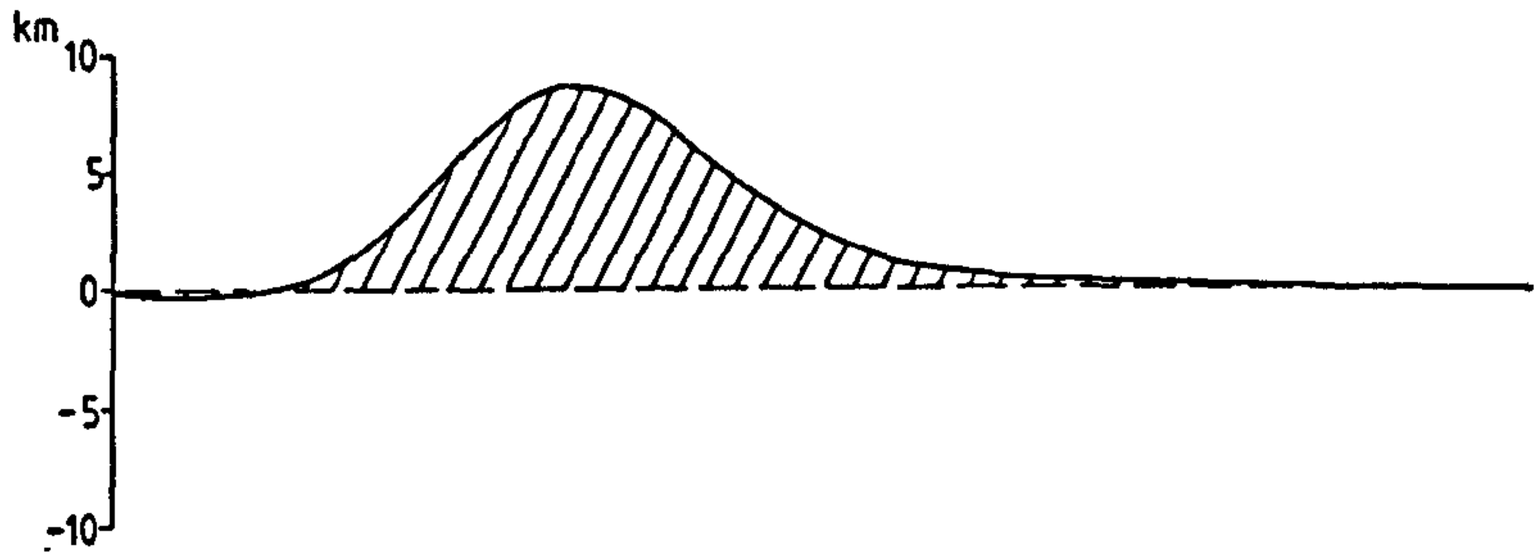

c) Subsidence Due To Pure Shear

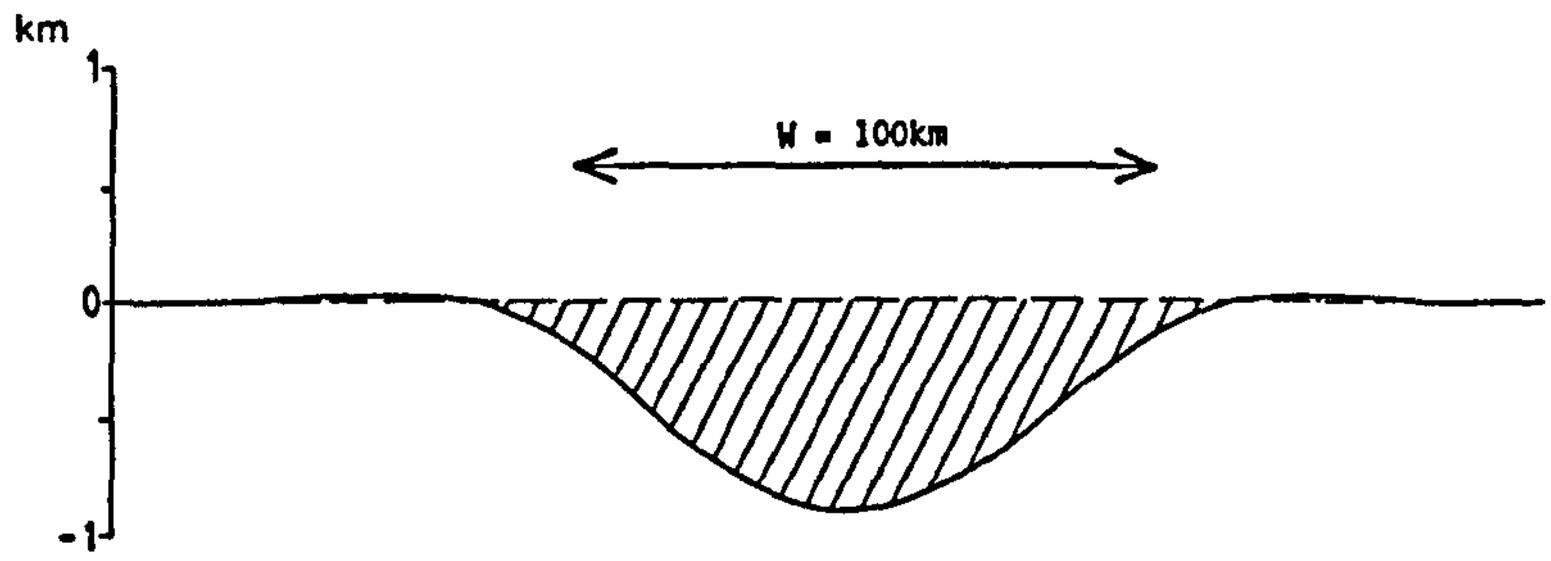

d) Thermal Uplift

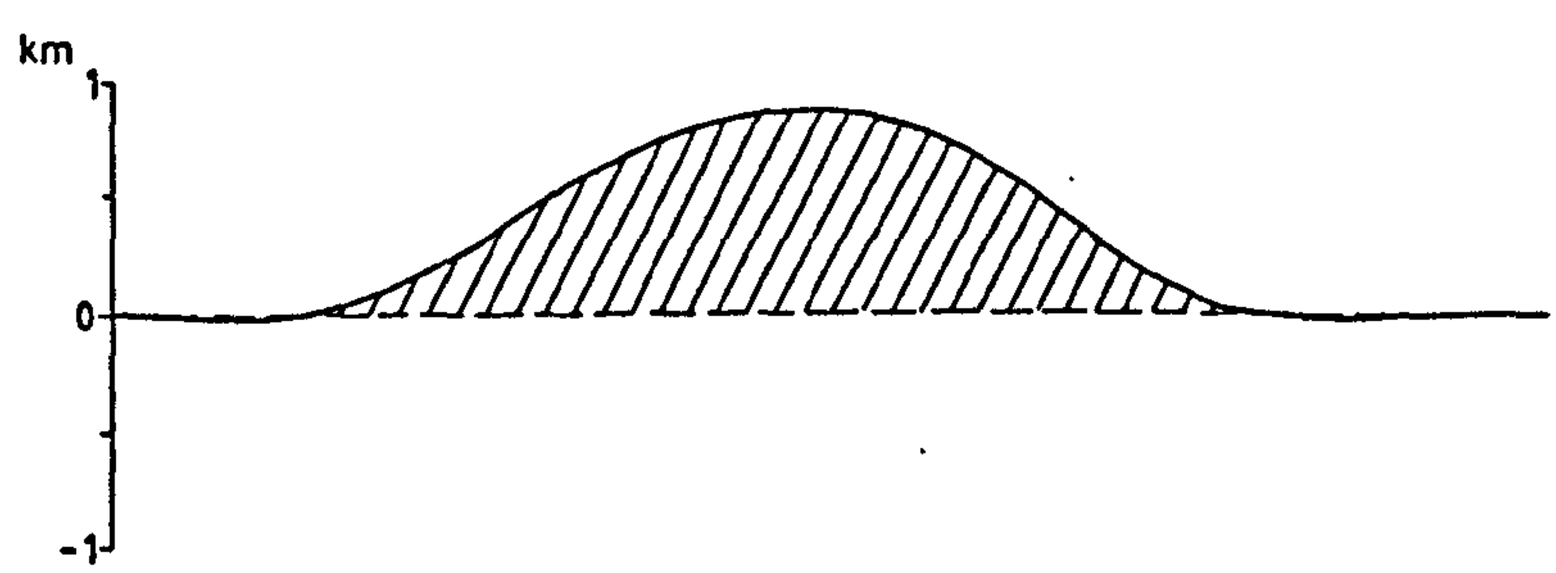

e) Resultant Basin

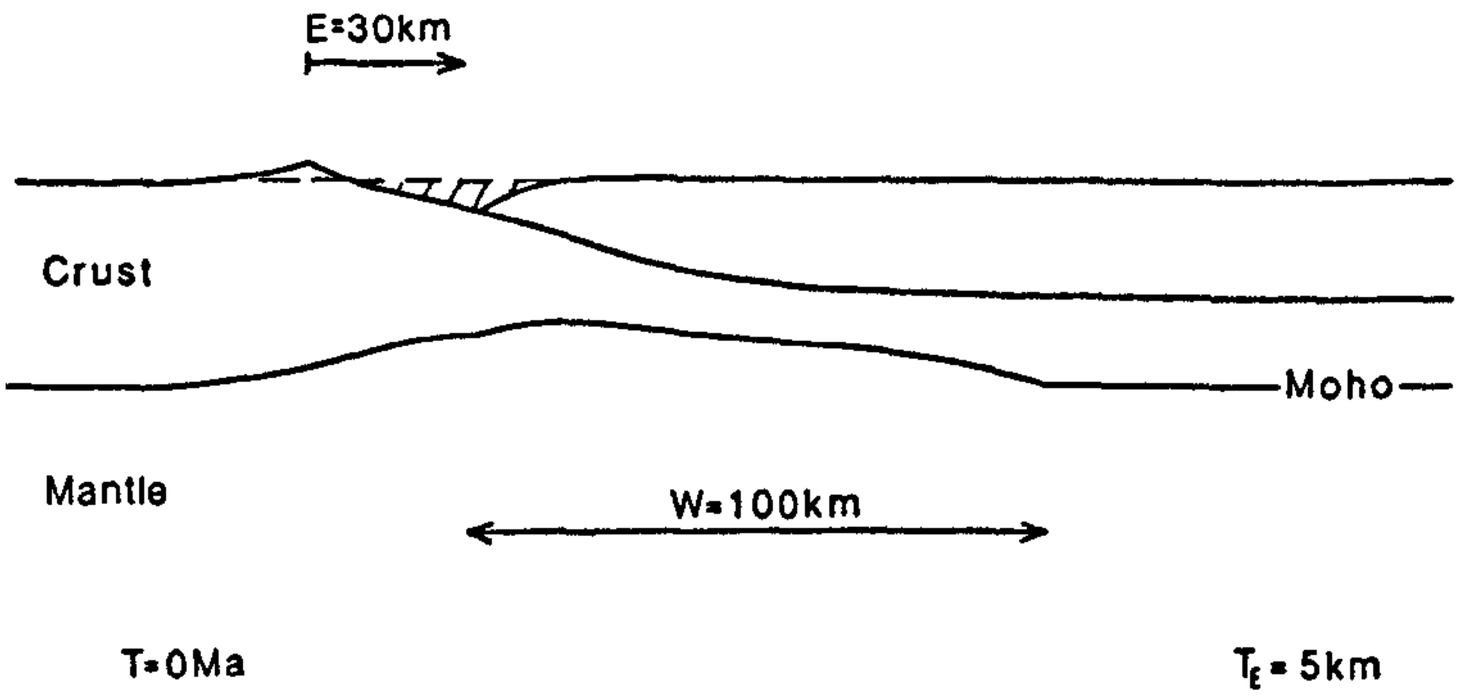

Figure 4.2 - The flexural response of the lithosphere to loads created at rifting following fault controlled extension (a) can be divided into a flexural isostatic uplift (b), subsidence due to pure shear thinning of the lower crust (c) and thermally induced uplift (d). The resultant basin and crustal structure (e) represents the combined effect of these load functions.

thickness of 5km, which is an average value displayed by actively rifting regions at present (Cochran 1979). The following sequences of loads and their resulting flexural effect on the lithosphere are shown:

a) A surficial hole is created by 30km of extension along a low angle fault with exponential geometry, which detaches at a depth of 20km (figure 4.2a).

b) The lithosphere flexes upwards in response to the simple shear crustal thinning as mantle material compensates for the loss of material at the surface (figure 4.2b).

c) An intracrustal detachment allows thinning by pure shear of the lower crust. The space vacated by the thinned crust is replaced by relatively dense mantle material and subsidence results (figure 4.2c).

d) Flexural uplift occurs due to the perturbation caused to the geotherm (figure 4.2d).

The resulting basin geometry and crustal structure (figure 4.2e) represents the modification of the surficial hole caused by the above sequence of flexural isostatic responses. The basin shows uplift of both the footwall shoulder and the distal region. The originally listric fault has a strong upward flexing, while Moho topography is relatively smooth and subdued.

4.4 The Flexural Isostatic Control on the Magnitude of Footwall Uplift and Basin Depth.

The flexural origin of the uplift of the footwall shoulder

is well documented (eg Jackson and McKenzie 1983), and was first formulated by Vening Meinesz (1950), who suggested that following extension along normal faults the hanging wall flexurally subsides to form a rift valley, while the footwall rises due to elastic upbending (see also Heiskanen and Vening Meinesz 1958, Bott 1976, Hellinger and Sclater 1983). The Vening Meinesz theory is limited in application as it assumes that the dip of the fault, along which extension is taking place, to be the main controlling parameter on the flexural behaviour of the footwall and hanging wall blocks. The methodology has also been criticised by Jackson and McKenzie (1983) for yielding approximate predictions for the effects of asymmetric loads and by Weissel and Karner (in press) for being speculative about the interaction between the faulted blocks during extension. The algorithm used for the calculations shown in figure 4.2 assumes that the footwall and hanging wall remain in contact during the rift process and as a result the associated load functions are continuous across the extended region. The method makes it possible therefore to accurately assess the effects of parameters such as extension, pure shear configuration, flexural rigidity and fault dip on basin geometry and crustal structure.

a) The effect of the amount of extension on the magnitude of footwall uplift.

Extension along the fault controls the amount of simple shear crustal thinning which, in turn, controls the magnitude of the flexural isostatic rebound. In figure 4.3 the maximum height of footwall uplift has been plotted

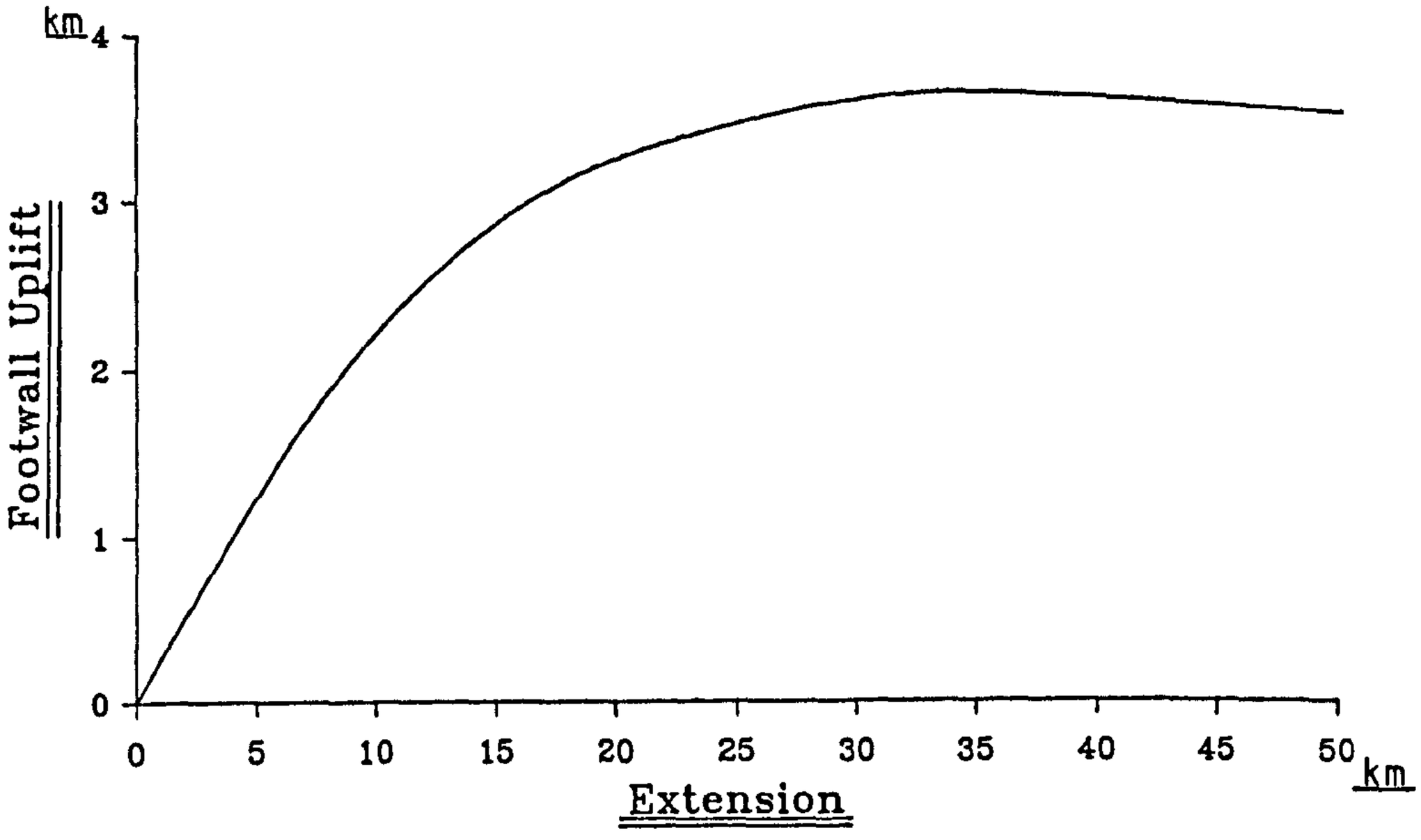

Figure 4.3 - The control of extension on the maximum height of footwall uplift. Extension occurs along a listric fault, which detaches within the crust at a depth 20km. Footwall uplift represents the flexural adjustment of the lithosphere to the simple shear crustal thinning resulting from this extension. Flexural rigidity is defined by a constant elastic thickness of 5km.

against increasing extension along a listric fault detaching at a depth of 20km. The footwall uplift reflects flexural rebound to simple shear crustal thinning only and both pure shear and thermal effects have been ignored in these calculations. Flexural rigidity has been kept constant and defined by a constant elastic thickness of 5km. The plot shows that after extensions greater than about 35km the maximum height of the footwall uplift stabilises at around 3.5km. This is caused partly by the fact that an extreme extension does not cause very much additional crustal thinning as it is mostly accommodated by movement on the horizontal detachment. Also the height of the footwall uplift stabilises when the amount of extension equals or exceeds the flexing wavelength of the lithosphere (see section 8.3b).

b) The effect on footwall uplift and basin depth of increasing flexural rigidity .

In figure 4.4a maximum footwall uplift generated by an extension of 30km along a listric fault with a surface dip of 45° is plotted against elastic thickness. At zero elastic thickness no footwall uplift results - the lithosphere has no flexural strength. At an elastic thickness of 10km the footwall reaches a maximum height of 3.6km, but with a further increase in flexural rigidity the height of the footwall uplift is reduced, until it again becomes zero as elastic thickness approaches infinity. The lateral extent of the uplift of the footwall shoulder is also controlled by flexural strength and in figure 4.4b a widening of the region of footwall uplift is predicted as

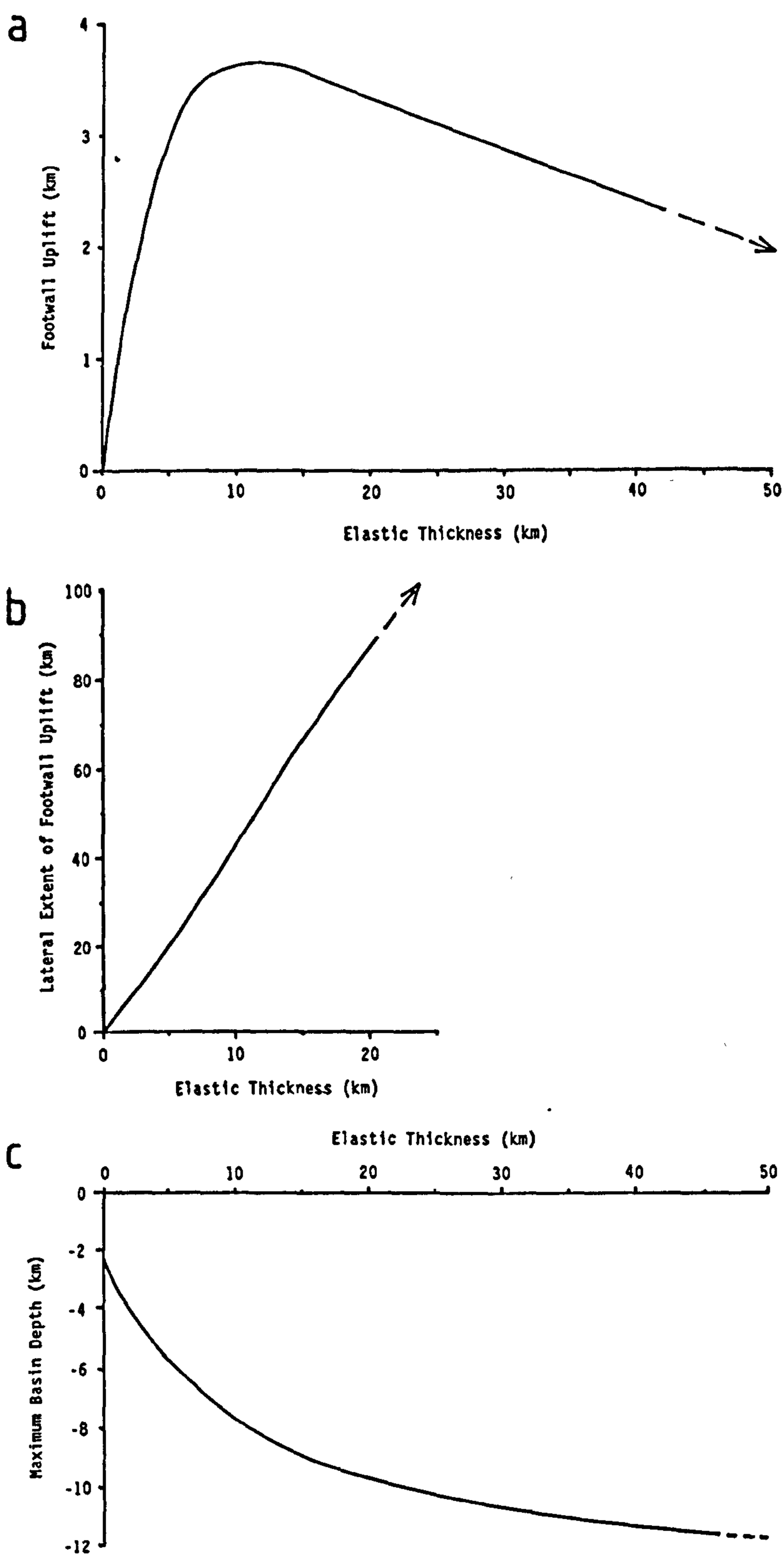

Figure 4.4 - The control of maximum footwall uplift, the lateral extent of footwall uplift and maximum basin depth by elastic thickness are shown in plots a, b, and c. The flexural isostatic response to simple shear crustal thinning only has been considered and both pure shear and thermal effects have been ignored.

flexural rigidity becomes greater.

In figure 4.4c maximum basin depth has been plotted against elastic thickness and shows a basin deepening with increasing flexural rigidity. Airy isostasy (T_e=0) allows maximum rebound to crustal thinning and relatively shallow basins result. As flexural strength increases the lithosphere resists this buoyancy force, resulting in an increased basin depth and therefore reduced Moho topography.

c) The effect of fault dip on the magnitude of footwall uplift.

The angle of dip of the fault controls the geometry of the surficial hole created by the simple shear extension. A steep fault generates a strongly asymmetric buoyancy load, and as a result maximum footwall uplift is increased. This is illustrated in figure 4.5 where flexural rebound resulting from extension along faults with surface dips of 45° and 60° are compared. The amount of flexural rebound is greater from the fault dipping at 60° which reflects the strongly asymmetric and deeper surficial hole created by extension along this fault.

4.5 The Flexural Isostatic Response of the Lithosphere to Basin Infill with Sediment.

Once a basin has formed it rarely remains empty as both water and/or sediment from the surrounding region are deposited in it. The infilling of a basin constitutes an additional load on the lithosphere, causing it to flex downwards (figure 4.6). The calculation of the response of

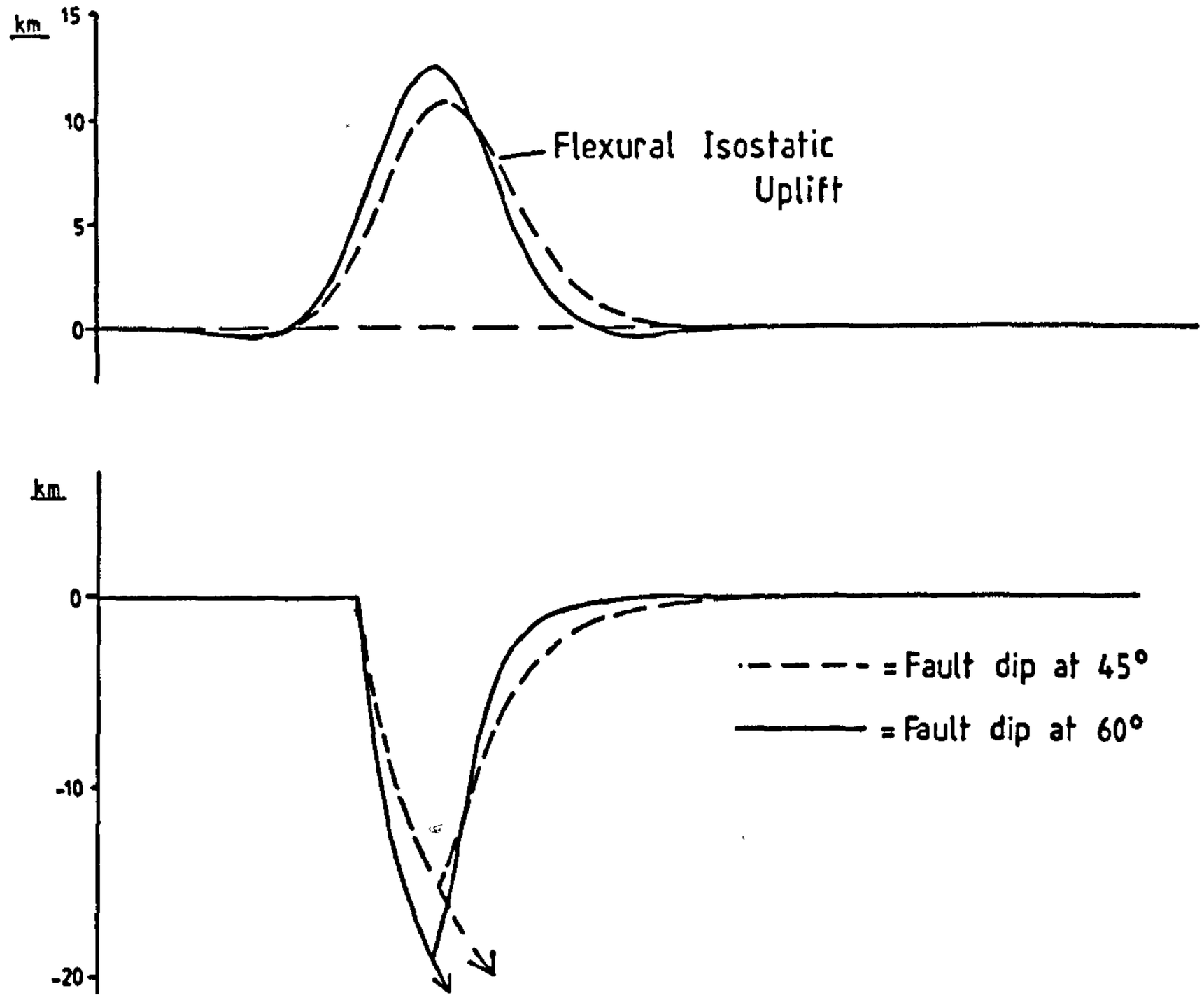

Figure 4.5 - Basin geometry following flexural adjustment to 30km extension along faults dipping at 45° (dotted line) and 60° are compared. The steeper fault generates a greater footwall topography due to the strongly asymmetric flexural uplift profile that has resulted from isostatic adjustment to crustal thinning by simple shear.

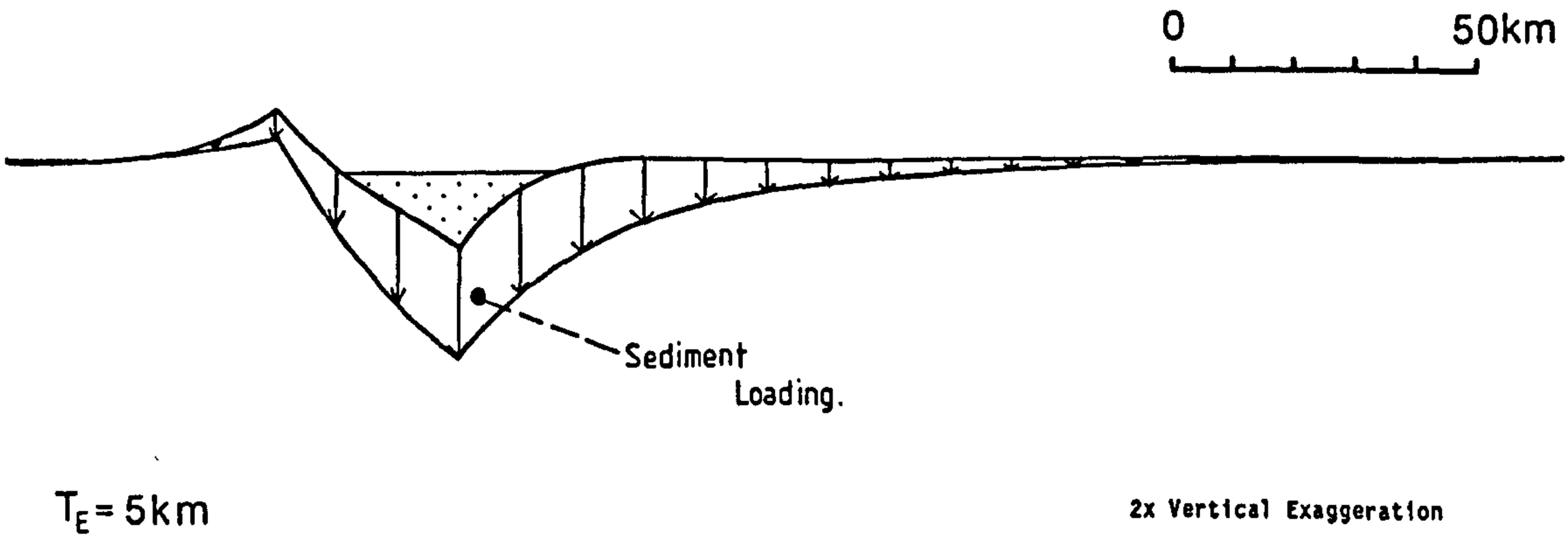

Figure 4.6 - Sediment filling of a basin creates a downward load on the lithosphere and causes a regional downward flexing. However, there is still uplift of the footwall shoulder.

the lithosphere to sediment loading has to take into account that the isostatic restoring force may not be constant across the region of extension. A sediment filled basin has an isostatic restoring force arising from sediment, deposited at the surface, which causes a displacement of mantle material at depth. However, in areas of no sediment deposition, for example the uplifted footwall shoulder, the isostatic restoring force incorporates the replacement of air by mantle material. In order to include this variation in density contrasts across the basin the flexural response of the lithosphere to sediment loading has to be calculated iteratively such that:

a) The initial sediment load is defined by the magnitude of the airfill basin such that:

$$L'_{sa}(x) = B_{(x,t=o)}.p_s.g \quad \text{---- 4.23}$$

where $B_{(x,t=o)}$ is given by equation 4.7.

b) The flexural response due to this load is calculated using a solution to the following equation to define the subsidence $w'_{sa}(x)$:

$$((d^2/dx).(D.d^2w_{sa}(x)/dx^2)) + ((p_m-p_{air}).g.w_{sa}(x)) = L_{sa}(x) \quad \text{---- 4.24}$$

c) The subsidence created by this flexural response defines the next sediment load such that:

$$L''_{sa}(x) = w'_{sa}(x) \quad \text{----- 4.25}$$

d) Steps b and c are repeated. The additional

subsidence created by each additional load increment becomes less and less until convergence occurs.

e) The subsidence created by each increment of sediment load is monitored and when it is less than a prescribed amount the calculation of sediment loading is complete.

4.6 Flexural Rigidity During Thermal Subsidence.

After rifting flexing loads are imposed on the lithosphere due to its overall cooling and additional sediment infill resulting from the extra subsidence created by that cooling. The flexural response of the lithosphere to these load functions can be quantified by solving equation 4.6 and following the sediment loading procedure in section 4.5 respectively. The effect of flexural strength during the post rift thermal subsidence on basin geometry and crustal structure is shown in figure 4.7, where an Airy isostatic rift phase of 30km extension is followed by 100Ma of flexurally compensated (T_e=5km) thermal subsidence. The main effect of the post-rift flexural rigidity is to disperse the thermal subsidence over a substantially broader area compared with the Airy models, which gives the basin a characteristic "Steer's Head" or "Texas Longhorn" geometry (Dewey 1982). At the same time, however, the thickness of this thermal component is reduced considerably compared to the models assuming Airy compensation in chapter 3.

Post-rift flexure has little effect upon fault geometry and Moho topography. This suggests that the deformed fault geometry and extreme Moho topography apparent in figure 4.7 have been "frozen in" from the Airy compensated rift phase.

a

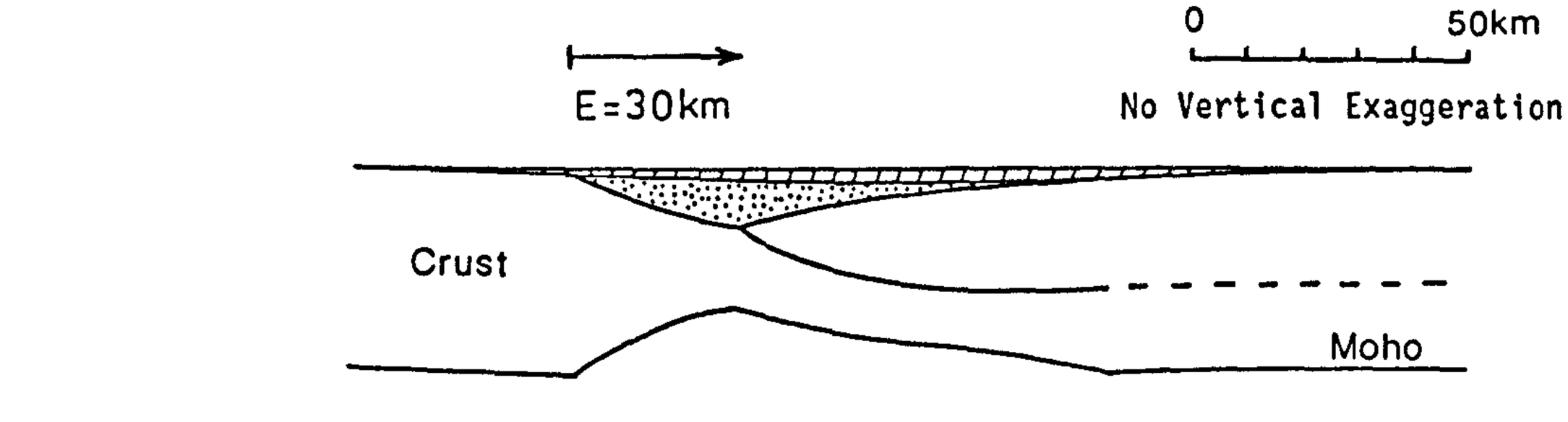

b

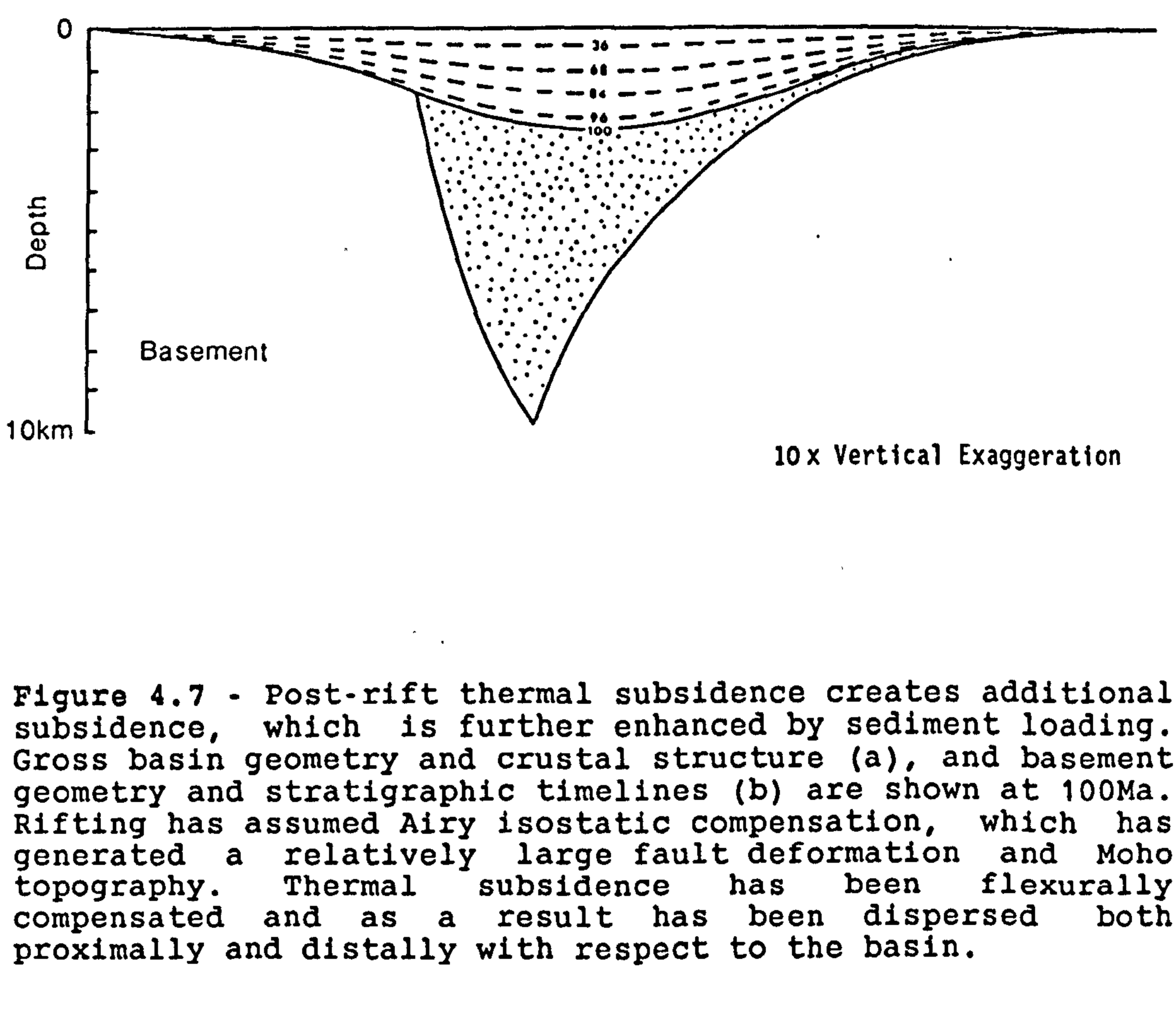

Figure 4.7 - Post-rift thermal subsidence creates additional subsidence, which is further enhanced by sediment loading. Gross basin geometry and crustal structure (a), and basement geometry and stratigraphic timelines (b) are shown at 100Ma. Rifting has assumed Airy isostatic compensation, which has generated a relatively large fault deformation and Moho topography. Thermal subsidence has been flexurally compensated and as a result has been dispersed both proximally and distally with respect to the basin.

4.7 Simple Shear - Pure Shear Model Results Incorporating Flexural Rigidity in Syn- and Post-Rift Components of Basin Evolution.

The coupled simple shear-pure shear model has been used to predict basin geometry and crustal structure following 30km extension along a low angle fault. A finite flexural rigidity, defined by an elastic thickness of 5km, has been assumed throughout both syn- (dotted ornament) and post-rift (shaded ornament) phases of basin evolution. The effects of sediment loading to sea level have also been calculated. Basin geometry and crustal structure are shown 100Ma after rifting.

a) The effect of position and width of pure shear on basin geometry.

In figures 4.8a and 4.8b the effect of increasing the offset of the pure shear deformation with respect to the simple shear is shown, while in figure 4.8c the effect of a reduced width of pure shear deformation is illustrated. The models show an uplift of the footwall shoulder caused by the flexural rebound of the lithosphere to simple shear crustal thinning. The basins are shallower compared to those generated under Airy isostatic conditions (eg. figure 3.2) and, in turn, fault deformation and Moho topography are more subdued. These features are a further consequence of flexurally dampened lithosphere rebound to simple shear crustal thinning. The flexural strength of the lithosphere during the post-rift stages of basin evolution causes a broadening of the basin into the distal region due to

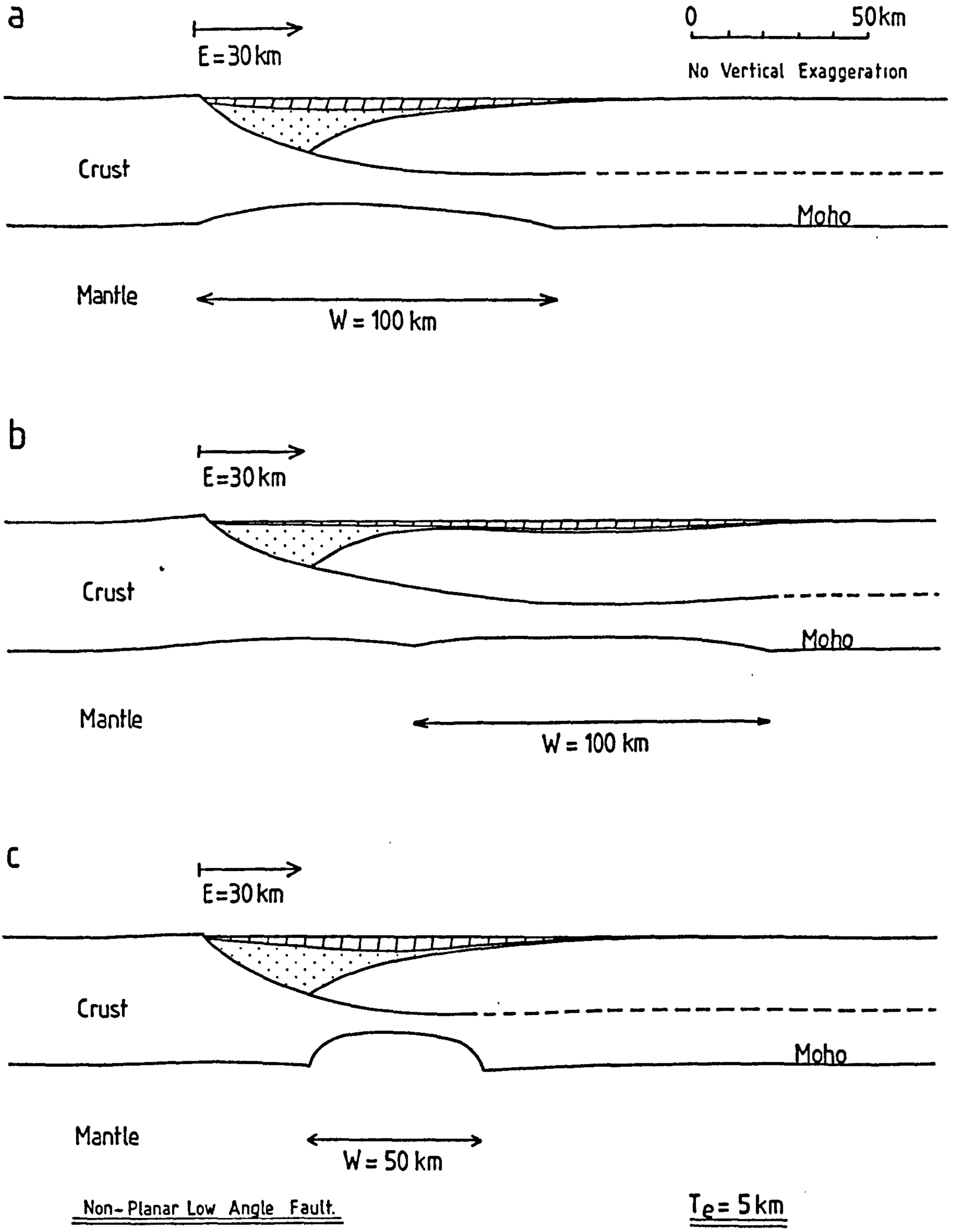

Non-Planar Low Angle Fault. T_e= 5km

Figure 4.8 - Sedimentary basin geometry and crustal structure predicted by the coupled simple shear-pure shear model at 100Ma after an extension of 30km on a listric fault. The detachment depth is 20km and flexural rigidity is defined by an elastic thickness of 5km.

The distribution and geometry of both rift (dotted ornament) and thermal (shaded ornament) components are dependent upon the relative lateral positions of pure and simple shear deformations with respect to one another (compare a and b).

W indicates the width of the pure shear, which has been reduced in c to 50km, causing and extreme Moho topography and exaggerated thermal subsidence.

thermal and sediment loading being dispersed over a wider region. In figure 4.8b 60km offset between the simple and pure shear deformations has caused a broadening of the basin distally, as the pure shear depocentre is laterally displaced with respect to the simple shear sub-basin. The basin is not widened in the proximal region as footwall uplift prevents any sediment deposition in this area.

In figure 4.5c the width of the pure shear has been reduced to 50km and as a result its deformational effects have been concentrated into a relatively small region. A narrow, deep basin with an exaggerated thermal subsidence component results.

b) The effect of detachment depth.

Increasing the detachment depth from 20km to a basal crustal depth of 35km is shown in figures 4.9a and 4.9b respectively. Deepening the detachment produces a narrower basin as pure shear thinning of the crust is eliminated. However, the differences between the two models are not as pronounced as the similar Airy models in figure 3.4 because the effect of finite flexural rigidity is to dampen and disperse the deformational forces generated by the loading of the lithosphere.

A flexural Wernicke-type model (figure 4.9c) also generates a relatively narrow basin. Pure shear produces a thermally driven uplift in the distal region at rifting, which, in the absence of erosion, is brought back down to sea level by the post rift thermal subsidence.

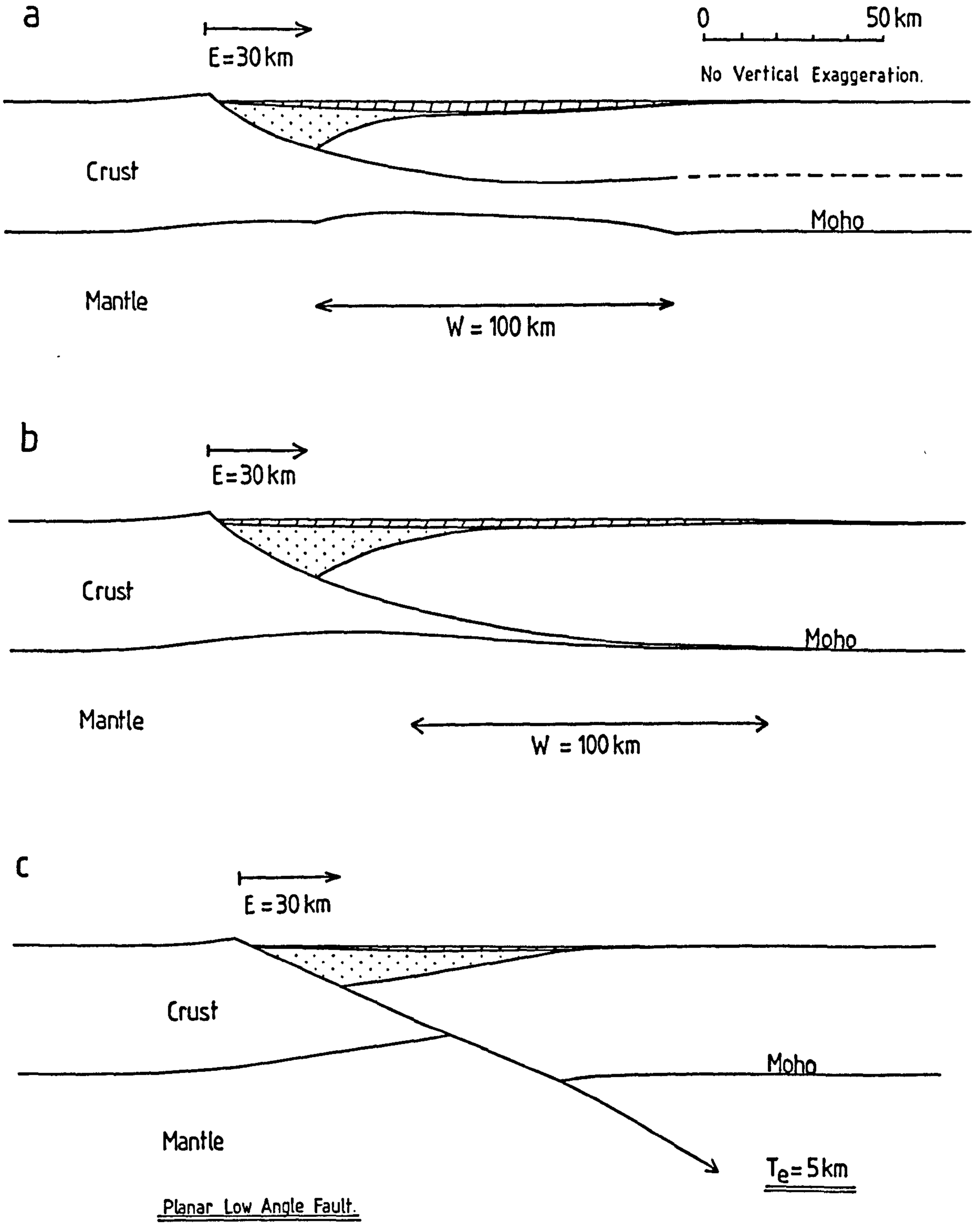

Figure 4.9 - The effect of detachment depth; intracrustal (a), moho (b) and base of lithosphere (c). An intracrustal detachment allows thinning of the crust by pure shear, whereas deepening the detachment to the base of the crust or into the mantle ensures that the pure shear is responsible only for perturbing the geotherm. This causes uplift of the surface in the distal region at rifting, followed by its return back to sea level during thermal subsidence.

c) The effect of fault dip.

One of the most powerful influences on basin geometry is the shape of the fault. The equation defining the depth of a listric fault, $D_{(x)}$, has been given in equation 2.1 such that:

$$D_{(x)} = 0 \qquad \text{for } x \leq x_o$$

$$D_{(x)} = Z_d \,.\, (1-\exp(-x/Z_d)) \qquad \text{for } x > x_o \quad \text{---- 4.26}$$

where Z_d is the depth of the detachment and x_o defines the position of the footwall cut-off.

Differentiation of equation 4.26 with respect to x gives:

$$dD_{(x)}/dx = \exp(-x/Z_d) \quad \text{---- 4.27}$$

If x=0 then equation 4.27 can be solved to give the surface dip, Θ, of the fault such that:

$$dD_{(x)}/dx = 1$$

$$= \tan \Theta \quad \text{---- 4.28}$$

For equation 4.26 Θ will be 45°.

In order to vary the angle of dip of the fault a scaling factor, k, can be applied to equation 4.26 such that:

$$D_x = Z_d \,.\, (1-\exp(-x.k/Z_d)) \quad \text{---- 4.29}$$

where $k = \tan \Theta$

In figure 4.10a to 4.10c three models are shown with exponential faults originally dipping at 30°, 45° and 60° respectively. All other parameters, that is extension, pure

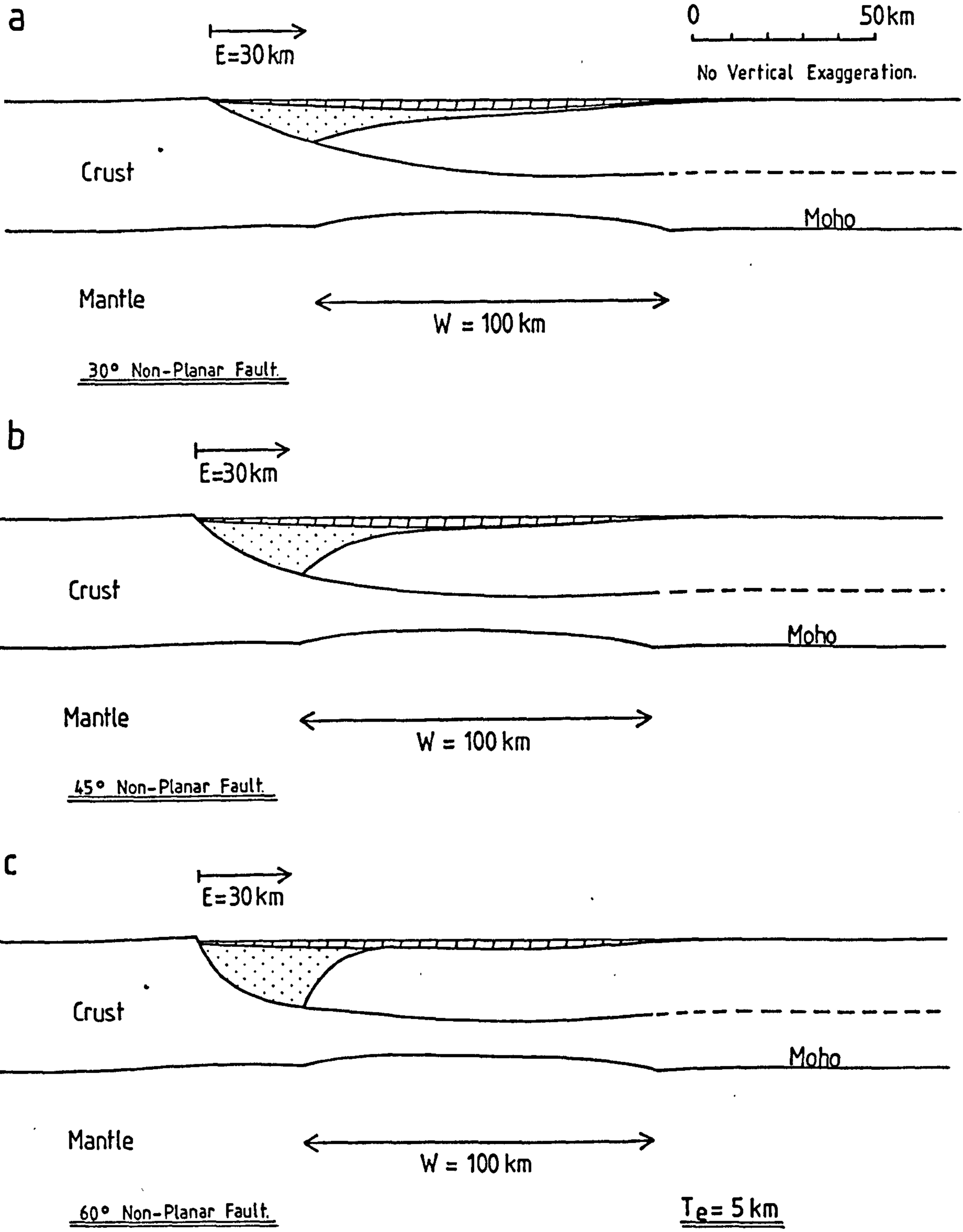

Figure 4.10 - Basin development and crustal structure following extension along faults with original near surface dips of 30° (a), 45° (b) and 60° (c). Basin depths are increased, but lateral extent is reduced as the dip of the fault increases.

shear configuration, etc., have been kept constant for each of the models. Extension along a shallowly dipping fault (figure 4.10a) produces a rift basin with a maximum thickness of about 12km and a lateral extent of approximately 130km. In figure 4.10c the fault was originally steeply dipping at 60° and shows an increase in the maximum thickness of the rift component by some 6km, whereas cross-sectional width is reduced by some 50km compared to the model in figure 4.10a. Therefore, a steepening of the fault increases the amount of simple shear crustal thinning in the depth dimension but reduces it laterally. This is because a steep fault flattens into a horizontal detachment within a relatively small lateral distance and as a consequence the hanging wall collapses directly onto a more or less horizontal detachment, thus a large maximum basin thickness results.

d) The effect of fault shape.

In figure 4.11a and 4.11b models generated by extension along a listric and planar fault are shown respectively. Extension along an originally planar fault has generated a symmetrical basin with a flat base due to hanging wall collapse onto a flat detachment. The implications of this are further discussed in chapter 10.

The vertical stacking of brittle and plastic layers within the lithosphere supports the existence of ramped fault-detachments. In figure 4.11c extension along a fault with a ramped geometry is shown. This produces two distinct basins - the most proximal of the basins has formed due to hanging wall collapse directly onto the footwall, whereas the distal

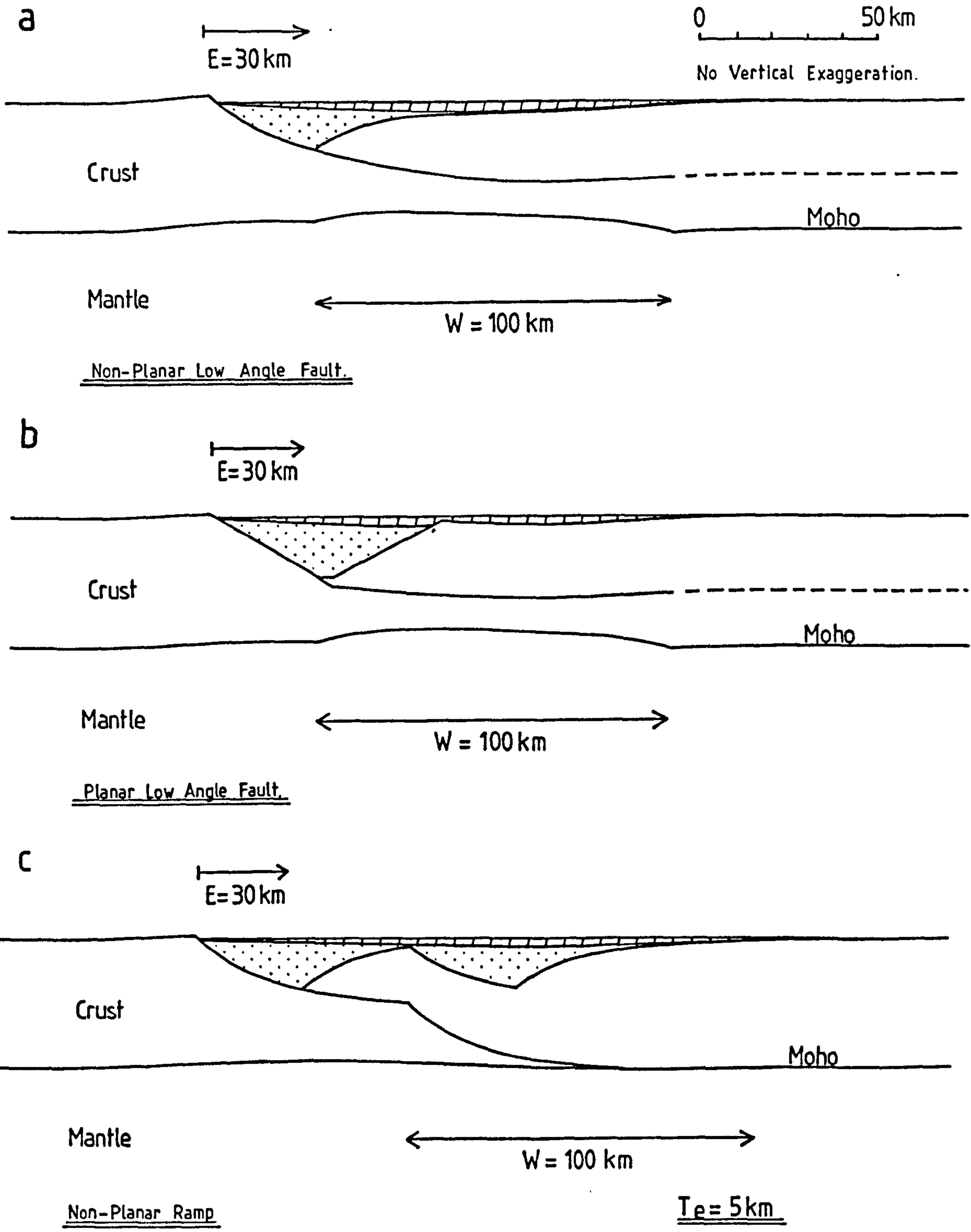

Figure 4.11 - Extensions on listric (a) and planar faults (b) are compared. A symmetrical basin geometry is created by extension along a planar fault due to hanging wall collapse onto a flat detachment.

Extension along a ramped fault-detachment geometry (c) generates two basins. The distal basin is caused by hanging wall sag following movement over the ramp. Post-rift thermal subsidence blankets both basins.

basin has formed by hanging wall sag following movement over the ramp. The position of the distal basin is therefore determined by the lateral position of the ramp while its shape is controlled largely by shape of the ramp cusp.

4.8 Summary.

This chapter has included a description of both the theory of flexural rigidity and its effect on extensional basin formation. It has been shown that flexural strength during rifting produces an uplift of the footwall shoulder, a relatively deep basin, a smooth fault geometry and a less extreme Moho topography relative to the Airy isostatic models (see chapter 3). Flexural rigidity during post rift thermal subsidence reduces this component to about 20 percent of the basin thickness, but at the same time thermally induced deposition is promoted in the distal region of the basin.

CHAPTER 5

A Numerical Study of the Jeanne d'Arc Basin and Implications on the Evolution of Extensional Sedimentary Basins.

5.1 Introduction.

In the previous chapters a coupled simple shear-pure shear model has been used to investigate sedimentary basin formation and crustal structure following extensional tectonics. In this section model predictions are tested and compared against geological and seismic data from an extensional sedimentary basin in the Grand Banks region, Newfoundland. At the same time, modelling techniques are applied so as to provide quantitative explanations of some of the features apparent in the stratigraphic record of the basin.

5.2 The Jeanne d'Arc Basin.

The Grand Banks region forms the continental shelf off the east coast of Newfoundland (figure 5.1) and consists of a series of extensional sedimentary basins bounded by low angle faults, with a north-south orientation in the northern part of the region and a gradual re-orientation to a north-east/south-west alignment in the southern part. These faults range in age from the Precambrian to Early Palaeozoic when the Grand Banks region was built-up from the accretion of numerous terrains. Extension during the Mesozoic made use of these inherited crustal weaknesses and produced the present configuration of sedimentary basins seen in figure 5.1. In this chapter the simple shear-pure shear lithosphere extension model has been used to predict the extensional

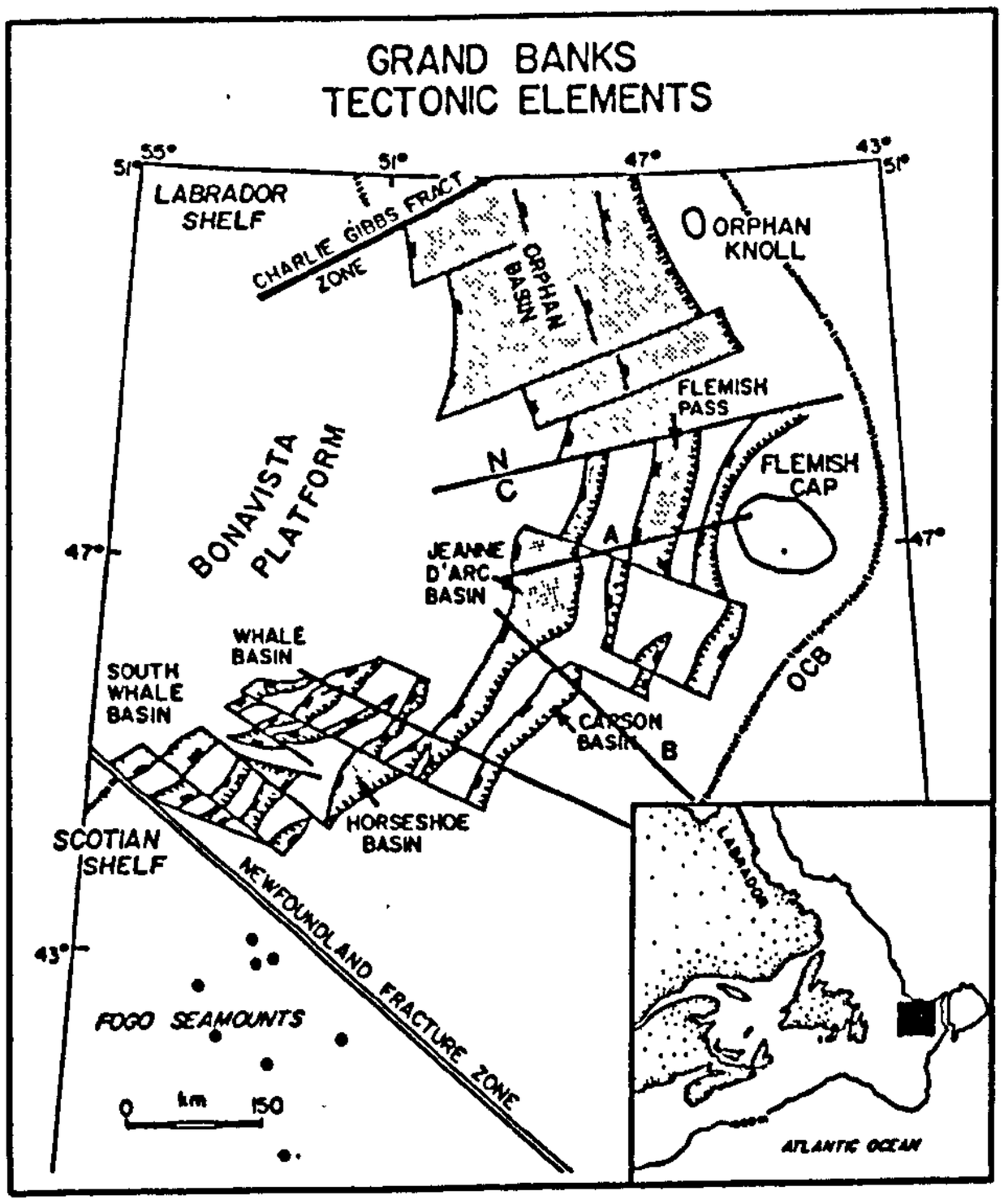

(adapted from Tankard & Welsink, 1987)

Figure 5.1 - The Grand Banks region contains Mesozoic sedimentary basins bounded by easterly dipping major low angle faults. The Jeanne d'Arc basin, in the centre of the region, has been numerically modelled using information derived from deep seismic reflection profiles A and B across the north and south of the basin, and from regional exploration data summarised by Tankard and Welsink (1987).

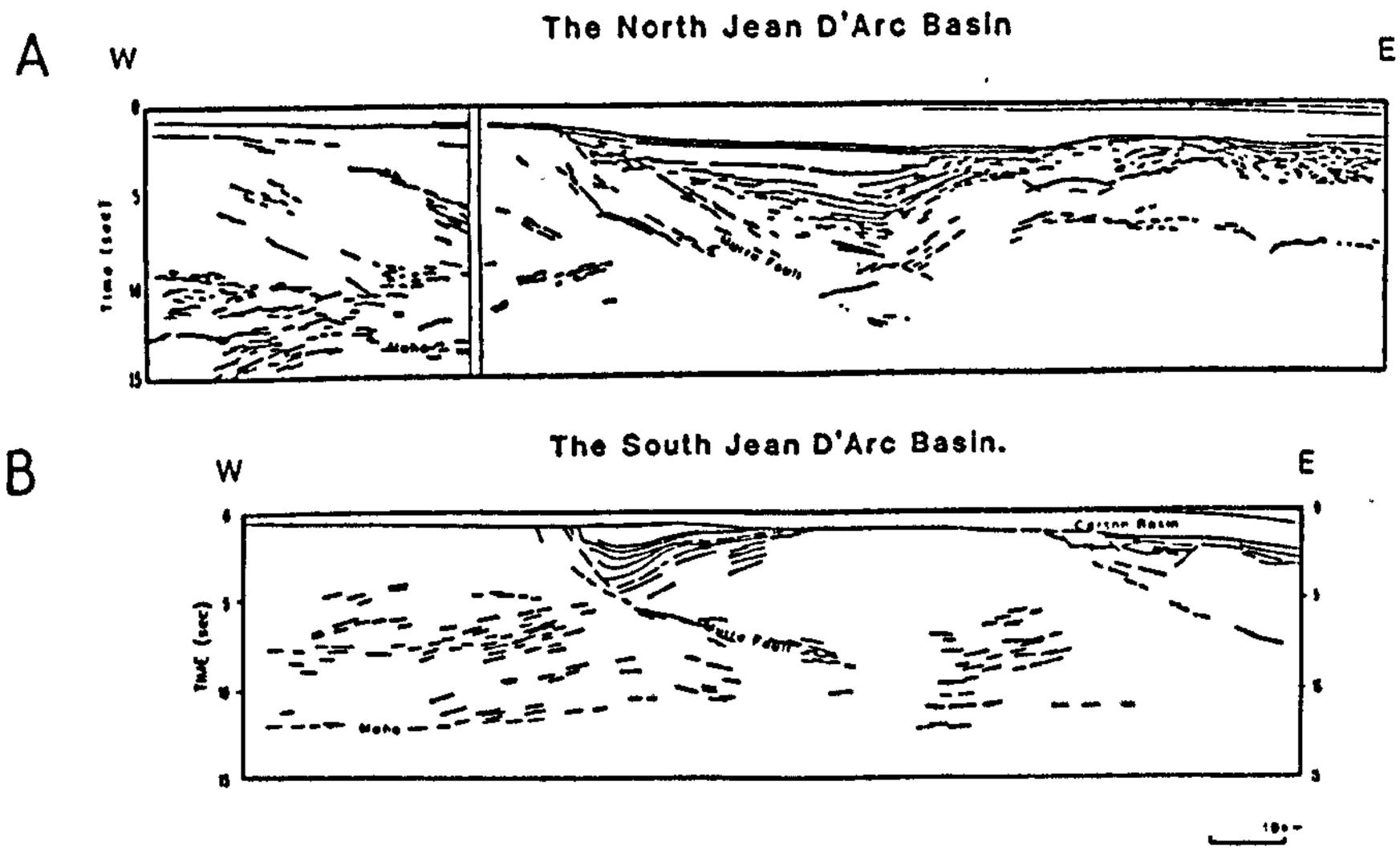

Figure 5.2 - Seismic reflection profiles (Keene et al 1987) across the North Jeanne d'Arc basin (profile A) and the South Jeanne d'Arc basin and adjacent Carson basin (profile B). The Jeanne d'Arc basin has formed in the hanging wall of the Murre fault.

evolution of the Jeanne d'Arc basin, located in the centre of the Grand Banks region. Geological and seismic data on the basin has been obtained from a variety of sources including Jansa and Wade (1975), Enachescu 1987), Keen et al (1987), Tankard and Welsink (1987).

Deep seismic reflection lines (Keen et al, 1987) show major crustal reflectors across the North and South Jeanne d'Arc basin and adjacent Carson basin respectively (figure 5.2). The seismic data shows the clear relationship between the Jeanne d'Arc basin and the Murre fault, whereby the basin has formed by hanging wall collapse following extension along this fault. The Murre fault has a near surface dip of approximately 35°, an exponential geometry and detaches at a depth of about 26km (ie. 8s TWT).

The northern Jeanne d'Arc basin has been formed following some 30 km of extension along the Murre fault and has a maximum sediment thickness of approximately 18 km. The southern part of the basin is much smaller with approximately 8 km extension along the fault and a maximum sediment thickness of around 6 km. The Moho is identified by the lower termination of strong reflections in the lower crust and is relatively flat at about 35km (ie. 10s TWT).

The tectono-stratigraphic construction and cross-section shown in figures 5.3a and 5.3b, and taken from Tankard and Welsink (1987), suggest that the Jeanne d'Arc basin evolved by the following sequence of events:

a) Triassic rifting, accounting for between 5km and 10km of movement along the fault.

a

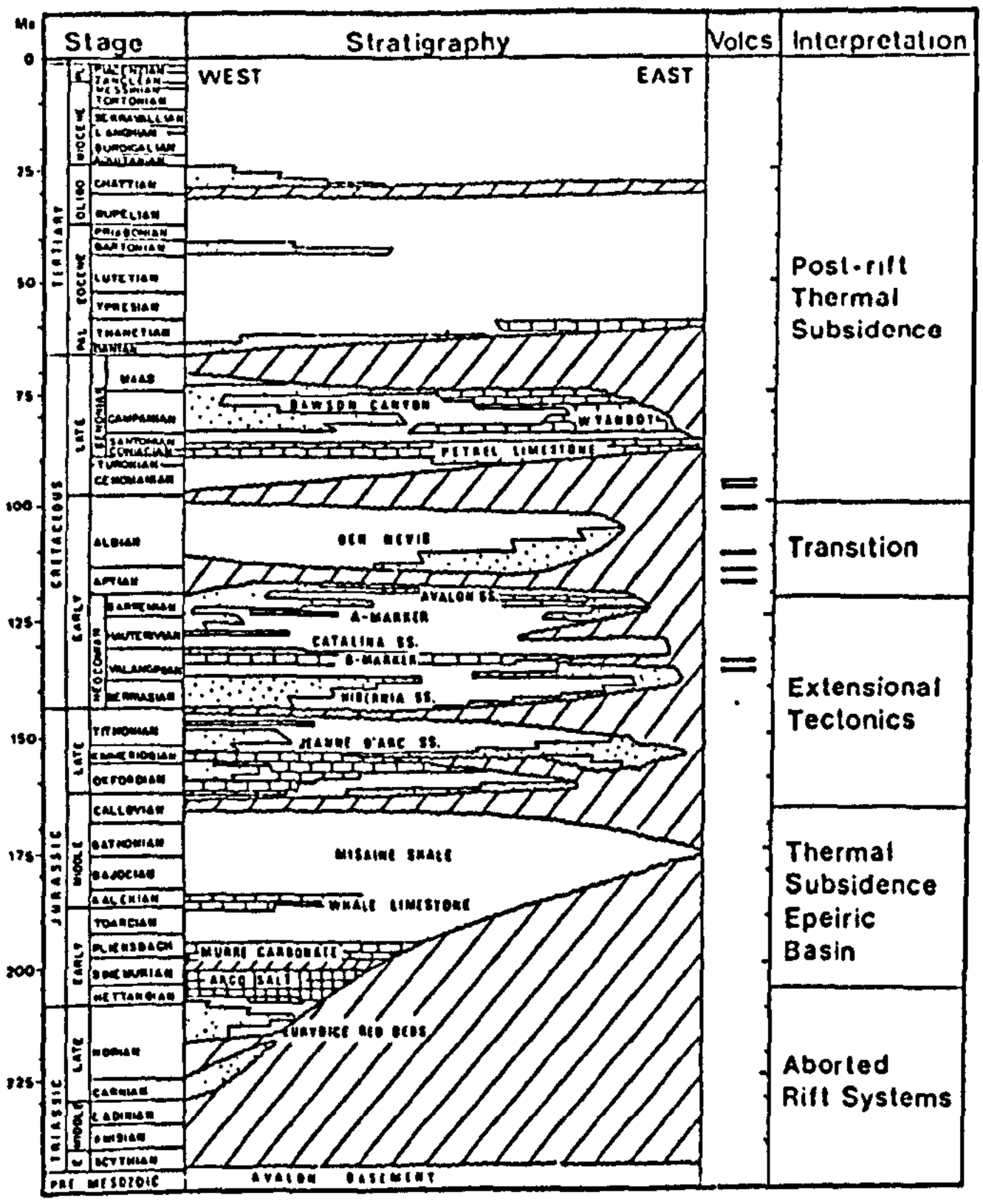

b

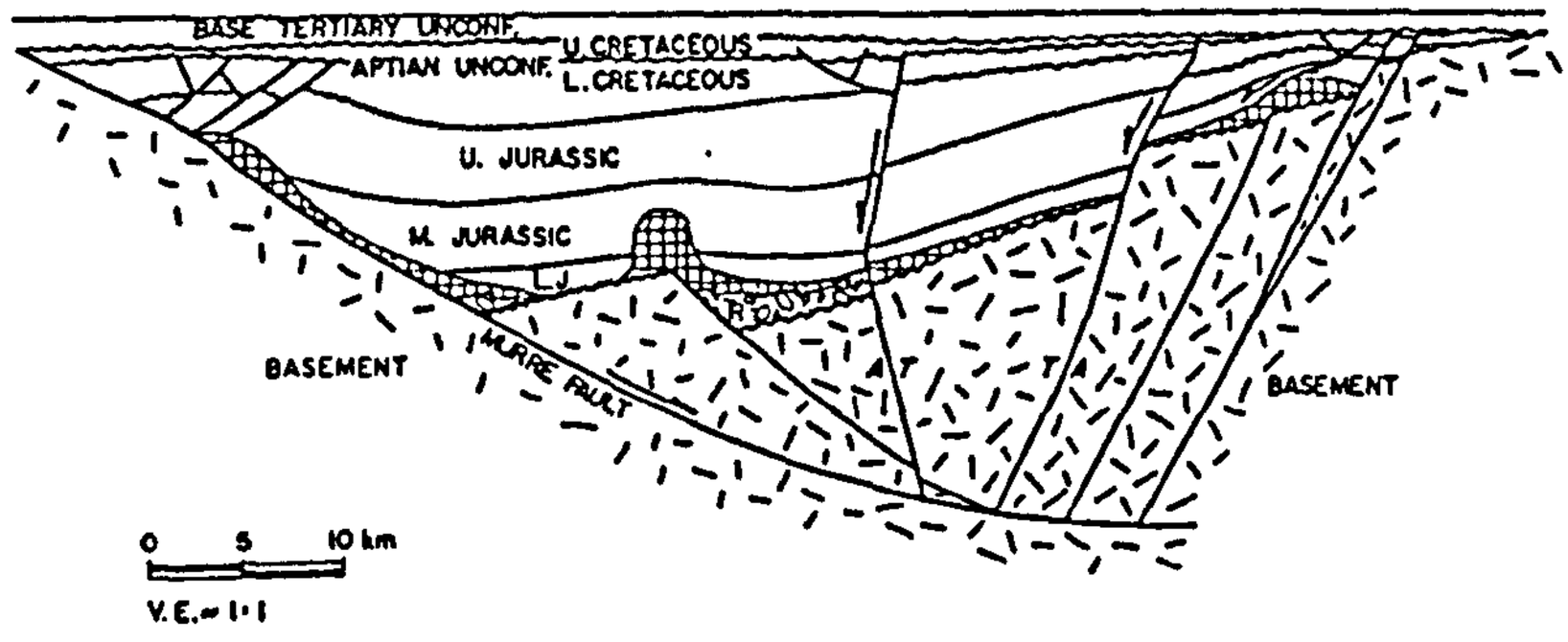

(after Tankard & Welsink 1987)

Figure 5.3 -

a) The evolution of the Jeanne d'Arc basin began with Triassic rifting. This was followed by a period of post-rift thermal subsidence during the Early to Mid Jurassic. Rifting resumed in the late Jurassic, and continued to the end of the Late Cretaceous, which was marked by a period of regional uplift and erosion to form the Avalon unconformity. Thermal subsidence then occurred to the present day.

b) Schematic cross-section across the Jeanne d'Arc basin shows the initial Triassic rift event to be relatively minor. Most of the deposition in the basin occurred from the Upper Jurassic to Lower Cretaceous.

b) Early to Middle Jurassic thermal subsidence.

c) Late Jurassic to Early Cretaceous rifting in which approximately 20km to 25km of movement occurred along the Murre fault.

d) Regional uplift and erosion at the end of the Early Cretaceous, which led to the formation of the Avalon/Aptian unconformity (Jansa and Wade 1975, Enachescu 1987).

e) Post Early Cretaceous subsidence to the present day.

5.3 Application of the Coupled Simple Shear - Pure Shear Model to the Formation of the Jeanne d'Arc Basin.

a) Airy isostatic model.

The coupled simple shear-pure shear model has been used to investigate the evolution of the North Jeanne d'Arc basin. In figure 5.4a sedimentary basin geometry and crustal structure are shown arising from the geometric, thermal and Airy isostatic response of the lithosphere to 30km of extension along a shallowly dipping listric fault, which flattens into an intracrustal detachment at a depth of 26km. The syn-rift basin component is denoted by dotted ornament, while post-rift thermal subsidence is denoted by diagonal ornament. 100Ma of the post-rift subsidence is shown in order to represent the post Early Cretaceous deposition recorded in the present stratigraphy of the Jeanne d'Arc basin. The assumptions made for the modelling are:

a) Rifting is instantaneous.

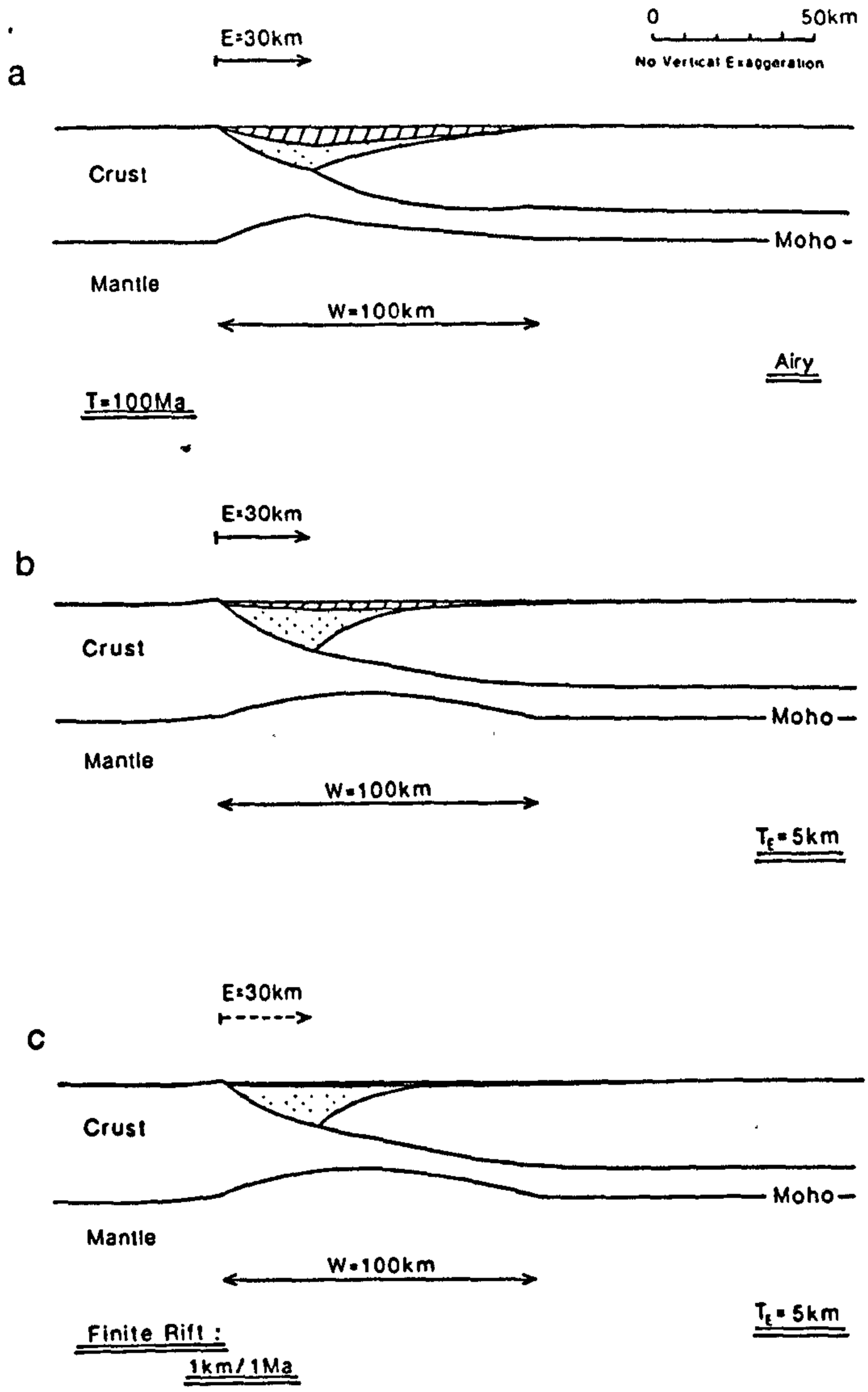

Figure 5.4 -

Numerical models of the formation of the North Jeanne d'Arc basin. 30 km of extension has been modelled along a shallowly dipping fault with exponential geometry and detaching at 26km depth. Dotted and shaded ornaments represent syn- and post-rift basin components respectively. Basin geometry and crustal structure are shown at 100Ma after rifting.

a) Airy compensation generates relatively shallow basin depths, a large fault deformation and extreme Moho topography. The proportion of post-rift thermal subsidence is also much larger than suggested by the geological and seismic data.

b) A flexural model removes the problems arising from Airy compensation - the basin is deepened to about 18 km, the fault geometry is smooth and Moho topography subdued. The predicted thickness of the post-rift subsidence is very similar to the 3km of Post Early Cretaceous thermal phase seen in the basin at present.

c) Finite or non-instantaneous rifting does not have a great effect on the gross structure of the basin. However, it considerably reduces the proportion of post-rift thermal subsidence.

b) Sediment loading occurs to sea level throughout all phases of basin evolution.

c) Pure shear deformation in the lower lithosphere has zero offset with respect to the upper simple shear and is distributed over 100 km.

The maximum basin depth predicted by the Airy isostatic model is 13.5 km, which is less than the thickness of over 18 km indicated by the seismic data. The model also shows a significant deformation of the fault geometry and substantial Moho topography. The amount of thermal subsidence accounts for approximately 50% of the total sediment thickness - substantially more than is observed in the basin.

b) Flexural isostatic model.

The initial model assumed that any loads imposed on the lithosphere were compensated by Airy isostasy (chapter 2), which is unrealistic, as the lithosphere flexes in response to superimposed loads - it possesses a finite flexural rigidity (eg. Watts et al 1982). Figure 5.4b assumes the lithosphere to have flexural strength in both syn- and post-rift phases of basin evolution. The flexural rigidity is defined by a constant elastic thickness of 5 km and its effect during rifting is to both dampen and laterally distribute the isostatic rebound in response to crustal thinning by simple shear. As a consequence, the basin is deepened to 17.5 km, the footwall rift shoulder is uplifted, the fault geometry is smooth and Moho topography is relatively subdued. Flexural strength during thermal

subsidence reduces this component to about 20% of the total sediment thickness, but at the same time thermally induced deposition is promoted in the distal region of the basin.

c) Finite rifting model.

The tectano-stratigraphic analysis of the Jeanne d'Arc basin by Tankard and Welsink (1987) in figure 5.3 shows it did not evolve with a single instantaneous rift but over a finite time period. Figure 5.4c shows a finite rifting model in which 30km of extension exhibited in the North Jeanne d'Arc basin has been modelled at a rate of 1 km per Ma over 30Ma. The effect of this finite rifting is not great on the gross structure of the basin, although it does have a significant effect on the thickness of the post-rift subsidence. The perturbation of the geotherm during an individual rift increment will have time to re-equilibrate during successive rift events. At the completion of rifting, less unequilibrated geotherm remains and post-rift thermal subsidence is therefore reduced. The algorithm used to calculate the temperature structure following finite rifting by a simple shear-pure shear process allows the perturbation caused to the geotherm by an individual rift increment to be added onto those arising from successive rift increments. The calculations also take into account the movement of the perturbation in the hanging wall due to incremental movements along the fault. A formulation of the geometric, thermal and isostatic components of finite rifting is given in Appendix 5 at the end of the chapter.

5.4 Flexural Erosion and the Avalon-Aptian Unconformity.

The Avalon-Aptian unconformity separates the main rift phase from the post-rift thermal sag in the Jeanne d'Arc basin (Enachescu 1987) and most likely explains the removal of the footwall uplift predicted by the models shown in figures 5.4b and 5.4c. Erosion of the discrete pockets of topography caused by the syn-rift flexural strength of the lithosphere (figure 5.5a) can provide the driving force for regional uplift across the whole basin as the lithosphere flexurally rebounds to a new isostatic equilibrium (figure 5.5b). The amount of flexural rebound, $w_{er}(x)$, occurring in response to this erosion is given by the solution of the following equation:

$$d^2/dx^2.(D.d^2w/dx^2) + (p_m-p_{air}).g.w_{er}(x) = p_c.g.U_{(x,t=0)} \quad \text{----- 5.1}$$

where D is flexural rigidity, g is acceleration due to gravity, $U_{(x,t=0)}$ is uplifted basement following rifting and p_m, p_c and p_{air} are the densities of mantle, crust and air respectively.

Further erosion of this regional uplift generates a regional unconformity (figure 5.5c). This process is iterative as erosion induces yet more flexural rebound, but on a smaller scale due to flexural dampening. Calculation of this iterative uplift requires not only the isostatic adjustment to eroded basement to be taken into account (equation 5.1), but also erosionally induced uplift arising from the removal of sediment from within the basin. The flexural rebound caused by the erosion of sediment, $w_{erx}(x)$, has been

a Erosion of Peripheral Topography

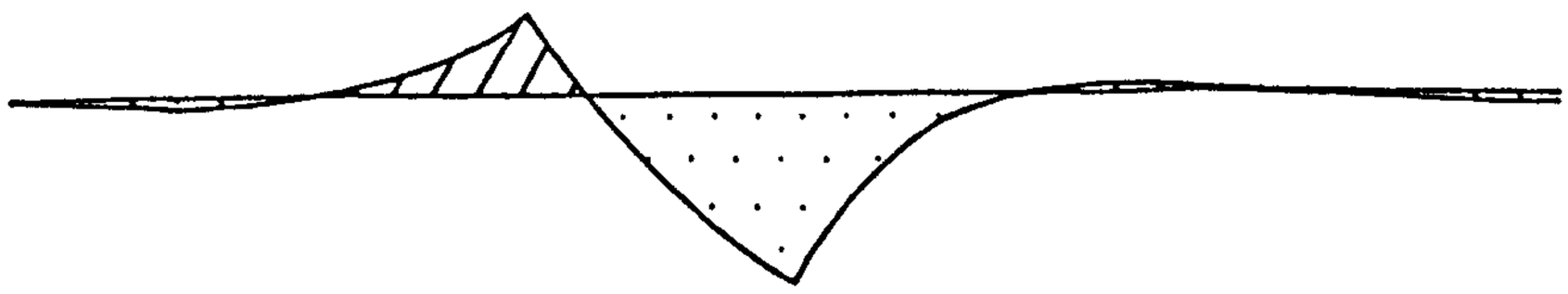

b Erosionally Induced Uplift

C Regional Erosion Surface

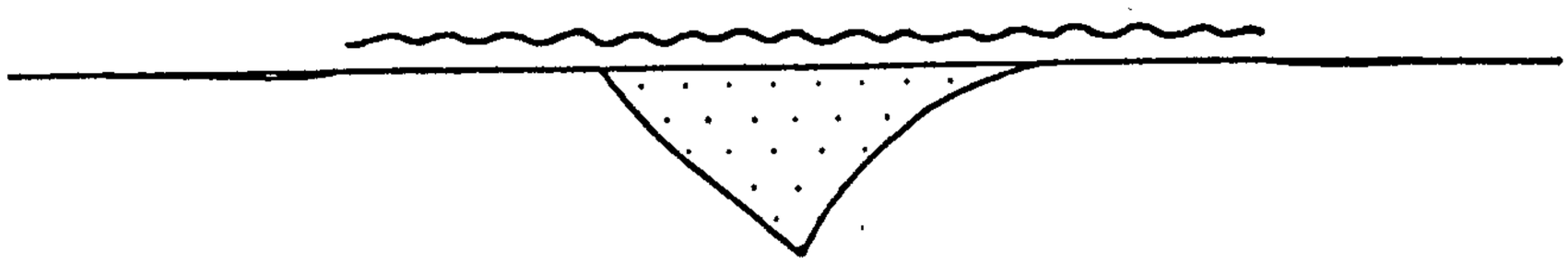

Figure 5.5 - The erosion of topography at the basin periphery (a) induces regional uplift due to flexural isostatic rebound (b). Further erosion of this new topography generates a regional erosion surface (C).

calculated using a solution to the following equation:

$$d^2/dx^2.(D.d^2w_{(x)}/dx^2 + (p_m-p_{air}).g.w(x) = p_s.g.US_{(x)} \quad \text{---- 5.2}$$

where $US_{(x)}$ defines the amount of sediment within the basin that has been uplifted through isostatic adjustment to erosion.

The regional erosion surface created in the Jeanne d'Arc basin has been buried due to thermal subsidence. This is illustrated in figure 5.6 where instantaneous rifting has been followed by erosion of uplifted topography and, in turn, 100Ma of thermal subsidence.

The above hypothesis relies upon the flexural isostatic response of the lithosphere to generate a regional erosion surface. There are two immediate weaknesses with this hypothesis:

a) The basin is assumed to be filled to sea level so that erosionally induced uplift brings material above sea level to be eroded.

b) The rate of thermal subsidence is assumed not to be greater than the rate of erosionally induced uplift.

The feasibility of the second assumption is tested in figure 5.7 where predicted thermal subsidence for the proximal (110km), central (130km) and distal (180km) regions of the basin are compared to erosionally generated uplift (dotted line). The proximal region shows 500m of erosionally induced uplift, which takes 25 Ma to thermally subsided below sea

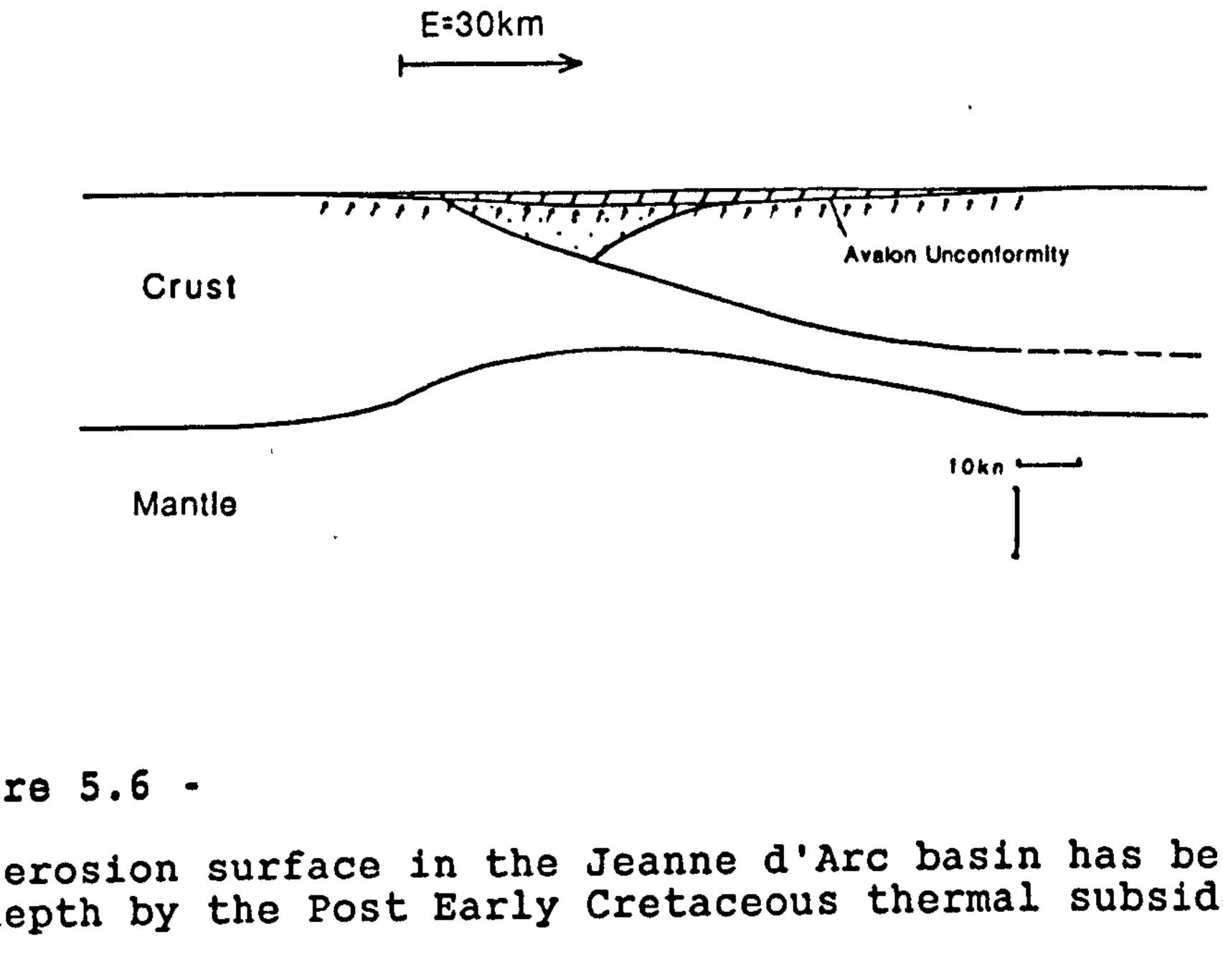

Figure 5.6 -

The erosion surface in the Jeanne d'Arc basin has been taken to depth by the Post Early Cretaceous thermal subsidence.

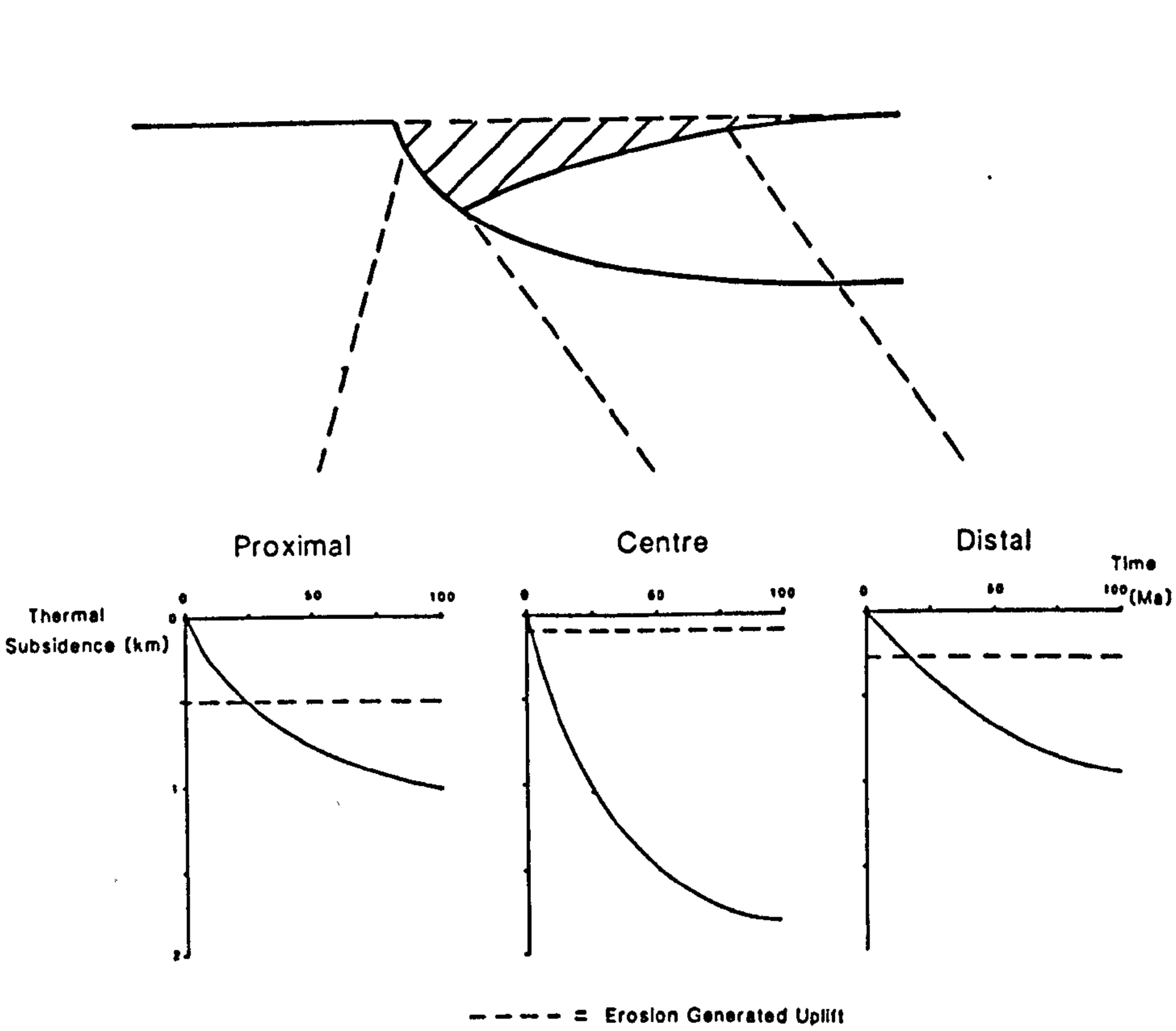

Figure 5.7 - The validity of the flexural erosion hypothesis can be questioned on the grounds that flexural rebound induced by the peripheral erosion will be offset by thermal subsidence. A comparison, however, of thermal subsidence against erosionally induced uplift does not invalidate the idea.

level. In the centre of the basin, however, the uplift due to erosion is about 100m and this subsides below sea level in less than 3Ma. Erosion rates must have therefore been very fast in the centre of the basin in order for the footwall uplift erosion hypothesis to be a viable mechanism to generate the Avalon unconformity. However, the proximity of Atlantic rifting to the Jeanne d'Arc basin may have aided uplift by regional heating of the lower lithosphere and by magmatic underplating of the crust (White et al 1987[1] and 1987[2], Keen and de Voogd 1988, McKenzie and Bickle in press). A drop in sea level could also have exposed new basement to the effects of subaerial erosion, although there is a lack of consistent and accurate eustatic data to investigate this possibility.

5.5 Multi-phase Rifting.

Figure 5.8a shows a model based on Tankard and Welsinks' (1987) interpretation, in which the evolution of the basin is shown to be a two stage rift process. A formulation of this finite rifting method is given in Appendix 5. The model contains a small rift increment due to Triassic extension in addition to the main rift phase in the Upper Jurassic-Lower Cretaceous. Sandwiched between these two syn-rift sequences (represented by dotted ornament) are 40Ma of pre-Upper Jurassic thermal subsidence (diagonal ornament). Post Early Cretaceous thermal subsidence blankets the whole of the basin.

Subsidence versus time plots are shown (figure 5.8b) for the proximal (110km), central (130km) and distal (180km) regions

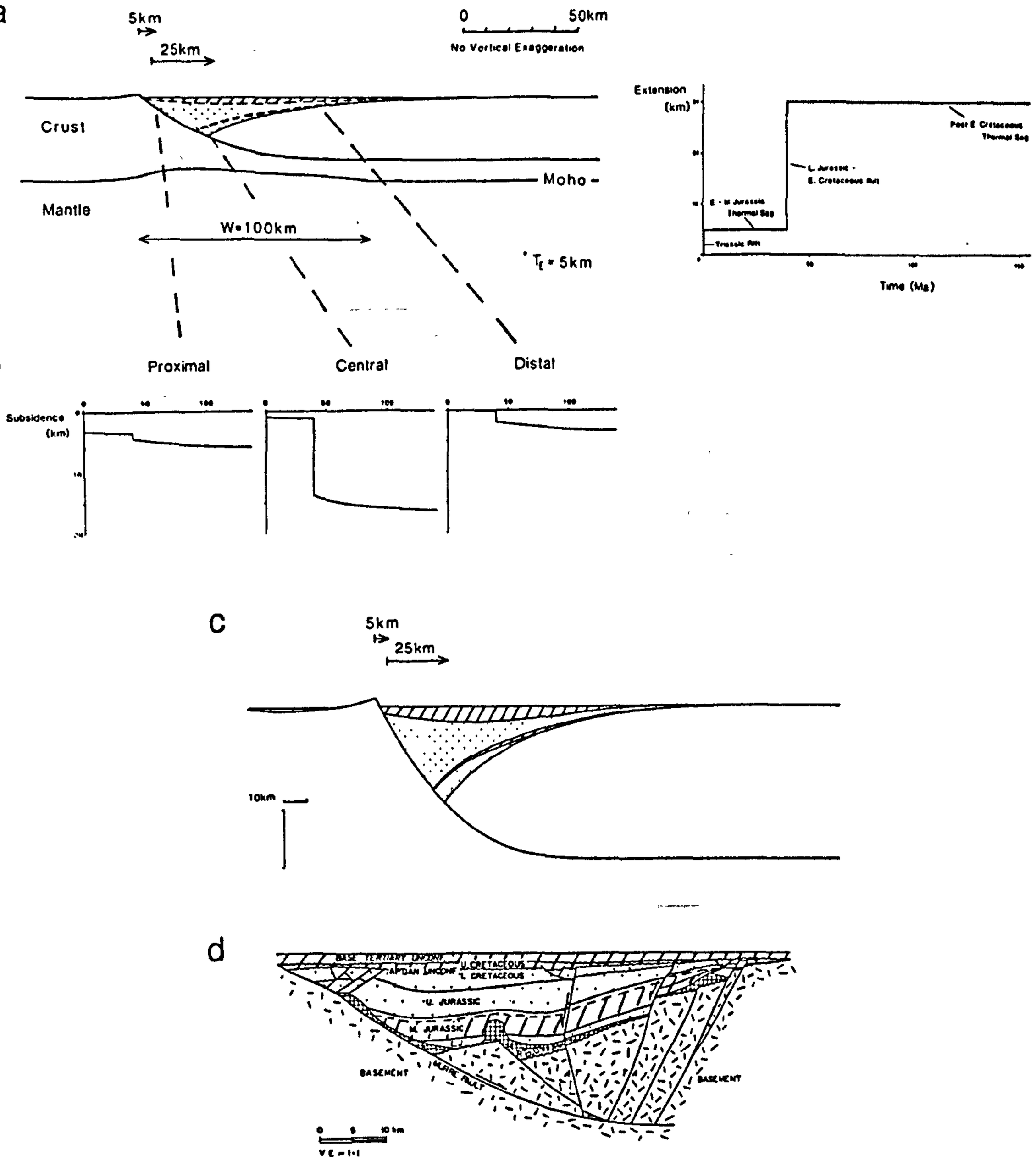

(after Tankard & Welsink, 1987)

Figure 5.8 -

a) Modelled crustal structure and basin geometry for the Jeanne d'Arc basin assuming two rifting events - Triassic and Late Jurassic/Early Cretaceous.

b) Modelled subsidence curves for proximal, central and distal regions of the Jeanne d'Arc basin.

c) Modelled basin fill with vertical exaggeration showing two rift and thermal subsidence sequences.

d) For comparison, geological cross-section of the Jeanne d'Arc basin constructed from seismic and borehole data (after Tankard and Welsink 1987).

of the basin. The period of rift subsidence in the curves reflects the amount of hanging wall collapse followed by flexural adjustment. Thermal subsidence is denoted by the section of the curve with exponential geometry.

The stratigraphic pattern predicted by the model is very similar to Tankard and Welsinks' (1987) interpretation (compare figures 5.8c and 5.8d) except that the thermal subsidence phase immediately following the Triassic rifting has a thickness of 1km. This is too small compared to the 4km thickness indicated by Tankard and Welsinks' information. There are two possible causes for this relatively subdued thickness of pre Upper Jurassic thermal subsidence predicted by the model:

a) Representation of Triassic rifting by 5km of movement along the fault is an underestimate, which, in turn, causes a low amount of post-rift thermal subsidence. In figure 5.9a Triassic extension has been represented by 10km of movement along the fault and in response to this the thickness of following thermal subsidence has risen to 2km.

b) The Triassic rift phase may have been sediment starved, thus giving an exaggerated thermal subsidence phase as the basin is gradually filled. This is illustrated in figure 5.9b where no sediment infill has been assumed during the initial 5km of extension. However, the basin produced by this initial rift phase is allowed to fill with sediment during the following thermal subsidence phase, which increases the total thickness of this component to 5.5km.

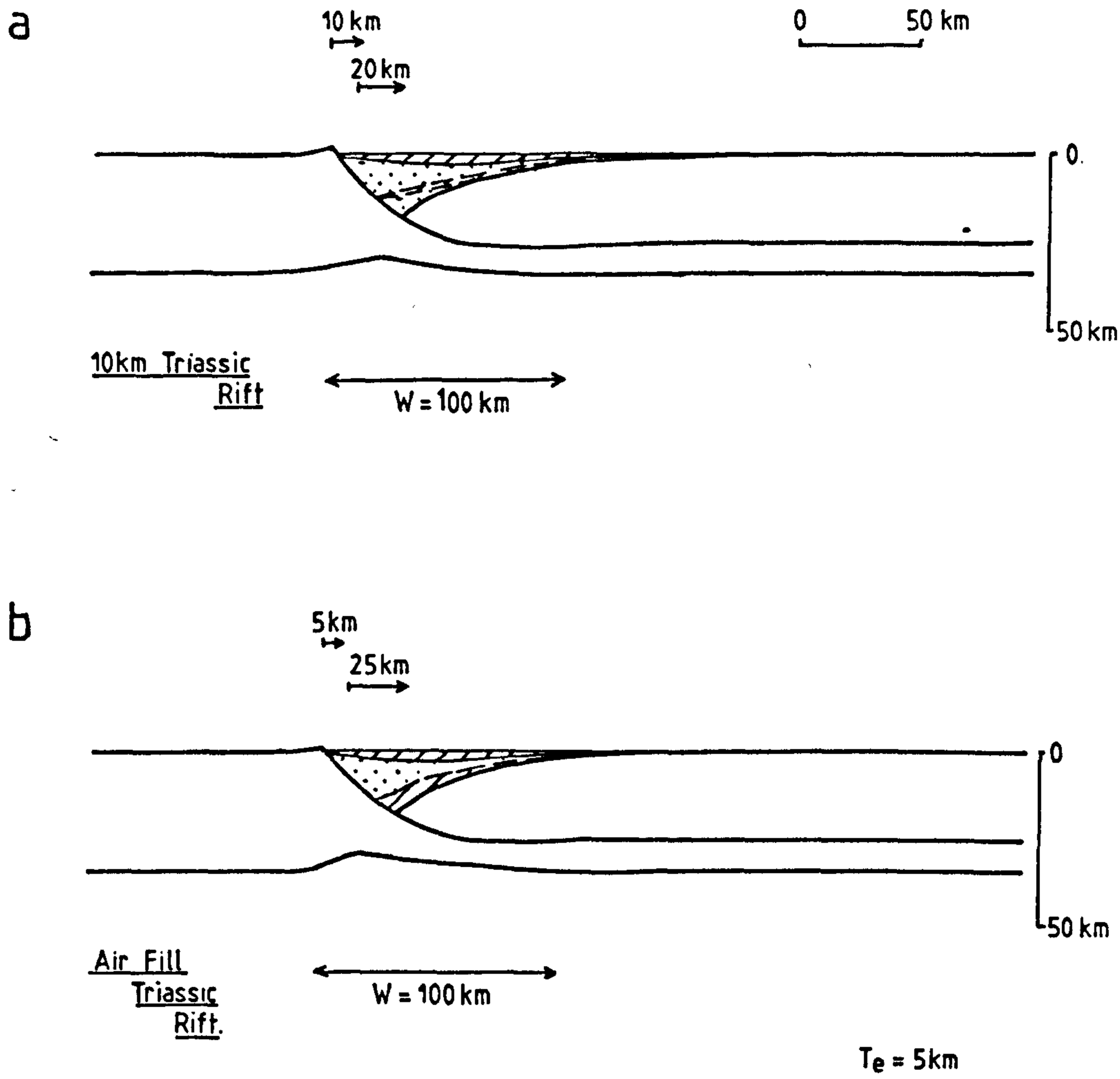

Figure 5.9 -

a) Model prediction for 10km Triassic rifting (instead of 5km). The thickness of the post Triassic thermal subsidence component has been increased to 2km. This amount is still low compared to the thickness indicated by the seismic and borehole data.

b) A sediment starved initial rift phase allows increased sediment deposition during the following period of thermal subsidence. The effect of this is to produce an exaggerated thermal subsidence thickness in the stratigraphic record.

It is clear that by modelling the Jeanne d'Arc basin as a multi-phase series of rift events it is possible to obtain an accurate representation of basin structure and stratigraphy. The modelling also reveals that in order to explain some of the more detailed features apparent in the stratigraphic record it is necessary to include the effect of other factors apart from gross amounts of extension and thermal subsidence. Such factors include erosion, base level for sedimentation, sediment supply, decompaction, rate of extension, etc.

5.6 Summary.

The following conclusions can be drawn from the above work:

a) The Jeanne d'Arc basin is a clear example of basin formation following extension along a single major low angle fault.

b) Numerical modelling of the Jeanne d'Arc basin shows that the deformational loads imposed on the lithosphere have to be flexurally compensated in order to achieve realistic basin depths, a smooth fault geometry, a relatively flat Moho topography and sensible amounts of thermal subsidence.

c) Erosion of uplifted basement at the basin peripheries is a possible driving mechanism for the Avalon unconformity, although additional factors such as magmatic underplating should also be considered.

d) The evolution of the Jeanne d'Arc basin has included

at least two separate rift phases and as a consequence finite rifting models most accurately predict the basin stratigraphy.

Appendix 5

Finite Rifting Formulation and Test.

a) Crustal thinning component.

In figure 5.10 the increase in crustal thinning by simple shear following three pulses of extension along a fault-detachment, $D_{(x)}$, is shown. The individual increments of extension, E1, E2 and E3, generate associated crustal thinning components $S1_{(x)}$, $S2_{(x)}$ and $S3_{(x)}$ respectively. Each of these amounts of crustal thinning can be calculated such that:

$$S1_{(x)} = D_{(x)} - D1_{(x-E)} \quad \text{-----} \quad 5.3$$

$$S2_{(x)} = [D_{(x)} - S1_{(x)}] - [D_{(x-E2)} - S1_{(x-E2)}] \quad \text{-----} \quad 5.4$$

$$S3_{(x)} = [D_{(x)} - S1_{(x)} - S2_{(x)}] -$$

$$[D_{(x-E3)} - S1_{(x-E3)} - S2_{(x-E3)}] \quad \text{-----} \quad 5.5$$

The model of the Jeanne d'Arc basin in figure 5.4c, which incorporates this finite rifting formulation, shows basin geometry and crustal structure following fifteen increments of extension. Simple shear crustal thinning caused by this fifteenth pulse of extension, E15, is given by:

$$S15_{(x)} = [D_{(x)} - S'_{(x)}] - [D_{(x-E15)} - S'_{(x-E15)}] \quad \text{-----} \quad 5.6$$

where $S'_{(x)}$ combines the crustal thinning caused by extension increments one to fourteen.

Crustal thinning by pure shear has been calculated for the first finite rift stage using the methodology described in section 2.2a, such that:

Figure 5.10 - Incremental extension on an exponential low angle fault causes a surficial hole with gradually increasing magnitude.

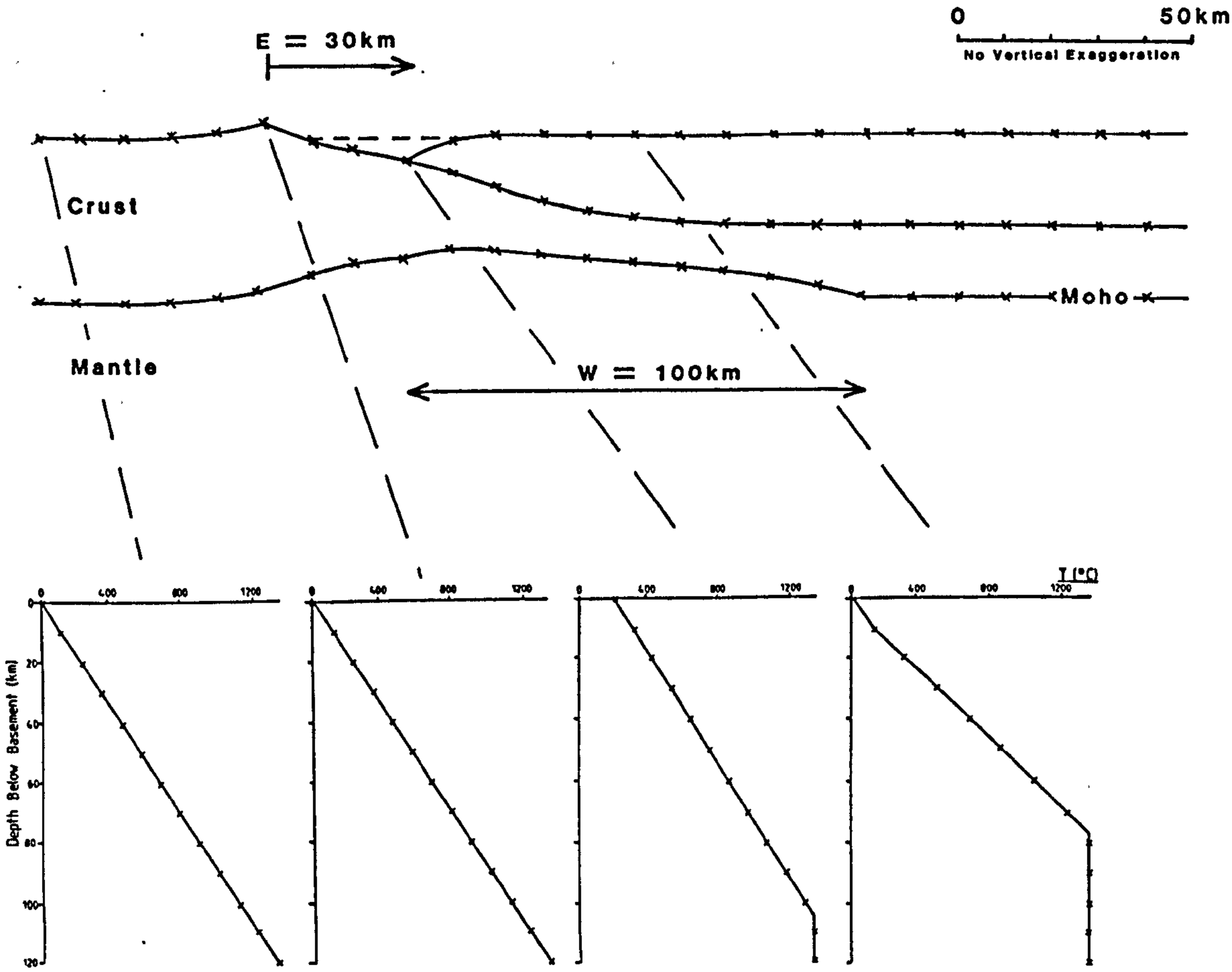

Figure 5.11 - Basin geometry, crustal structure and geotherms following 30km instantaneous extension (solid line) and 30 x 1km incremental extension (crossed line) are compared.

$$P'_{(x)} = (C_o - Z_a) \cdot (1 - 1/\beta'_{(x)}) \quad \text{-----} \quad 5.7$$

where C_o is original crustal thickness, Z_a is detachment depth and $\beta'_{(x)}$ is the extension factor defining the pure shear extension, which balances the simple shear.

After the second rift phase the total amount of pure shear crustal thinning, $P''_{(x)}$, is given by:

$$P''_{(x)} = (C_o - Z_a) \cdot (1 - (1/\beta'_{(x)} . 1/\beta''_{(x)})) \quad \text{-----} \quad 5.8$$

where $\beta''_{(x)}$ defines the pure shear associated with the second rift phase.

Similarly, at the nth rift component the total amount of crustal thinning by pure shear, $P^T_{(x)}$, is given by:

$$P^T_{(x)} = (C_o - Z_a) \cdot (1 - 1/\beta^T{}_{n(x)}) \quad \text{----} \quad 5.9$$

where $\beta^T{}_{n(x)} = \beta'_{(x)} . \beta''_{(x)} . \beta'''_{(x)} \ldots . \beta^n{}_{(x)}$

b) Thermal component.

As described in section 2.2b the equilibrated geotherm defining the lithosphere temperature field is given by:

$$T_{(x,z)} = T_o/a . z \quad \text{-----} \quad 5.10$$

where T is the temperature at horizontal position x with respect to depth, z, below basement, T_o is the temperature at the base of the lithosphere and a is lithosphere thickness.

After the first increment of simple shear extension the temperatures in the footwall are modified by simple shear deformation such that:

$$T'_{(x,z)} = T_{(x,z+S1x)} \quad \text{-----} \quad 5.11$$

The temperatures in the hanging wall are defined such that:

$$T'_{(x,z)} = T_{(x,z)} \quad \text{----} \quad 5.12$$

Between successive finite rift increments the geotherm re-equilibrates such that:

$$T'_{(x,z)} = T'_{(x,z)} + T'_{(x,z)} \quad \text{-----} \quad 5.13$$

where $T'_{(x,z)}$ defines the re-equilibration of the lithosphere temperature field between the first and second finite rift components, which has been calculated using the finite difference method as described in section 2.3.

The second increment of rifting modifies the temperatures again so that in the footwall:

$$T''_{(x,z)} = T'_{(x,z+S2x)} \quad \text{-----} \quad 5.14$$

Temperatures in the hanging wall are laterally translated by the extensional movement such that:

$$T''_{(x,z)} = T'_{(x-E2,z)} \quad \text{-----} \quad 5.15$$

In the time between the second and third rift phases re-equilibration of the temperature field continues by an amount $T_{(x,z)}$ such that:

$$T''_{(x,z)} = T''_{(x,z)} + T_{(x,z)} \quad \text{----} \quad 5.16$$

after the third increment of extension, E3, the temperatures in the footwall and hanging wall are modified such that in the former:

$$T'''_{(x,z)} = T''_{(x,z+S2x)} \quad \text{-----} \quad 5.17$$

and in the hanging wall:

$$T'''_{(x,z)} = T''_{(x-E3,z)} \quad \text{----} \quad 5.18$$

Pure shear deformation perturbs the geotherm beneath the horizontal detachment such that:

$$T'_{(x,z)} = T_{(x,z')} \quad \text{-----} \quad 5.19$$

where $z' = Z_a + [(z+S1_{(x)}+Z_a).\beta1_{(x)}]$ for the first increment of rifting and $z' = Z_a + [(z+S2_{(x)}+Z_a).\beta2_{(x)}]$ for the second increment, etc.

c) Isostatic component.

The load forces imposed upon the lithosphere by each increment of rifting are compensated by either Airy or flexural isostasy as described in sections 2.2b and 4.2 respectively.

d) Finite rifting test.

In order to test the finite rifting algorithm the following test was carried out:

a) Basin geometry and crustal structure were calculated following 30km instantaneous extension by a simple shear-pure shear process (figure 5.11). The effects of sediment loading are not included. Geotherms are also shown at several positions across the basin.

b) Similar predictions have been made for a 30km rift in 1km increments.

A comparison of the results from a (solid line) and b (crossed line) are also shown in figure 5.11. Both sets of

results are identical, which demonstrates the accuracy of the finite rifting algorithm used.

Chapter 6

Extensional Basin Formation on Multiple Low Angle Faults.

6.1 Introduction.

The small thickness of thermal subsidence recorded in the stratigraphy of many extensional sedimentary basins, for example the Jeanne d'Arc basin (chapter 5) and the Whale basin (figure 6.1a), can be explained by a combination of the flexural strength of the lithosphere and non-instantaneous extension. However, the Orphan basin in the northern Grand Banks region (figure 6.1b), shows a much larger thickness of thermally induced deposition. This basin is relatively wide, extending over some 400km, and exhibits a very similar Mesozoic extensional evolution to the Jeanne d'Arc and Whale basins. However, it differs from its contempories in the south in that it contains a relatively thick post-rift thermal subsidence sequence up to 6km deep. Keen (in press) has attributed this difference to a large thinning of the sub crustal lithosphere relative to the attenuation of the crust for the Orphan basin, while for the basins in the southern Grand Banks region (eg. the Whale and Jeanne d'Arc basins) she proposes a large thinning of the crust with a relatively small extension of the sub crustal lithosphere, resulting in a high proportion of syn- to post-rift sediment thickness.

The weakness with Keen's explanation is its reliance upon a large contrast between the amounts of extension experienced by the crustal and sub crustal lithosphere. The seismic data over the Orphan basin suggests that the crust was thinned by a factor of about 2, which must be matched by a stretching

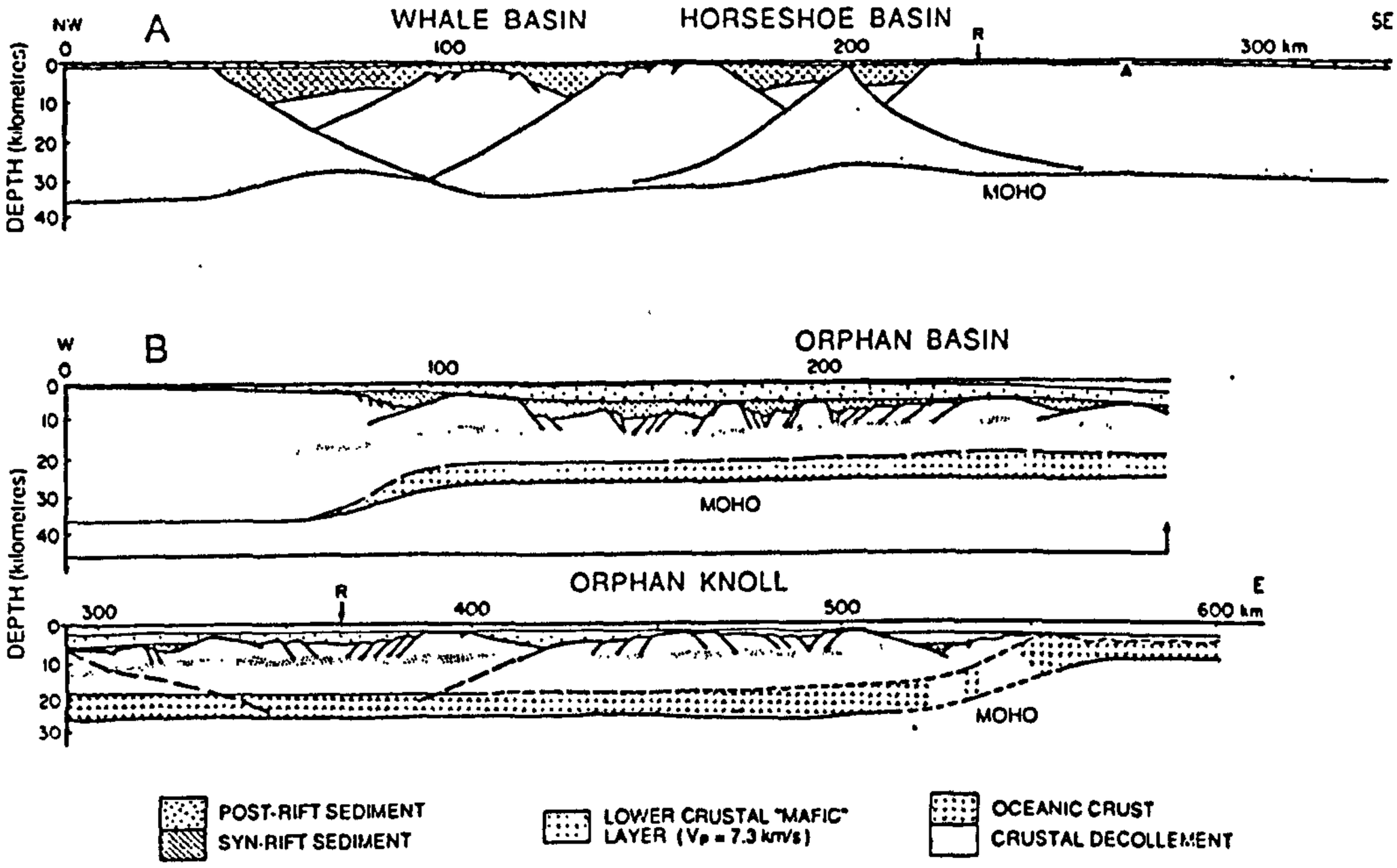

(after Keen, in press)

Figure 6.1 - The Whale (a) and Orphan (b) basins in the southern and northern regions of the Grand Banks respectively have very similar Mesozoic extensional histories (Keen, in press). The Whale basin has formed by extension dominantly along a single low angle fault and exhibits a small thickness of post-rift deposition. In contrast, the Orphan basin has formed by extension along a series of closely spaced faults and possesses a relatively large thickness of post rift thermal subsidence.

factor of 4 to 8 in the mantle lithosphere in order to generate the correct syn- to post-rift sediment thicknesses (Keen, in press). A contrast such as this must introduce severe mass balance problems into the extending system.

It is suggested here that an alternative, more feasible, explanation can be found in the structural evolution of the Orphan basin, which has formed as a series of half grabens by extension along several closely spaced faults. In a single half graben the simple shear rift depocentre may overly pure deformation in the lower lithosphere. On a regional scale the superposition of several half grabens causes the simple shear component of one half graben to overly the pure shear deformation associated with both itself and several others. This produces a pattern of discrete rift depocentres overlain by a broad, relatively thick blanket of thermal subsidence due to the regionally distributed pure shear in the lower lithosphere. This effect can be demonstrated by applying the simple shear-pure shear model to extension on multiple faults.

6.2 A Geometric, Thermal and Isostatic Consideration of Extension Along Multiple Faults.

a) Geometric component.

The required number of faults are defined at suitable positions in the hanging wall before extension occurs (figure 6.2a) such that the proximal fault, $D1_{(x)}$, is defined by the equation:

$$D1_{(x)} = 0 \quad \text{for} \quad x \leq x1_o$$

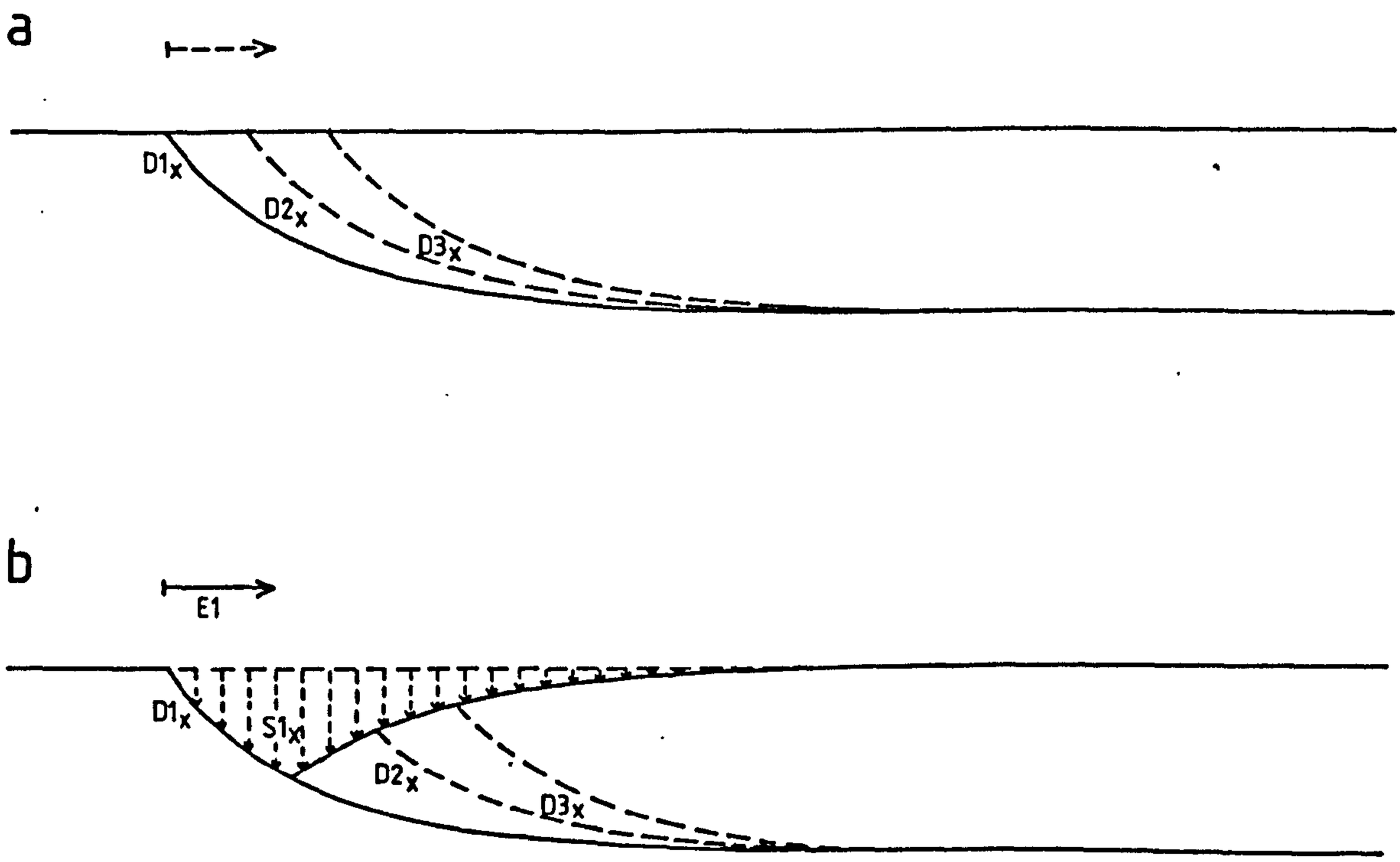

Figure 6.2 -

Geometric consideration of in-sequence extension on multiple faults.

a) A sequence of faults are defined before extension.

b) Extension, E1, along the proximal fault, $D1_{(x)}$, thins the crust by an amount $S1_{(x)}$ and creates a surficial hole. The middle and distal faults in the hanging wall are both displaced laterally and subsided.

c) Extension, E2, along the middle fault causes additional thinning of the crust, $S2_{(x)}$. Total crustal thinning by simple shear is $S1_{(x)} + S2_{(x)}$.

$$D1_{(x)} = Z_a \cdot (1 - \exp(-x/Z_a)) \quad \text{for} \quad x > x1_o \quad \text{-----} \quad 6.1$$

The middle fault, $D2_{(x)}$, is given by:

$$D2_{(x)} = 0 \quad \text{for} \quad x \leq x2_o$$

$$D2_{(x)} = Z_a \cdot (1 - \exp(-x/Z_a)) \quad \text{for} \quad x > x2_o \quad \text{-----} \quad 6.2$$

The distal fault, $D3_{(x)}$, is defined such that:

$$D3_{(x)} = 0 \quad \text{for} \quad x \leq x3_o$$

$$D3_{(x)} = Z_a \cdot (1 - \exp(-x/Z_a)) \quad \text{for} \quad x > x3_o \quad \text{-----} \quad 6.3$$

where Z_a is the detachment depth and $x1_o$, $x2_o$ and $x3_o$ denote the horizontal positions of the original outcrops of the proximal, central and distal faults at the surface

If extension, E1, occurs along the most proximal fault, $D1_{(x)}$, the amount of crustal thinning, $S1_{(x)}$, is given by:

$$S1_{(x)} = D1_{(x)} - D1_{(x-E1)} \quad \text{----} \quad 6.4$$

The predefined faults (eg. $D2_{(x)}$) in the hanging wall of this initial fault are laterally displaced and subsided by the extension and lithospheric thinning respectively (figure 6.2b), such that:

$$D2_{(x)} \text{ -----> } D2'_{(x)} \quad \text{----} \quad 6.5$$

and

$$D2'_{(x)} = D2_{(x-E1)} + S1_{(x)} \quad \text{----} \quad 6.6$$

If extension, E2, occurs along $D2'_{(x)}$ (figure 6.2c) an additional crustal thinning component, $S2_{(x)}$, is generated such that:

$$S2_{(x)} = [D2'_{(x)} - S1_{(x)}] - [D2'_{(x-E2)} - S1_{(x-E2)}] \quad \text{---- } 6.7$$

substituting for $D2'_{(x)}$ into equation 6.4 gives:

$$S2_{(x)} = D2_{(x-E1)} - D2_{(x-E1-E2)} \quad \text{---- } 6.8$$

The total crustal thinning, $S_{(x)}$, along both faults is given by the following:

$$S_{(x)} = S1_{(x)} + S2_{(x)}$$

$$= [D_{(x)} - D_{(x-E1)}] + [D2_{(x-E1)} - D2_{(x-E1-E2)}] \quad \text{----- } 6.9$$

This equation can easily be modified to calculate the amount of crustal thinning by simple shear caused by extension along three faults such that:

$$S_{(x)} = [D_{(x)} - D_{(x-E1)}] + [D2_{(x-E1)} - D2_{(x-E1-E2)}]$$

$$+ [D3_{(x-E1-E2)} - D3_{(x-E1-E2-E3)}] \quad \text{---- } 6.10$$

The amount of crustal thinning caused by pure shear, $P_{(x)}$, in the lower lithosphere is dependent upon detachment depth and is given by the following equation:

$$P_{(x)} = (C_o - Z_d) \cdot (1 - 1/\beta_{(x)}) \quad \text{----- } 6.11$$

where C_o is original crustal thickness, Z_d is detachment depth and $\beta_{(x)}$ defines the extension factor distribution.

The amount of extension by simple shear must balance the amount of regionally distributed pure shear deformation in the lower lithosphere. This implies for extension along three faults:

$$(E1+E2+E3) = \int_0^{w'} (\beta_{(x)} - 1)\, dx$$

$$= \int_{o}^{w'} D_o \,.\, \sin(\pi.x/W) \quad \text{-----} \quad 6.12$$

where W defines the width of the region over which the pure shear has been distributed, W' = W-(E1+E2+E3) and D_o+1 defines the maximum extension factor at the centre of the pure shear, which has been distributed sinusoidally.

If W is much greater than the total amount of simple shear extension, the following equation becomes valid:

$$D_o = (\pi/2) \,.\, [(E1+E2+E3)/(W-(E1+E2+E3))] \quad \text{----} \quad 6.13$$

b) Thermal component.

The lithosphere temperature field is initially defined by an equilibrated geotherm such that:

$$T_{(z)} = T_o/a.z \quad \text{-----} \quad 6.14$$

where T is the temperature at a particular depth below basement z and T_o is the temperature at the base of the lithosphere of thickness a.

Both simple and pure shear perturb the geotherm during rifting as described in chapter 2. The calculation of this perturbation is more complex for extension along multiple faults due to the continual tectonic denudation of the hanging wall as extension occurs on the distal faults.

For extension on the initial, most proximal, fault (figure 6.2a), the temperatures in the footwall, $T'_{(z)}$, are defined such that:

$$T' = T_{(z+s1(x))} \quad \text{-----} \quad 6.15$$

where $S1_{(x)}$ is the crustal thinning by simple shear.

The temperatures in the hanging wall remain as defined in equation 6.14 provided z defines depth with respect to top basement. Thus:

$$T' = T_{(z)} \quad \text{-----} \quad 6.16$$

Extension on the middle fault (figure 6.2b) causes hanging wall material, related to the first fault, to now be part of the footwall of the middle fault. The temperatures in the footwall, $T''_{(z)}$, are now defined such that:

$$T'' = T'_{(z+S2(x))} \quad \text{-----} \quad 6.17$$

where $S2_{(x)}$ is simple shear crustal thinning due to extension along the central fault.

The temperatures in the hanging wall of the middle fault are defined such that:

$$T'' = T_{(z)} \quad \text{-----} \quad 6.18$$

Similarly, extension along the third, most distal, fault (figure 6.2c) modifies the footwall temperatures such that:

$$T''' = T''_{(z+S3(x))} \quad \text{-----} \quad 6.19$$

where $S3_{(x)}$ is crustal thinning associated with movement along the third fault.

In the hanging wall:

$$T''' = T_{(z)} \quad \text{----} \quad 6.20$$

Below the detachment depth, Z_a, pure shear deformation

perturbs the geotherm such that:

$$T_{(z)} \text{ ----> } T_{(z')} \quad \text{-----} \quad 6.21$$

where z' for in-sequence extension along three faults is given by:

$$z' = Z_a + [(z+S1_{(x)}+S2_{(x)}+S3_{(x)}-Z_a).\beta_{(x)}] \quad \text{-----} \quad 6.22$$

c) Isostatic component.

The load forces generated by simple and pure shear crustal thinning, temperature perturbations and sediment loading following extension along multiple faults can be expressed as a continuous function across the extended region. For example, the buoyancy load arising from crustal thinning following extension along three faults can be defined as:

$$L_{(x)m} = -[(S1_{(x)}+S2_{(x)}+S3_{(x)}).\rho_c.g] \quad \text{-----} \quad 6.20$$

The flexural response of the lithosphere to these loads can be calculated therefore using the methodology described in chapter 4.

6.3 The Application of the Simple Shear - Pure Shear Model to Extension on Multiple Faults.

In figure 6.3a the geometric aspect of simple shear-pure shear extension along four faults has been combined with thermal and flexural isostatic components to show basin geometry and crustal structure at 100Ma after rifting. Extension began on the most proximal fault and then continued in sequence onto the synthetic faults in the hanging wall. Rifting was assumed to be instantaneous and the faults flatten into an intracrustal detachment at 20km,

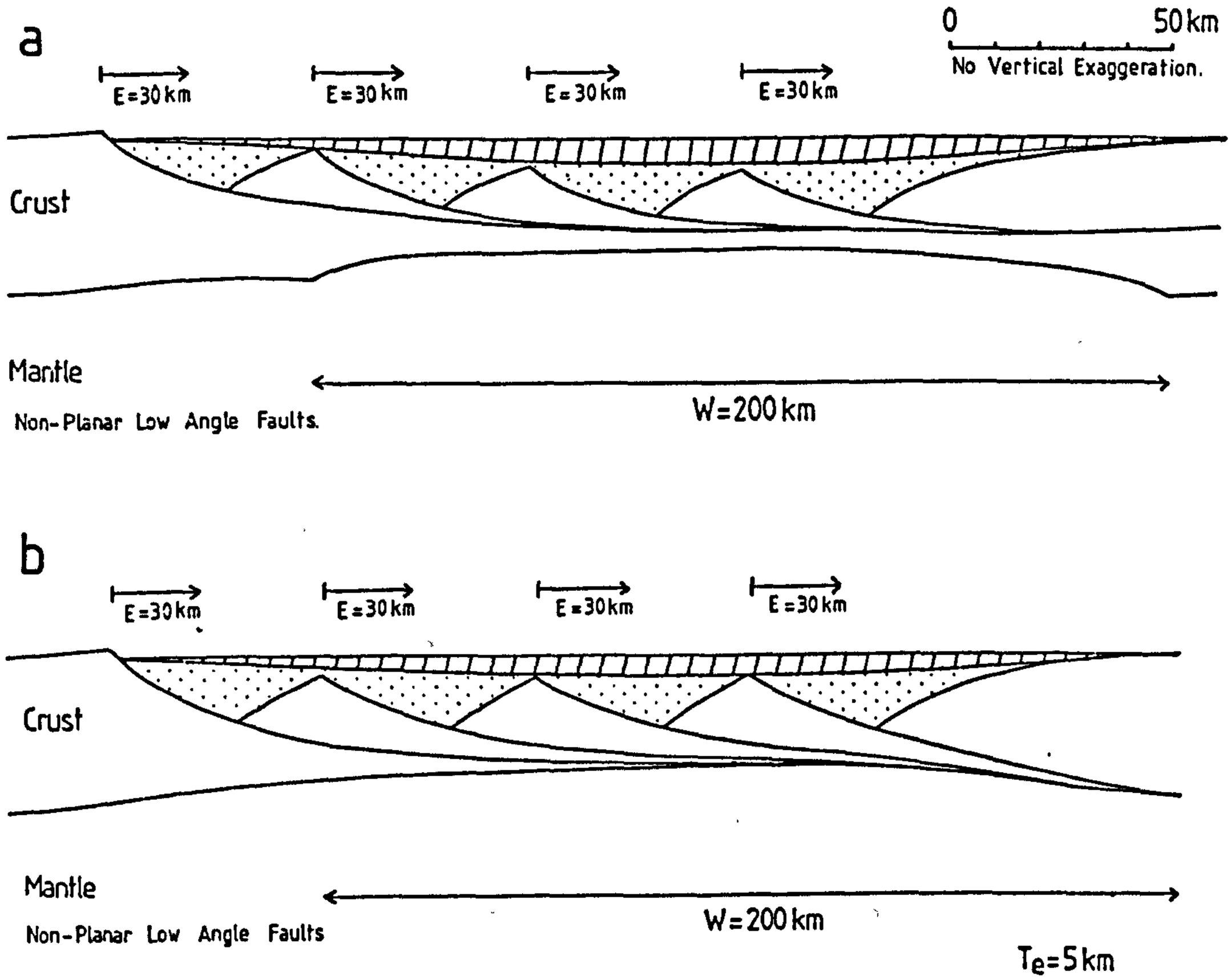

Figure 6.3 - Large sedimentary basins are formed by lithosphere extension on several major low angle faults. The pattern of discrete syn-rift (simple shear) depocentres overlain by a continuous blanket of post-rift thermal subsidence is a feature common to most large sedimentary basins. Basin geometry and crustal structure are shown 100Ma after in-sequence extension along four major low angle faults which detach at depths of 20km (a) and 35km at the base of the crust (b).

which has caused a pure shear thinning of the lower crust. In figure 6.3b the effect of a detachment at the base of the crust is shown and as a result the predicted crustal structure shows no pure shear thinning of the lower crust. In both models the pattern of discrete rift depocentres caused by simple shear extension are overlain by a broad thin blanket of thermal subsidence.

6.4 Numerical Modelling Constraints on the Evolution of the Viking Graben in the Northern North Sea.

The Viking Graben, a major Mesozoic rift basin in the northern North Sea, has been studied extensively (eg. Ziegler 1982, Glennie 1986, Beach 1986, Beach et al 1987, Gibbs 1987) and, like the Orphan basin in the Grand Banks region, has evolved as a series of closely spaced half grabens. The evolution of the Viking Graben is complex with rifting beginning in the Permian, although the main phase of fault movement occurred in the Middle Jurassic and continued through to the Early Cretaceous. A flexural thermal subsidence phase began during the Upper Cretaceous and continued through the Tertiary.

Studies using uniform stretching models to explain the evolution of the Viking Graben cannot generate the thickness of thermal subsidence evident in the present stratigraphy of the basin (Beach et al 1987, Badley et al 1988) and as a consequence depth-dependent models of lithosphere extension have been suggested to most accurately represent the extensional evolution of the basin (Beach 1986, Beach et al 1987, Badley 1988, Klemperer, 1988). The deep seismic

reflection section in figure 6.4a across the Viking Graben and surrounding region has been interpreted by Beach (1986) as a series of closely spaced faults along which the region has extended (figure 6.4b). In figure 6.5a simple shear-pure shear model predictions are shown using structural elements from the Beach interpretation and assuming a lower crustal detachment depth at 20km. The total amount of apparent fault controlled extension across the Viking Graben and surrounding area is about 22km (G. Marsden, personal communication). However, it is suggested that this is an underestimation due to the effects of erosion, which has removed parts of the footwall blocks to leave an unconformity across the top of the present fault blocks, separating the Jurassic (plus older) sequences from the almost horizontal Upper Cretaceous and Tertiary strata (Badley et al 1988).

The model in figure 6.5a has included therefore the effect of erosion of uplifted basement following in-sequence extensions on each of the seven faults and the total amount of extension along the faults has been increased to 32km in order to compensate for this erosion. Loads imposed on the lithosphere have been flexurally compensated, as defined by an elastic thickness of 5km. Pure shear has been regionally distributed over 150km beneath the area of fault controlled extension. The maximum thickness of syn-rift sediment predicted by the model is 3km, while post-rift thermally induced deposition reaches a maximum thickness of 1.5km. These amounts compare to approximately 2km and 4km for maximum syn- and post-rift deposition as shown in the section in figure 6.5b, which has been constructed from

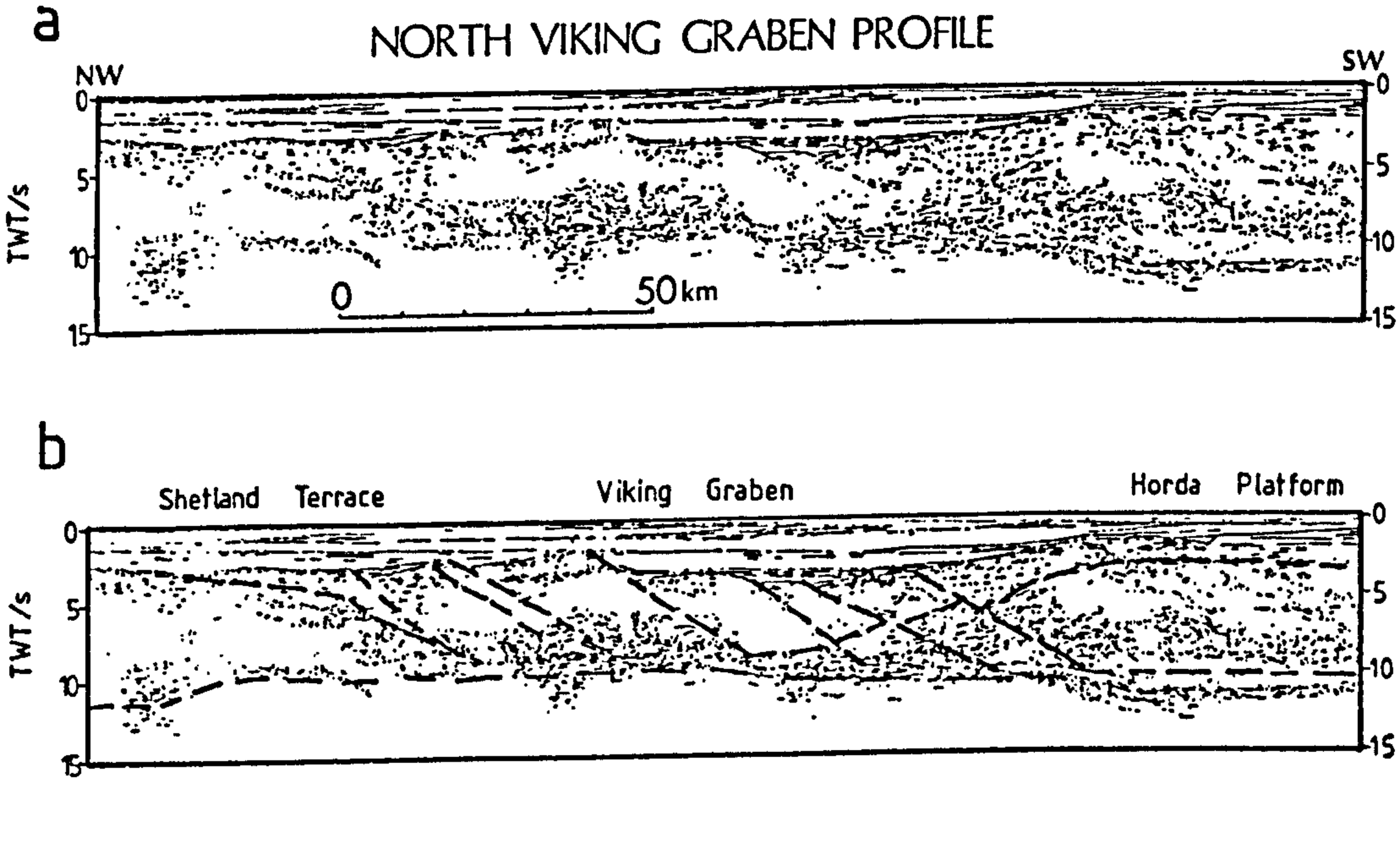

Figure 6.4 -

a) Line section of the deep seismic reflection survey across the North Viking Graben.

b) The interpretation of this section shows major eastward dipping faults and pre-erosion estimates of extension. The Moho is denoted by the depth limit of crustal reflectors and occurs at about 12s TWT in unextended regions (Beach 1986).

seismic and borehole data (Badley et al 1988). It can be concluded therefore depth dependent lithosphere extension models suffer from the same problem as the uniform extension examples in that they also predict an underestimation of post-rift thermal subsidence for the Viking Graben. The importance of the problem is indicated by the fact that:

a) Modelling calculations have assumed instantaneous rifting and the amount of post-rift subsidence has therefore been maximised. If the effect of finite rifting were included, the thickness of the thermal component would be further reduced.

b) The apparent thickness of syn-rift sediment has been reduced due to the inclusion of the effects of erosion of uplifted basement at the end of the extension event. The flexural response of the lithosphere to localised erosion causes a regional uplift and, in turn, removal of syn-rift material from within the basin (see figure 5.5).

A possible cause for the high proportion of thermal subsidence compared to rift subsidence in the Viking graben is a varying base level for sedimentation. Modelling calculations have assumed so far that sediment loading occurs to sea level throughout all phases of basin evolution. Alternatively, the Viking Graben may have been sediment starved during rifting and gradually filled during thermal subsidence. The proportion of syn-rift sedimentation will therefore strongly influence the amount of thermally induced deposition and no sediment deposition during rifting

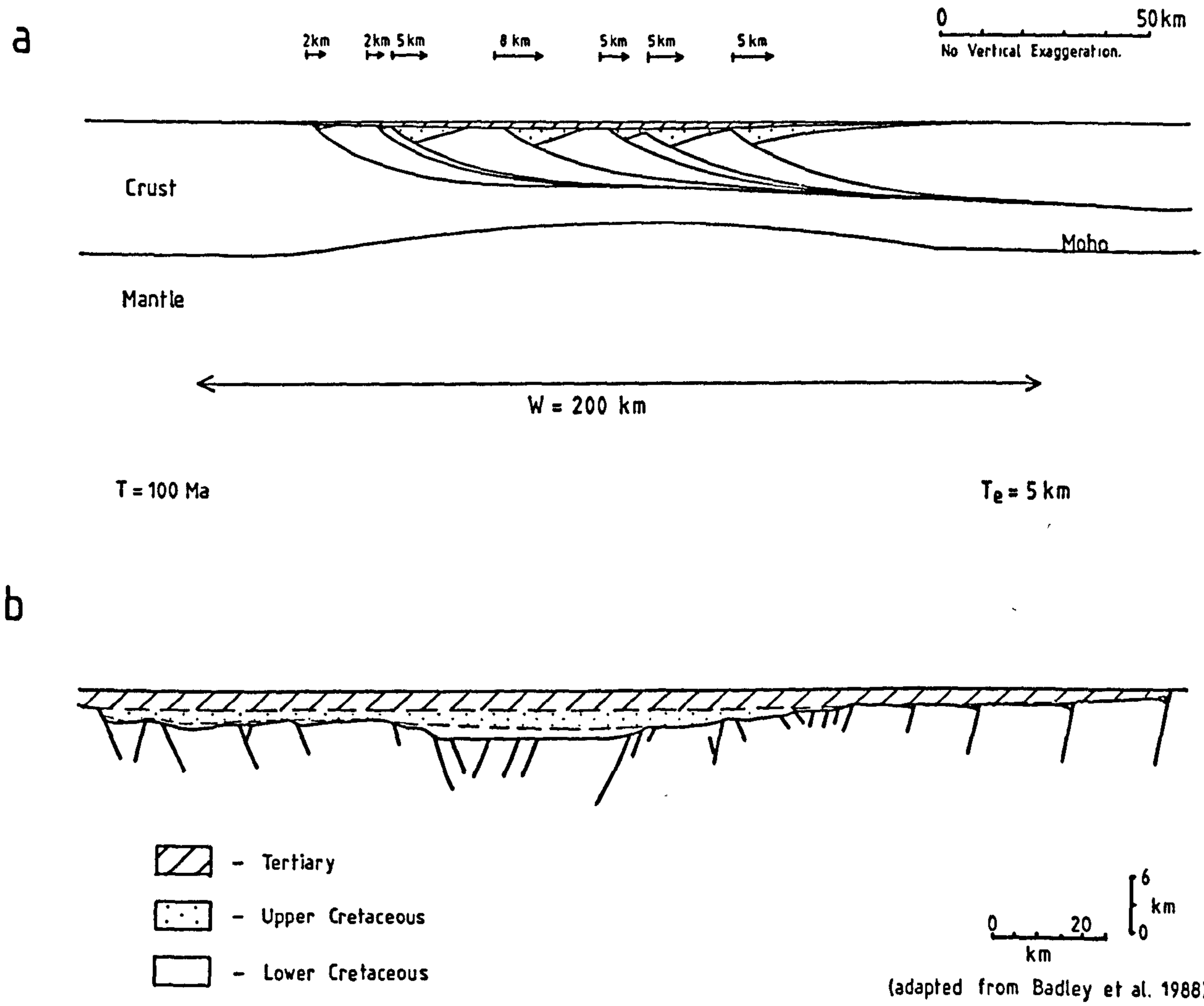

Figure 6.5 -

a) Model predictions for the extensional evolution of the Viking Graben. The total amount of fault controlled extension is 32km, while pure shear thins the lithosphere below a detachment depth of 20km and is distributed over 150km. Erosion of the uplift of the footwall rift shoulder has been assumed following an instantaneous rift phase. This initial model fails to show the planar thermal sag phase forming the Cretaceous and Tertiary sequence in the Viking Graben.

b) Section across the East Shetland Terrace and the Viking Graben, showing a relatively thin Lower Cretaceous syn-rift sequence overlain by a larger thickness of thermally induced subsidence occurring in the Upper Cretaceous and Tertiary.

maximises the thickness of the post-rift thermal component. On the other hand, it is suggested that restricting sediment deposition to the thermal subsidence phase of basin evolution does not generate the almost planar geometry exhibited by the post Early Cretaceous sediments present in the Viking Graben.

The parameter of base level for sedimentation is further complicated by a temporal variation both due to eustatic changes (eg. Vail et al 1977) and regional changes in the thermal state of the lithosphere. The steady-state equilibrium geotherm, assumed in the modelling calculations above corresponds to a surface heat flow of about 45mW.m^{-2}, which is common to regions of stable continental shield. Such areas are considered too strong to extend by the naturally arising tensile forces created in the lithosphere (Kusznir and Park 1987) and extending forces are usually transmitted to regions of warmer (and hence rheologically weaker) lithosphere, typically with surface heat flows within the range of 57mW.m^{-2} to 75mW.m^{-2}. In figure 6.6a model predictions are shown after extending warm lithosphere with a geotherm producing a surface heat flow of 75mW.m^{-2}. The finite difference method, as described in chapter 2, has been adapted to define the geotherm such that:

a) The initial temperature of each node in the finite difference grid is set to 1333°C.

b) The temperature of both the surface and bottom of the lithosphere are maintained at temperatures of 0°C and 1333°C respectively, while other depths experience cooling. The heat equation (equation 2.12) is solved

using the finite difference method and the amount of cooling experienced by each of the nodes is calculated after a small time increment, dt.

c) Step b is repeated for further time increments and the cooling of the lithosphere is monitored by the calculation of surface heat flow, Q, at every million year interval such that:

$$Q = k.dT/dz \quad \text{----} \quad 6.21$$

where k is the coefficient of thermal conductivity, which is assumed to be 3.3 $W.m^{-1}.{}^{o}K^{-1}$, and dT is the temperature difference over a suitable surface depth increment (eg. 5km).

For the model in figure 6.6a the cooling lithosphere was extended when Q was equal to $75mW.m^{-2}$, which caused an additional heating of the rifted region. After rifting, lithosphere cooling is calculated from the combined effect of both a post-rift thermal re-equilibration and regional loss of heat as the geotherm decays to an equilibrated state.

At 0Ma the surface is regionally uplifted due to isostatic effects arising from the warm geotherm. After rifting (figure 6.6b) the thermal subsidence arising from the re-equilibration of the geotherm is superimposed onto a regional subsidence due to the overall cooling of the lithosphere. This has a dramatic effect on the sediment deposition pattern within the basin and, depending on the availability of sediment fill, it is possible to generate a

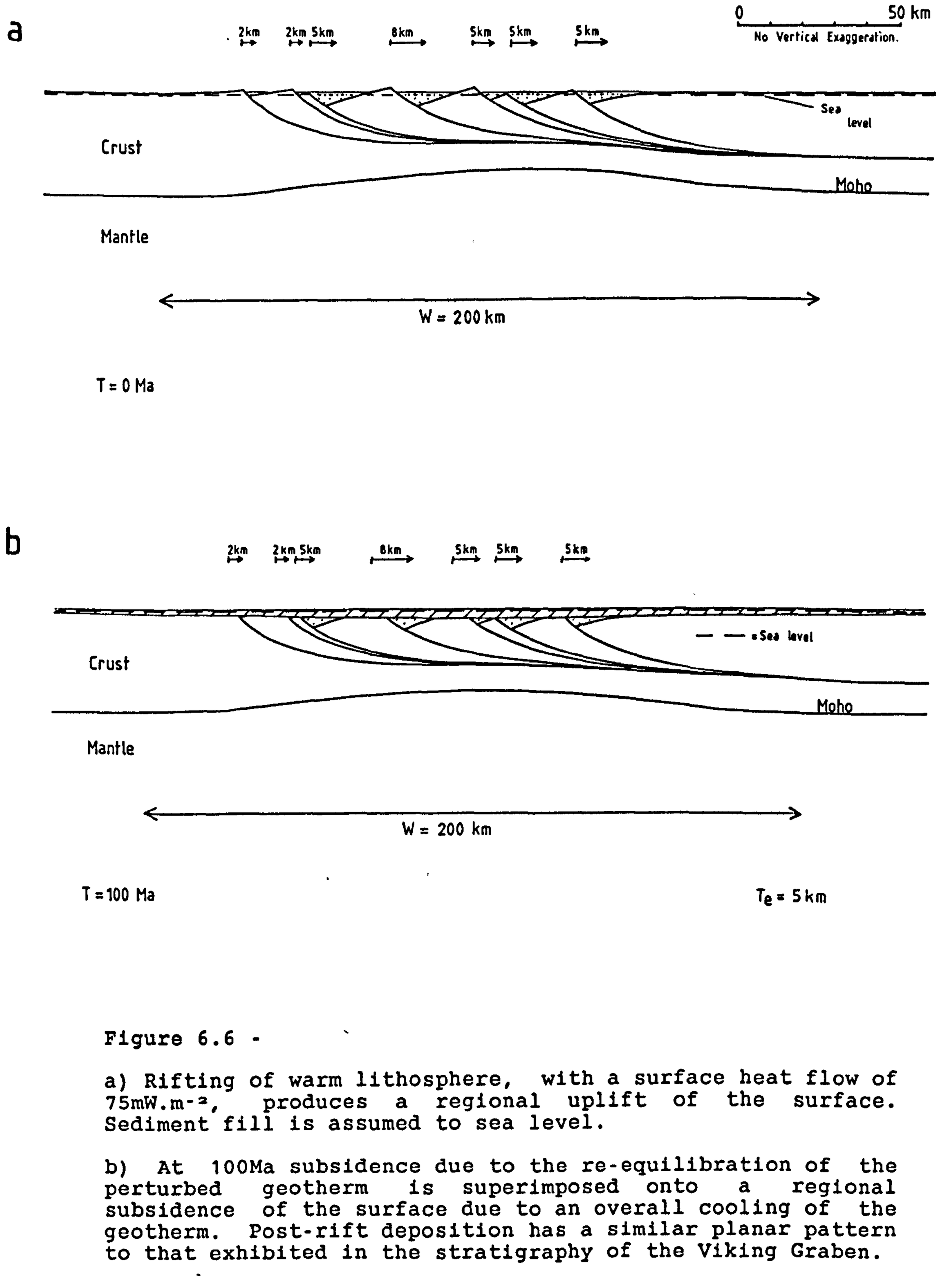

Figure 6.6 -

a) Rifting of warm lithosphere, with a surface heat flow of 75mW.m^{-2}, produces a regional uplift of the surface. Sediment fill is assumed to sea level.

b) At 100Ma subsidence due to the re-equilibration of the perturbed geotherm is superimposed onto a regional subsidence of the surface due to an overall cooling of the geotherm. Post-rift deposition has a similar planar pattern to that exhibited in the stratigraphy of the Viking Graben.

planar thermal subsidence component that is analogous to the Cretaceous and Tertiary sequences in the Viking Graben at present.

6.5 Summary.

The above work shows that a depth dependent simple shear-pure shear lithosphere extension model, incorporating flexural isostatic compensation, can be used to accurately predict the extensional evolution of both small and large sedimentary basins. The versatility of the model has also been illustrated by the ease with which the effects of such phenomena as erosion and a varying base level for sedimentation can be included. It is only by addressing such parameters that some of the complexities arising in the stratigraphic record of many basins can begin to be understood.

Uniform lithosphere extension models (McKenzie 1978) predict a lateral coincidence between syn- and post-rift depocentres (see figure 1.3). It has been shown in figure 6.3 that the simple shear-pure shear model can also produce this lateral coincidence of basin components through extension along multiple faults. This suggests that the superposition of simple shear and pure shear components, caused by extension on a series of closely spaced faults, is, on a regional scale, a close approximation to a wholly pure shear process. Furthermore, this might also explain the apparent success of the relatively simple uniform extension models in predicting the evolution of many complex extensional sedimentary basins (eg. Sclater and Christie 1980, Barton and Wood 1984).

Chapter 7

Thermo-Rheological Implications of Simple Shear - Pure Shear Lithosphere Extension.

7.1 Introduction.

The strength of the continental lithosphere controls both the site of rifting and the subsequent evolution of the extensional deformation (eg. Steckler and ten Brink, 1986). A useful representation of lithospheric strength is the yield-stress envelope, which shows the value of either tensile or compressive deviatoric stresses (σ_1 - σ_3) at which failure of the lithosphere occurs. The form of the yield-stress envelope represents the varying rheological behaviour of the lithosphere with depth, that is the vertical distribution of brittle and ductile strength. The brittle behaviour of a material is controlled by lithostatic pressure and therefore increases with depth. It is limited to relatively low temperatures and pressures because at higher temperature and pressure values other physical processes occur allowing crystalline rock material to creep. Three well documented forms of creep are:

a) Diffusion or Herring-Nabarro creep, which occurs at relatively low stress levels and results from the diffusion of atoms through the interiors of crystal grains on the application of applied stress. Coble creep is another type of diffusion creep where the diffusion of atoms takes place along grain boundaries.

b) Dislocation or power law creep occurs when imperfections or dislocations in the crystalline

lattice structure migrate under the application of stress.

The relationship between strain rate, $\dot{\epsilon}$, and each of these creep mechanisms has been defined by Weertman (1970) such that:

$$\dot{\epsilon} = F(\sigma) \cdot \exp(-(E+(p.V))/(k.T)) \quad \text{----- 7.1}$$

where $F(\sigma)$ is a non-linear stress dependent function, E is activation energy, V is the volume for diffusion, k is Boltzmann's constant, T is temperature and p is pressure. In order to constrain these values a number of experimental studies have been made on granitic, basaltic and ultra-basic rocks representative of the lithosphere. For example, Kohlstedt and Goetze (1974) and Goetze (1978) have shown that dislocation creep provides the dominant creep mechanism for olivine provided the deviatoric stresses are greater than 2kb. For higher levels of stress Goetze suggests, following Stocker and Ashby (1973), that Dorn law creep is more applicable and that diffusion creep may also be significant for large stresses. Koch et al. (1980) suggests that dislocation creep in quartz is the dominant mechanism controlling creep deformation and the strength of this process is determined by water content.

Integration of the yield-stress envelope over the thickness of the lithosphere, a, gives a tensile or compressive force, F_t, which provides a convenient definition of lithosphere strength for a given strain rate at a particular time.

$$F_t = \int_0^a (\sigma_1 - \sigma_3)\, dz \quad \text{----} \quad 7.2$$

F_t has units of kbars.km.

7.2 Formulation of the Thermo-Rheological Model.

In this chapter a thermo-rheological model has been used to calculate yield-stress envelopes associated with lithosphere extended by a simple shear-pure shear process. For modelling purposes the lithosphere has been simplified compositionally into a crust of wet quartz and a mantle of olivine. As described in Kusznir (1982) and Kusznir and Park (1984) the following relationships between creep rate, stress and temperature (in ^{o}k) for both dislocation (equation 7.3) and Dorn law creep (equation 7.4) for the olivine rheology of the mantle have been used:

$$\dot{\epsilon} = 7x10^{11} \cdot \exp(-53030/T) \cdot (\sigma_1 - \sigma_3)^3 \quad (s^{-1}) \text{ ---- } 7.3$$

$$\dot{\epsilon} = 5.7x10^{11} \cdot \exp(-55556/T) \cdot$$

$$1 - (\sigma_1 - \sigma_3)/85)^2 \ (\ s^{-1}) \text{ ---- } 7.4$$

Equation 7.3 applies for $(\sigma_1 - \sigma_3)$ less than 2kb, while equation 7.4 applies for $(\sigma_1 - \sigma_3)$ greater than 2kb.

The creep rate used for wet quartz is based on experimental work by Koch et al (1980) and is given by:

$$\dot{\epsilon} = 4.36 \cdot \exp(-19332/T) \cdot (\sigma_1 - \sigma_3)^{2.44} \quad (s^{-1}) \text{ ---- } 7.5$$

The brittle deformation of the lithosphere has been predicted by the use of Griffith's theory (1924) as modified by McKlintock & Walsh (1962). The physical parameters within the modified Griffith theory, which control the failure, are tensile strength, the frictional coefficient and the

critical stress required to close the Griffith crack. The corresponding values assigned to these values are 0.2kb, 0.5 and 1kb respectively. A more detailed explanation of the thermo-rheological model used can be found in Kusznir (1982) and Kusznir and Park (1986 and 1987).

Figure 7.1 shows steady-state temperature-depth distributions for lithosphere with thermo-tectonic ages of 150Ma and 50Ma, corresponding to surface heat flows of 45 $mW.m^{-2}$ and 75 $mW.m^{-2}$ respectively. The temperature structure of the lithosphere has been calculated using a cooling plate model as described in section 6.4, which has been modified to include radiogenic heat input as used in Kusznir and Park (1986 and 1987).

Yield-stress envelopes are calculated from the application of a tensile force equivalent to a strain rate of 10^{-15} s^{-1} for both thermally young and old lithosphere. This strain rate is geologically significant (Dewey 1982), producing 30% strain in 10Ma. The yield stress envelopes show brittle zones in the upper crust, while at mid-crustal levels the increased temperatures cause plastic failure and the deviatoric stresses ($\sigma_1 - \sigma_3$) sharply decrease to zero. The stronger olivine rheology of the mantle causes the stresses to again rise until the increase in temperature with depth is high enough to induce plastic failure.

7.3 The Rheological Strength of the Lithosphere Following Simple Shear-Pure Shear Extension.

a) The effect of pure shear position.

In figure 7.2 basin geometry and crustal structure are shown

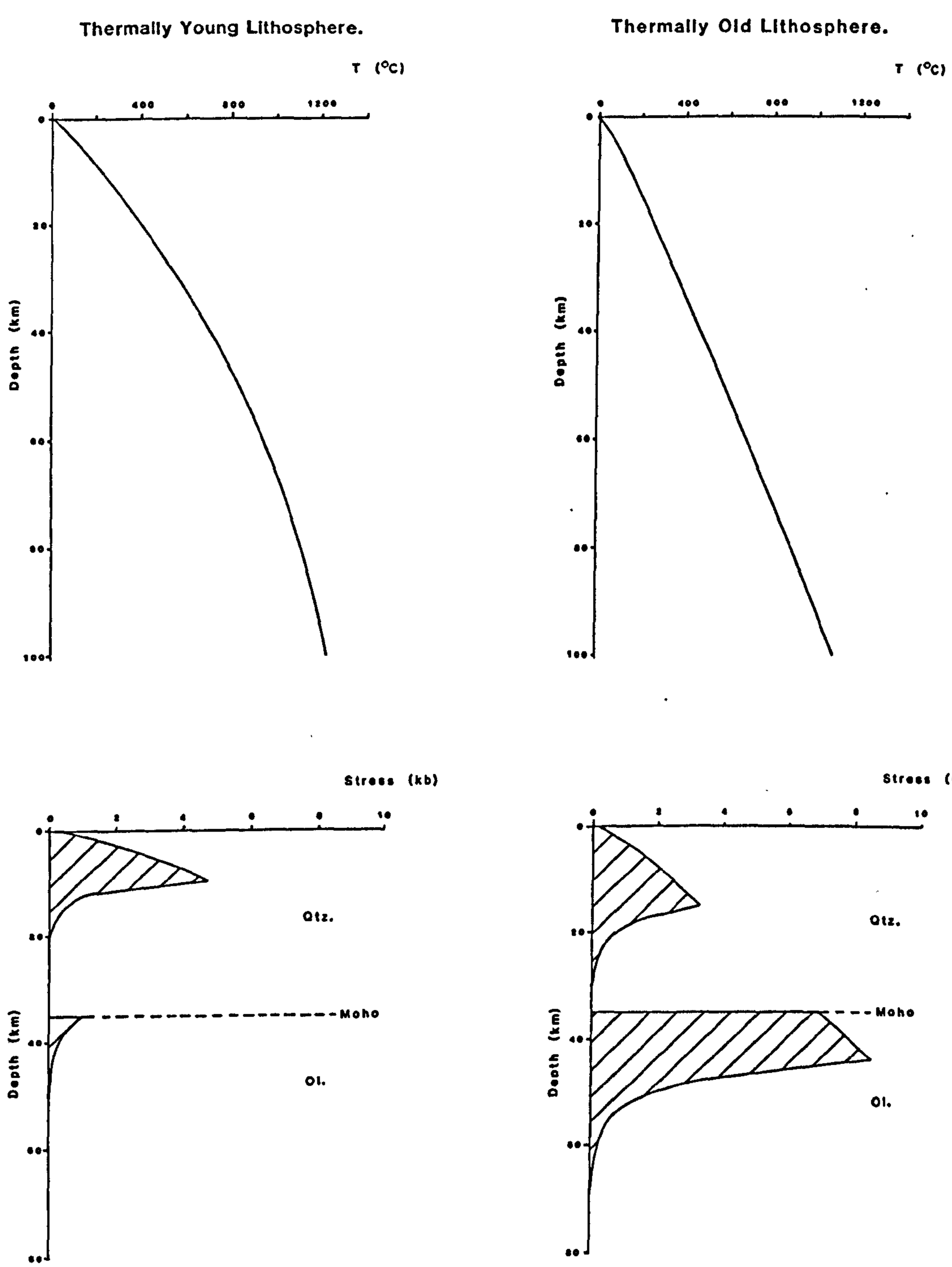

Figure 7.1 - Geotherms and corresponding yield-stress envelopes for thermally old and young lithosphere with surface heat flows of 45mW.m^{-2} and 75mW.m^{-2} respectively. The yield-stress envelopes are generated in response to a tensile force equivalent to a strain rate of $10^{-15}s^{-1}$. The stresses resulting from thermally young lithosphere are significantly less than those for thermally old lithosphere - younger (and hence warmer) lithosphere is rheologically weaker.

directly following 30km extension along a low angle fault with an exponential geometry, which detaches at a depth of 20km. A cool pre-rift geotherm has been assumed with a surface heat flow of 45mW.m^{-2} and includes radiogenic heat input. Rifting is assumed to be instantaneous, while an applied strain rate of 10-15 s^{-1} has been assumed for the stress calculations. All subsidence remains starved of sediment fill.

Pure shear deformation thins the lower crust and causes some of the subsidence at the surface. In this example there is no lateral offset between the start of simple and pure shear, and so both upper and lower lithosphere deformation are concentrated into a relatively small region and as a consequence a relatively narrow basin is formed.

The weakening of the lithosphere shown by the force distribution in figure 7.2 reflects both crustal thinning and temperature perturbations caused by simple shear-pure shear extension. The weakest part of the extended region is shown to be in the deepest part of the basin, where crustal thinning has been greatest. Yield-stress envelopes are shown at selected positions; peripheral to the extension, at the point of maximum simple shear, at a region of interference between simple and pure shear and within the region of pure shear only. In each case the distribution of stress in the crust is dictated by the amount of thinning experienced by the hanging wall. For example, where the simple shear deformation has been greatest (130km) the thickness of the cool hanging wall is effectively zero. The implications of this removal of the hanging wall is a denudation of the

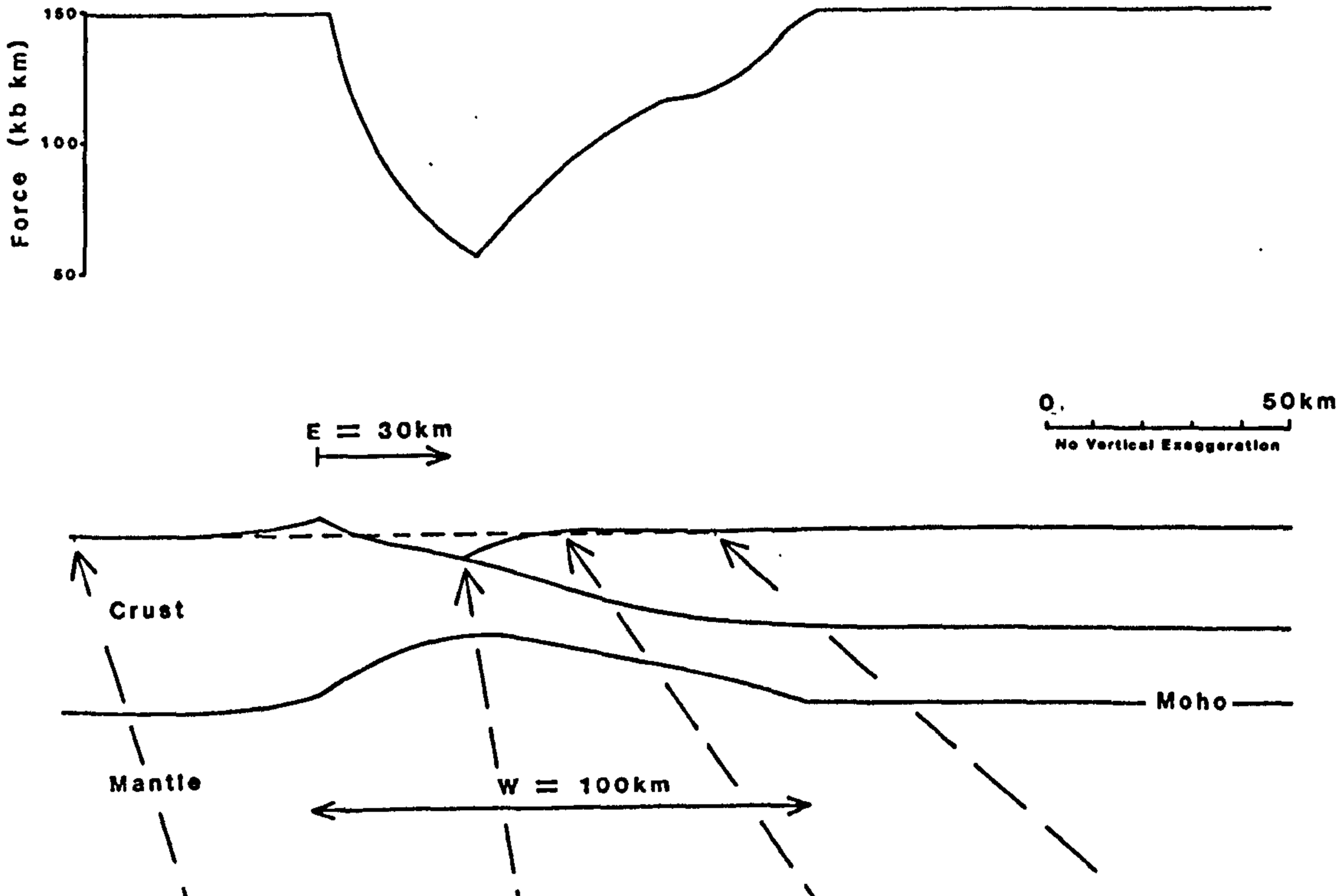

Figure 7.2 - Simple and pure shear rifting of thermally old lithosphere showing resulting basin geometry and crustal structure after 30km extension along a listric fault which detaches at a depth of 20km. A lithospheric strength profile and several yield-stress envelopes have been generated by an applied strain rate of $10^{-15}s^{-1}$, even though temperature perturbation calculations have assumed rifting to bbe instantaneous. The force/unit length distribution across the extended region shows that the rheological strength of the lithosphere is controlled by the amount of crustal thinning and heating induced by both simple and pure shear deformation.

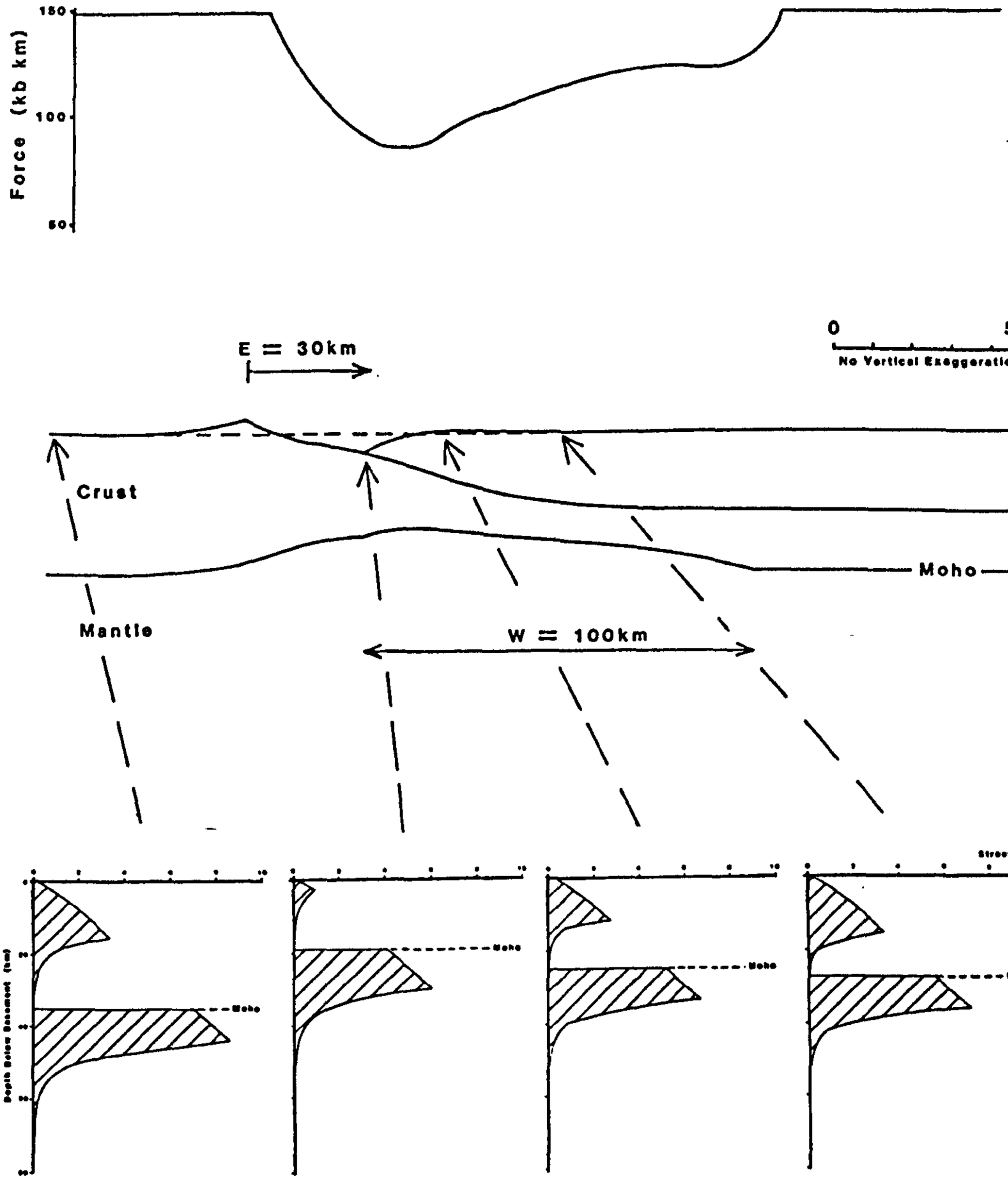

Figure 7.3 - Pure shear has been offset 30km distally with respect to the simple shear. In response to this offset the force profile shows lithospheric weakening in the distal region where deformation has occurred by pure shear.

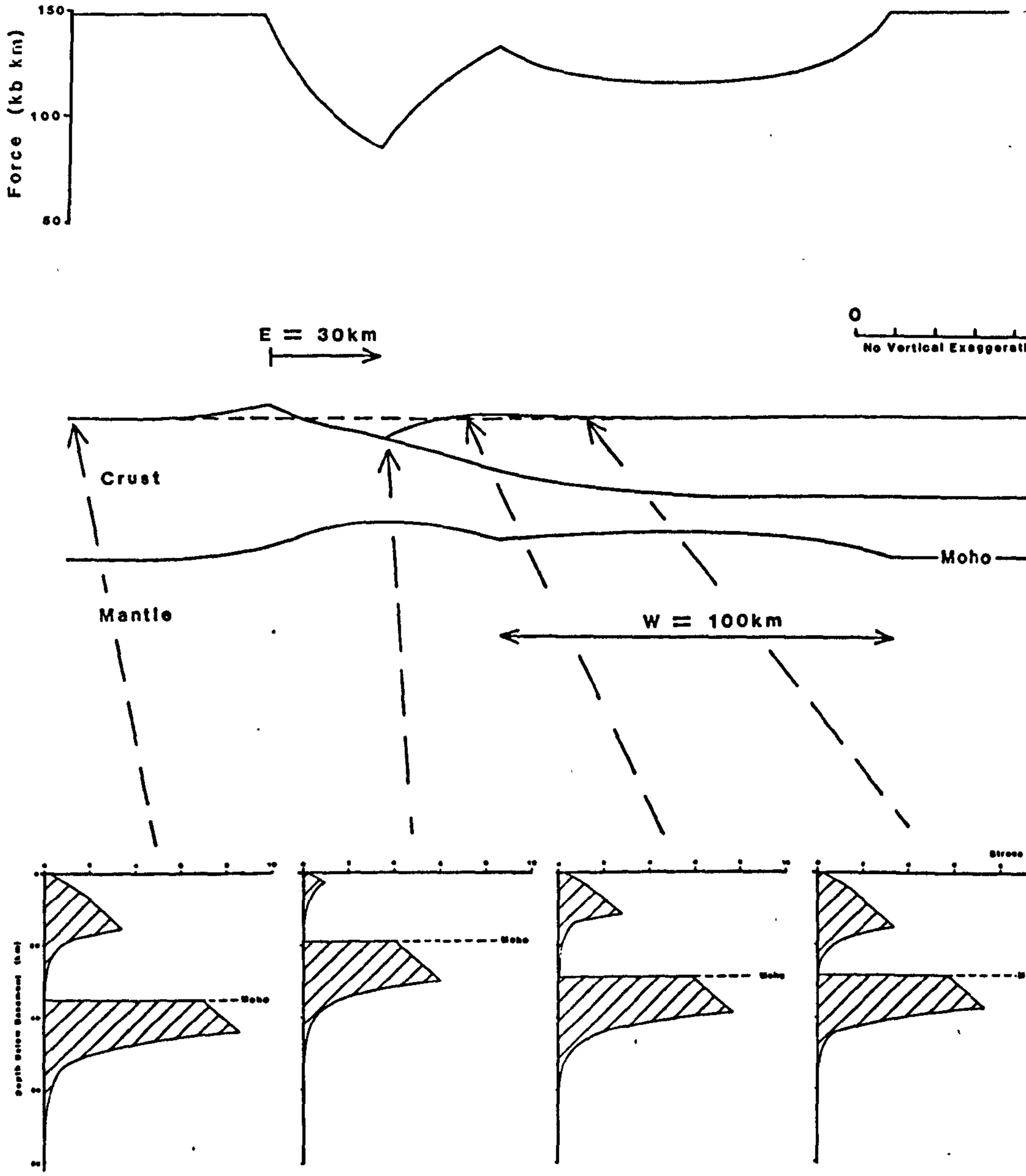

Figure 7.4 - Pure shear has been offset by 60km with respect to the start of simple shear (ie. the footwall cut-off). This separation produces two almost separate regions of lithosphere weakening. However, the point of minimum strength remains within the rift depocentre (30km from the footwall cut-off) where crustal thinning has been greatest.

brittle layer and as a consequence the stresses in the crust are considerably reduced. Stresses within the mantle are also reduced due to the higher temperatures. It is clear that the weakest point across the basin is laterally coincident with the position of maximum crustal thinning.

Offsetting the lower lithosphere pure shear deformation with respect to the simple shear separates the effects of the two deformational regimes. In figures 7.3 and 7.4 distal offsets of 30km and 60km are investigated. The effect of this offset is to cause a distally positioned broad depression in the force distribution, which is laterally coincident with the region of pure shear. This is most evident in figure 7.4 where there is greatest lateral offset between simple and pure shear. The pure shear is primarily responsible for adding heat to the base of the lithosphere, which, in turn, weakens the olivine component. However, despite the generation of this second low strength minimum, the position of greatest weakening still remains within the rift depocentre (30km from the footwall cut-off)

b) The effect of detachment depth.

A detachment depth at the Moho (figure 7.5) means that there is no thinning by pure shear of the lower crust. However, this change in the attenuation pattern of the crust is not reflected by a significant difference in the overall rheological strength of the lithosphere (compare figure 7.4). At lower crustal depths the temperatures are sufficiently high to cause plastic failure of the quartz rheology. Thinning of the lower crust mostly affects this

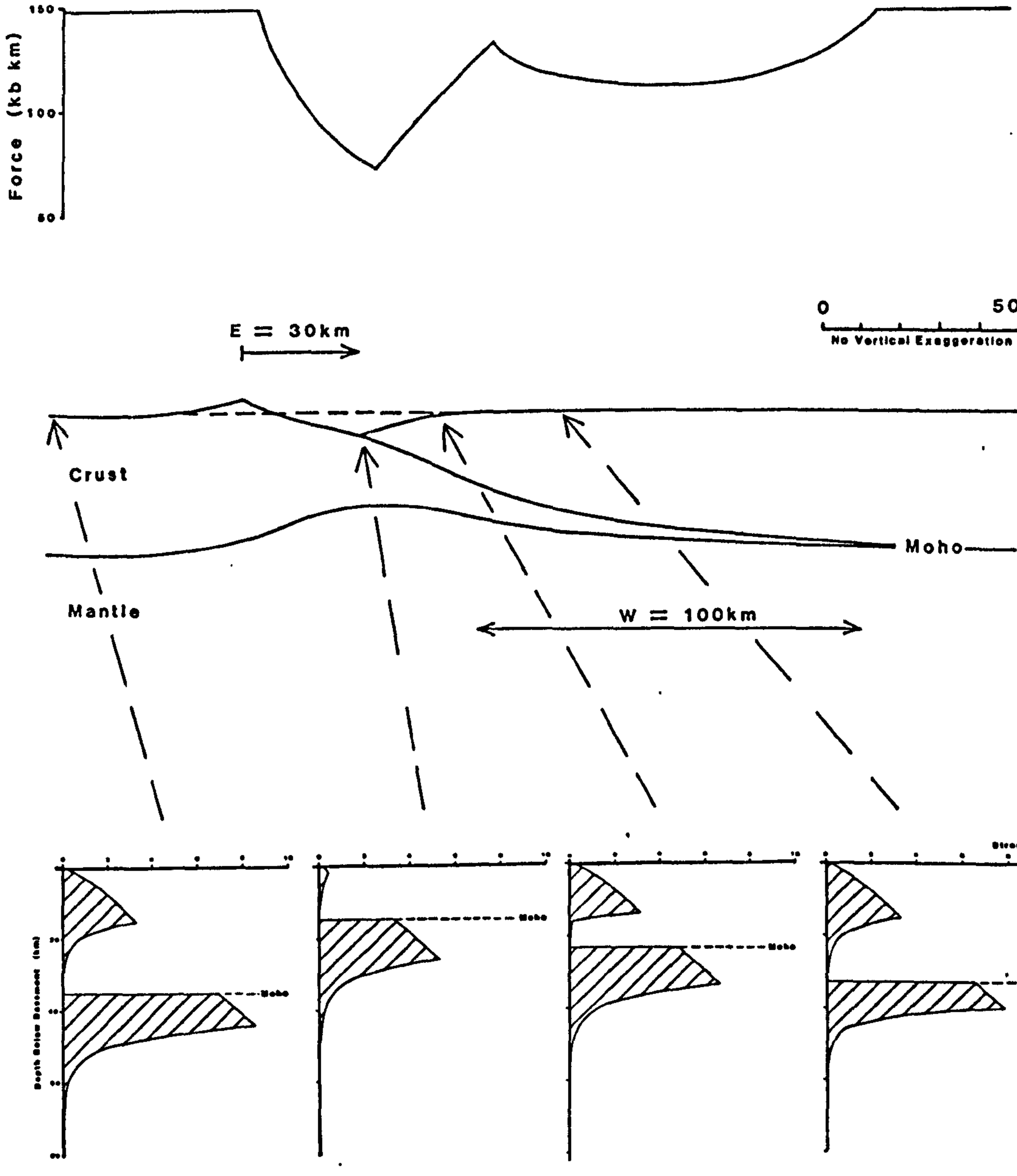

Figure 7.5 - Extension along a fault flattening into a horizontal detachment at the base of the crust means that there is no pure shear thinning of the crust. However, deepening of the detachment from the mid crust to the Moho does not significantly change the overall rheological strength of the lithosphere (cf. figures 7.4 and 7.5).

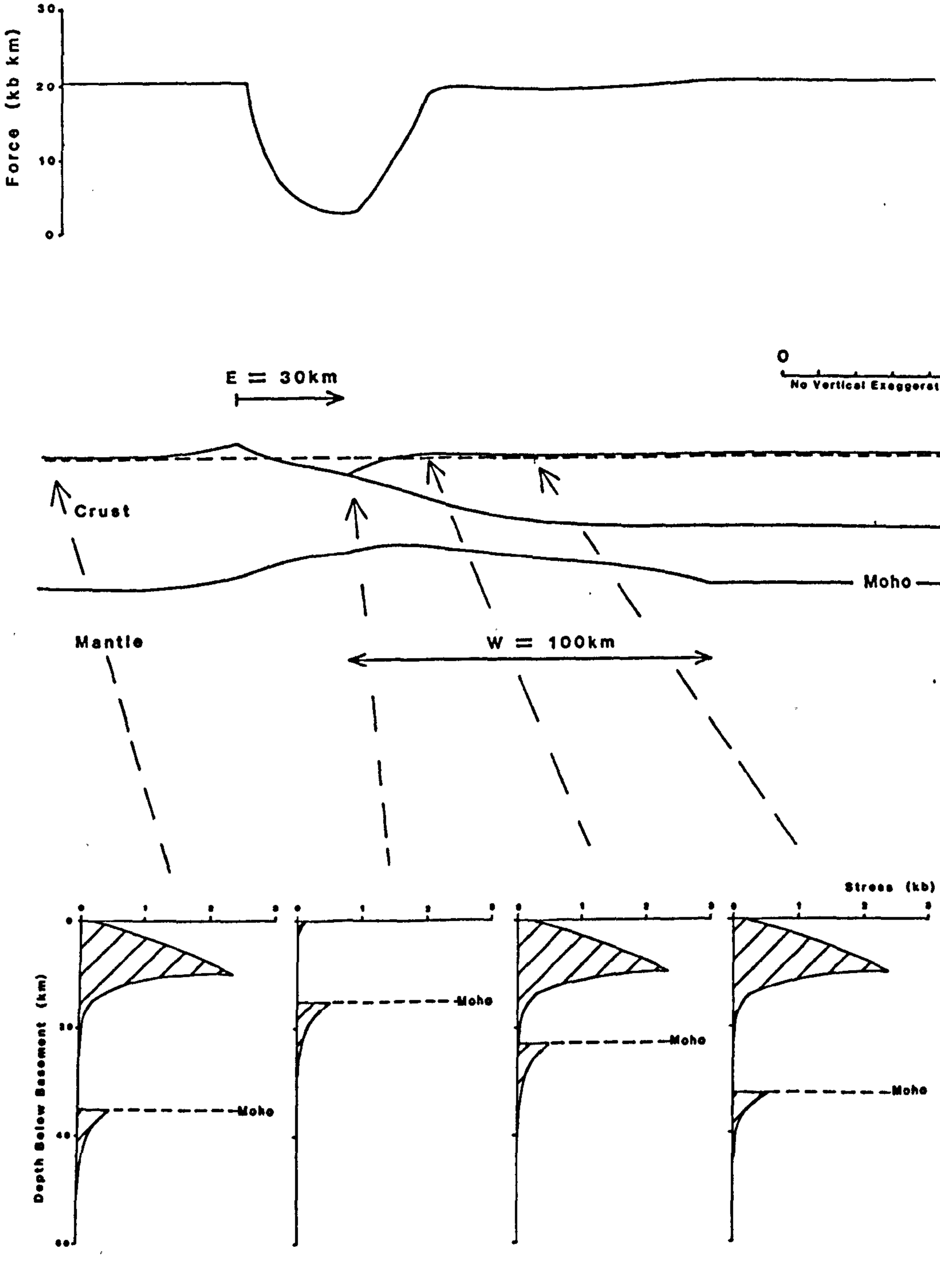

Figure 7.6 - Thermally young lithosphere is shown to be very weak in an unextended state. Rifting causes even more weakening of the lithosphere so that it possesses negligible strength.

region of plastic failure, where the stresses are negligible, and therefore does not have a dramatic effect on the integrated strength of the lithosphere.

c) The effect of geothermal gradient.

Figure 7.6 shows basin geometry and crustal structure resulting from the extension of thermally young lithosphere with a surface heat flow of 75 $mW.m^{-2}$. The rifting of warm (and hence weak) lithosphere means that the forces required for extension are reduced for a particular strain rate, although the overall pattern of lithospheric weakening generated by the rifting is very similar to that obtained from the extension of cool lithosphere (cf. figure 7.3).

7.4 Modelling Implications on the Site of the Continent-Ocean Boundary.

The above work shows that the rheologically weakest part of the lithosphere following rifting coincides with the region of maximum crustal thinning, irrespective of pure shear position and detachment depth. Studies of passive continental margins however reveal that in certain cases continental extension, leading to sea floor spreading, takes place in areas of relatively thick crust. For example, the separation of South America from Africa took place close to the present Brazilian margin where the crust is relatively thick (figure 7.7). In order to explain this phenomena there are several factors which can further modify the rheological strength of the lithosphere and that have not been included in the above work:

a) The inclusion of other crustal and/or mantle

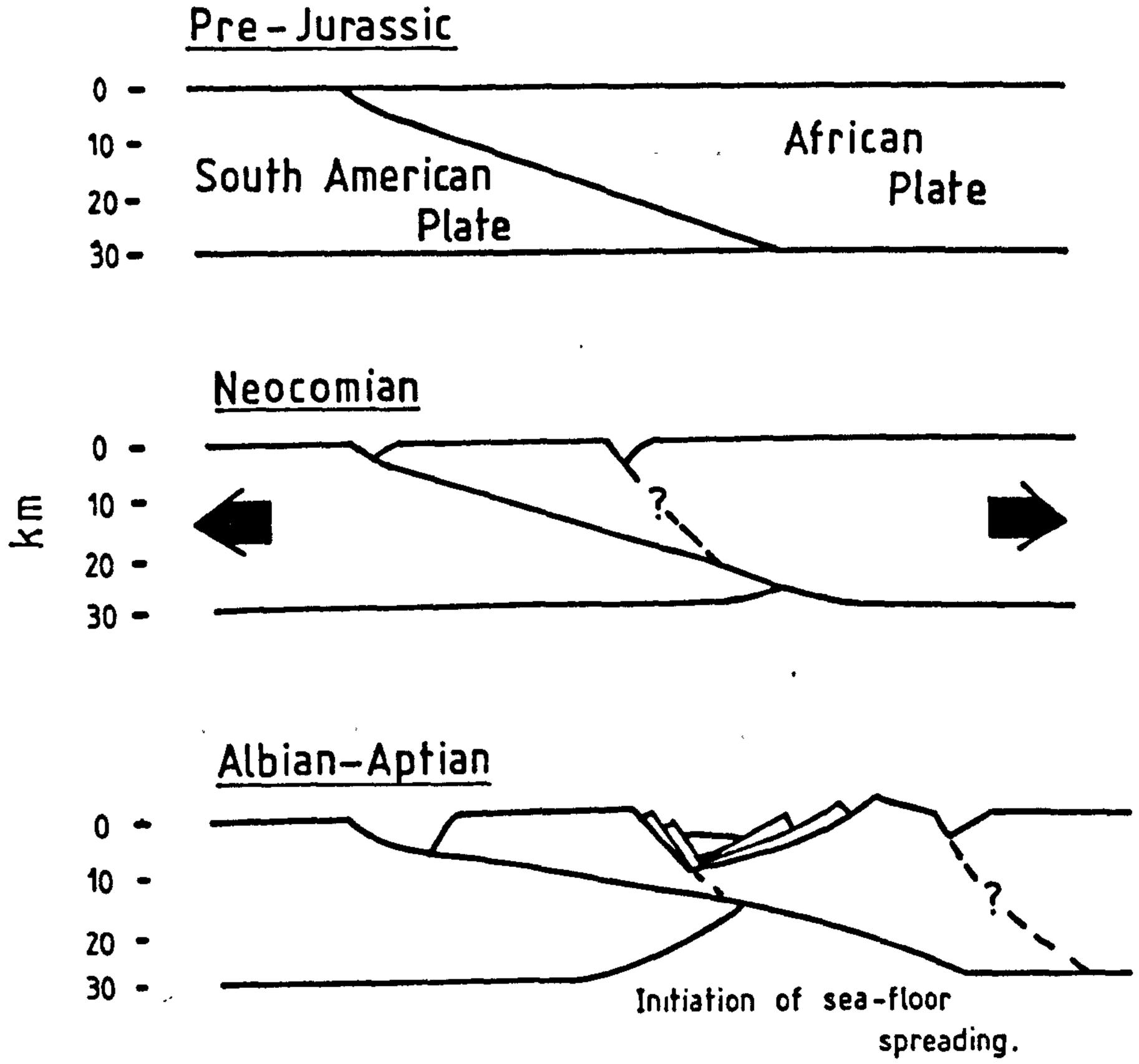

Figure 7.7 - The separation of South America from Africa began in the Jurassic, where the initiation of sea floor spreading began distally to the initial rift centre in a region of relatively thick crust (Ussami et al., 1986).

rheologies such as pyroxenes and feldspars.

b) The post-rift re-equilibration of the lithosphere temperature field.

c) Finite or non-instantaneous rifting.

d) Sediment infilling of the rift basin.

e) Magmatic underplating of the crust by rift-induced partial melting of mantle lithosphere.

f) Reactivation of crustal weaknesses from past tectonic events.

a) The effect of additional lithosphere rheologies.

The effect of including a more complex compositional structure on the rheological strength of the lithosphere is shown in figure 7.8 where both force distribution and yield-stress envelopes are shown for extended thermally old lithosphere with a crust of wet quartz, a lower crust (20 to 35km) of anorthosite and a mantle of olivine. The lithosphere has been extended by 30km and the pure shear deformation has been offset 30km with respect to the start of simple shear. The creep rate of anorthosite or plagioclase is predicted by the following equation and based on experimental work by Shelton and Tullis (1981):

$$\dot{\epsilon} = 8.2 \times 10^{2} \cdot \exp(-28788/T) \cdot (\sigma_1 - \sigma_3)^{3.2} \quad s^{-1} \quad \text{---- 7.6}$$

The addition of plagioclase to control the rheological behaviour of the lower crust generates an overall stronger

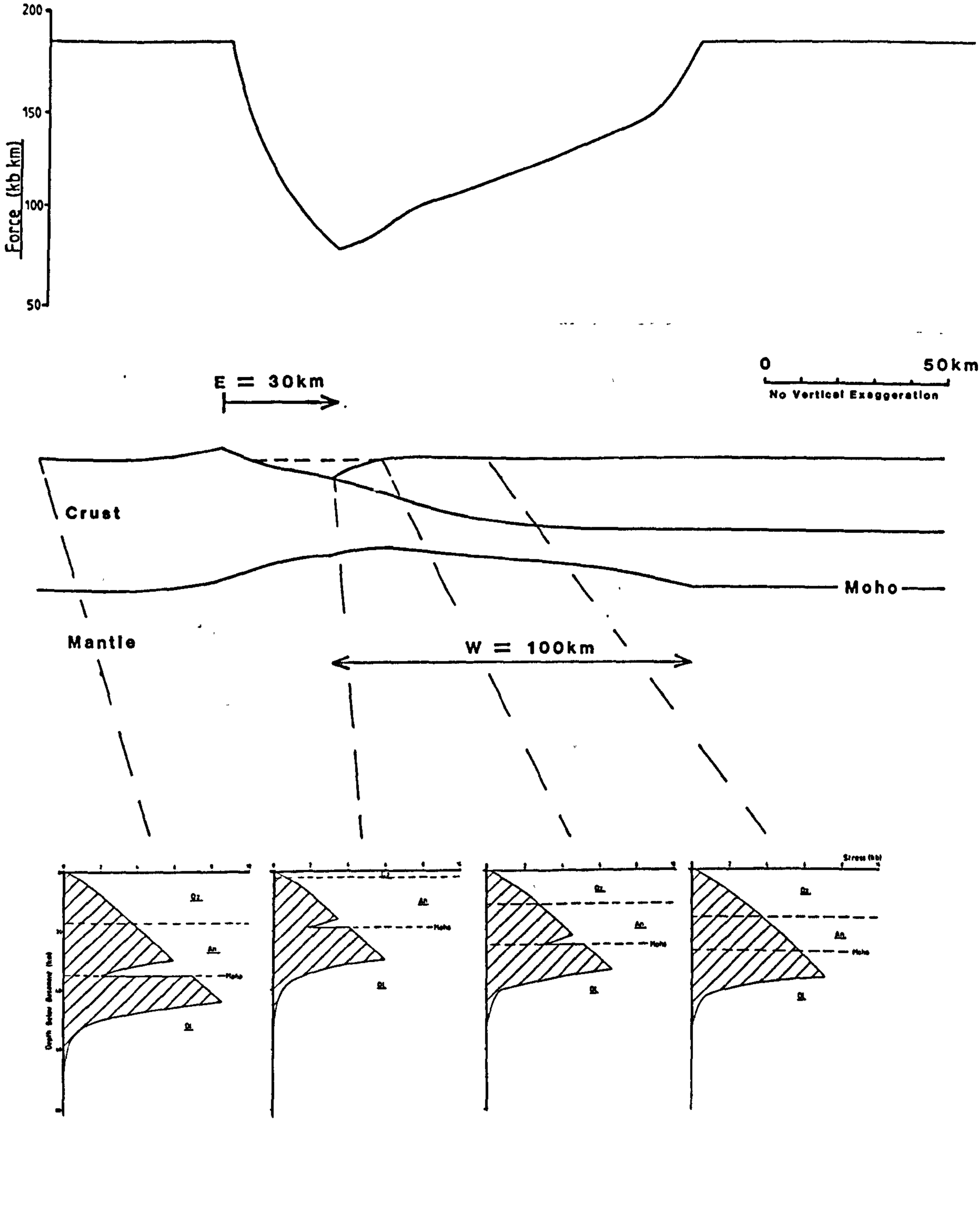

Figure 7.8 - Strength profile and yield-stress envelopes resulting from the extension of a three layered lithosphere; an upper crust of wet quartz, a lower crust of plagoclase and a mantle of olivine. Plastic failure is reduced in the crust (cf. figure 7.3) due to the strong plagioclase rheology of the lower crust, and as a result the overall strength of the lithosphere is increased.

lithosphere in both undeformed and rifted states. This is because the mineral plagioclase is sufficiently strong in the lower crust to deform by a brittle process. Despite the increased lithosphere strength, however, the force profile across the basin shows a very similar pattern to that generated by the rifting of the two layer lithosphere (compare figure 7.3). It is suggested, therefore, that the compositional variation with depth is not an important consideration when investigating relative positions of weakness over an extended region.

b) The effect of the post-rift re-equilibration of the lithosphere temperature field.

After rifting perturbations caused to the lithosphere geotherm gradually re-equilibrate over a time span of the order of 100Ma to 300Ma. This re-equilibration, which represents a cooling of the isotherms back to their original state, involves both the lateral and vertical transfer of heat. This is reflected in the sequence of force profiles shown in figure 7.9, which show the rheological state of the lithosphere at various stages from rifting (0Ma) through the post-rift re-equilibration of the temperature field. Again the initial rift phase consisted of 30km of extension along a listric fault, with pure shear positioned 30km distally to the footwall cut-off. At 0Ma the familiar situation of weakened lithosphere with a minimum at the point of maximum crustal thinning (30km from the footwall cut-off) is generated adjacent to a lesser weakened area arising from the pure shear deformation.

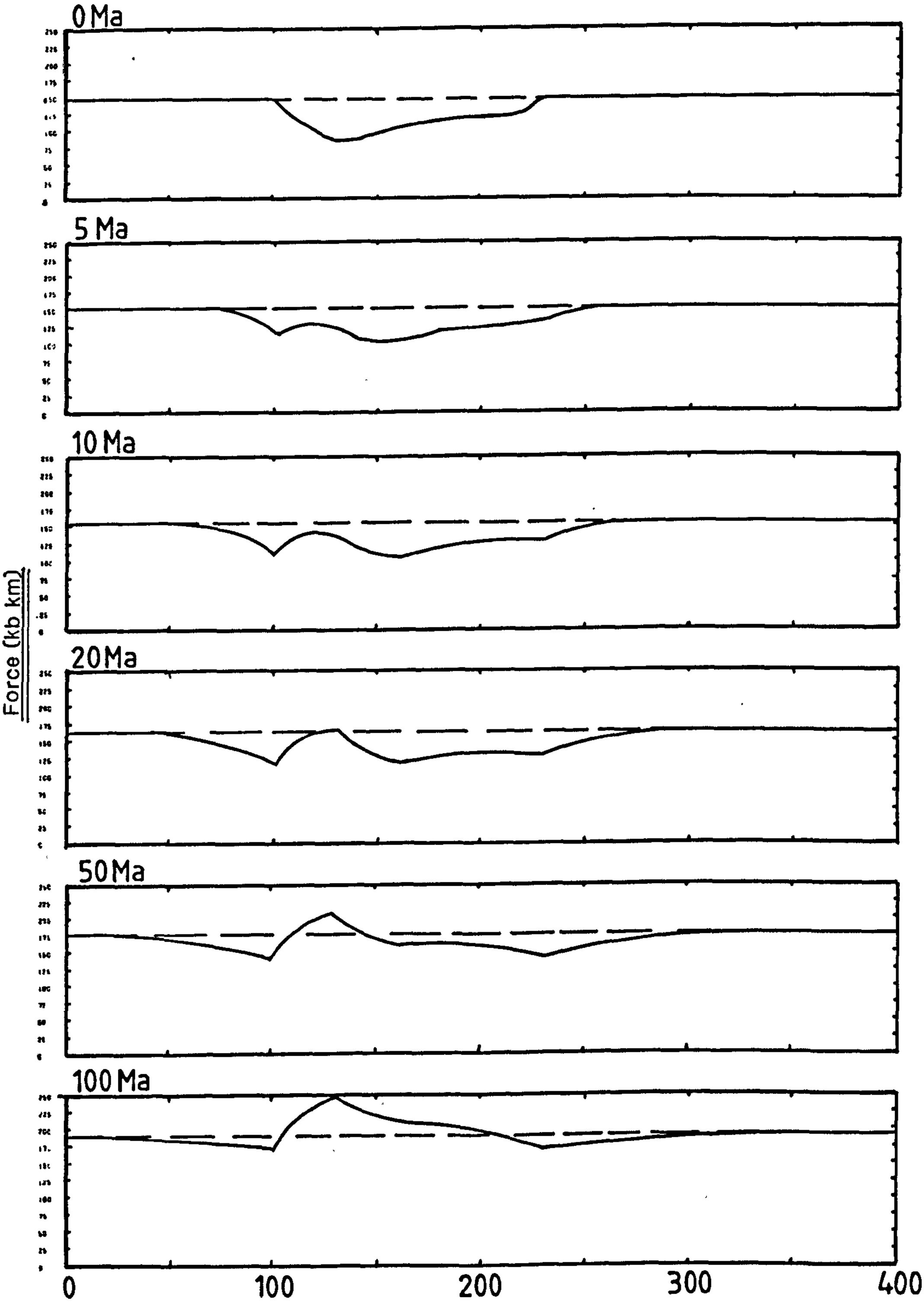

Figure 7.9 - Force profiles shown at various stages from rifting (0Ma) by 30km along a fault detaching at a depth of 20km and during the re-equilibration of the lithosphere temperature field. Pure shear has been offset 30km distally to the start of simple shear. The strength of the lithosphere within the simple shear depocentre gradually increases until at 20Ma it becomes stronger than its surroundings. By 10Ma the region of pure shear is the weakest. Lateral heat diffusion accounts for low strength in areas peripheral to the extension.

After rifting two dramatic changes occur to the pattern of weakening:

a) The extreme weakening within the rift basin gradually decreases until at about 20Ma it becomes stronger than the adjacent pure shear region.

b) Strength reductions are predicted in the areas surrounding the extensional deformation due to lateral diffusion of heat into these peripheral regions.

How can the initial strength minimum, controlled by the simple shear deformation, quickly become so strong compared to the region of pure shear? Simple shear tectonically denudes the hanging wall so that hot rock material is exposed at the surface. The temperature disturbances caused are essentially shallow and, therefore, re-equilibration occurs very quickly by heat loss from the surface. In contrast, pure shear has a negligible effect on crustal temperatures at rifting, although it creates a large perturbation to the geotherm within the mantle. After a finite time period the heating effects from the pure shear diffuse upwards into the crust, thereby enhancing plastic failure of quartz and resulting in a lower integrated strength. The most notable changes take place in the force profile during the first 10Ma after rifting, which reflects the exponential decay path followed by the equilibrating geotherm.

By 100Ma the whole of the area of crustal thinning is stronger than the surrounding undeformed lithosphere. This is caused by the rift attenuation of the quartz component in

the crust so that the lithosphere is now effectively composed of a greater proportion of the stronger olivine mantle. This phenomena has been previously noted by Kusznir and Park (1987) and the results of their studies are shown in figure 7.10 where lithosphere strength as a function of heat flow is shown for models with a range of crustal thicknesses. A thinned crust means that the lithosphere is essentially composed of a greater proportion of olivine mantle at the expense of the weaker quartz rheology. This situation at average surface heat flow values of 70mw.m^{-2} makes the lithosphere relatively strong. However, at both low and high geothermal gradients lithosphere strength is independent of crustal thickness, except at zero crustal thickness. For high geothermal gradients the temperatures in the mantle lithosphere are sufficiently high to induce plastic failure and the brittle-ductile transition is within the crust, causing low stresses, whereas the opposite is true for low geothermal gradients because the brittle-ductile transition is always within the olivine mantle.

The implications of this study on the evolution of ocean-continent boundary is quite profound because it demonstrates how the locus of lithosphere weakening is transferred from the position of initial extension, and hence greatest crustal attenuation, to the surrounding regions. Within the first 10Ma after rifting strength minimum moves to the region of pure shear deformation, after which it migrates into areas both proximal and distal to the deformation in response to lateral heat movement.

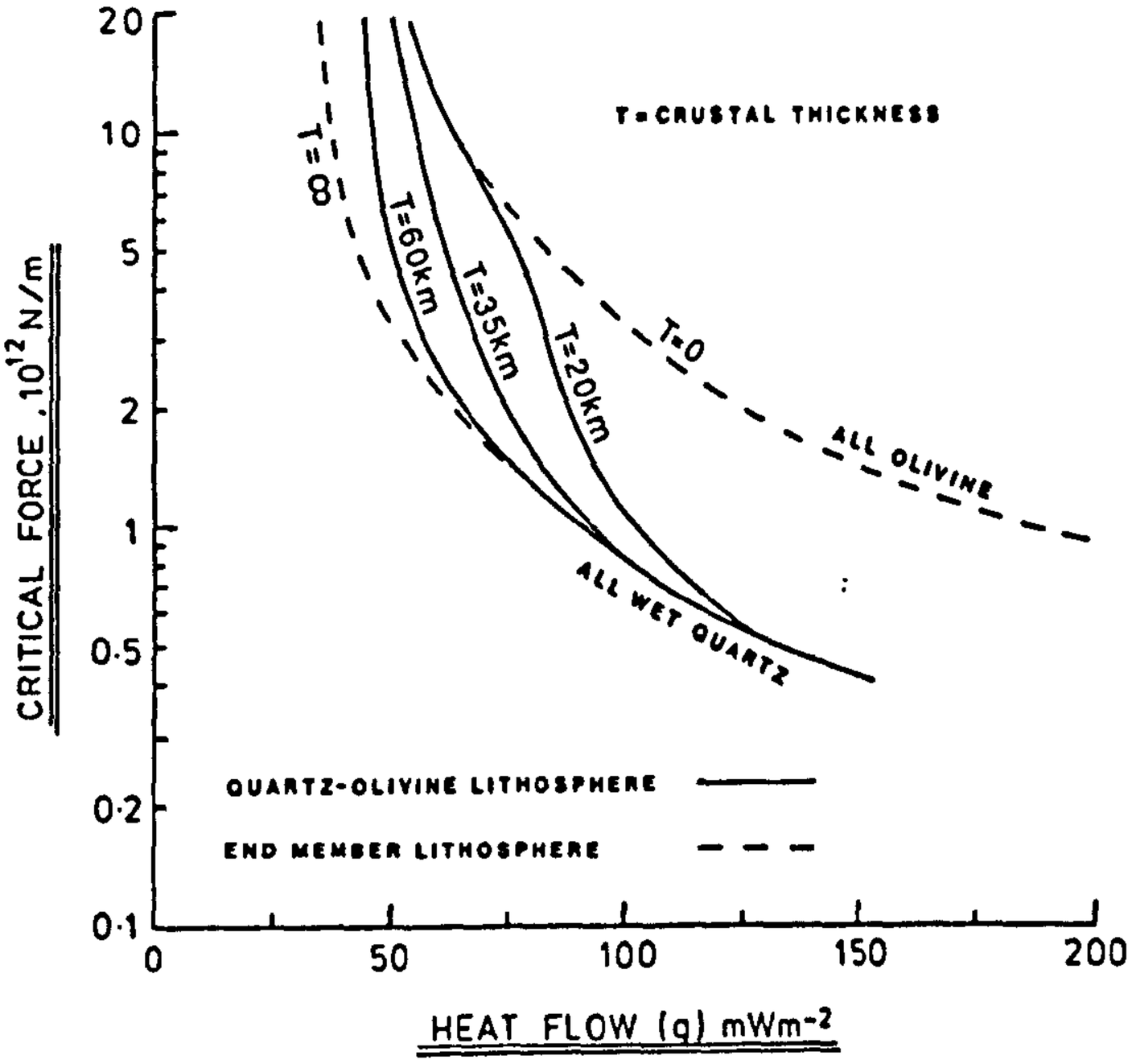

Figure 7.10 - The effect of crustal thickness on lithosphere strength (Kusznir and Park, 1987). Decreasing crustal thickness increases lithosphere strength except at very high and low geothermal gradients.

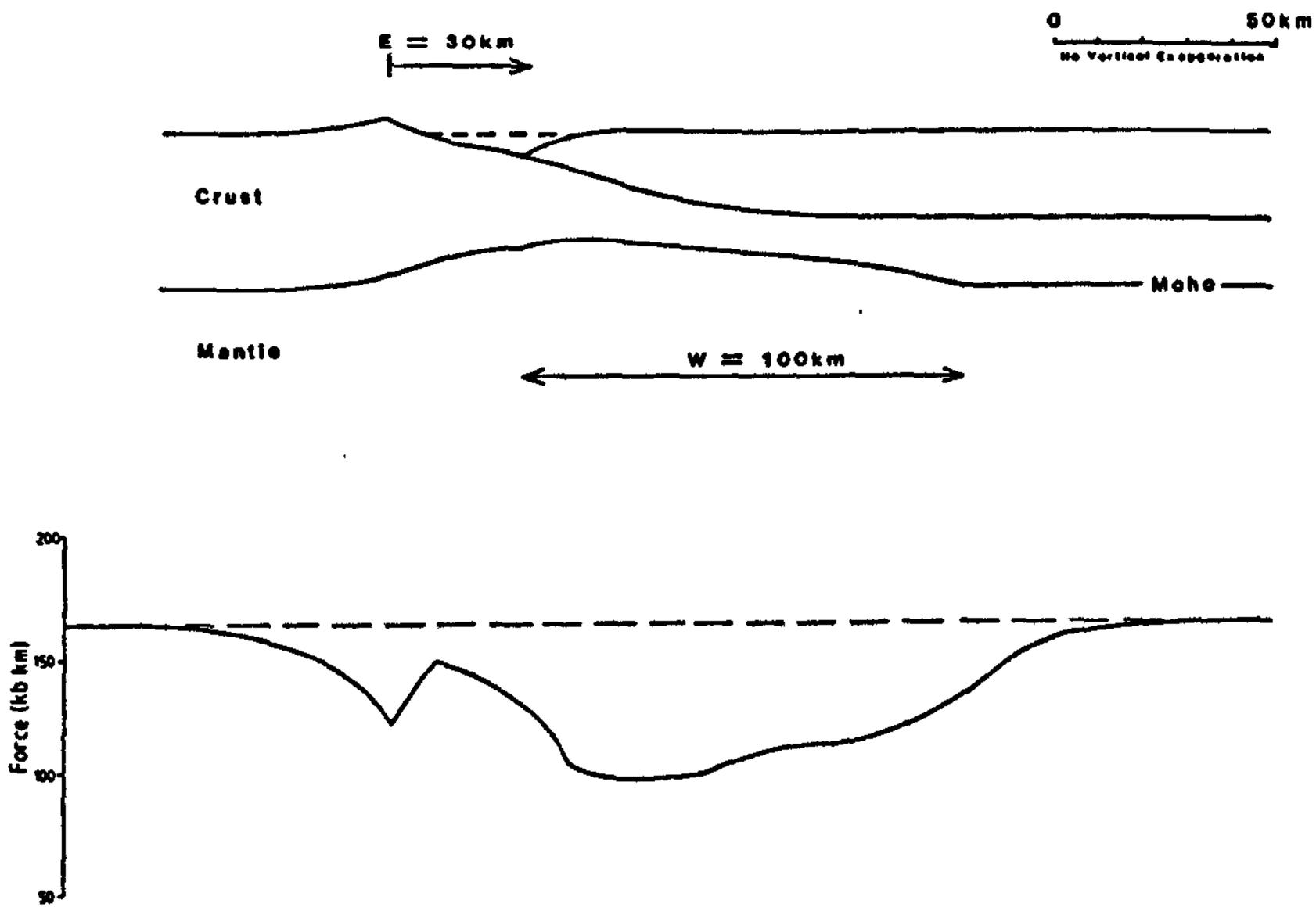

Figure 7.11 - Rheological strength shown after non-instantaneous rifting at a rate of 2km per 1Ma for 15Ma. Shallow temperature perturbations caused by simple shear re-equilibrate relatively quickly during the finite rift phase. The deep-rooted temperature disturbances resulting from pure shear reach crustal levels at the end of the rift phase (15Ma) and induce plastic failure at shallow depths in the crust. This weakens the lithosphere so that the region of pure shear has the lowest strength across the basin. Lateral heat flow also causes both proximal and distal weakening.

c) The effect of non-instantaneous rifting.

In chapter 5 the effects of instantaneous and finite rifting were contrasted in the context of the evolution of the Jeanne d'Arc basin. In the former case the heat available directly after rifting is at a maximum, which is reflected by the extreme amounts of thermal subsidence produced. Rifting over a finite time period, on the other hand, allows heat diffusion and cooling to occur during extension so that the temperature field is partially equilibrated after the rift event - a reduced thermal subsidence component results.

In figure 7.11 the effects of finite rifting, at a rate of 2km per 1Ma for 15Ma, on the rheological strength of the lithosphere are examined. The strength profile shows that the weakest part of the basin after the finite rift phase is within the region of pure shear. There are also more localised strength minima both proximally and distally to the deformation. The pure shear minimum arises initially from thermal weakening of olivine in the mantle lithosphere. During the finite rift increments heat induced by the deformation has time to diffuse vertically into the crust, which, in turn, is weakened and the integrated strength of the lithosphere is reduced. The effect is very similar to that described for temporal changes in lithosphere strength occurring during post-rift thermal re-equilibration of the geotherm following instantaneous extension (figure 7.9).

Similar effects to the above have been previously noted by Kusznir and Park (1987) from their experiments on extension at a finite time rate. They concentrated on the rheological

effects of varying strain rates and showed that fast strain rates produce a larger increase in geothermal gradient and, in turn, a net weakening of the lithosphere. Slow strain rates, for the same amount of stretching, produce a net strengthening of the lithosphere due to thinning of the crust in the presence of a relatively unperturbed geotherm.

d) The effect of infilling the rift basin with sediment.

Steckler and ten Brink (1986) have contrasted yield-stress envelopes for oceanic lithosphere without sediment deposition and for oceanic lithosphere loaded with 10km of sediments. They show that the lower thermal conductivity of the sediments insulates the basement below so that the plastic failure envelope is brought nearer to the surface. Given that many passive continental margins show sediment accumulations of 12-15km (eg. Steckler and Watts, 1978), the modification of the rheological strength of the lithosphere by sediment blanketing is an important factor.

e) The effect of magmatic underplating of the crust by rift-induced partial melting of mantle lithosphere.

Recent work has illustrated the importance of the underplating of continental margins by mantle melt generated by rifting (eg. White et al 1987[1] and 1987[2], McKenzie and Bickle, 1988). Direct evidence of a basal crustal basaltic layer comes from both sampling by drilling (Roberts et al, 1984) and from seismic velocity measurements (White et al 1987[1]). The generation of magma occurs due to pressure release - as the lithosphere is thinned asthenospheric material, at a more or less constant temperature, is brought

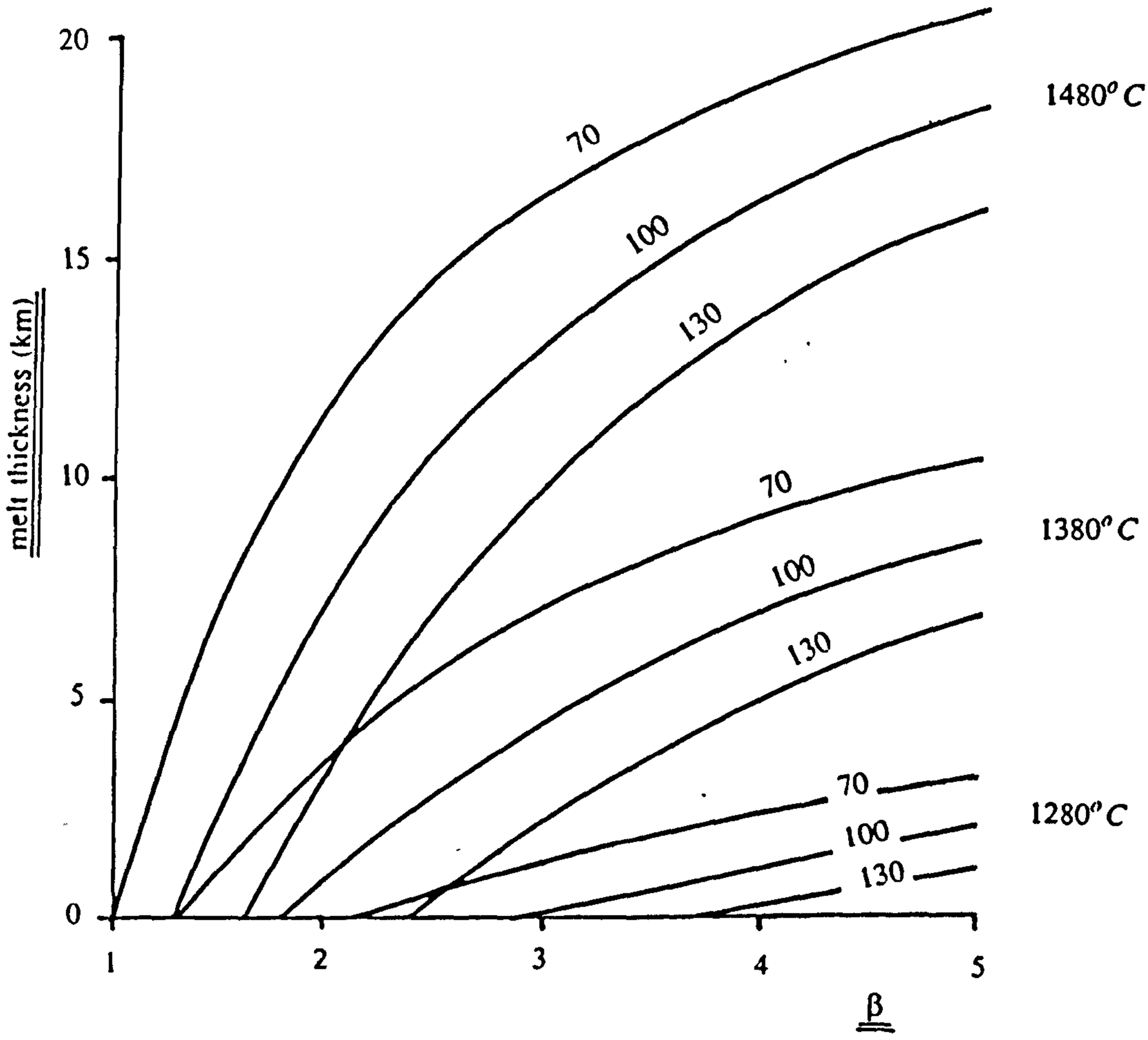

Figure 7.12 - Total melt thickness generated by various amounts of lithosphere extension as defined by β (McKenzie and Bickle, 1988). The numbers against the curves give the thickness of the mechanical boundary layer and the temperatures on the right are the asthenospheric potential temperatures. This melt will add heat to the lithosphere and weaken it rheologically.

to shallower depths where the pressure is lower. The solidus temperature, denoting the temperature at which rock material first melts, is less at lower pressures and when the temperature of the raised asthenospheric rock equals the solidus temperature melting occurs. It follows that the amount of melt produced is controlled by the amount of extension and the temperature of the asthenospheric mantle (figure 7.12). For the models presented above the extension of the lithosphere, β, does not exceed 2 and the temperature of the asthenosphere is assumed to be 1333°C, which means the thickness of melt generated will be between 0 and 4km. At a typical passive margin, however, extension factors exceed values of 2, especially in near proximity to the ocean-continent boundary, causing the thickness of melt generated to be much greater.

The effect of magmatic underplating on the rheological strength of the lithosphere will be to cause a fairly rapid weakening caused by the extra heating from the emplaced melt. Strength reduction will be greatest where the thickness of magma emplacement has been most pronounced, which, from figure 7.12, is indicated to be at the point of maximum lithospheric thinning.

f) Reactivation of crustal weaknesses from post tectonic events.

The fact that basin formation is controlled by the extensional reactivation of existing faults has already been mentioned in chapter 5 where the Mesozoic extension of the Grand Banks region of Newfoundland took place on an inherited structural framework from the PreCambrian/Early

Palaeozoic. Does the presence of potential breaching horizons have a greater influence on lithosphere failure than rheological strength? It is suggested that the attenuation of the upper crust takes place by extensional reactivation of existing weaknesses if they exist , whereas the lower lithosphere more readily deforms in the region of lowest rheological strength. But, the answer as to which of these is the dominant in controlling lithosphere strength must again be determined by factors such as geothermal gradient, time since rifting and rates of extension.

7.5 Summary.

The strength of the lithosphere after instantaneous rifting has been shown to be critically dependent upon:

a) its pre-rift thermal state - thermally young (and hence warm) lithosphere is weaker than thermally old (cool) lithosphere.

b) the amount of simple and pure shear extension - simple shear extension causes a stress reduction in the crust by tectonically denuding the hanging wall. Both simple and pure shear crustal thinning effectively raise the stress envelope in the mantle nearer to the surface where the lower confining pressures generate lower stresses. Also the heating of the lithosphere by the raising of the lithosphere-asthenosphere boundary and the intervening isotherms serves to decrease the stresses in the mantle by inducing plastic failure at shallower depths.

c) the interference between simple and pure shear components - a lateral displacement of the pure shear deformation causes a corresponding weakening of the lithosphere in the distal region. However, greatest lithosphere weakening is always at the point of maximum crustal thinning in the rift depocentre.

d) Deepening the detachment depth from the mid crust to the Moho does not appear to have any significant effect upon the rheological strength of the lithosphere.

The main conclusion to arise from the investigations carried-out in section 7.4 is that the distribution of rheological strength across a region of rifting is mostly determined by the temporal behaviour of the lithosphere temperature field. The implications of this on the position of the ocean-continent boundary are twofold:

a) If continental breakup is fast then the site of lithosphere rupturing will be within the original rift depocentre. Rheological weakening will also be aided by the magmatic underplating of the crust.

b) If continental breakup is more prolonged then a migration of the breaching centre is likely, its final position being determined either by the position of sub-crustal stretching or lateral heat flow into regions of unthinned crust.

CHAPTER 8

Numerical Models of Continental Lithosphere Shortening.

8.1 Introduction.

The coupled simple shear-pure shear model, which has been previously used to examine the thermo-mechanical behaviour of the lithosphere during extensional tectonics, has been adapted for lithosphere shortening. The model assumes that the compressional deformation of the upper lithosphere is achieved by simple shear on thrusts, and by pure shear below the horizontal detachment horizon into which the thrusts flatten.

8.2 Application of the Coupled Simple Shear - Pure Shear Model to Continental Lithosphere Shortening.

The model quantifies the geometric response of the lithosphere to shortening by simple shear using a chevron construction (Verall 1982, Gibbs 1983), which has been modified to allow the unsupported hanging wall following compression to collapse directly downwards onto the footwall shoulder. Figure 8.1a shows crustal thickening resulting from 10km, 20km and 30km of shortening along a low angle thrust with exponential geometry, which detaches at a depth of 20km. 10km of compression generates up to a maximum of 7.5km of lithosphere thickening, while 30km gives a maximum of 15km thickening. The amount of simple shear thickening, $S_{(x)}$, is quantified by:

$$S_{(x)} = D_{(x)} - D_{(x+E)} \quad \text{---- 8.1}$$

where E is the amount of shortening and $D_{(x)}$ defines the

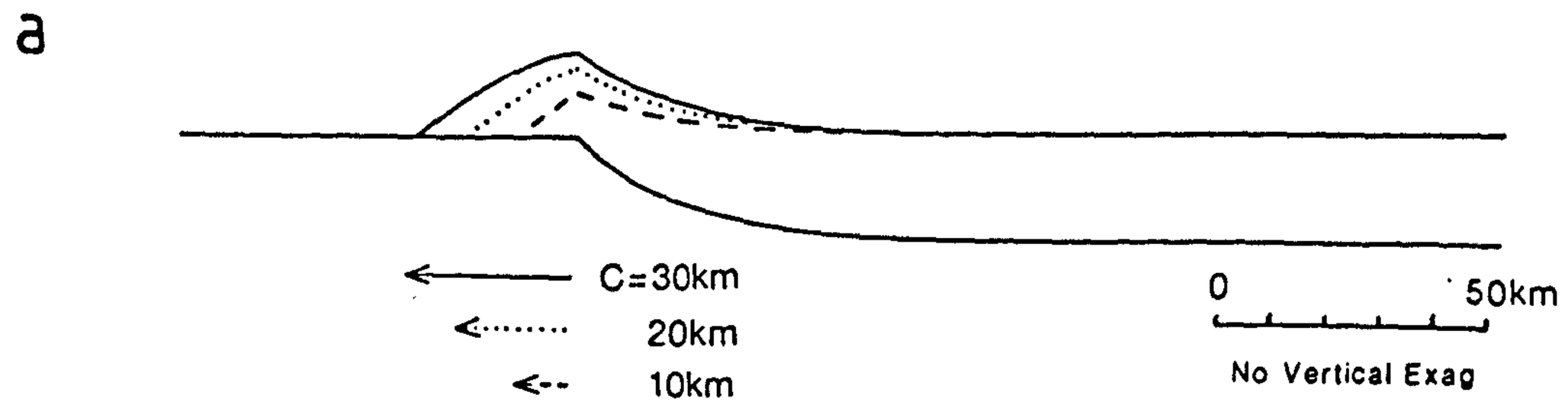

Figure 8.1 -

a) Lithosphere thickening by simple shear along a low angle fault following shortening amounts of 10km, 20km and 30km.

b) Simple shear deformation in the upper lithosphere gives way below the horizontal detachment to compression by pure shear. Lateral temperature gradients are created due to the overthrusting of warm hanging wall onto relatively cool footwall. Pure shear deepens the lithosphere/asthenosphere boundary - cooling results.

c) Geotherms following both extensional and compressional deformation respectively. Extension causes an initial heating of the lithosphere, whereas compressional deformation causes a cooling and a discontinuity in the geotherm at a depth of 17km, which defines the depth to the decollement along which thrusting is taking place.

thrust geometry such that:

$$D_{(x)} = 0 \quad \text{for} \quad x \leq x_o$$

$$D_{(x)} = Z_a \cdot (1 - \exp(-x/Z_a)) \quad \text{for} \quad x > x_o \quad \text{---- 8.2}$$

Z_a is the depth of detachment and x_o is the horizontal position of the outcrop of the fault at the surface.

Below the depth of detachment of the thrusts shortening occurs by pure shear, which is defined as a series of Beta factors (McKenzie 1978) such that:

$$\beta = 1+\epsilon \quad \text{----- 8.3}$$

where the maximum Beta value is 1, describing undeformed lithosphere, and the minimum Beta value is zero, representing the hypothetical situation of lithosphere infinitely compressed to zero horizontal length. The Beta factors defining the pure shear compressional deformation can be placed at any required lateral position and can be quantified by using equations 2.6 to 2.8 in which E denotes the amount of shortening, whereby E = -10km defines a shortening of 10km, E = -20km represents a shortening amount of 20km, etc. The amount of crustal thickening caused by pure shear is given by equation 2.5.

Both simple and pure shear perturb the lithosphere temperature field (figure 8.1b), in such a manner that the resulting effects are opposite to those arising from extensional tectonics. In figure 8.1c geotherms following simple shear extension and shortening are compared. In the former situation tectonic denudation of the hanging wall

Table 8

List of Symbols.

α	Flexural parameter	-----
D	Flexural rigidity	-----
$D_{(x)}$	Thrust geometry	-----
$\beta_{(x)}$	Shortening factor	-----
E	Amount of shortening	-----
g	Acceleration due to gravity	$9.81 m.s^{-2}$
ρ_c	Density of crustal rock	$2800 kg.m^{-3}$
ρ_m	Density of mantle rock	$3300 kg.m^{-3}$
$P_{(x)}$	Crustal thickening by pure shear	-----
$S_{(x)}$	Crustal thickening by simple shear	-----
T_e	Elastic thickness	-----
x_o	Horizontal position of fault outcrop	-----
v	Poisson's ratio	0.25
w	Flexural uplift or subsidence	-----
Y	Young's modulus	$70 x 10^9 Pa$
Z_a	Detachment depth	-----

causes an elevation of the geotherm and warm crustal material to be exposed at the surface. Crustal thickening after shortening depresses the geotherm and produces a marked temperature discontinuity across the fault surface showing that warm hanging wall material is emplaced on top of the footwall. In addition, pure shear deepens the lithosphere-asthenosphere boundary, causing further cooling and inducing subsidence at the surface. After the shortening event the temperature field re-equilibrates to its original state causing a gradual uplift of the surface over a time period of the order of 100Ma to 300Ma. The calculation of the perturbation to the lithosphere temperature field caused by simple shear - pure shear shortening can be calculated by following the steps in section 2.2b. The post shortening re-equilibration of the temperature field is again calculated using the finite difference method as described in section 2.3. The assumption is made that the base of the lithosphere, at 125km depth, is maintained at 1333°C even though lithospheric thickening displaces this thermal boundary downwards into the asthenosphere.

In figures 8.2 and 8.3 loading of the lithosphere, resulting from the simple shear-pure shear compression, has been compensated by Airy isostasy (chapter 2). Figure 8.2a shows surface topography, thrust geometry and crustal structure at 100Ma, following 30km of shortening along an exponential thrust which detaches at a depth of 20km. The original surface and undeformed fault geometry are denoted by dotted lines. The maximum topographic relief is 3km above the original footwall cut-off. Isostasy has accommodated most of the crustal thickening and a large downward displacement of

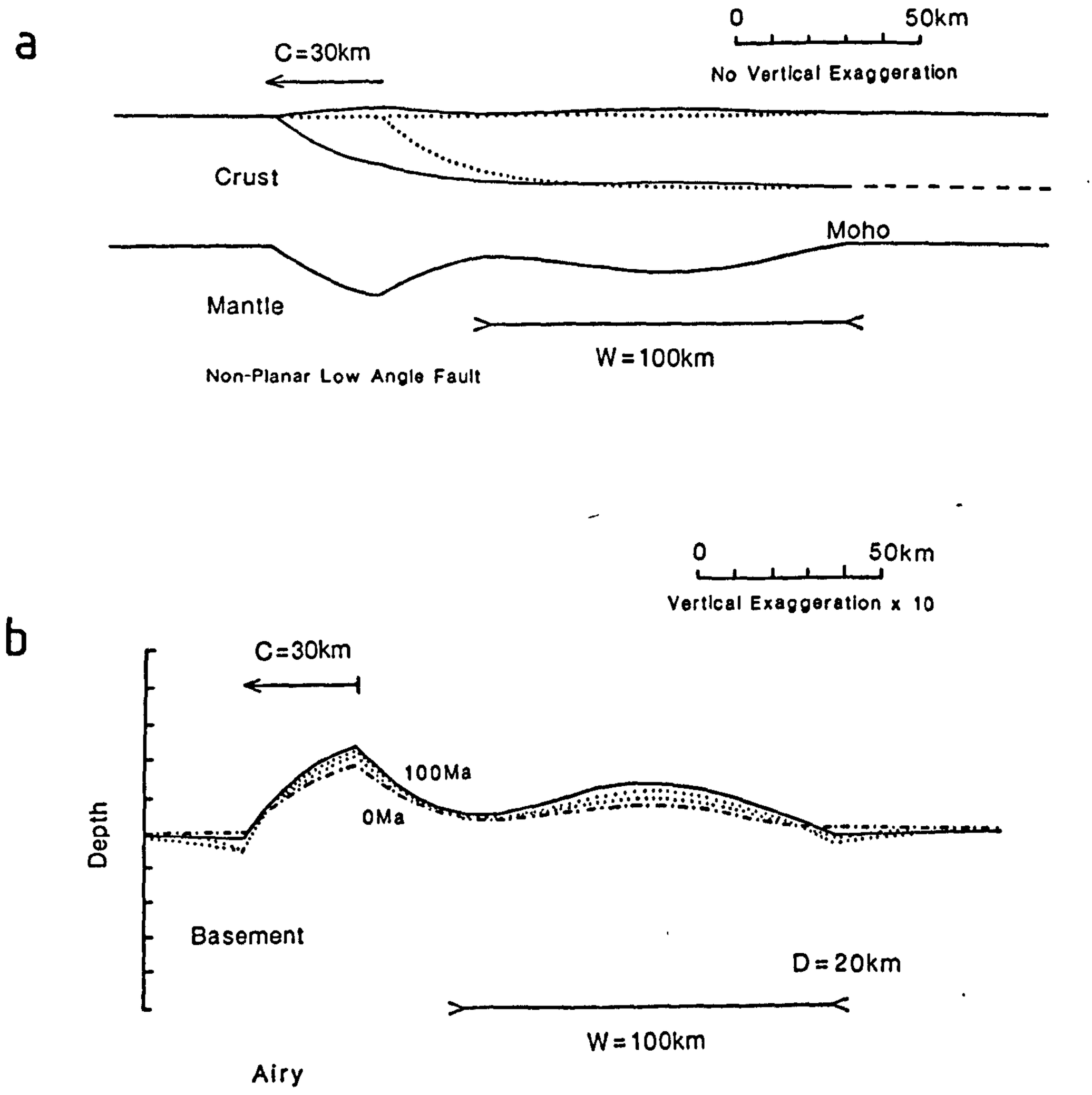

Figure 8.2 -

a) Surface topography and crustal structure are shown at 100Ma following 30km of shortening along a low angle thrust, detaching within the crust at a depth of 20km (dotted line). About 3km of surface topography is generated by the shortening. Most of the crustal thickening has been accommodated by isostatic adjustment. Pure shear thickens the lower crust and induces uplift of the surface above.

b) Basement is compared at 0Ma and 100Ma following instantaneous shortening. Uplift is caused due to the re-equilibration of the lithosphere temperature field, after its initial cooling.

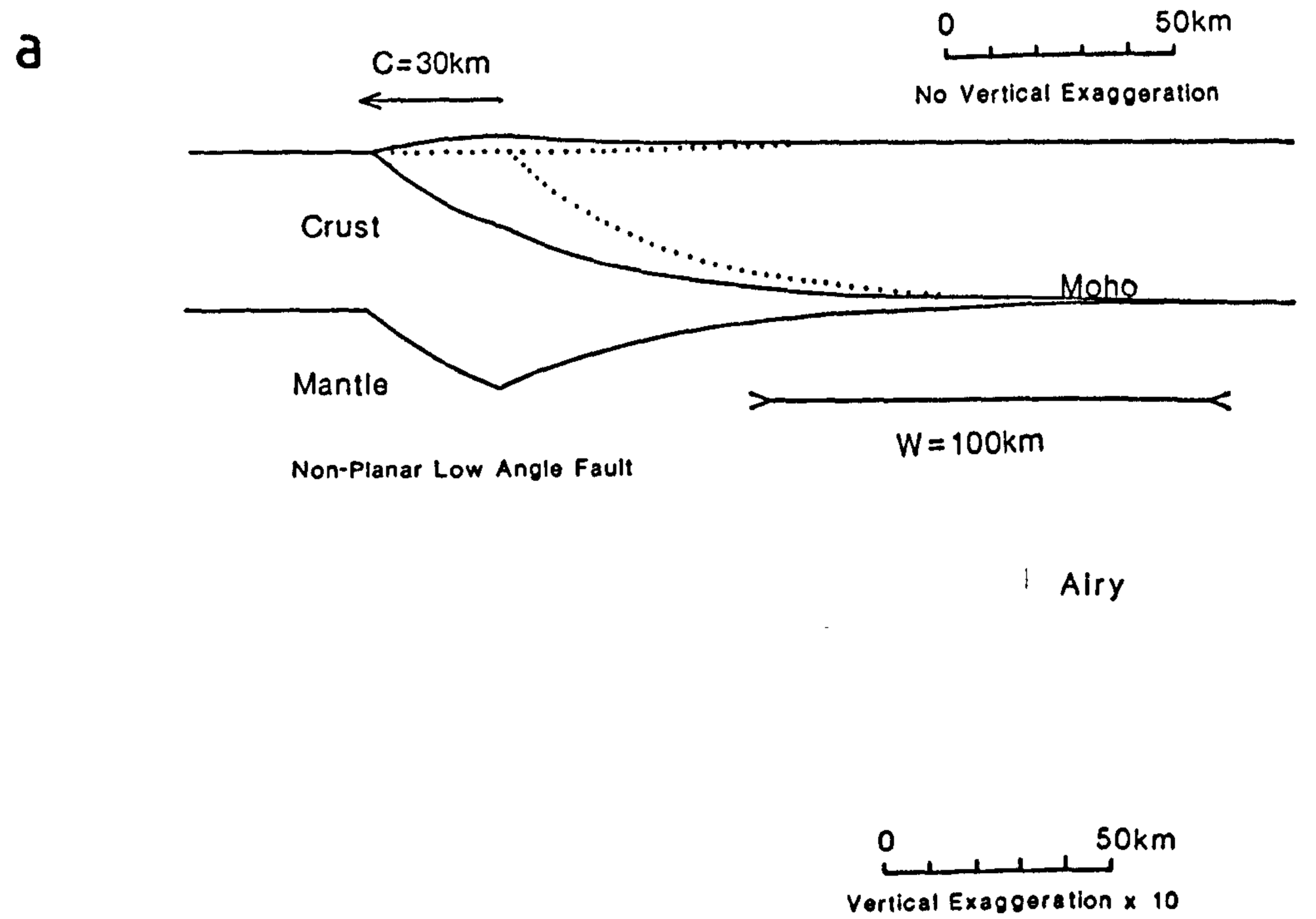

Figure 8.3 -The detachment has been deepened to the base of the crust and as a consequence there is no pure shear thickening of the lower crust (a). The distal pure shear sub-basin, which is caused by initial lithosphere cooling, gradually diminishes as the surface rises in response to post shortening thermal re-equilibration (b).

the original surface, thrust and Moho result. Pure shear deformation below the detachment is positioned 30km in the distal direction of the start of simple shear and is distributed over a width of 100km. A thickening of the lower crust arises from the pure shear compression and approximately 1km of overlying surface topography is produced.

After compression, thermal uplift occurs across the region of deformation. This is shown in figure 8.2b where basement is plotted at shortening (0Ma) and at 100Ma after the shortening event. The amount of uplift varies across the region due to changes in the interference between simple and pure shear deformational regimes; nevertheless thermal uplift reaching thicknesses of 1km are attained.

Figure 8.3 shows the detachment at the base of the crust and as result there is no crustal thickening by pure shear, although his distally positioned deformational regime perturbs the geotherm and an overlying sub-basin 1.5 km deep results. Post shortening thermal uplift gradually returns the subsided region to a position at or near sea level. At the peripheries of the compressional deformation small transient basins, approximately 500m deep, are generated (figures 8.2b and 8.3b) and are caused by lateral temperature gradients promoting cooling of peripheral regions.

8.3 Flexural Constraints on Foreland Basin Development.

Regions of thrusting are always bordered by a wedge-shaped basin with its maximum depth adjacent to the thrust loading.

Such basins are termed foredeep or foreland basins and result from the downward flexing of the lithosphere in response to thrust sheet loading (Beaumont 1979, 1981, Jordan 1981, Beaumont et al 1982 and Royden and Karner 1984).

Beaumont et al (1982) contrasted foreland basins with those arising from lithosphere extension; both types of basin exhibit a rapid initial subsidence caused by rifting in extensional tectonics and thrust sheet emplacement in compression. Extensional basins exhibit a post rift thermal subsidence phase, which is not seen in foreland basins

Jordan (1981) attempted a two-dimensional modelling of the thrust loading of the Idaho-Wyoming thrust belt. Regional isostatic compensation by flexure of an elastic lithosphere was found to be sufficient to explain the formation of the adjacent foreland basin. Similarly, Royden and Karner (1984) site the examples of the Appenine and Carpathian thrust belts where thrust sheet loading of relatively stable foreland has occurred. In both cases foreland basins about 8km deep have developed adjacent to the thrust complexes.

Geometric, thermal and flexural isostatic components of simple shear-pure shear shortening have been combined in figures 8.4 and 8.5 to show basement geometry and associated foreland basin formation. Figure 8.4a shows crustal structure, surface topography and foreland basin geometry at 100Ma after lithosphere shortening by 30km along a single major thrust detaching at a depth of 20km. Flexural rigidity is defined by a constant elastic thickness of 10km and the

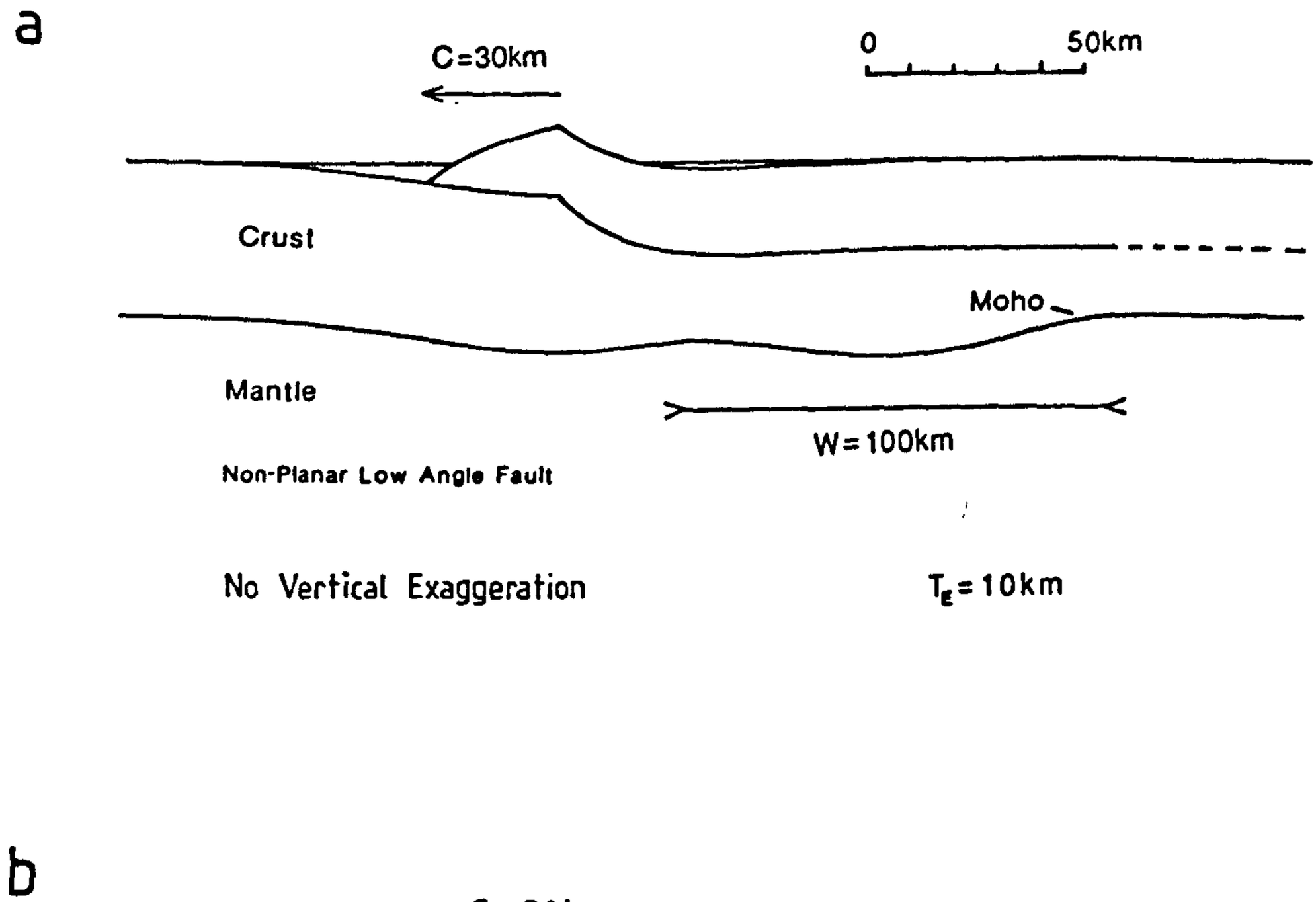

Figure 8.4 -

a) Loading imposed upon the lithosphere due to the compressional tectonics has been flexurally compensated and as a result an increased surface topography is produced along with foreland basins peripheral to the deformation.

b) Post shortening thermal uplift is shown over 100Ma following compression and is regionally distributed due to the flexural strength of the lithosphere.

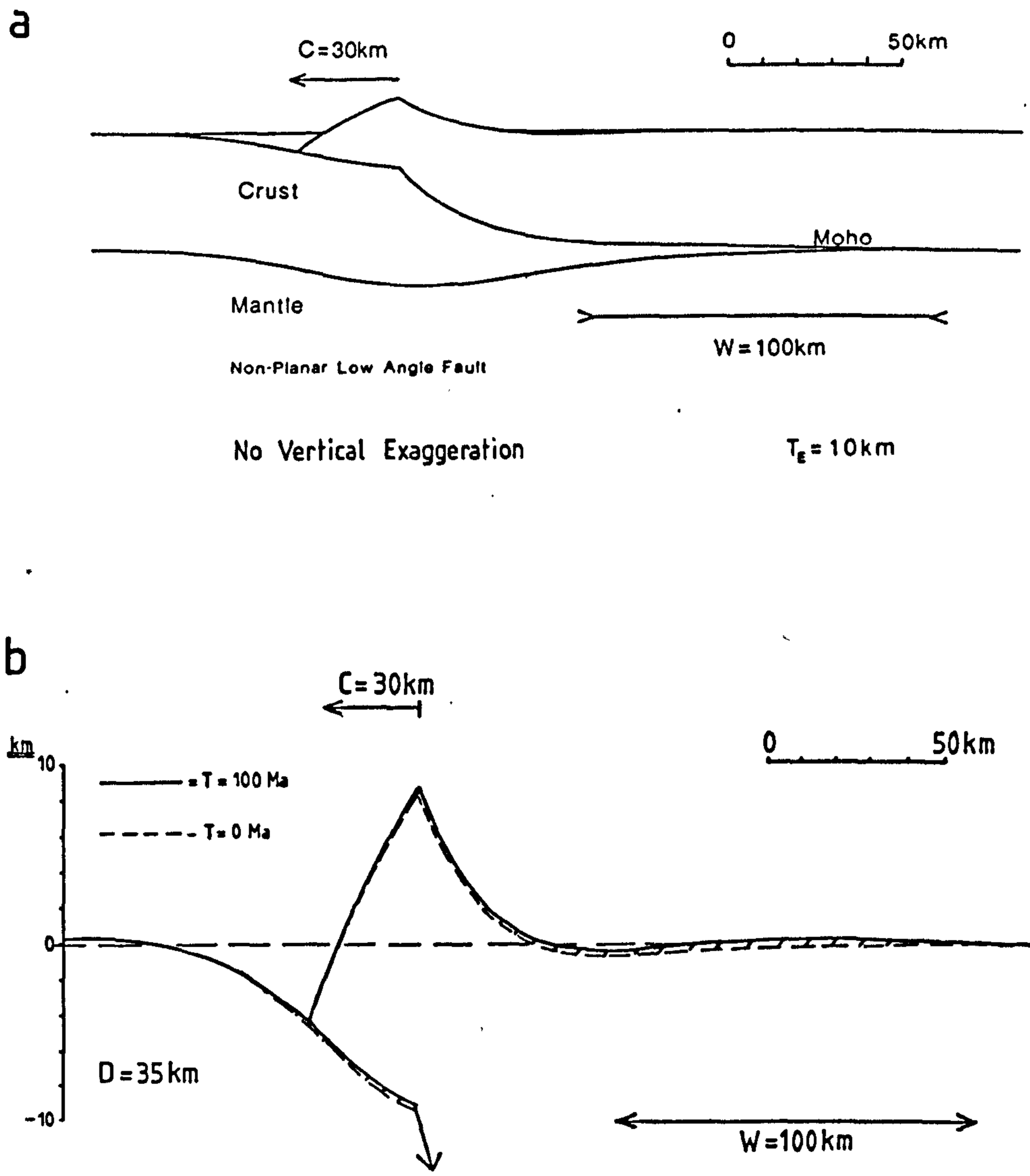

Figure 8.5 - Geometric, thermal and flexural isostatic consequences of 30km of shortening along a thrust detaching at a depth of 35km.

flexural response of the lithosphere to simple and pure shear crustal thickening and thermal subsidence are calculated using the formulation described in section 4.2. The maximum topography produced by the shortening is increased to about 5km (cf. 3km for the Airy model in figure 6.2). This is because the flexural strength of the lithosphere supports some of the emplaced thrust sheet load. Flexure also produces the foreland basin adjacent to thrust emplacement, which shows an asymmetric shape with a maximum depth of about 5km. Pure shear creates an upward flexing load due to a thickening of the lower crust. Figure 8.4b shows basement at 0Ma and 100Ma to illustrate the amount of uplift caused by post shortening re-equilibration of the geotherm.

Model predictions for a detachment at the base of the crust (figure 8.5) shows a similar configuration, although there is no uplift due to pure shear. However, both simple and pure shear cause an initial cooling of the lithosphere temperature field which is followed by its re-equilibration (figures 8.5b). Finite flexural rigidity causes a reduction in thickness of post shortening thermal uplift compared to the Airy isostatic predictions, although, it is regionally dispersed both proximally into the foreland basin and distally with respect to the compressional deformation. This thermally generated uplift, along with flexural isostatic uplift resulting from the erosion of the thrust sheets (see section 5.4), probably explains the generation of regional erosion surfaces recorded in the stratigraphy of the Swiss Molasse foreland basin which post date the main period of thrust sheet emplacement (Rigassi in Matter and Homewood

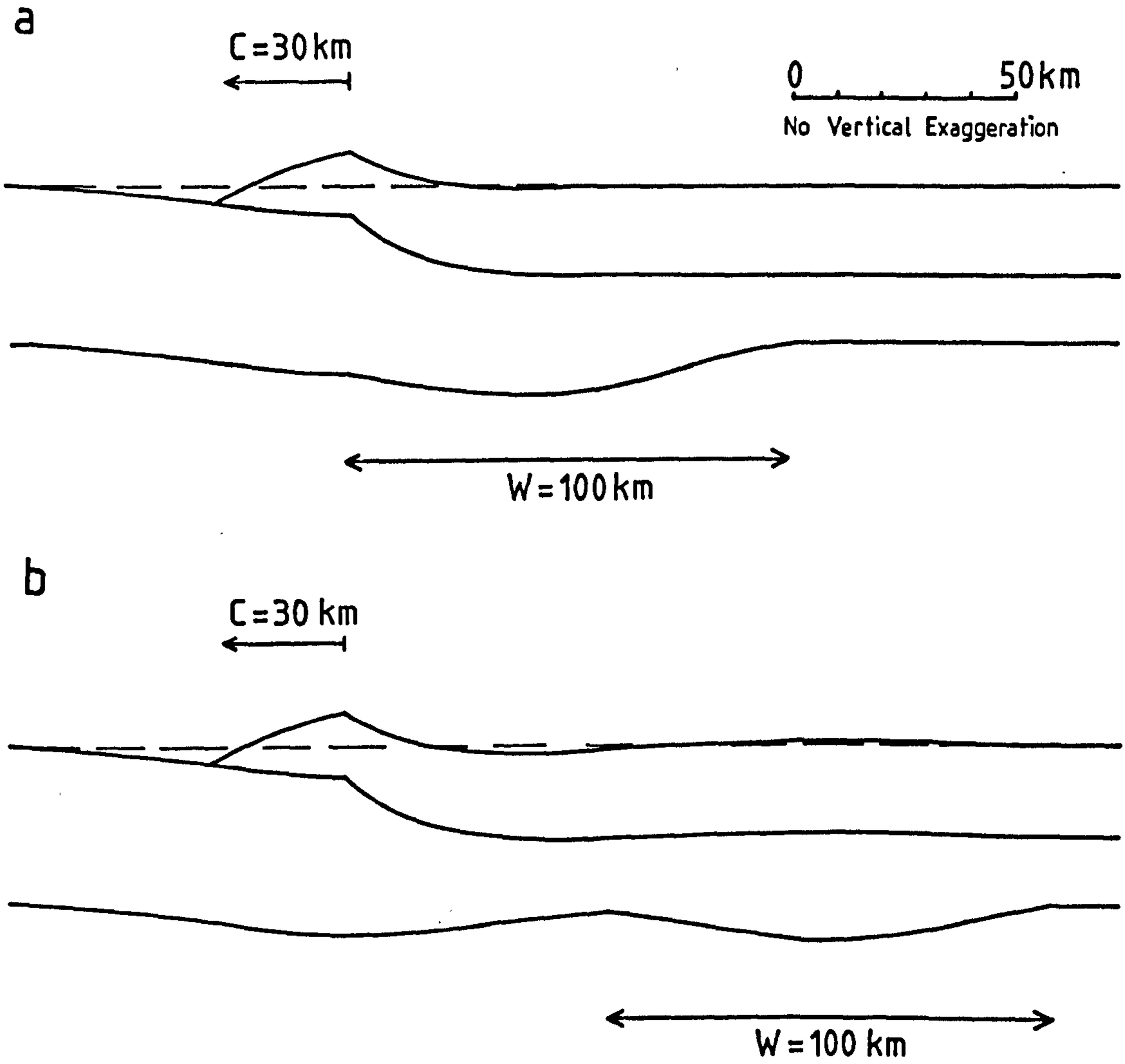

Figure 8.6 - Zero offset between the start of simple and pure shear (a) causes an interference of the deformational effects arising from the two compressional regimes. However, an increased offset of 60km (b) produces two distinct regions of crustal thickening and post shortening thermal uplift due to simple shear and pure shear respectively.

1980, Lemcke 1981, Bamford, personal communication).

Figure 8.6 shows the effect of laterally offsetting the pure shear with respect to the upper lithosphere simple shear. Zero offset between the two deformational regimes (figure 8.6a) causes a concentration of their deformational effects into a relatively small region - increased relief and post shortening thermal uplift result. A displacement of 60km between simple and pure shear (figure 8.6b) causes two almost separate regions of crustal thickening and a wider distribution of the thermal uplift.

Foreland basins result from the flexing of the lithosphere from thrust sheet loading. It seems likely therefore that two of the main controlling parameters affecting the geometry of foreland basins are flexural rigidity and the amount of shortening. Furthermore, once the basin has formed it will be modified by effects such as sediment infill.

a) The effect of flexural rigidity.

Figure 8.7a shows flexural rigidity, defined by elastic thickness, plotted against the maximum depth of the foreland basin produced by loading resulting from 30km of shortening by simple shear. The effects of pure shear, temperature perturbations and sediment loading have not been included. No foreland basin is generated at zero flexural rigidity (T_e=0), but as the elastic thickness rises to 10km the depth of the foreland basin correspondingly increases to a maximum depth of 3.7km. As flexural rigidity further increases the foreland basin depth begins to decrease, due to the thrust

a

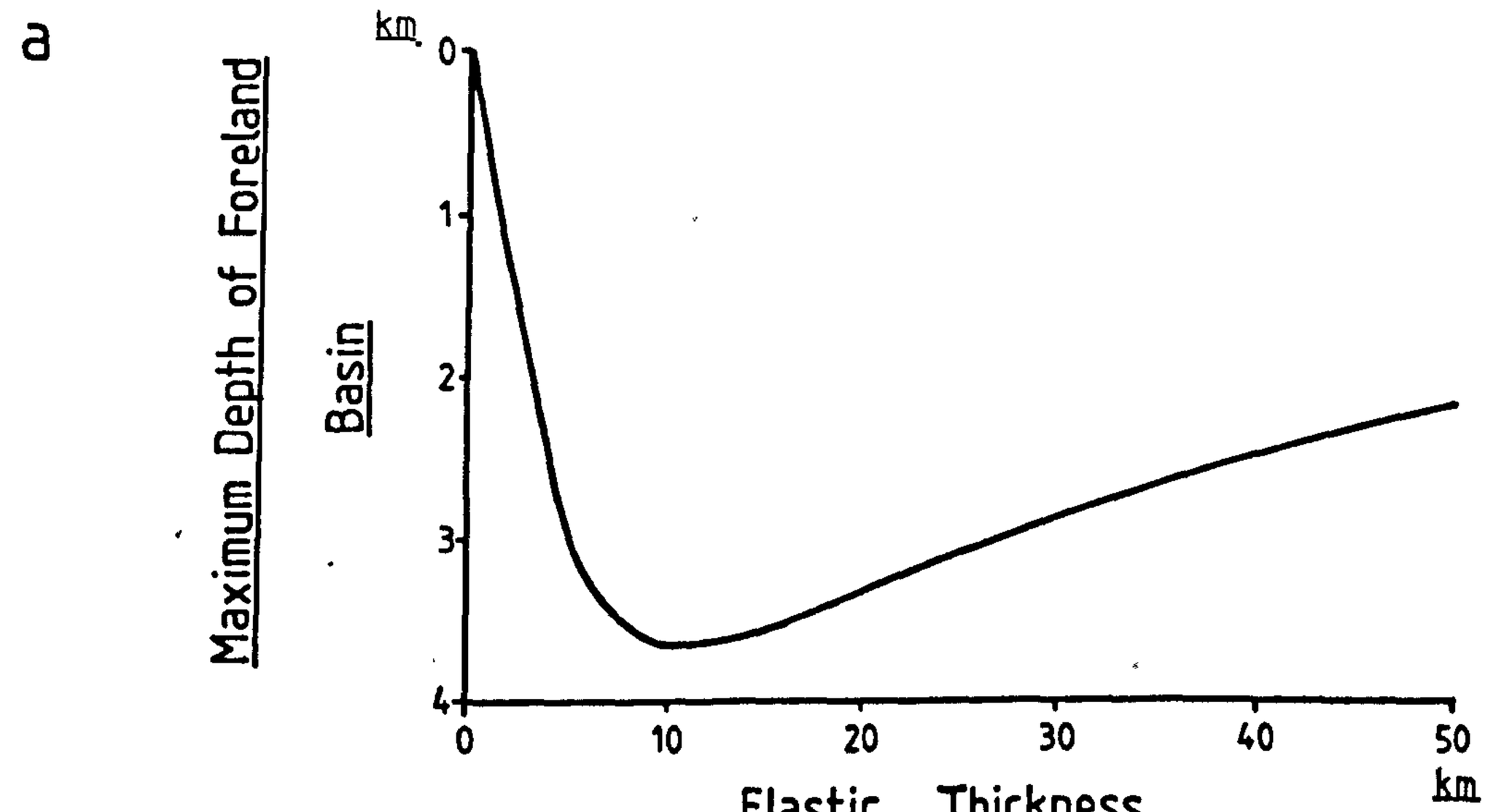

b

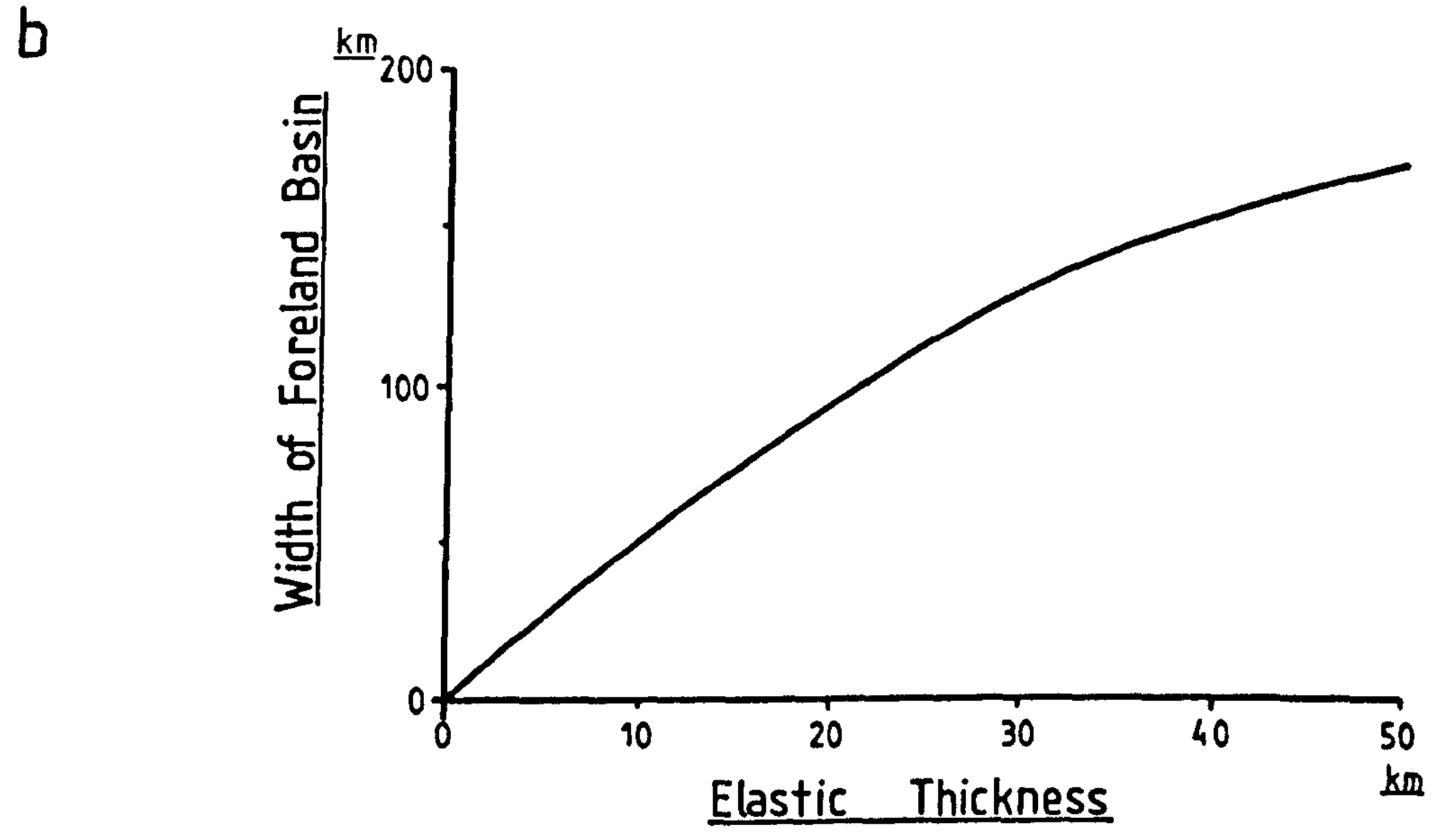

Figure 8.7 - Maximum foreland basin depth and width are related to the elastic thickness of the lithosphere in plots a and b respectively. Loading is calculated due to 30km of shortening along a low angle thrust.

load being increasingly supported by the flexural strength of the lithosphere rather than isostatic restoring forces. The flexural wavelength of the lithosphere, which is directly proportional to flexural rigidity ensures that the width of the foreland basin becomes greater as flexural rigidity rises (figure 8.7b)

b) The effect of increasing the amount of shortening.

Increasing amounts of thrusting impose a greater downward loading force upon the lithosphere and a relatively deep foreland basin initially results. The relationship between the maximum depth of the foreland basin and the amount of shortening is shown in figure 8.8. Flexural rigidity has been kept constant constant and defined by an elastic thickness of 10km. The maximum depth of the foreland basin is shown to gradually increase as the amount of thrust sheet emplacement onto the foreland becomes greater. The maximum foreland basin depth predicted is 4.25km and is generated by a shortening of 50km. As the wavelength of the load is increased the depth of the associated foreland basin stabilises. This indicates that the wavelength of the crustal load now exceeds the flexural wavelength of the lithosphere and therefore additional loading does not cause increased subsidence. An indication of the flexural wavelength of the lithosphere is provided by the flexural parameter, α (Turcotte and Schubert 1982), which for a point load is defined such that:

$$\alpha = [(4.D) / ((p_m - p_1).g)]^{\frac{1}{4}} \quad \cdots\cdots \quad 8.4$$

where g is acceleration due to gravity, p_m and p_1 are the

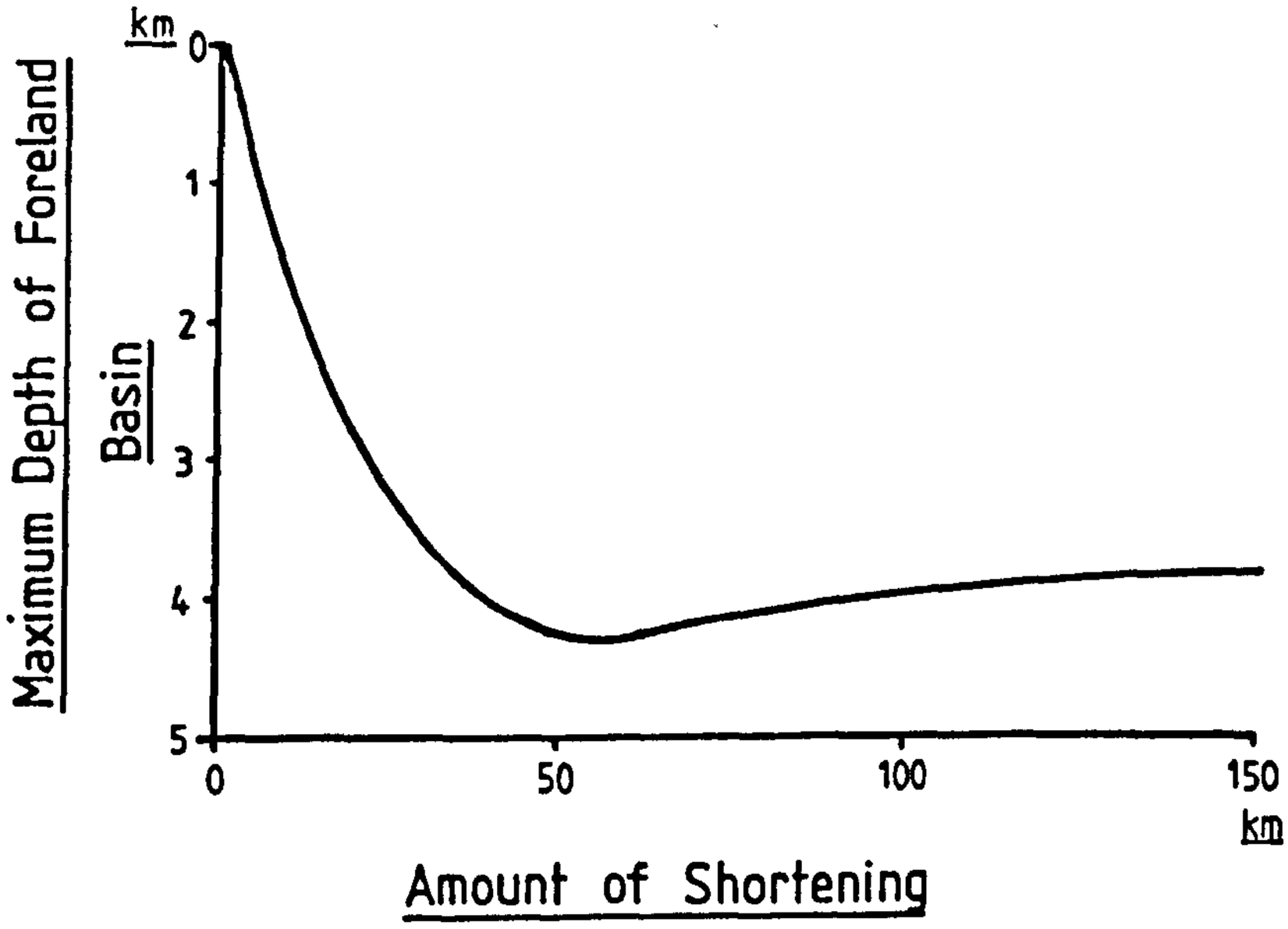

Figure 8.8- The control of lithosphere shortening on maximum foreland basin depth.

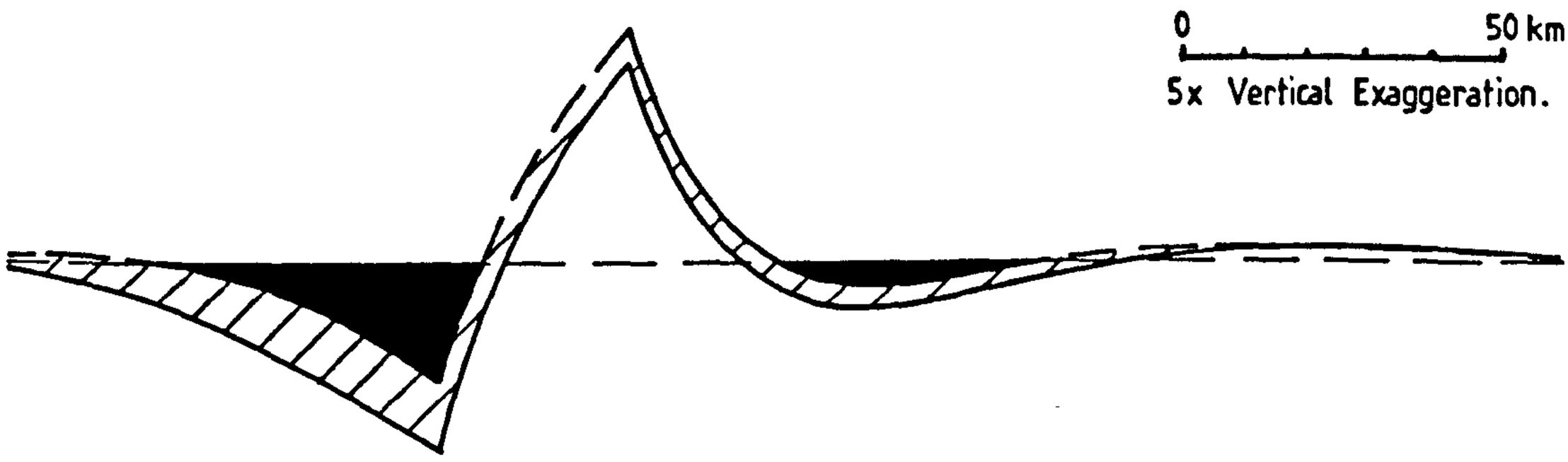

Figure 8.9 - Sediment loading of the basement below sea level in the proximal and distal regions causes regional subsidence.

densities of mantle and replacing loads respectively, and D is flexural rigidity, which is defined such that:

$$D = (Y.T_e^3) / (12.(1-v^2)) \quad \text{-----} \quad 8.5$$

and Y is Young's modulus, T_e is elastic thickness and v is Poisson's ratio.

The flexural parameter is approximately 50km for an elastic thickness of 10km and using values for the other parameters as described in Table 8. This agrees with figure 8.8 which shows that the depth of the foreland basin more or less stabilises at shortening amounts of 50km and greater.

c) The effect of sediment loading.

In figure 8.9 the effect of infilling subsided regions with sediment is shown. This causes regional subsidence, which is most noticeable in the foreland basin where deposition has been greatest. It is anticipated that these model predictions are more complicated in reality due to the following factors:

a) Sediment fill of the foreland basin will mostly be derived from material eroded from the adjacent thrust sheets. This erosion will, in turn, cause unloading of the lithosphere which responds by flexural uplift as described in section 5.4.

b) Deepening of the foreland basin by sediment loading will be offset by post shortening thermal uplift.

The overall effect of the above factors must be to subdue the amount of sediment loading related subsidence as

illustrated in figure 8.9.

8.4 Summary.

In this chapter the coupled simple shear - pure shear model, used in previous sections to investigate extensional tectonics, has been applied to lithosphere shortening. Model predictions, rather expectedly, show that compressional deformation produces opposite effects to those caused by extension of the lithosphere and crustal thickening and cooling of the geotherm occur as opposed to a thinning of the crust and heating of the lithosphere. Despite the different basement geometries and crustal structures however, the formulation of the geometric, thermal and isostatic components of extension and compression are almost identical.

Emphasis has been placed upon the factors governing the evolution of foreland basins following compressional deformation. The strong control of flexural rigidity on the magnitude of these basins is undisputed.

CHAPTER 9

Sedimentary Basin Inversion.

9.1 Introduction.

It has been shown that lithosphere deformation is controlled by either extensional and compressional movement along major low angle faults. Most of these major faults have exhibited a complex history of extensional and compressional events throughout geological time (Etheridge 1986). The MOIST seismic reflection line shown in figure 1.6b has imaged the Lewis and Orcadian basins in the west and east of the section respectively (eg. Smythe et al 1982, Brewer et al 1984, Blundell et al 1985). These basins have formed following extension along low angle faults during the Mesozoic. The same faults, however, had been active earlier as thrusts during the Caledonian earth movements. Alternatively, there are examples of compressional reactivation of faults that were previously active in a region of extension, in which case existing sedimentary basins are inverted by the compressional event.

In Chapter 5 the Jeanne d'Arc basin was modelled as a series of rift events, separated by periods of relative stability or thermal subsidence. The effect of this finite rifting was to generate a vertical stacking of rift and post-rift basin components. The Mesozoic basins of North-West Europe have exhibited a similar multi-phase evolution. These basins, however, are characterised by the fact that their extensional evolution was terminated by compressional forces during the Tertiary, causing inversion of the normal faults

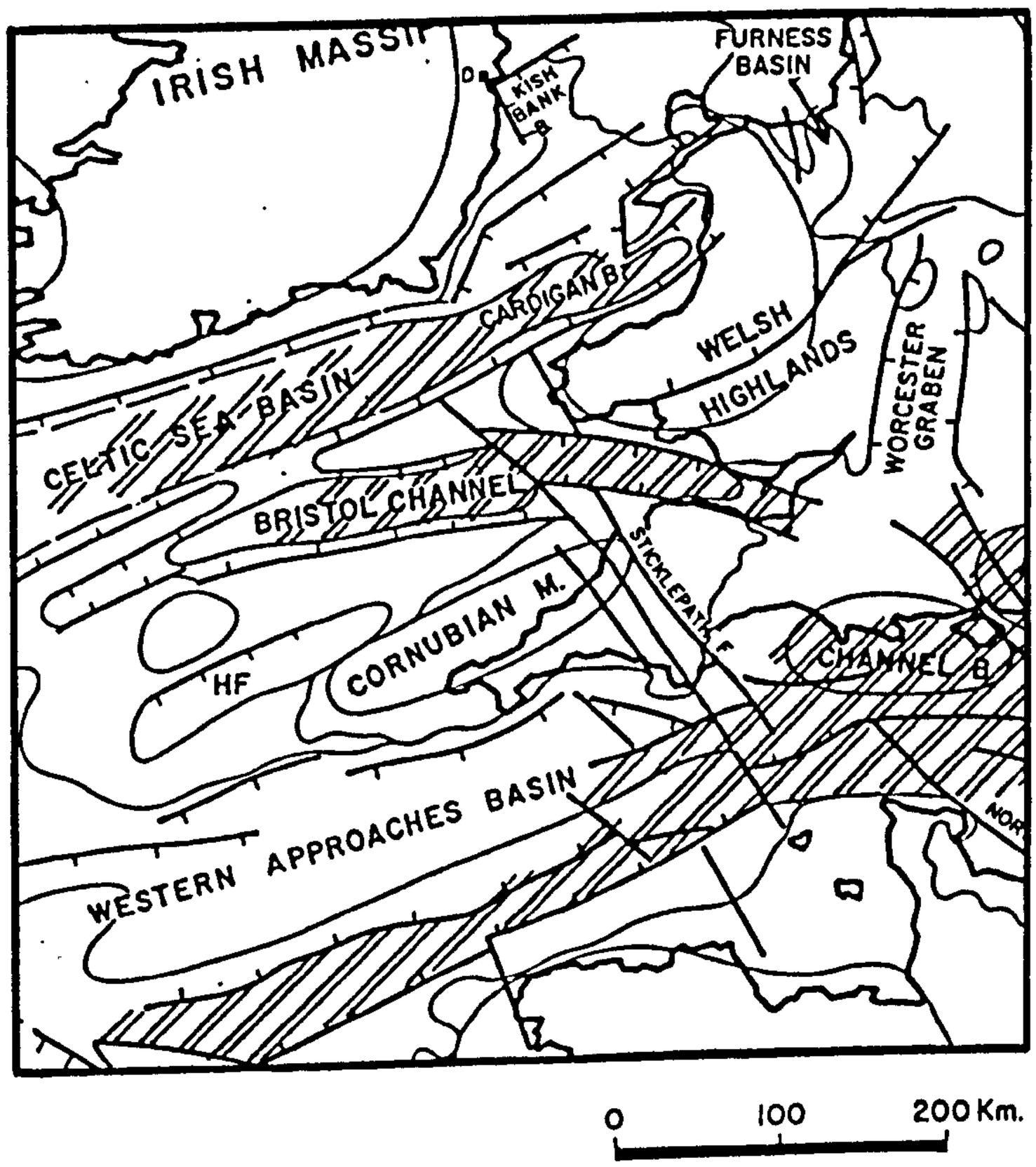

Figure 9.1 - Permian and Mesozoic basins off the coast of South-West England. Shaded ornament represent basins affected by Late Cretaceous- Tertiary inversion (after Ziegler 1982).

in the basins to high angle reverse or thrust faults. The Mesozoic basins of southern England, the Celtic Sea and the Western Approaches all show clear evidence of inversion on inherited structural frameworks. The Wessex basin, for instance, evolved originally by normal reactivation of Variscan basement thrusts (Shackleton 1984, Lake and Karner 1987). The basin was inverted during the Late Cretaceous to Early Tertiary along the same fault framework that had earlier accommodated the Mesozoic crustal extension (Kusznir et al 1987).

The Celtic Sea basin and adjacent Western Approaches basin, the Brittany Trough and also the South West Channel basin, which together compose the Western Approaches basin (figure 9.1), experienced similar compressive forces during the Late Cretaceous and Tertiary due to the Pyrenean and Alpine earth movements to the south (Ziegler 1987[1]). In the Celtic Sea basin, Brittany Trough and South-West Channel basin this compression induced reverse movements on the originally normal faults, causing upwarpings of between 1km and 3km (Tucker and Arter 1987, Ziegler 1987[2]). There is a lack of evidence for compressional fault reactivation in the Western Approaches basin (Ziegler 1982), although chalk porosity-depth data does indicate that uplift of the basin took place during the Tertiary (Hillis, in press). This situation might be explained by compression, and hence thickening, of the lower crust by pure shear beneath the Western Approaches basin in the absence of simple shear deformation in the upper crust (see figure 8.6b).

a

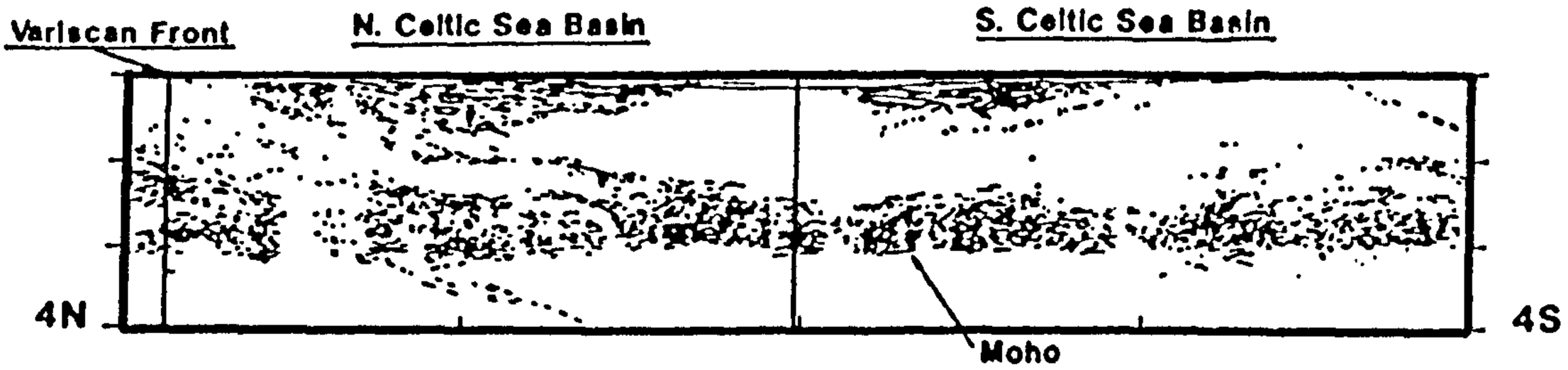

b

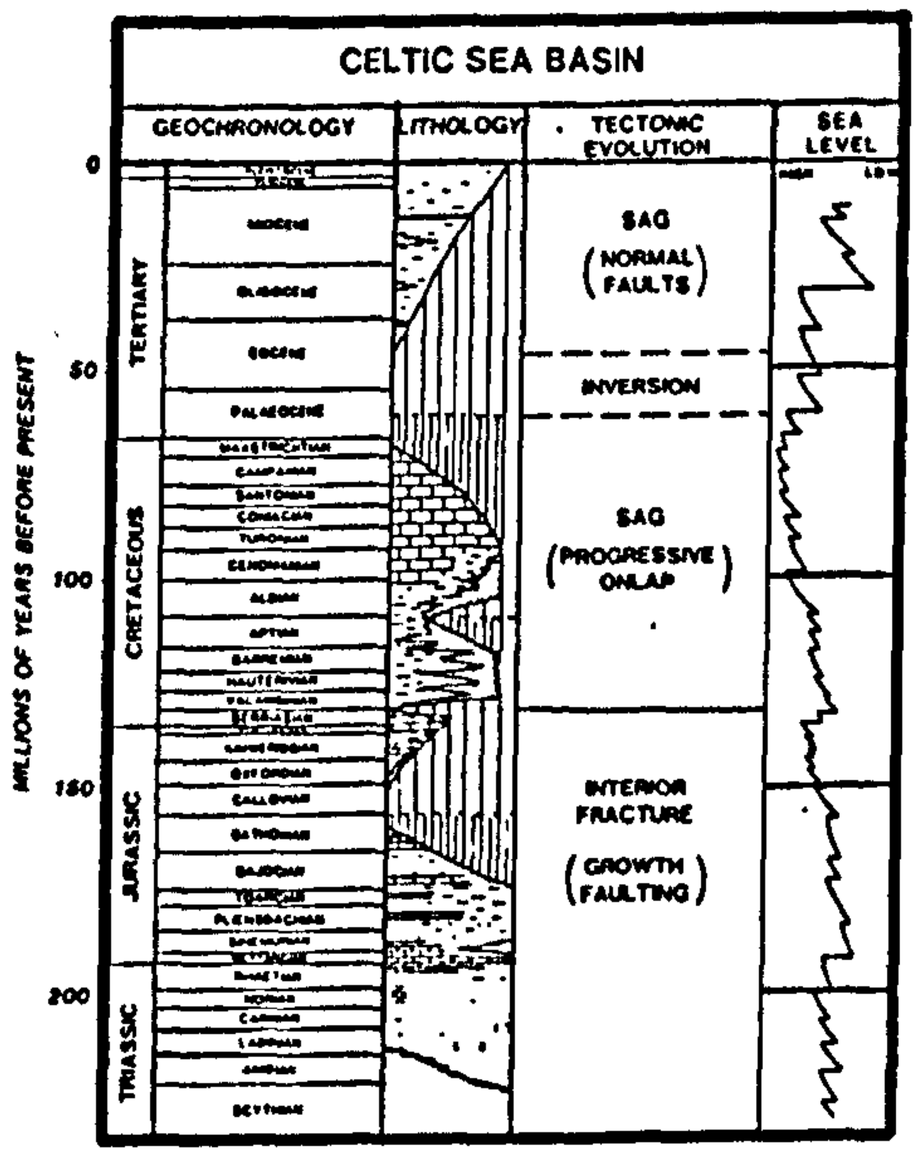

c

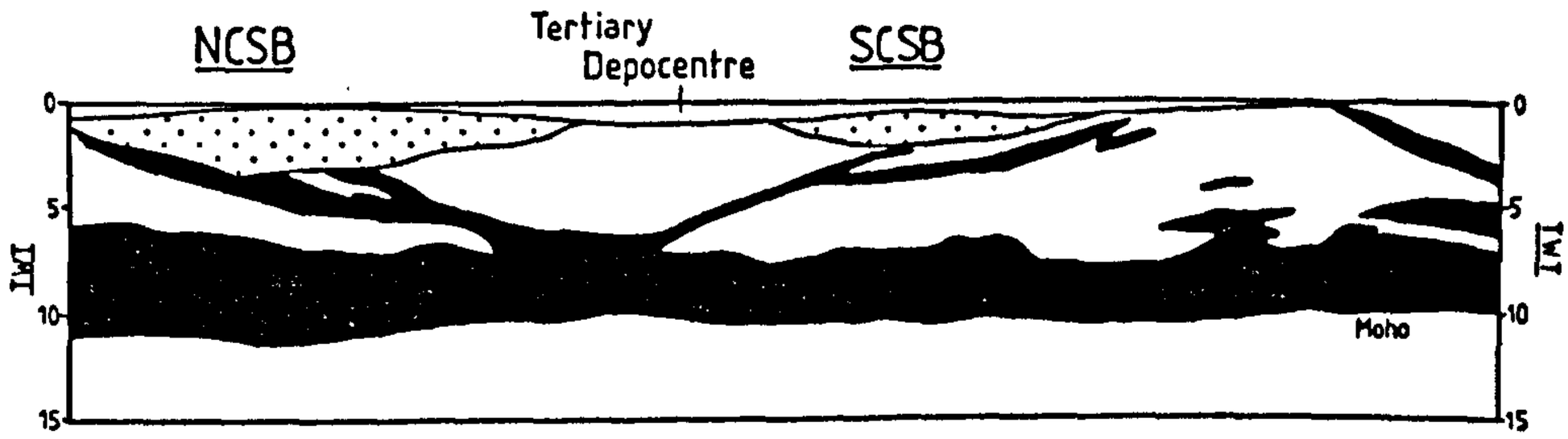

(G. Williams, personal communication)

Figure 9.2 - SWAT4 deep seismic reflection section (a) across the North and South Celtic Sea basins. The extensional evolution of the North Celtic Sea basin occurred from the Triassic to Late Cretaceous (b). Inversion of this Mesozoic depocentre occurred during the Tertiary and was followed by deposition at the basin flanks (c).

9.2 The Inversion of the North Celtic Sea Basin.

In this chapter the processes responsible for sedimentary basin inversion in the context of the North Celtic Sea basin are explored. Deep seismic reflection data across the basin, which is located between south-eastern Ireland and western England, is provided by the SWAT4 deep seismic reflection line shown in figure 9.2a (BIRPS and ECORS 1986). The stratigraphic table in figure 9.2b shows that basin formation was initiated in the Triassic, when north-western Europe was subjected to tensional stresses related to the opening of the Tethys ocean in southern Europe and rifting in the Arctic North Atlantic (Ziegler 1981). The fault that dominantly controlled the formation of the North Celtic Sea basin during the Mesozoic is denoted by the strong set of reflectors in the left of the section in figure 9.2a, which dip shallowly from the surface down to a detachment depth of approximately 20km. Fault movement ended in the Jurassic, to be followed by thermal sag with gradual sediment onlap onto the margins (Tucker and Arter 1987). This thermal subsidence phase was terminated abruptly during the Tertiary due to compressional forces created by the Alpine-Pyrenean Orogeny. Slip reversals occurred in response to this Tertiary shortening, causing 1km to 2.5km of uplift of the Mesozoic depocentre. Basin inversion was followed by the deposition of thicknesses of up to 300m of Tertiary clastic sediments,which are seen at present at the flanks of the basin (figure 9.2c).

During the extensional evolution of the North Celtic Sea basin both synthetic and antithetic faults developed in the

a) Basin Formation.

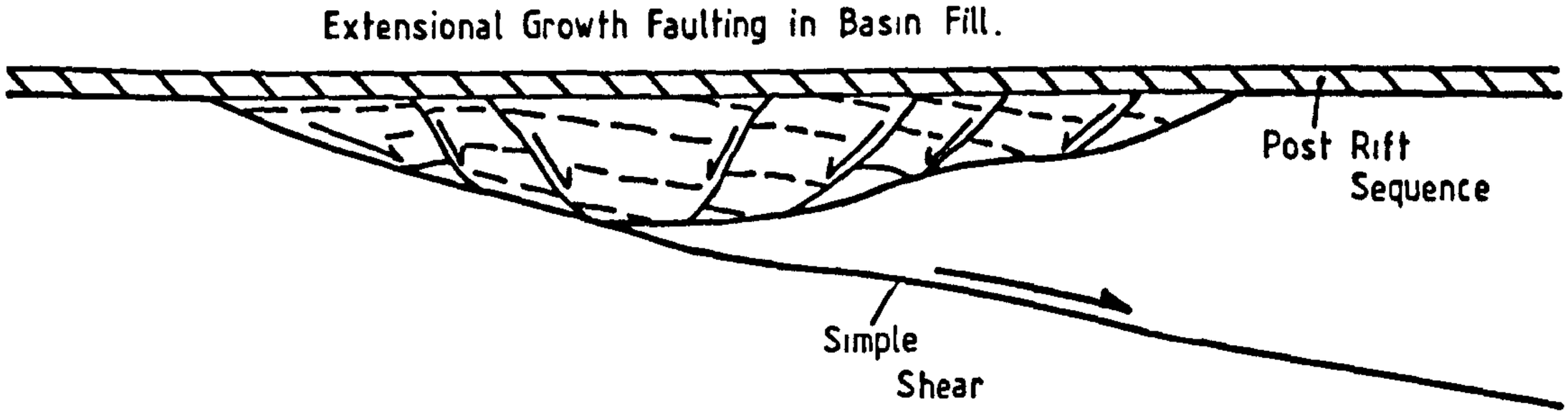

b) Basin Inversion.

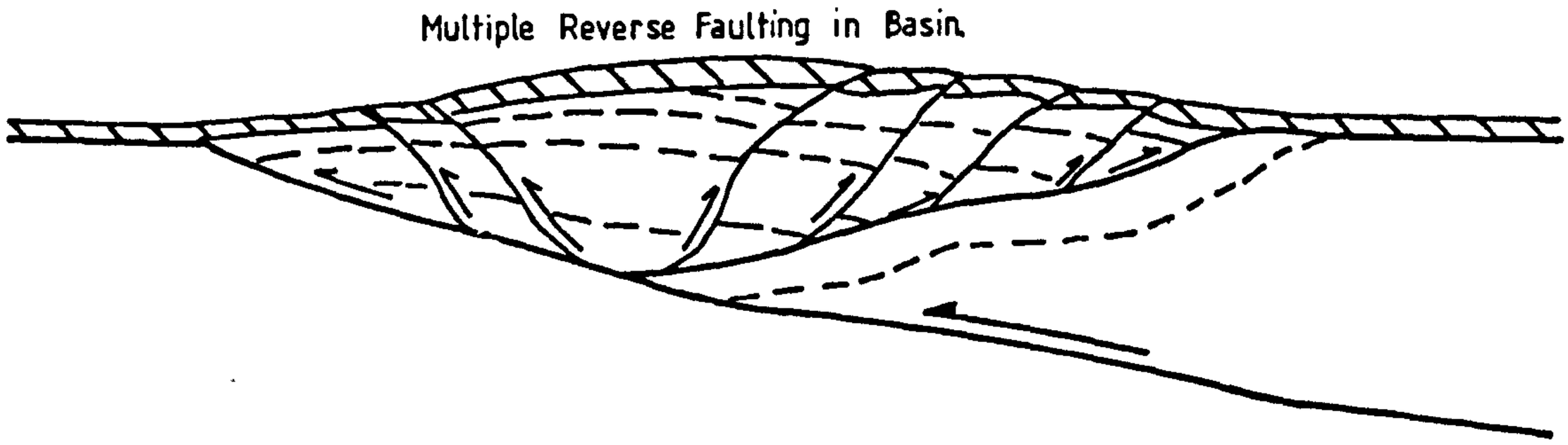

Figure 9.3 - Diagrammatic representations (after G. Williams, personal communication) of the extensional evolution of the North Celtic Sea basin (a) and its inversion (b).

basin fill (figure 9.3a). Tertiary shortening caused hanging wall basement to wedge into the sediment pile of the Mesozoic depocentre, both squeezing and uplifting it as it did so (figure 9.3b). It has been suggested that this chisel-like action produced a reverse motion on the originally normal synthetic and antithetic faults (G. Williams, personal communication) and thus caused the lateral motion of the hanging wall to be translated to a dominantly vertical motion by movement on these minor faults - the Mesozoic depocentre experienced substantial updoming.

9.3 The Application of the Simple Shear - Pure Shear Model to Basin Inversion.

The extensional and compressional modelling techniques described earlier have been combined in order to explore the inversion of the North Celtic Sea basin. Figure 9.4a shows a listric detachment along which 25km extension has taken place. Perturbations caused to the lithosphere temperature field by this extension have been allowed to equilibrate, and a constant flexural rigidity defined by an elastic thickness of 10km has been assumed. A shortening of 10km along a similar listric fault is shown in figure 9.4b, and substantial crustal thickening results. Flexing of the lithosphere in response to loading due to crustal thickening causes foreland basin development in the areas adjacent to the main deformation. It is suggested that the superposition of these two models produces an inverted basin.

The geometry of the inverted structure is determined by the response of the sediment fill within the extensional basin

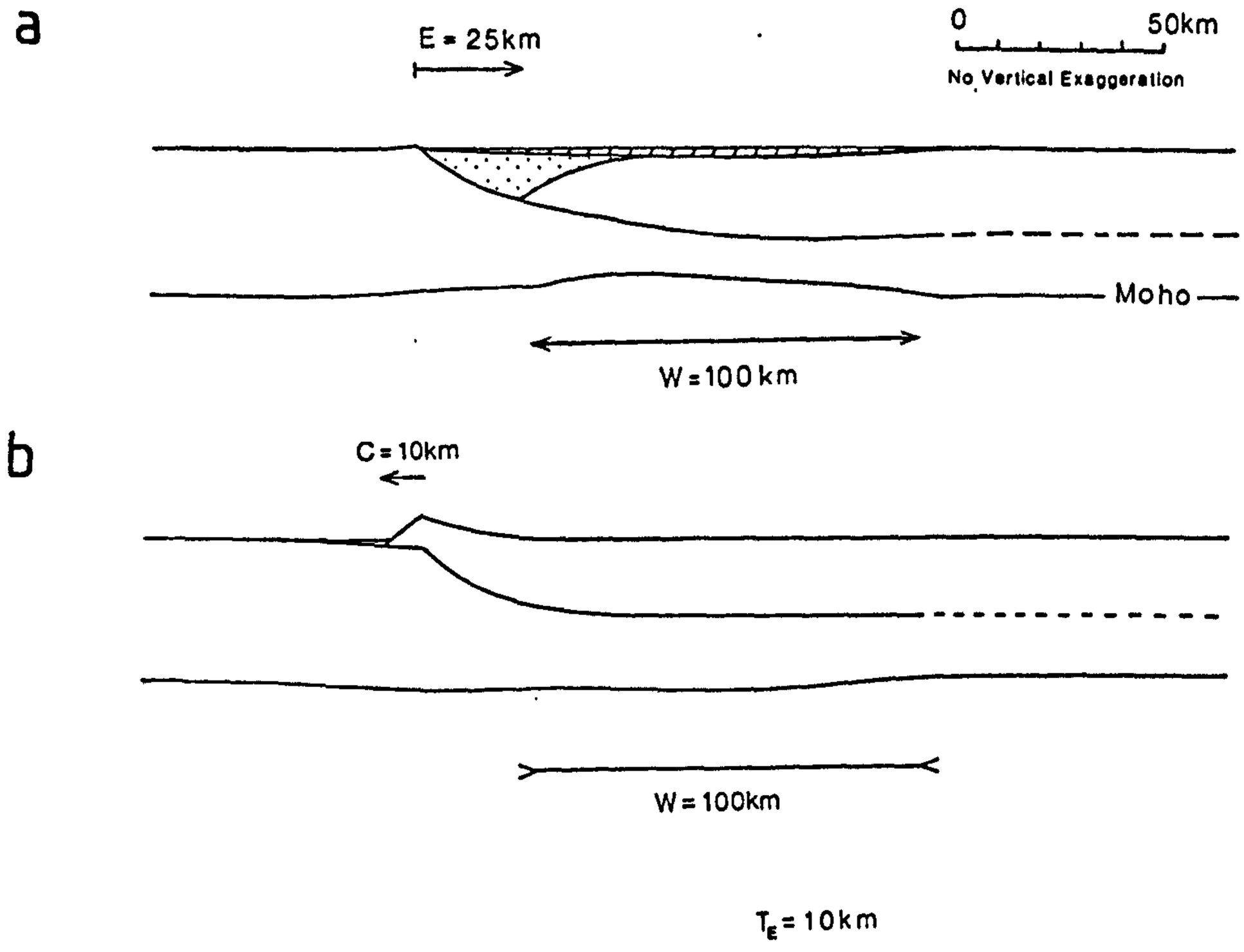

Figure 9.4 - The process of sedimentary basin inversion can interpreted as the superposition of extensional (a) and shortening (b) components.

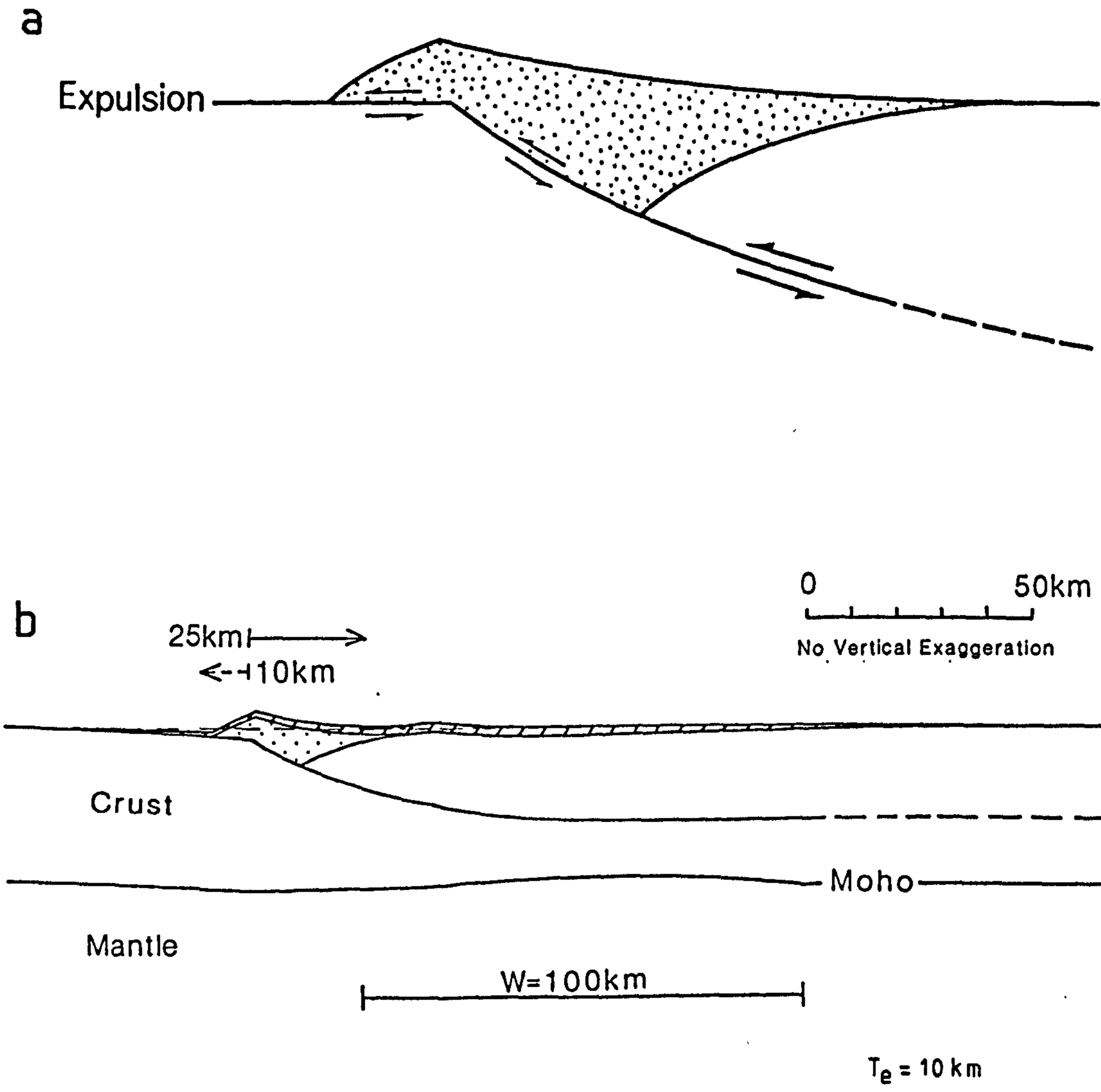

Figure 9.5 -

a) Compressional reactivation of the major basin bounding fault causes expulsion of sediment onto the footwall.

b) Model predictions for 25km of lithosphere extension followed by 10km of shortening to generate basin inversion. In this model sediment within the basin is assumed to be part of the hanging wall and shortening displaces sediment out of the basin onto the footwall shoulder.

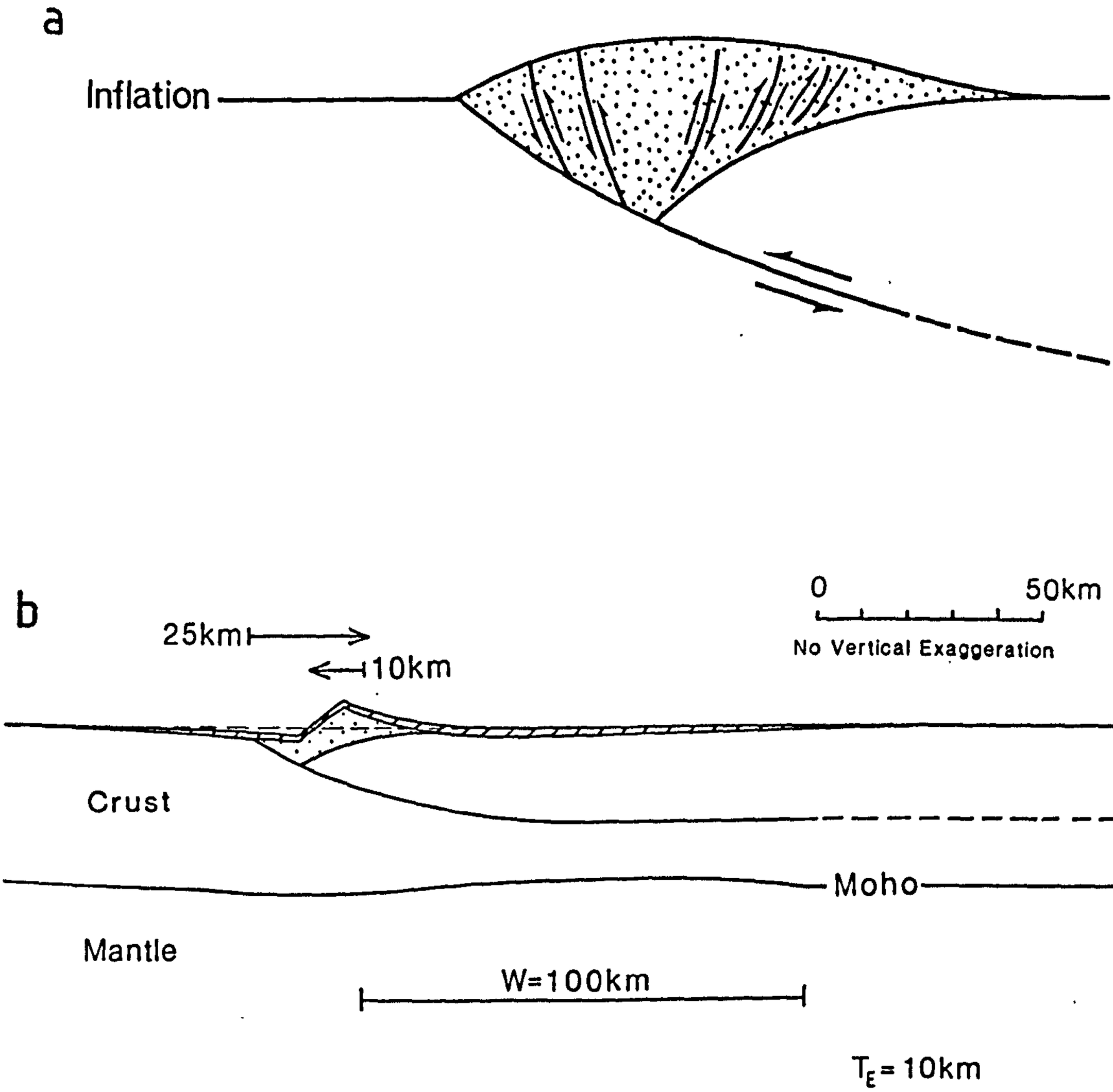

Figure 9.6 -

a) Shortening can induce reverse motion on minor faults within the basin fill. Inflation of the extensional depocentre results.

b) Model predictions for 25km of lithosphere extension followed by 10km of shortening. Sediment within the extensional depocentre is assumed to have no strength and shortening causes its uplift into an anticlinal structure.

to the inversion related shortening. A consolidated basin fill takes up the movement of the hanging wall during shortening and expulsion of sediment onto the footwall shoulder results (figure 9.5). Alternatively, if the basin fill is assumed to have no strength, hanging wall movement induces direct uplift of the extensional depocentre (figure 9.6). It is the latter alternative which appears to best describe the structure created by the Tertiary inversion of the Celtic Sea basin (cf. figure 9,3b).

Basin upwarping by inversion is shown by the models in figure 9.7, which illustrate the relationship between the amount of shortening and the resulting uplift of the inverted depocentre. 25km of extension followed by 2km of shortening (figure 9.7a) causes up to 1.5 km of sediment uplift, whereas 10km of shortening (figure 9.7c) produces a maximum of 4km of basin uplift. The angular inversion geometries predicted by these models are caused by the geometrical construction used. It is suggested that in the case of the North Celtic Sea basin reverse motion on numerous minor faults within the basin fill produced a rounded anticlinal structure as shown in figure 9.8a. In order to generate the upwarping shown in these models, the 10km shortening phase has been assumed to have occurred by pure shear. The dotted and shaded ornament represent the inverted Mesozoic basin, which has been uplifted by about 4km during the Tertiary shortening. The thickening of the crust by the lateral movement of hanging wall basement during inversion imposes an additional load on the lithosphere and causes it to flex downwards, generating sub-basins both proximally and distally to the basin. Erosion of

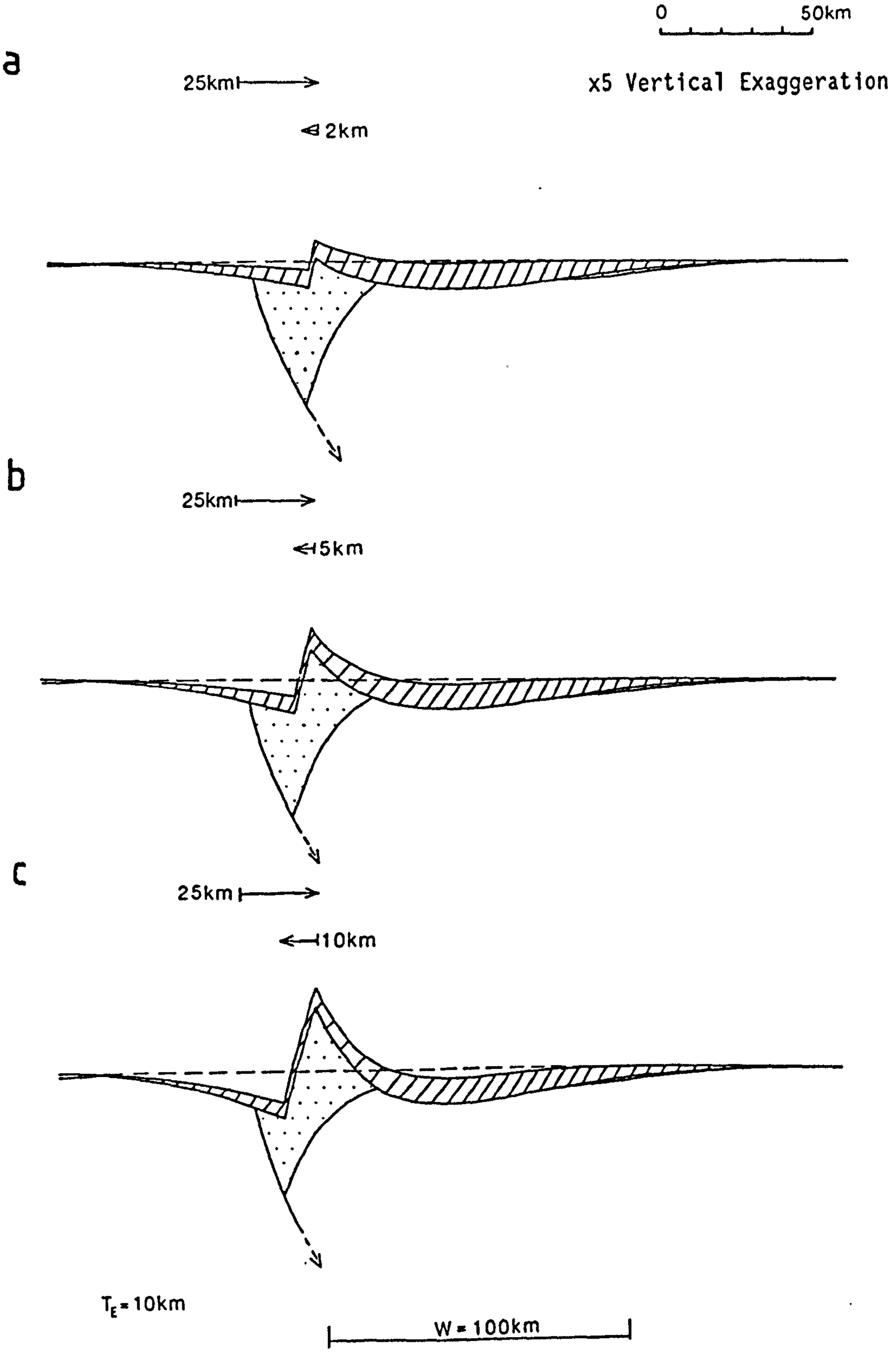

Figure 9.7 - Model predictions for 25km of extension along a low angle fault detaching at 20km followed by 2km (a), 5km (b) and 10km (c) of shortening. The sediments within the basin are assumed to have no strength, so that inversion causes an overlying uplift of both syn- and post-rift basin components.

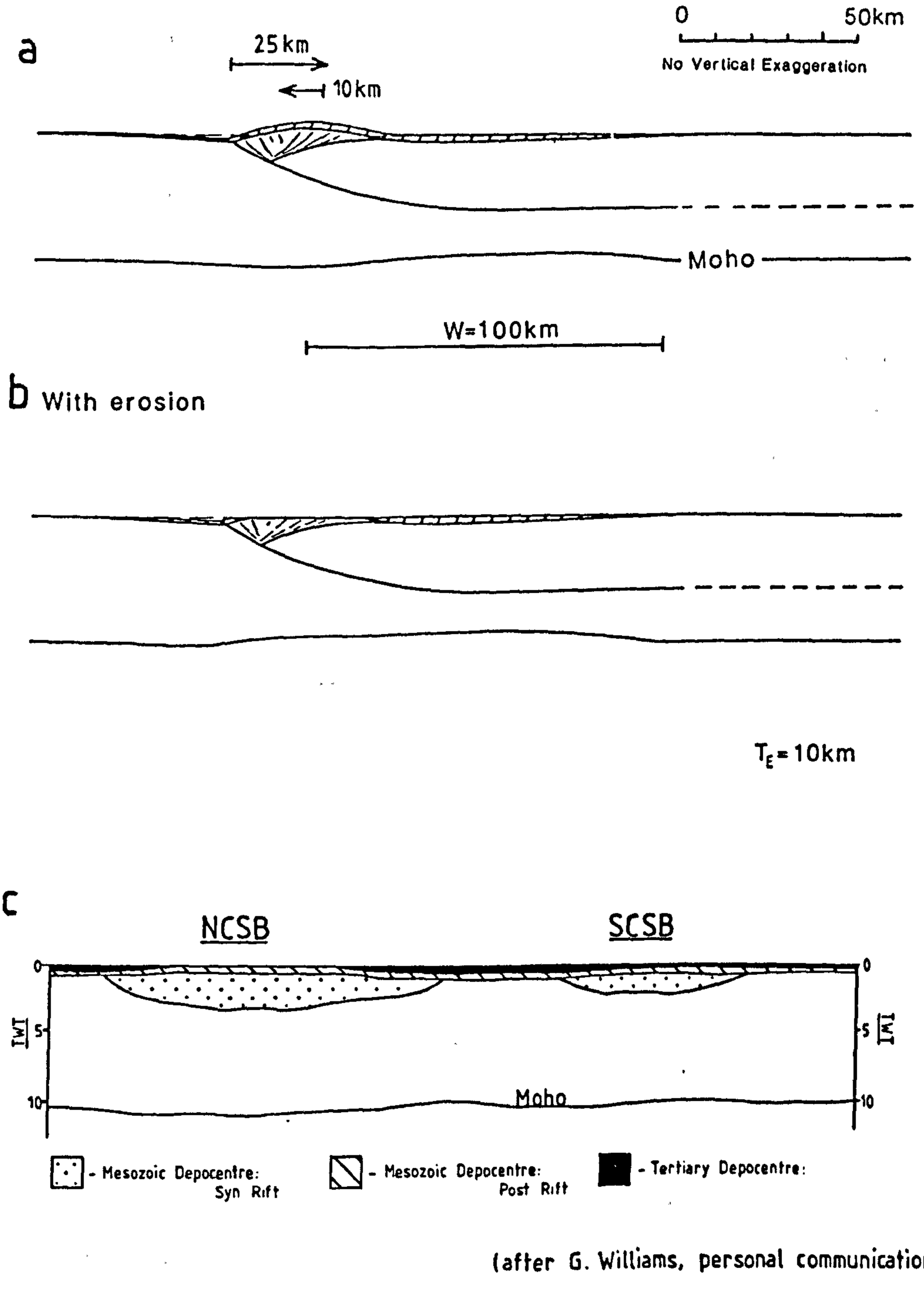

Figure 9.8 - The accommodation of inversion by reverse motion on minor faults within the basin fill creates an anticlinal geometry (a). Erosion of this uplift (b) provides infill for the flexurally generated peripheral basins which are seen as the Tertiary depocentres surrounding the Celtic Sea basin at present (c).

any uplifted material (figure 9.8b) has provided infill for the flanking foreland basins, which are at present seen as Tertiary depocentres peripheral to the North Celtic Sea basin (figure 9.8c).

9.4 Summary

Tertiary inversion of the North Celtic Sea basin appears to have caused inflation of the original basin, rather than reactivation along the main basin bounding fault, due to the absence of Mesozoic sediment on the footwall. Gillcrist et al (1987) cite many examples of basin inversion in the Alpine foreland, North Sea, Bristol Channel and Saxony basins, etc., and similarly conclude that the inversion of a sedimentary basin does not typically involve the reactivation of the major basin bounding fault and therefore sediment expulsion onto the footwall. Moreover, steeply dipping normal faults are more likely to act as buttresses to the compression of the extensional depocentre, enhancing the development of a compressive anticline. The steepness of this upwarping reflects the intensity of the inversion. It is unlikely, however, that there is no sediment expulsion at all onto to the footwall during inversion (C. Powell, personal communication), especially where the basin bounding fault is shallowly dipping, and evidence of deposition onto the footwall due to inversion is usually not seen in the stratigraphic record due to the effects of subaerial erosion.

Chapter 10

Extension on Planar Faults and Its Implications on Sedimentary Basin Formation and Modelling Methods.

10.1 Introduction.

Deep seismic reflection data shows unequivocally that the extensional and compressional deformation of the upper lithosphere takes place on major low angle faults. Much of the seismic data available, however, depicts post deformational features and does not give a direct indication of how the footwall and hanging wall respond structurally during extensional and compressional tectonics. The coupled simple shear-pure shear model used in previous sections has relied upon the chevron construction (Verall 1981, Gibbs 1983, 1984) to define the surficial hole created by extensional movement along the fault. This construction allows any unsupported area of the hanging wall, following extension, to collapse directly downwards onto the footwall (see figure 2.1b).

Despite its simplicity, it has been shown that the chevron construction, when combined with thermal and flexural isostatic components of simple shear-pure shear extension along listric faults, generates basin geometries and crustal structures very similar to those shown in the seismic record. Model predictions for extension along planar faults using the chevron construction show a strong symmetry (figure 10.1), which is caused by the constant angle of dip of the fault and the flat horizontal detachment along which a large amount of the extension has been accommodated. The

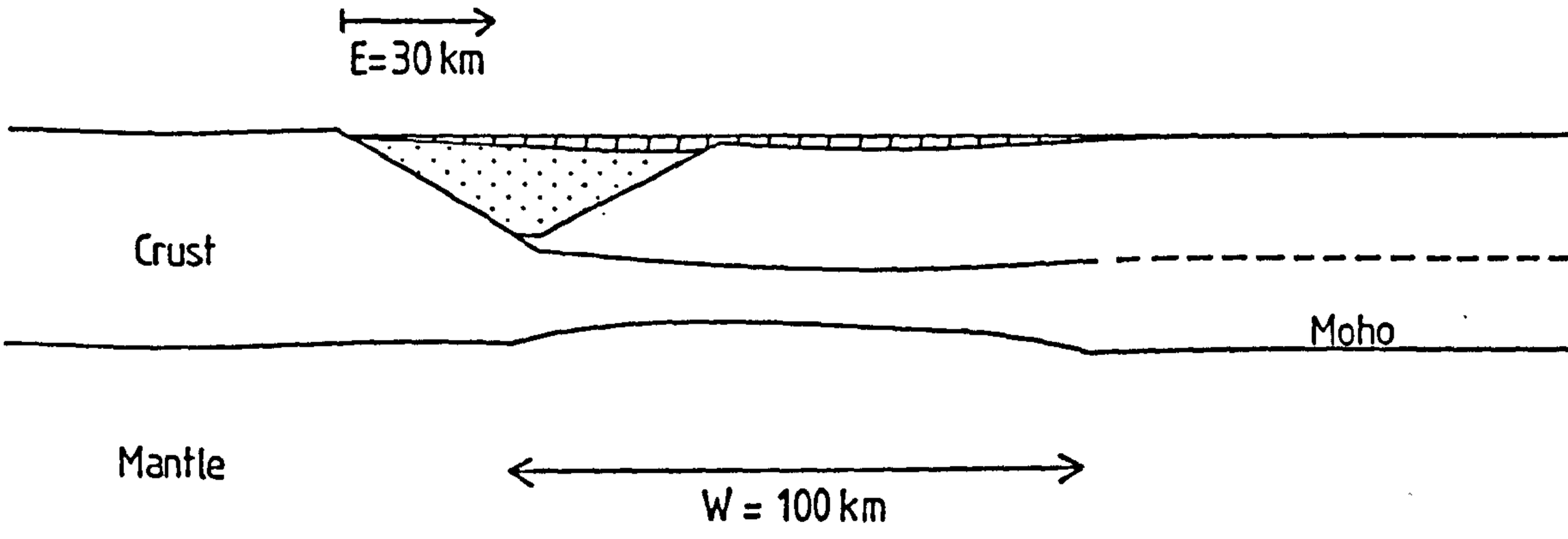

Planar Low Angle Fault

Figure 10.1 - The chevron construction predicts flat bottomed and symmetrical basins following extension along planar faults. This is caused by a large proportion of the extension being accommodated along the horizontal detachment.

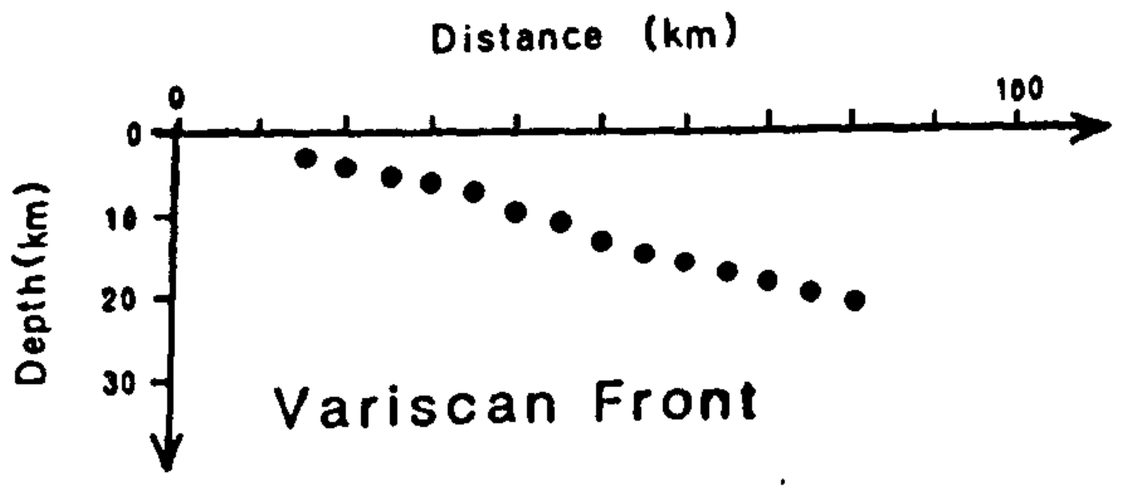

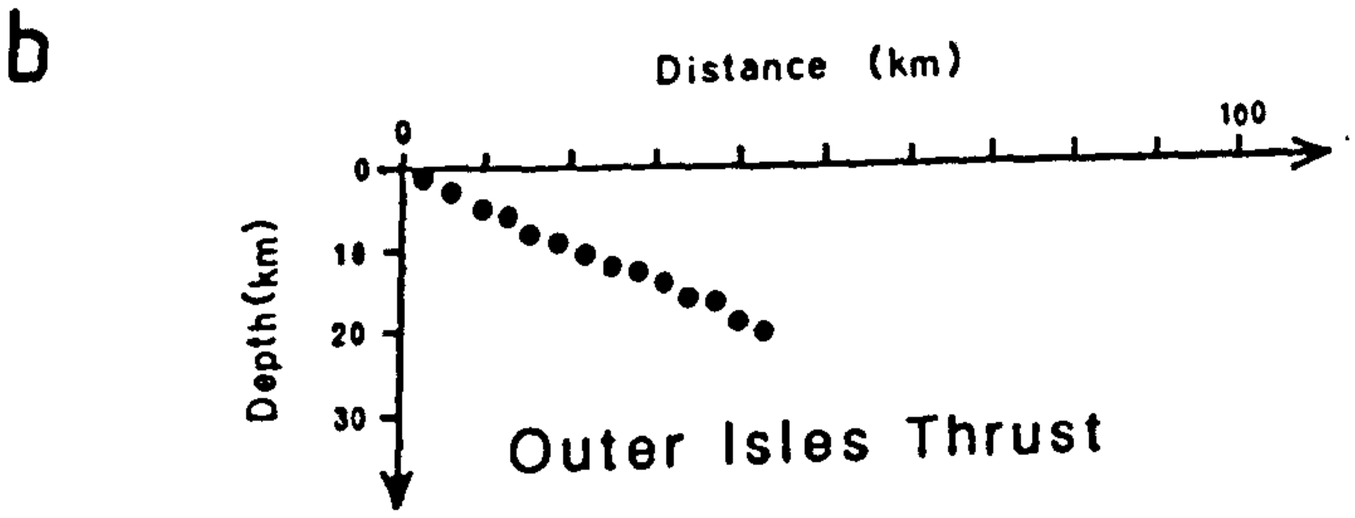

Figure 10.2 - Depth sections of the Outer Isles Fault (a), related to the Lewis basin, and the Variscan Front fault (b), related to the North Celtic Sea basin. These faults are shown to be more or less planar (P. Caban, personal communication).

underlying reasons for this symmetry can be found in two inherent assumptions within the chevron construction:

a) Hanging wall collapse, following extension, occurs by movement along vertical simple shear planes.

b) The hanging wall is infinitely weak, following simple shear extension, whereas the footwall possesses an infinite strength and as a consequence does not deform following simple shear extension.

These assumptions question the use of the Chevron construction for predicting basin geometries following lithosphere extension, particularly along planar faults where both seismological investigations of presently active faults (Jackson and McKenzie 1983) and depth conversions of seismic data (figure 10.2) show that a large number of major basement faults are in fact planar.

The literature reveals a variety of methods to predict the structural deformation of the upper lithosphere following extension along both listric and planar faults (eg. Wernicke and Burchfiel 1982, Le Pichon et al 1983, White et al 1986, Williams and Vann 1987, Barr 1987, Moretti et al. in press). These methods also possess inherent weaknesses and many rely upon a variety of geometric manipulations of the basic chevron construction. For example, Wernicke and Burchfiel (1982) note that both listric and planar normal faults are common in extended terrains. They qualitatively explain extension on planar faults as producing a "domino-style" set of fault blocks, but fail to account satisfactorily for space problems that exist both at the base of the fault

blocks and at the proximal and distal boundary faults. The former boundary is rather unjustifiably represented as a listric fault, while the internal fault blocks have evolved by extension on a series of planar faults.

The work of White et al (1986) is more convincing as they analytically relate the shape of a fault in cross-section to the shape of the bedding horizons in its hanging wall block. Their method is an improvement upon the chevron construction in that the hanging wall can deform upon inclined shear planes. The weakness in their approach, however, and in the approach of the other workers mentioned above, has been to study only the geometrical aspect of the deformation associated with extensional tectonics; the effects of perturbing the temperature field and isostasy have been ignored. While it is necessary to understand the geometrical aspect of fault movement, it is not possible to consider this component separate from thermal and isostatic effects - all play a contributory role in basin formation.

10.2 The flexural isostatic consequences of extension on planar faults.

In this section a quantitative method for extension on planar faults, which combines geometric aspects of the hanging wall and footwall deformation with associated thermal and flexural isostatic effects, is described (see also Kusznir et al, in press). The method allows both footwall and hanging wall to deform during the extensional process. The simple shear component of this formulation is obtained by quantifying the Wernicke model (Wernicke 1985), whereby extension occurs along a planar fault dipping at a

constant angle from the surface down to the asthenosphere (figure 10.3a). The depth of the fault in the x-coordinate frame, $D_{(x)}$, is given by:

$$D_{(x)} = 0 \qquad \text{for} \quad x \leq x_o$$

$$D_{(x)} = \tan\theta.x \qquad \text{for} \quad x > x_o \quad \text{----} \quad 10.1$$

where θ is the angle of dip of the fault and x_o is the position of the outcrop of the fault at the surface.

A purely geometric consideration of extension along this fault is shown in figure 10.3b, and the surface subsidence, $SS_{(x)}$, is given by:

$$SS_{(x)} = D_{(x)} - D_{(x-E)} \quad \text{------} \quad 10.2$$

where D_x defines the fault and E is extension.

The surface is prevented from attaining the geometry illustrated in figure 10.3b due to the resistance created by flexural isostatic forces. These forces arise due to:

a) The replacement of mantle material by air as the surface subsides due to extension along the fault.

b) The replacement of mantle rock by lower crust, as defined by $CR_{(x)}$ in figure 10.3b.

The magnitude of the uplift described in a, $w_{(x)}$, can be obtained by solving the following differential equation:

$$d^2/dx^2.(D.d^2w_{(x)}/dx^2) + (\rho_m-\rho_{air}).g.w_{(x)} = \rho_c.g.SS_{(x)} \quad \text{----} \quad 10.3$$

Figure 10.3 - The geometric consequences of extension along a planar fault dipping uninterrupted down to the lower lithosphere (a) is to produce a "wedge" of surface subsidence due to a downward displacement of the hanging wall (b). Isostatic restoring forces maintain areas of unthinned crust at sea level, while the basin reflects the region of attenuated crust (c).

where D is flexural rigidity, g is acceleration due to gravity and p_m, p_c and p_{air} are the densities of mantle, crust and air respectively.

Flexural isostatic modification of the surface subsidence by uplift, $w_{(x)CR}$, arising from the replacement of mantle material by lower crust, is given by the solution to the following equation:

$$d^2/dx^2.(D.d^2w_{(x)CR}/dx^2) + (p_m-p_{air}).g.w_{(x)CR} = (p_m-p_c).g.CR_{(x)} \quad -- \quad 10.4$$

where $CR_{(x)} = SS_{(x-Of)}$ and Of defines the horizontal distance between the outcrop of the fault at the surface and the position at which it cuts the Moho.

The resultant basin shown in figure 10.3c reflects a superposition of the above geometric and flexural isostatic components, and shows an upbending of the footwall as well as flexural downbending of the hanging wall, which results in an uplift of the footwall rift shoulder and rift basin respectively. The magnitude of this basin, $B_{(x)}$, is given by:

$$B_{(x)} = SS_{(x)} - W_{(x)==} - W_{(x)CR} \quad ---- \quad 10.5$$

Deep seismic reflection data does not support the existence of faults dipping uninterrupted from the surface down to the deep lithosphere. Instead, extension in the upper lithosphere occurs along faults that appear to merge into or detach at lower crustal depths (see chapter 1). In figure 10.4a this has been taken into account by allowing extension

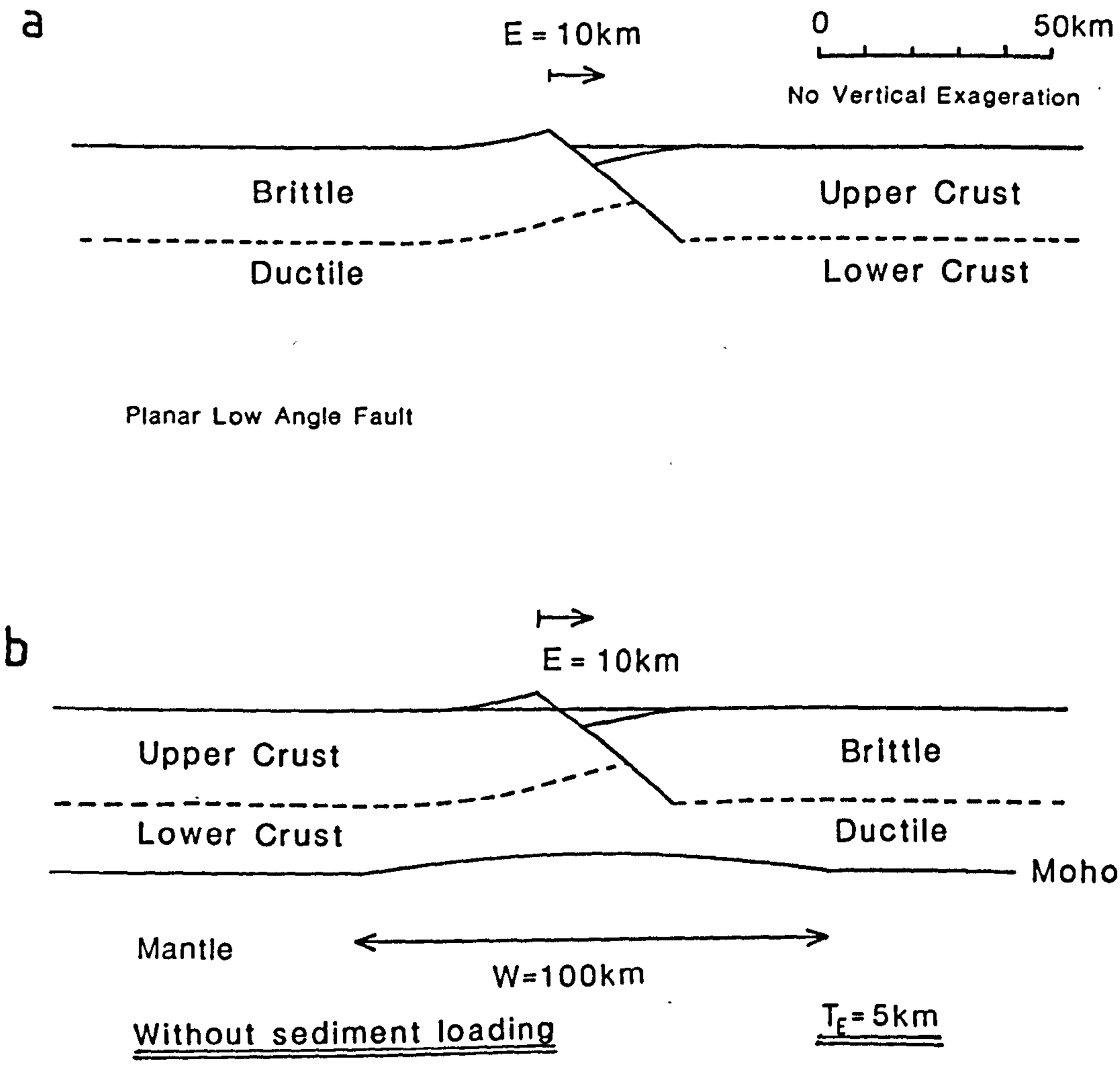

Figure 10.4 - Seismic data and thermo-rheological modelling suggests that major low angle faults are consumed in the plastic lower crust (a). This plastic layer must therefore accommodate the extensional deformation of the fault blocks above. The basin and crustal structure produced by the simple shear process is modified by an upward flexing isostatic force in response to the thinned crust, thermally induced uplift and pure shear thinning of the lower crust (b).

to occur along a planar fault in the upper crust, and this gives way with depth to ductile pure shear in the lower crust. This initial model assumes the deforming medium to be composed entirely of crustal rocks. A geometric consideration of this situation again produces a surface subsidence component, as quantified by equation 10.2, which, in turn, is modified by uplift due to flexural isostasy. Quantification of this uplift is provided by equation 10.3, which has been modified to take into account the fact that extension along the fault is caused by the replacement of crust by air. The modified equation is given by:

$$d^2/dx^2.(D.d^2w_{(x)}/dx^2) + (\rho_c-\rho_{air}).g.w_{(x)} = \rho_c.g.SS_x \quad \text{----- 10.6}$$

In figure 10.4b mantle lithosphere has been added to the model and the flexural isostatic effects of the following loads have also been considered:

a) Pure shear thinning of the lower crust and mantle lithosphere.

b) Perturbation of the lithosphere temperature field.

c) Isostatic compensation by mantle material for crustal thinning generated by brittle faulting

The effects of pure shear deformation and temperature perturbations have been described in chapter 2 and equations quantifying the flexural response of the lithosphere to these two phenomena are given in section 4.2. The isostatic response of the lithosphere to the loss of mass from the thinning of the crust, $w_{(x)tc}$, can be quantified by solving

the following equation:

$$d^2/dx^2.(D.d^2w_{(x)tc}/dx^2) + (p_m-p_{air}).g.w_{(x)tc} = (p_m-p_c).g.tc_{(x)} \quad \text{---- 10.7}$$

where $tc_{(x)}$ defines the thinning of the crust such that:

$$tc_{(x)} = Z_a \cdot (1-1/\beta_{(x)}) \quad \text{----- 10.8}$$

where Z_a defines the thickness of the brittle layer and $\beta_{(x)}$ defines a series of extension factors, which are defined according to equations 2.6 to 2.8.

Although the above formulation is new, the isostatic consequences of extension along planar faults have previously been investigated by Vening Meinesz, 1950 (see Heiskanen and Vening Meinesz 1958) who provided a formulation for the flexural origin of the footwall shoulder uplift seen to flank many rift valleys. The Vening Meinesz method takes two crustal blocks, separated by a planar fault and, on extension, allows them to behave as two independent cantilevers. Flexural isostatic rebound causes uplift of the footwall due to unloading of the fault surface by tectonic denudation of the hanging wall, and also subsidence of the hanging wall, caused by the replacement of the thinned crust with rock of mantle density (figure 10.5). A major drawback with the Vening Meinesz method is that it relates the post-extensional restoring forces acting on each of the cantilevers, and hence basin geometry, to the dip of the fault (see Weissel and Karner, in press). While the angle of dip of the fault on which extension is taking place does influence of flexural response of the lithosphere, a more

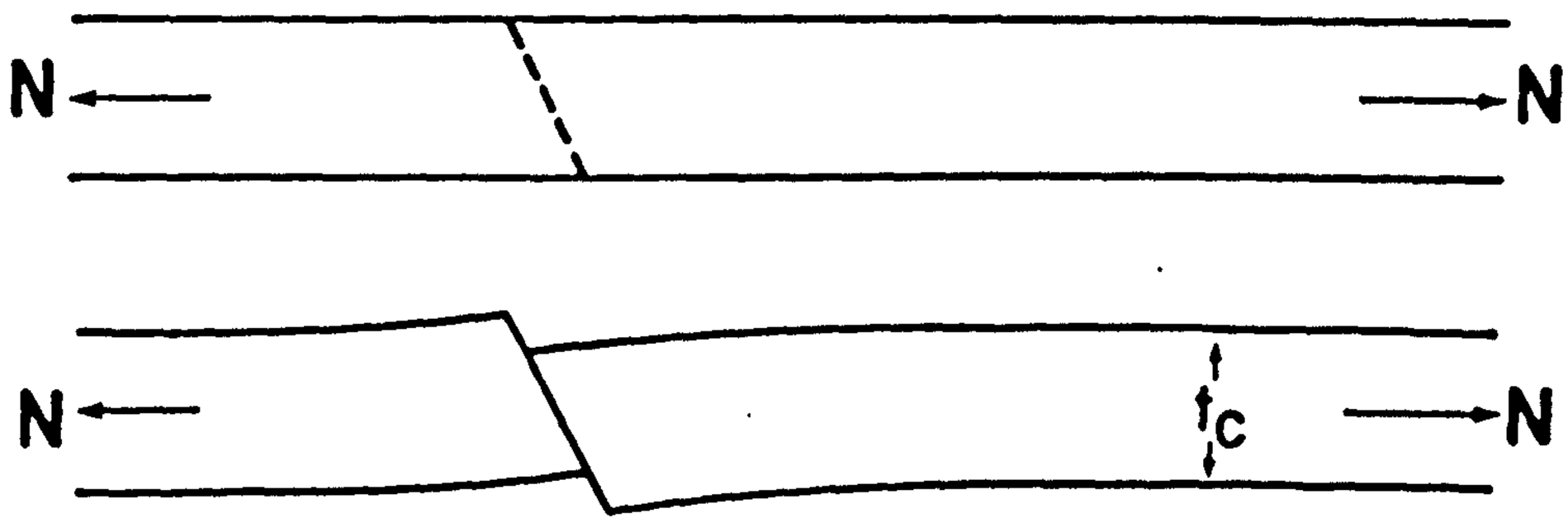

Figure 10.5 - The Vening Meinesz model (1950) divides the crust, via a planar fault, into two blocks. Extension on this fault causes an uplift of the footwall rift shoulder and a downbending of the hanging wall to form a basin.

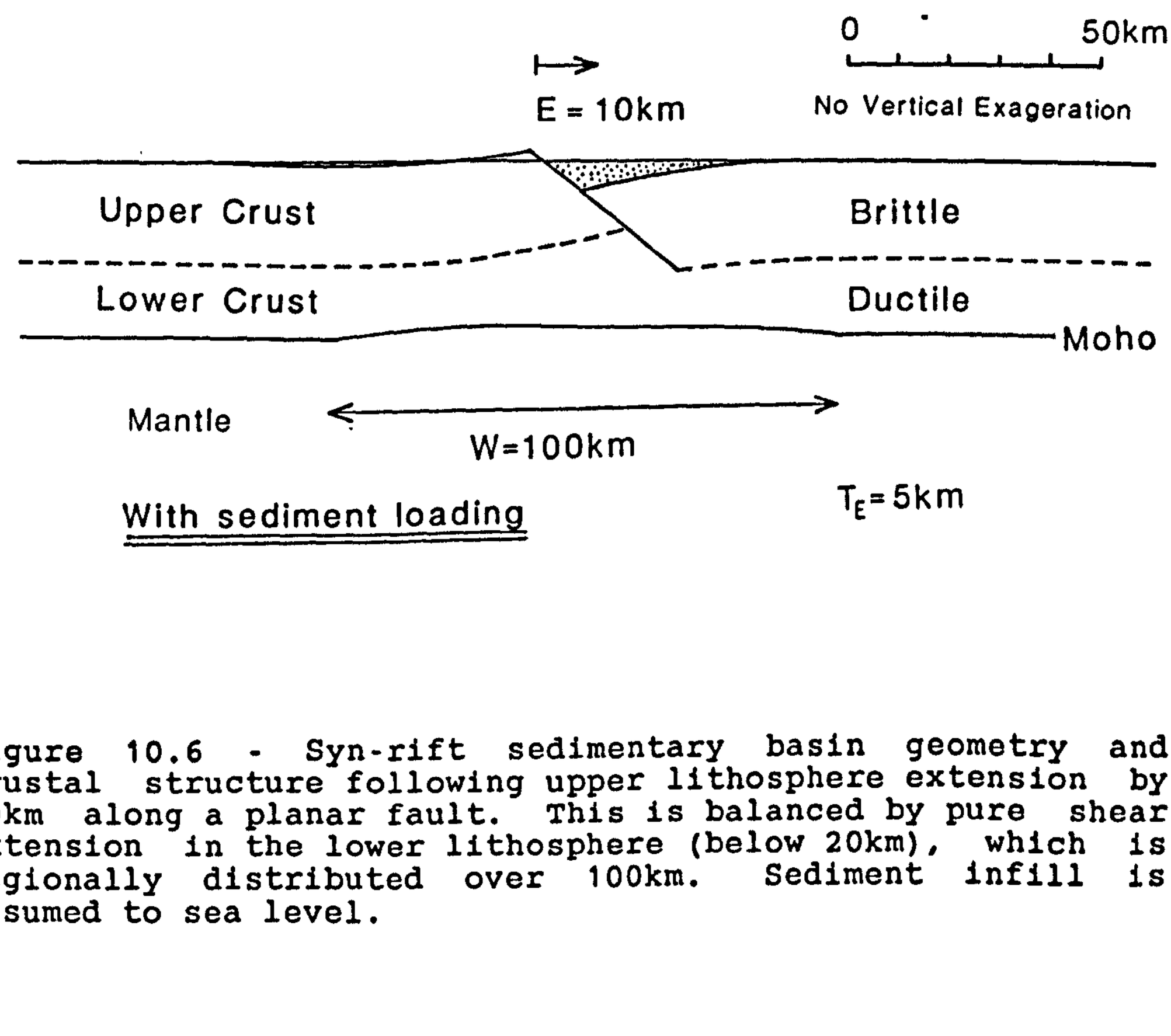

Figure 10.6 - Syn-rift sedimentary basin geometry and crustal structure following upper lithosphere extension by 10km along a planar fault. This is balanced by pure shear extension in the lower lithosphere (below 20km), which is regionally distributed over 100km. Sediment infill is assumed to sea level.

important controlling factor is the amount of extension along the fault. The Vening Meinesz method also treats the footwall and hanging wall as two independent cantilevers, while the method used here maintains contact between the footwall and hanging wall and as a consequence treats the isostatic restoring forces as acting on a continuous elastic plate. Thus the control on basin geometry by factors such as fault dip, amount of extension and sediment loading etc. can be accurately assessed.

10.3 Simple shear-pure shear model predictions for extension on planar faults.

In figure 10.6 syn-rift (0Ma) basin geometry and crustal structure are shown as predicted by simple shear-pure shear extension by 10km along a planar fault dipping at 45° and reaching down to a depth of 20km. Below this depth plastic failure is assumed and deformation is taken up by pure shear, regionally distributed over 100km and positioned beneath the fault controlled extension in the upper lithosphere. A finite flexural rigidity is assumed and is defined by an elastic thickness of 5km. Footwall uplift and hanging wall collapse are mainly the result of flexural isostatic movement arising from the effects of simple shear, although both the effects of pure shear crustal thinning and perturbation of the geotherm have also been included. In addition basin geometry has been modified following rifting by sediment loading to sea level.

In figure 10.7a the flexibility of the model is illustrated by showing the effect of in-sequence extension on a set of four faults. Temperature and isostatic calculations have

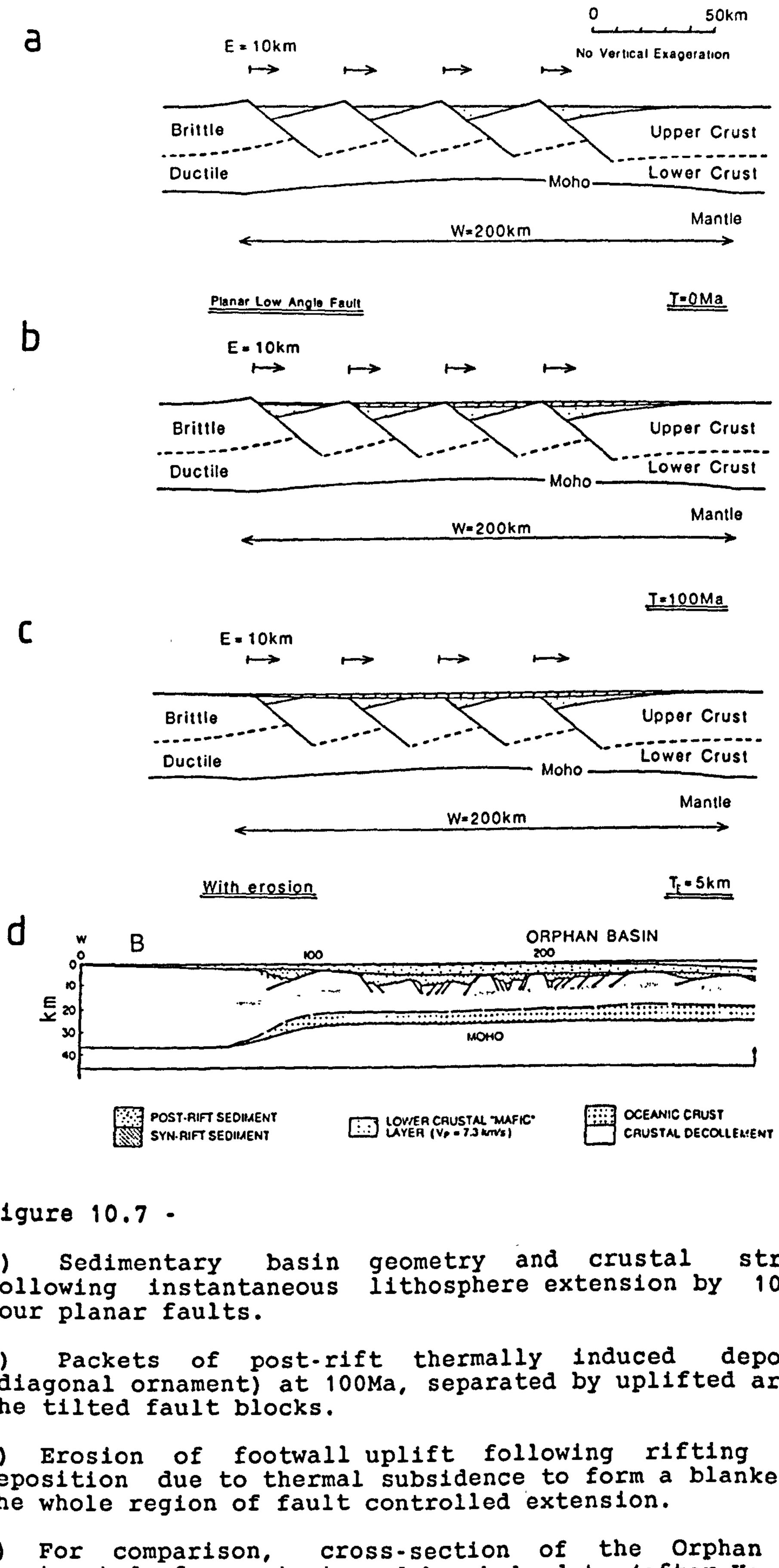

Figure 10.7 -

a) Sedimentary basin geometry and crustal structure following instantaneous lithosphere extension by 10km on four planar faults.

b) Packets of post-rift thermally induced deposition (diagonal ornament) at 100Ma, separated by uplifted areas of the tilted fault blocks.

c) Erosion of footwall uplift following rifting allows deposition due to thermal subsidence to form a blanket over the whole region of fault controlled extension.

d) For comparison, cross-section of the Orphan basin constructed from seismic and borehole data (after Keen, in press).

assumed instantaneous rifting. The flexural bending of the footwalls and hanging walls, related to movement on the individual faults, destructively interfere to produce the familiar "domino-style" block rotation of multiple fault systems. The upper surfaces of the blocks are more or less planar after extension, although they have been tilted. Mass balance problems are avoided at the boundaries of the tilted fault blocks due to an upward and downward flexing of both footwall and hanging wall blocks respectively. It is anticipated that the precise angular form of the base of the fault blocks illustrated in the model are purely hypothetical and, in reality, would merge into the series of anastomosing shear zones within the plastic lower crust (Reston 1988).

At 100Ma (figure 10.7b) deposition is induced by thermal subsidence, although its lateral continuity is interrupted by uplift of the block shoulders, particularly in the proximal region of the basin. Flexural erosion of the footwall uplift immediately after rifting (figure 10.7c), however, allows the post-rift sequence to form a continuous blanket above discrete syn-rift sub basins. This sedimentation pattern is common to large extensional basins such as the Viking Graben in the northern North Sea (chapter 6) and the Orphan basin in the Grand Banks region, Newfoundland (figure 6.1d)

10.4 Discussion.

In previous chapters the chevron construction has been used to predict crustal thinning by simple shear arising from

extensional movement along a listric fault. This resulting surficial hole is then modified by the combined effects of pure shear deformation, thermal uplift and isostatic forces. In this chapter a flexural cantilever model has been used to investigate extension on planar faults. The two methods are not compatible; the chevron construction predicts unrealistic basin geometries when used in conjunction with planar fault extension, and conversely it is not easily possible to consider the footwall and hanging wall as two interacting cantilevers when they are separated by a listric fault. The question arises as to which construction is the most appropriate, taking into account the fact that geological and seismic data show that both planar and listric faults exist in regions of extension, sometimes in close proximity to one another (eg. Bally 1984, Wernicke and Burchfiel 1982). An initial answer might be to question the existence of syn-extensional planar faults as it may be that the planar geometry of many faults in the seismic record are the result of isostatic forces created by the extensional deformation. Isostatic rebound following extensional fault movement can produce a planar or even concave upward fault from a listric geometry. Conclusive evidence of fault geometry, however, has been provided by the work of Jackson and McKenzie (1983), who have studied many examples of normal faults, from both Greece and Turkey, in their active state. The application of a variety of seismological techniques shows that these faults appear to be more or less planar down to depths of about 10km and dip at angles between 40° and 50°.. At depths greater than 10km these planar faults take on an exponential geometry as they

gradually flatten out into the rheologically weak plastic layer in the lower crust. It appears, therefore, that faults may appear to have an overall listric form from the surface down to the depth at which they detach in the lower crust, but they are planar in the brittle region near the surface.

The above evidence suggests that the cantilever construction, presented in this chapter, is the more appropriate method of modelling extensional tectonics, as it allows the deformation of hanging wall and footwall to occur as essentially two brittle blocks along a planar fault, while the lower crust is represented as a plastic layer which both accommodates the fault block movement above and provides a medium into which the major low angle faults can flatten out. The chevron construction, on the other hand, assumes the footwall to be infinitely strong compared to the hanging wall, and rather unrealistically allows the detachment horizon to be a rigid boundary onto which the hanging wall can collapse following extension - the variation of the rheological behaviour of the lithosphere with depth indicates that this is not true.

10.5 Summary.

In this chapter a quantitative method predicting sedimentary basin geometry and crustal structure following extension on planar faults has been described. The method, unlike other formulations described in the literature, combines the geometric aspect of faulting with associated thermal and flexural isostatic effects, and as a result both footwall and hanging wall are allowed to deform during the extensional process. It is suggested that only by using such

an integrated approach can a correct understanding of sedimentary basin evolution be achieved. Finally, the method is compatible with the rheological structure of the lithosphere and it is therefore suggested that it is superior to modelling techniques incorporating the chevron construction, which have been shown to contain several inherently weak assumptions.

Chapter 11

Conclusions

11.1 Introduction.

The work carried out for this thesis has concentrated upon the development of a depth dependent lithosphere extension model. Geological and seismic evidence have not only been used to both test and develop the model, but also to demonstrate its use as a powerful tool for the forward modelling of the evolution of many sedimentary basins. Furthermore, the flexibility of the model has been demonstrated by showing that it can be focused onto specific parameters involved in basin evolution so that their effect can easily be assessed and quantified.

11,2 Summary Points and Conclusions.

In this final chapter a summary of the findings and implications made in the previous sections are described:

1. Existing numerical models of lithosphere extension and sedimentary basin formation are pure shear models, and thus fail to take into account fault controlled deformation in the upper lithosphere. Seismic evidence shows that low angle faults and the detachments into which they flatten play a major role in extensional and compressional tectonics. They provide a line of weakness within the lithosphere and allow the formation of sedimentary basins in regions of tension and the formation of mountain ranges in a compressional environment.

2. Detachments are the product of either a rheological

zonation of the crust or an inherited collisional fabric. The seismic record shows them to be restricted to crustal depths in a continental setting.

3. The depth dependent lithosphere extension model presented in this thesis combines the geometric, thermal and isostatic components of extensional tectonics. The upper lithosphere is extended by simple shear along low angle faults, while the lower lithosphere is extended by pure shear. The surficial hole created by simple shear extension is calculated using the chevron construction. Both simple and pure shear perturb the lithosphere temperature field, while loads imposed upon the lithosphere due to its deformation are isostatically compensated. The amount of simple shear extension, the lateral offset of the lower lithosphere pure shear with respect to the simple shear deformation, and the depth of detachment are the main controlling parameters on sedimentary basin geometry and crustal structure.

4. The extensional deformation of the lithosphere has been shown to exert loads of both varying magnitude and polarity on the lithosphere. The resulting sedimentary basin geometry and crustal structure reflect a superposition of these loads after they have been compensated by either Airy or flexural isostasy. Airy compensation, however, leads to shallower basins than indicated by the seismic record, unrealistic deformation of the low angle fault and an extreme moho topography. Post rift thermal subsidence is also exaggerated. On the other hand, models assuming flexural compensation yield most accurate predictions of sedimentary basin evolution. The flexural strength of the lithosphere

during rifting causes an uplift of the footwall shoulder, a relatively deep basin, a smooth fault geometry and a subdued moho topography. The flexural strength of the lithosphere during post-rift thermal subsidence causes a reduction in the thickness of this component, but at the same time a broadening of thermally induced deposition into the distal region.

5. The amount of post-rift thermal subsidence is critically dependent upon the rate at which extension occurs. Instantaneous rifting maximises the perturbation to the geotherm, causing a large amount of thermally induced subsidence. Non-instantaneous rifting allows re-equilibration of the lithosphere temperature field during the finite rift phase - the apparent thickness of post-rift thermal subsidence is reduced. Furthermore, the superposition of several distinct rift phases produces a vertical stacking of syn- and post-rift basin components. This situation most closely resembles the stratigraphic pattern seen in many sedimentary basins.

6. It has been shown that uplift of basement can occur during rifting due to heating of the lithosphere and/or flexural isostatic rebound in response to simple shear crustal thinning. Erosion of these discrete pockets of topography is accompanied by isostatic compensation, which produces a regional uplift. Further erosion of this uplift can cause both the removal of both more basement and sediment fill from within the basin. A regional erosion surface results, which, on burial, forms an unconformity in the stratigraphic record.

7. The simulation of rifting on several closely spaced faults in the crust, while the lower lithosphere extends by a regionally distributed pure shear process, produces a superposition of extensional components generating a broad blanket of thermally induced deposition on top of discrete rift depocentres. This lateral coincidence between syn- and post-rift sub basins is also predicted by the pure shear models.

8. The level to which a basin is filled with sediment is dictated by a combination of the availability of sediment, eustatic changes over time and the temporal behaviour of the thermal state of the lithosphere. Warm lithosphere has been shown to be regionally elevated compared to lithosphere with a cool geotherm. Furthermore, basins resulting from the extension of thermally young (and hence warm) lithosphere show a depositional sequence due to rifting superimposed onto a regional subsidence created by the overall re-equilibration of the geotherm. This can have dramatic implications of the pattern of sedimentation within a sedimentary basin.

9. Thermally young (and hence warm) lithosphere is rheologically weaker than thermally old (and hence cool) lithosphere. Fast rates of extension cause a weakening of the lithosphere such that the point of minimum strength occurs where the crust has been most attenuated by simple shear. Slow rates of extension, however, cause rheological weakening in areas that have experienced heating either due to pure shear deformation within the lower lithosphere or due to the lateral flow of heat. After the equilibration of

the geotherm, lithosphere with thinned crust is rheologically strongest due to it being composed of a higher proportion of olivine at the expense of the weaker quartz rheology, composing the crust.

10. Lithosphere shortening has also been shown to be best represented as a coupled simple shear-pure shear process, whereby the upper lithosphere shortens along thrusts and the lower lithosphere is compressed by a regionally distributed pure shear deformation. Both simple and pure shear shortening cause a deepening of the lithosphere-asthenosphere boundary and therefore an initial cooling and, in turn, subsidence of the surface. This is followed by thermally induced uplift in response to post-shortening re-equilibration of the lithosphere temperature field. Flexural isostatic compensation of the thrust sheet emplacement causes a downward flexing of the lithosphere and a foreland basin is produced adjacent to the region of lithospheric thickening.

11. Many major low angle faults have experienced a sequence of extensional and compressional events throughout geological time. The modelling shows that extensional reactivation along a fault produces a vertical stacking of rift and thermal sequences. Compressional reactivation along a fault leads to basin inversion which can lead to the loss of existing depocentres and the formation of new ones due to the additional loading of the lithosphere.

12. Extension on a planar fault separates the crust into two separate blocks, and are best considered as two cantilevers,

which respond to flexural isostatic forces created by movement along the fault. Sedimentary basin formation and crustal structure are produced by an upward flexing of the footwall block and a down bending of the hanging wall. Extension on multiple planar faults causes an interference of these two opposing flexural effects and the familiar "domino-style" fault block rotation is produced.

11.3 Future Work.

While the coupled simple shear-pure shear model is covered comprehensively in this thesis there is still plenty of scope for further development. Two immediate areas are anticipated to form the basis for future work:

a) The prediction of basin stratigraphy - while the effects of finite rifting and a temporally varying base level for sedimentation have been investigated, other factors such as decompaction and lateral variation in both sediment type and amount have been neglected. Work by Sclater and Christie (1980) supports the importance of the former parameter, while lateral sediment variation within a basin from proximal deltaic sands to distal, sometimes sparse, shale dominated lithologies in the distal region is well documented.

It is anticipated the temporal variation of flexural rigidity with time will have a strong effect on basin stratigraphy. Flexural rigidity is determined by the thermal state of the lithosphere (Kusznir and Karner 1985) and the heating of the lithosphere during rifting, promotes a low value of flexural rigidity, whereas post-rift cooling

following rifting is accompanied by an increase in flexural strength. It is anticipated that this will create an increasing resistance to thermal subsidence and as a consequence the thickness of this component will be reduced. At the same time, however, higher flexural flexural rigidities cause a corresponding increase in the flexing wavelength of the lithosphere - thermally induced subsidence is therefore promoted further and further onto peripheral regions.

In the shortening process more attention is required on the finite development of thrusts in order to investigate the stratigraphic evolution of foreland basins and particularly their continual modification as thrusting propagates onto the foreland.

b) Incorporation of simple shear-pure shear model predictions with other techniques and data-types - Forward modelling of the type carried out in this thesis can sometimes suffer from the inverse problem in that a combination of several differing factors can explain the pattern now seen in the geological record. It is suggested that use should be made of as many techniques and data types that are available. Gravitational data, palaeo heat flow data, chalk porosity data, etc. can be incorporated with simple shear-pure shear model predictions and perhaps alleviate some of the ambiguity that arises. For example, it is possible to use the crustal and basin profiles predicted by the simple shear-pure shear model to calculate gravity anomalies, by using either a line integral method or an admittance function technique (Karner 1982). These

predictions can be compared with gravity data over the sedimentary basins under investigation.

Finally, if the work carried out for this thesis has achieved nothing else, it has proven the usefulness of numerical modelling techniques in helping to understand many geological processes. At the same time it has become clear that the development of the modelling relies on accurate and detailed geological observations. The initial chapters were almost entirely theoretical and it was only by consultation of geological and geophysical data that the theory could be tested and further developed. This indicates, therefore, that future work must continue promoting this mutual beneficial relationship.

References.

Airy, G.B. 1855. On the computation of the effect of the attraction of mountain-masses, as disturbing the apparent astronomical latitude of stations in geodetic surveys. Phil. Trans. R. Soc., 145, pp.101-104.

Badley, M.E., Price, J.D., Rambech Dahl, C. & Agdestein, T. 1988. The structural evolution of the northern Viking Graben and its bearing upon extensional modes of basin formation. J. Geol. Soc. Lond., 145, pp.455-472.

Bally, A.W. 1982. Musings over sedimentary basin evolution. Phil. Trans. R. Soc. A305, pp.325-328.

Bamford, D. 1979. Seismic constraints on the deep geology of the Caledonides of Northern Britain. In: Harris, A.L., Holland, C.H. & Leake, B.E. (Eds.). The Caledonides of the British Isles -Reviewed. Spec. publ. geol. Soc. Lond., 8, pp.93-96.

Barr, D. 1987. Structural/stratigraphic models for extensional basins of half-graben type. J. Struct. Geol., 9, pp.491-500.

Barton, P. & Wood, R. 1984. Tectonic evolution of the North Sea basin: crustal stretching and subsidence. Geophys. J. R. astr. Soc., 79, pp.987-1022.

Beach, A. 1986. A deep seismic reflection profile across the northern North Sea. Nature, 33, pp.53-55.

Beach, A., Bird, T. & Gibbs, A. 1987. Extensional tectonics and crustal structure: deep seismic reflection data from the

northern North Sea Viking Graben. In: Coward. M.P., Dewey, J.F. & Hancock, P.L. (Eds.). Continental Extensional Tectonics. Spec. publ. geol. Soc. Lond. No. 28, pp.467-476.

Beaumont, C. 1978. The evolution of sedimentary basins on a viscoelastic lithosphere: theory and examples. Geophys. J. R. astr. Soc., 55, pp.471-498.

Beaumont, C. 1979. Foreland basins (abs.). International Union of Geodesy and Geophysics General Assembly, Abs., No. 17, pp.3-9.

Beaumont, C. 1981. Foreland basins. Geophys. J. R. astr. Soc., 65, pp.291-329.

Beaumont, C., Keen, C.E., & Boutilier, R. 1982. A comparison of foreland and rift margin sedimentary basins. Phil. Trans. R. Soc. London, A305, pp.295-317.

BIRPS & ECORS. 1986. Deep seismic profiling between England, France and Ireland. J. geol. Soc. London, 143, pp.45-52.

Blundell, D.J., Hurich, C.A. & Smithson, S.B. 1985. A model for the MOIST seismic reflection profile, N. Scotland. J. geol. Soc. London, 142, pp.245-258.

Bodene, J.H., Steckler, M.S. & Watts, A.B. 1981. Observations of flexure and the rheology of the oceanic lithosphere. J. geophys. Res. 86, pp.3695-707.

Bott, M.H.P. 1976. Formation of sedimentary basins of the graben type by extension of the continental crust. Tectonophysics, 36, pp.77-86.

Brewer, J.A. & Smythe, D.K. 1984. MOIST and the continuity

of crustal reflection geometry along the Caledonian-Appalachian orogen. J. geol. Soc. London, 141, pp.105-120.

Coward, M.P. 1986. Heterogeneous stretching, simple shear and basin development. Earth and Planet. Sci. Letts., 80, pp.325-336.

Dewey, J.F. & Bird, J.M. 1970. Mountain belts and the new global tectonics. J. Geophys. Res., 75, pp.2625-2647.

Dewey, J.F. 1982. Plate tectonics and the evolution of the British Isles. J. geol. Soc. Lond., 133, pp.371-412.

Enachescu, M.E. 1987. Tectonic and structural framework of the northeast Newfoundland continental margin. In: Beaumont, C. & Tankard, A.J. (Eds.). Sedimentary basins and basin forming mechanisms, Canad. Soc. Petrol. Geol. Mem. No. 12, pp.117-146.

Etheridge, M.A. 1986. On the reactivation of extensional fault systems. Phil. Trans. R. Soc. London, 317, pp.179-194.

Gibbs, A.D. 1983. Balanced cross-section constructions from seismic sections in areas of extensional tectonics. J. Struct. Geol., 5, pp.152-160.

Gibbs, A.D. 1984. Structural evolution of extensional basin margins. J. Geol. Soc. Lond., 141, pp.609-620.

Gibbs, A.D. 1987. Linked tectonics of the northern North Sea. In: Beaumont, C. & Tankard, A.J. (Eds.). Sedimentary basins and basin forming mechanisms, Canad. Soc. Petrol. Geol. Mem. No. 12, pp.163-171.

Gillcrist, R., Coward, M. & Mugnier, J.L. 1987. Structural inversion: examples from the Alpine foreland and the French Alps. Geodinamicu Acta (Paris), 111, pp5-35.

Glennie, K.W. 1986. Introduction to the Petroleum Geology of the North Sea. Blackwell Scientific Publications, 2nd ed.

Goetze, C. 1978. The mechanisms of creep in olivine. Phil. Trans. R. Soc. A288, pp.99-119.

Griffith, A.A. 1924. Theory of rupture. Proc. 1st int. Congr. Applied Mechanics, Delft, A221, pp.163-198.

Hall, J. & Al-Haddad, F.M. 1976. Seismic velocities in the Lewisian Metamorphic complex, north west Britain - "in situ" measurements. Scot. J. Geol., 12, pp.305-314.

Hall, J., Brewer, J.A., Matthews, D.H. & Warner, M.R. 1984. Crustal structure across the Caledonides from the WINCH seismic reflection profile: influences on the evolution of the Midland Valley of Scotland. Trans. R. Soc. Edinburgh: Earth Sciences, 75, pp.97-109

Hallam, A. 1973. A Revolution in the Earth Sciences: From Continental Drift to Plate Tectonics. Oxford University Press.

Heiskanen, W.A. & Vening Meinesz. 1958. The Earth and its Gravity Field. McGraw-Hill New York.

Hellinger, S.J. & Sclater, J.G. 1983. Some comments on two-layer extensional models for the evolution of sedimentary basins. J. Geophys. Res. 88, pp.8251-8269.

Hillis, R.R. in press. Chalk porosities from wireline logging and Tertiary uplift, Western Approaches Trough. J. geol. Soc. Lond.

Jackson, J.A. & McKenzie, D.P. 1983. The geometrical evolution of normal fault systems. J. struct. Geol., 5, pp.471-482.

Jansa, L.E. & Wade, J.A. 1975. Geology of the continental margin off Nova Scotia and Newfoundland. In: Offshore Geology of Eastern Canada. Geological Survey of Canada, Paper 74-30, 2, pp.51-105.

Jordan, T.E. 1981. Thrust loads and foreland basin evolution, Cretaceous, Western United States. Bull. Am. Ass. Petrol. Geol., 65. pp.2506-2520.

Karner, G.D. 1982. Spectral representation of isostatic models. J. Aust. Geol. and Geophys., 7, pp.55-62.

Karner, G.D. 1984. Continental tectonics - a quantitative view of the thermal and mechanical properties of the continental lithosphere in compressional and extensional stress regimes. Proceedings of the Summer School of Space Physics, Centre National d'Etudes Spatiales, Toulouse, France. pp.403-464.

Keen, C.E., Boutilier, R., De Voogd, B., Mudford, B. & Enacheseu, M. 1987. Crustal geometry and models of the evolution of the rift basins on the Grand Banks off eastern Canada: constraints from deep seismic reflection data. In: Beaumont, C. & Tankard, A.J. (Eds.). Sedimentary basins and basin forming mechanisms, Canad. Soc. Petrol. Geol. Mem. No.

12. pp.101-116.

Keen, C.E. & de Voogd, B. 1988. The continent-ocean boundary at the rifted margin off eastern Canada: new results from deep seismic reflection studies. Tectonics, 7, No. 1, pp.107-124.

Keen, C.E. In press. The mode of lithospheric extension determined from crustal studies across rift basins, eastern Canada. A.G.U. Geodynamics Series Vol. on Basins Arising from I.U.G.G. Symp., U19.

Kirby, S.H. 1983. Rheology of the lithosphere. Rev. Geophys. Space Phys., 21, pp.1458-1487.

Klemperer, S.L. in press. Crustal thinning and nature of extension in the northern North Sea from deep seismic reflection profiling. Tectonics.

Koch, P.S., Christie, J.M. & George, R.P. 1980. Flow law of 'wet' quartzite in the α-quartz field. Eos. 61, p.376.

Kohlstedt, D.L. & Goetze, C. 1974. Low-stress high-temperature creep in olivine single crystals. J. geophys. Res. 79, pp.2045-2051.

Kusznir, N.J. 1982. Lithosphere response to externally and internally derived stresses: a viscoelastic stress guide with amplification. Geophys. J.R. astron. Soc., 70, pp.399-414.

Kusznir, N.J. & Park, G. 1984. Intraplate lithosphere deformation and the strength of the lithosphere. Geophys. J. R. astr. Soc. 79, pp.513-535.

Kusznir, N.J. & Karner, G.D. 1985. Dependence of the flexural rigidity of the continental lithosphere on rheology and temperature. Nature, 316, pp.138-142.

Kusznir, N.J. & Park, G. 1986. Continental lithosphere strength: the critical role of lower crustal deformation. In: Dawson, J.B., Carswell, D.A., Hall, J. & Wedepohl, K.H. (Eds). The nature of the lower continental crust. Geol. Soc. Spec. Pub. No.24, pp.79-93.

Kusznir, N.J. & Park, G. 1987. The extensional strength of the continental lithosphere: its dependence on geothermal gradient, crustal composition and thickness. In: Coward. M.P., Dewey, J.F. & Hancock, P.L. (Eds.). Continental Extensional Tectonics. Spec. publ. geol. Soc. Lond. No. 28, pp.35-52.

Kusznir, N.J., Karner, G.D. & Egan, S.S. 1987. Geometric, thermal and isostatic consequences of detachments in continental lithsphere extension and basin formation. In: Beaumont, C. & Tankard, A.J. (Eds.). Sedimentary basins and basin forming mechanisms, Canad. Soc. Petrol. Geol. Mem. No. 12., pp.185-203.

Kusznir, N.J. & Egan, S.S. In press. Simple - shear and pure - shear models of extensional sedimentary basin formation: application to the Jeanne d'Arc basin, Grand Banks of Newfoundland. Canad. Soc. Petrol. Geol. Mem.

Kusznir, N.J., Marsden, G. & Egan, S.S. In press. A flexural cantilever model of continental lithosphere extension on planar faults. Geol. Soc. Lond. Spec. Pub.

Lake, S.L. & Karner, G.D. 1987. The structure and evolution of the Wessex basin, southern England: an example of inversion tectonics. In: Ziegler, P.A. (Ed.), European Union of Geosciences 3rd Symposium on Inverted Mesozoic Basins of the Alpine Foreland. Tectonophysics, 137, pp.347-378.

Leeder, M.R. 1983. Lithospheric stretching and North Sea Jurassic clastic sourcelands. Nature, 305, pp.510-513.

Lemcke, V.K. 1981. Das heutige geologische Bild des deutschen Alpenvorlandes nach drei Jahrzehnten Ol - und Gasexploration. Eclogae geol. Helv., 741. pp1-18.

Le Pichon, X., Angelier, J. & Sibuet, J.C. 1983. Subsidence and stretching. In: Watkins, J.S. & Drake, C.L. (Eds.). Studies in Continental Margin Geology. Am. Ass. petrol. Geol. Mem., 34, pp.731-741.

Matter, A. & Homewood, P. 1980. Flysch and Molasse of western and central Switzerland. In: Schweizerische Geologische Kommission (Eds.). The Geology of Switzerland. Basel, New York.

Matthews, D.H. & Cheadle, M.J. 1986. Deep reflections from the Caledonides and Variscides west of Britain and comparisons with the Himalayas. In: Barazangi, M. & Brown, L. (Eds.), Reflection Seismology: A Global Perspective. A.G.U. Geodynamics Series, 13, pp. 5-19.

Matthews, D.H. & Smith, C. 1987. Deep seismic reflection profiling of the continental lithosphere. Gephys. J. R. astr. Soc., 89.

McGeary, S. & Warner, M.R. 1985. Seismic profiling of the continental lithosphere. Nature, 317, pp.795-797.

McKenzie, D.P. 1969. Speculations on the consequences and causes of plate motion. Geophys. J. R. astr. Soc., 18, pp.1-32.

McKenzie, D.P. 1978. Some remarks on the development of sedimentary basins. Earth and Planet. Sci. Letts., 40, pp.25-32.

McKenzie, D.P. 1986. The extraction of magma from the crust and mantle. Earth and Planet. Sci. Letts., 74, pp.81-97.

McKenzie, D.P. & Bickle, M.J., in press. The volume and composition of melt generated by extension of the lithosphere. J. Petrol.

McLintock, F.A. & Walsh, J.B. 1962. Friction on Griffith cracks under pressure. Proc. 4th U.S. Nat. Congr. Applied Mechanics, pp.1015-21.

Moretti, I., Colletta, B., & Vially, R. In press. Theoretical model of block rotation along circular faults. Tectonophysics.

Murrell, S.A.F. 1976. Rheology of the lithosphere - Experimental Indications. Tectonophysics, 36, pp.5-24.

Noble, B & Daniel, J.W. Applied Linear Algebra. 2nd ed. Englewood Cliffs, NJ., Prentice-Hall, 1977.

Parsons, B. & Sclater, J.G. 1977. An analysis of the variation of ocean floor bathymetry and heat flow with age. J. Geophys. Res., 82, pp.803-827.

Post R.L. 1977. High temperature of Mt. Burnet Dunite. Tectonophysics. 42, pp.75-110.

Reston, T.J. 1988. Evidence for shear zones in the lower crust offshore Britain. Tectonics, 7, pp.929-945.

Roberts, D.G., Backman, J., Morton, A.C., Murray, J.W. & Keene, J.B. 1984. Evolution of volcanic rifted margins: synthesis of leg 81 results of the west margin of Rockall Plateau. Init. Rep. Deep Sea Drill. Proj., 81, pp.883-911.

Royden, L. & Keen, C.E. 1980. Rifting processes and thermal evolution of the continental margin of eastern Canada determined from subsidence curves. Earth and Planet. Sci. Letts., 51, pp.343-361.

Royden, L. & Karner, G.D. 1984. Flexure of the continental lithosphere beneath the Apennine and Carpathian foredeep basins. Nature. 309. pp.142-144.

Sclater, J.G., Royden, L., Harvath, F., Burchfiel, B.C., Semkin, S. & Stegena, L. 1980. Subsidence and thermal evolution of the intra-Carpathian basins. Earth Planet. Sci. Letts., 51, pp.139-162.

Sclater, J.G. & Christie, P.A. 1980. Continental stretching: an explanation of the post mid-Cretaceous subsidence of the central North Sea basin. J. geophys. Res., 85, pp.3711-3739.

Shackleton, R.M. 1984. Thin-skinned tectonics, basement control and the Variscan Front. In: Hutton, D.H.W. & Sanderson, D.J. (Eds.), Variscan Tectonics of the North Atlantic Region. Spec. Pub. Geol. Soc. Lond. No. 14, pp.125-

Shelton, G. & Tullis, T. 1981. Experimental flow laws for crustal rocks. Eos, 62, p.396.

Sleep, N.H. & Snell, N.S. 1976. Thermal contraction and flexure of mid continent and Atlantic marginal basins. Geophys. J. R. astr. Soc., 45, pp.125-154.

Smythe, D.K., Dobinson, A., McQuillin, R., Brewer, J.A., Matthews, D.H., Blundell, D.J. & Kelk, B. 1982. Deep structure of the Scottish Caledonides revealed by the MOIST reflection profile. Nature. 299, pp.338-340.

Steckler, M.S. & Watts, A.B. 1978. Subsidence of the Atlantic- type continental margin of New York. Earth Planet. Sci. Letts., 41, pp.1-13.

Steckler, M.S. & ten Brink, U.S. 1986. lithospheric strength variations as a control on new plate boundaries: examples from the northern Red Sea region. Earth and Planet. Sci. Letts., 79, pp.120-132.

Stocker, R.L. & Ashby, M.F. 1973. On the rheology of the upper mantle. Rev. Geophys., 11, pp391-497.

Tankard, A.J. & Welsink, H.J. 1987. Extension tectonics and stratigraphy of the Mesozoic Grand Banks of Newfoundland. In: Manspeizer, W. (Ed.), Triassic-Jurassic rifting and the opening of the Atlantic Ocean. Amsterdam: Elsevier.

Tucker, R.M. & Arter, G. 1987. The tectonic evolution of the North Celtic Sea and Cardigan Bay basins with special reference to basin inversion. In: Ziegler, P.A. (Ed.),

European Union of Geosciences 3rd Symposium on Inverted Mesozoic Basins of the Alpine Foreland.Tectonophysics, 137, pp.291-307.

Turcotte, D.L. & Schubert, G. 1982. Geodynamics : applications of continuum physics to geological problems. J. Wiley & Sons.

Ussami, N., Karner, G.D. & Bott, M.H.P. 1986. Crustal detachment during South Atlantic rifting and the formation of the Tucano- Gabon basin system. Nature, 322, pp.629-632.

Vail, P.R., Mitchum, R.M. & Thompson, S. 1977. Seismic stratigraphy: Applications to Hydro-Carbon Exploration. Mem. Am. Ass. Petrol. Geol. no. 26, pp.83-97.

Vening Meinisz, F.A. 1950. Les Graben africains, resultat de compression ou de tension dans la croute terrestre. Bull. Inst. R. Colon. Belge, 21, pp.539-552.

Verall, P. 1982. Structural interpretation with applications to North Sea problems. Course Notes No. 3. JAPEC.

Walcott, R.I. 1970. Flexural rigidity, thickness and viscosity of the lithosphere. J. Geophys. Res., 75, pp.3941-3954.

Watts, A.B., Karner, G.D. & Steckler, M.S. 1982. Lithospheric flexure and the evolution of sedimentary basins. In: Kent, P., Bott, M.H.P., McKenzie, D.P. and Williams, C.A. (Eds.), The Evolution of Sedimentary Basins. Phil. Trans. R. Soc., A305, pp.249-281.

Weertman, J. 1970. Rev. Geophys. Space Phys., 8,

p.145.

Weissel, J.K. & Karner, G.D. (to be submitted for publication). Flexural uplift of rift flanks due to tectonic denudation of the lithosphere during extension.

Wernicke, B. & Burchfiel, B.C. 1982. Modes of extensional tectonics. J. of Struct. Geol, 4, pp.105-115.

Wernicke, B. 1985. Uniform-sense normal simple shear of the continental lithosphere. Canadian Journal of Earth Sciences, 22, pp.108-125.

White, N.J., Jackson, J.A. & McKenzie, D.P. 1986. The relationship between the geometry of normal faults and that of the sedimentary layers in their hanging walls. J. Struct. Geol., 8, pp.897-909.

White, R.S., Westbrook, G.K., Fowler, S.R., Spence, G.D., Barton, P.J., Joppen, M., Morgan, J., Bowen, A.N, Prestcott, C. & Bott, M.H.P. 1987¹. Hatton Bank (northwest U.K.) continental margin structure. Geophys. J. R. astr. Soc., 89, pp.265-272.

White, R.S., Spence, G.D., Fowler, S.R., McKenzie, D.P., Westbrook, G.K. & Bowen, A.N. 1987². Magmatism at rifted continental margins. Nature, 330, pp.439-444.

Williams, G. & Vann, I. 1987. The geometry of listric normal faults and deformation in their hanging walls. J. Struct. Geol., 9, pp.789-795.

Wilson, J.T. 1966. Did the Atlantic close and then reopen? Nature, 211, pp.676-681.

Wilson, J.T. et al. 1972. Continents Adrift and Continents Aground. W.H. Freeman and Co., San Francisco.

Ziegler, P.A. 1981. Evolution of sedimentary basins in N.W. Europe. In: Illing, L.V. & Hobson, G.D. (Eds.), Petroleum Geology of the Continental Shelf of North-West Europe. Heyden, London, pp.3-43.

Ziegler, P.A. 1982. Geological Atlas of Western and Central Europe. Elsevier Scientific Publishing Company.

Ziegler, P.A. 1987¹. Celtic Sea - Western Approaches area: an overview. In: Ziegler, P.A. (Ed.), European Union of Geosciences 3rd Symposium on Inverted Mesozoic Basins of the Alpine Foreland. Tectonophysics, 137, pp.285-289.

Ziegler, P.A. 1987². Evolution of the Western Approaches Trough. In: Ziegler, P.A. (Ed.), European Union of Geosciences 3rd Symposium on Inverted Mesozoic Basins of the Alpine Foreland. Tectonophysics, 137, pp.341-346